Universität Stuttgart
Institut für Energiewirtschaft und
Rationelle Energieanwendung

Forschungsbericht

A model-based framework for the assessment of energy-efficiency and CO_2-mitigation measures in multi-cylinder paper drying

Hélène Godin

Band 151

A model-based framework for the assessment of energy-efficiency and CO_2-mitigation measures in multi-cylinder paper drying

Von der Fakultät für Energie-, Verfahrens- und Biotechnik der Universität Stuttgart zur Erlangung der Würde eines Doktor-Ingenieurs (Dr.-Ing.) genehmigte Abhandlung

Vorgelegt von
Hélène Godin
geboren in Paris, Frankreich

Hauptberichter:	Prof. Dr.-Ing. Peter Radgen
Mitberichter:	Prof. Dr. Martin Patel

Tag der Einreichung: 4.04.2022
Tag der mündlichen Prüfung: 14.11.2022

Institut für Energiewirtschaft und Rationelle Energieanwendung

2022

ISSN 0938-1228

D93 (Dissertation der Universität Stuttgart)

Acknowledgement

I would like to express my deepest gratitude to everyone who contributed to the completion of this thesis. First and foremost, I am extremely thankful to Prof. Peter Radgen for giving me the opportunity of being part of his research team and supervising my research work. His support and feedback made this thesis a reality.
Several industrial partners also contributed to this work, and I would like to particularly thank Mr. Thorsten Kaesler and Mr. Karsten Berlin for sharing their knowledge with me so generously.

Very special thanks to the colleagues of my department at IER, in particular to Matthias, Luís, Paula, Nils and Manuel for the excellent team spirit and the many nice discussions.

Thank you also to all the other dear colleagues from the Institute who made my time at IER wonderful. Your positive energy kept me motivated all along and I will never forget the good times we spent together!

Finally, I would like to thank very deeply my friends and my family for their encouraging words and constant support during this journey.

Stuttgart, March 2022

Hélène Godin

Table of Contents

List of Figures

List of Tables

List of Abbreviations

Abbreviation	Meaning
CAPEX	capital expenditure
CHP	combined heat and power
COP	coefficient of performance
EEM	energy-efficiency measure
GHG	greenhouse gas
HEN	heat exchanger network
IR	infrared
MACC	marginal abatement cost curve
MEMRC	marginal co_2-emissions reduction cost
MESC	marginal energy-saving cost
MINLP	mixed integer nonlinear programming
NC	no change
ODE	ordinary differential equation
OPEX	operational expenditure

Nomenclature

Parameters and Variables

Symbol	Unit	Description
A	m^2	area
AF	-	annuity factor
$Angle$	°	cover angle of paper contacting the cylinder
c	kJ/kg K	specific heat
$CAPEX$	EUR_{2021}	capital expenditure
COP	-	coefficient of performance of heat pump
D	m	cylinder diameter
d	%	discount rate
$Diff$	-	diffusivity of vapor in air
ef	g_{CO2}/kWh	emission factor
EMR	kt_{CO2}	emission reduction
ES	MWh	energy savings
FRF	-	fabric reduction factor
G	kg/m^2	basis weight of paper web
h	kW/m^2 K	heat transfer coefficient
H	kJ/kg	specific enthalpy
K	m/s	mass transfer coefficient
l	m	length
L_{vap0}	kJ/kg	latent heat of vaporization at 0 °C at atmospheric pressure
Le	-	Lewis number
Lt	a	economic lifetime of the energy-efficiency / CO_2-mitigation measures
m	kg	mass
$\dot{m}$	kg/s	mass flow
M	kg/kmol	molecular weight
$MEMRC$	EUR_{2021}/t_{CO2}	marginal co_2-emissions reduction cost
$MESC$	EUR_{2021}/MWh	marginal energy-saving cost

Nu	-	Nusselt number
NPV	EUR_{2021}	Net Present Value
$OPEX$	EUR_{2021}	operational expenditure
P	kW	power consumption
p	kPa	(partial) pressure
Pr	-	Prandtl number
$\dot{Q}$	kJ/s	heat flow rate
r	-	ratio of leakage to exhaust air
R	kJ/kmol K	ideal gas constant
Re	-	Reynolds number
Sc	-	Schmidt number
SF	-	steam margin factor
t	m	thickness
T	°C	temperature
TAC	EUR_{2021}	total annual cost
U	kW/m^2 K	overall heat transfer coefficient
V_0	m/s	bulk flow velocity of air
v	m/s	speed of paper machine
w	m	width of paper web
x	$kg_{water}/kg_{\text{(dry air or dry solid)}}$	humidity

Greek letters

Symbol	Unit	Description
Δ		difference between final and initial state
α	-	blow-through steam coefficient
β	-	hood thermal loss factor
η	-	efficiency
λ	kW/m K	thermal conductivity
μ	pa.s	dynamic viscosity at 100 °C
ρ	kg/m^3	density

ψ	-	share of the cylinder inlet steam from a certain steam group that is conducted to a thermocompressor in hybrid steam system configurations (the rest of the steam is conducted to the next cylinder group of the steam cascade)
ϕ	-	isotherm correction factor which accounts for the sorption of bound water in the paper web

Subscripts

a	air
aw	water vapor in the air
ah	air heater
$ambient$	ambient (outside the paper machine hall)
$base$	base of a cylinder
c	condensate
ca	between cylinder and air
$cont$	contact area
cp	between cylinder and paper
ds	discharge steam
dry	dry paper
$evap$	evaporation
ex	exhaust air from hood (numbering ex1, ex2, etc. corresponds to the state of exhaust air after successive heat recovery steps)
f	fiber
hr	heat recovery
i	infinitesimal section number
in	inlet of the (entire) drying section
j	cylinder number
k	steam group number
lam	laminar
$leak$	leakage air from paper machine hall
ms	motive steam
$non-covered$	lateral area of a drying cylinder which is not covered with the paper web
out	outlet of the (entire) drying section
p	paper web

pa	between paper and air
pre	pre-drying
$post$	post-drying
pw	water vapor at the paper web surface
$room$	paper machine hall
s	steam
sa	between steam and air
sat	saturation
sc	between steam and cylinder
sep	separator
$shell$	cylinder shell
$sink$	heat sink of the heat pump
$source$	heat source of the heat pump
sp	between steam and paper
sup	supply air (numbering sup1, sup2, etc. corresponds to the state of supply air after successive heating steps)
$thlosses$	thermal losses at the hood walls
tc	thermocompressor
tot	total
$turb$	turbulent
vap	vaporization
w	water

Abstract

Paper drying is the most energy-intensive step in paper making and leads to significant CO_2-emissions at paper mills where fossil fuels are used to generate the required heat. From the different technologies used for paper drying, multi-cylinder paper drying is the most widespread method constituting around 90% of the installed capacity. The techno-economic analysis of energy-efficiency and CO_2-mitigation measures related to multi-cylinder paper drying is therefore of key importance for the paper sector to achieve its emission reduction targets.

The first step of this work covers the review of literature on the analysis of energy-saving and CO_2-emission reduction measures in multi-cylinder paper drying. No existing model was found which encompasses all modules needed for the assessment of CO_2-saving measures. Furthermore, waste heat recovery from hood exhaust air using heat pumps and the interactions between different measures at the drying section of multi-cylinder paper machines have been very little analyzed.

Thus, a model representing energy and material flows in a multi-cylinder drying section was set-up in MATLAB which includes black-box models of the hood, the heat recovery system, the steam cascade and the energy supply system, and a grey-box model of the dryers. The dryer model was validated with data sets from literature from four different mills.

Thereafter, methods for the energy and economic assessment of measures and combinations of measures were developed on top of the model, and a new methodology for the construction of marginal energy-saving cost curves and marginal abatement cost curves accounting for interactions between measures was proposed to graphically represent the model results.

In the next section of the thesis the developed framework was applied to the drying section of a German mill to analyse the effect of the replacement of film sizing with curtain sizing, the replacement of iron cast cylinders with steel cylinders, the closure of the current semi-closed hood, and the integration of heat pumps using hood exhaust air as a heat source to heat the hood supply air and generate steam for the dryers. The model results showed that a reduction of the steam demand by 51.3% (1.79 GJ_{th}/t_{paper}) at the cost of an increase of the electricity demand by 72.1% (0.2 GJ_{el}/t_{paper}) due to the operation of heat pumps is expected at the drying section after implementing all energy-efficiency measures. For the same combination of measures, the calculated technical and economic CO_2-emissions reduction potentials are equal to 0.16 kg_{CO2}/t_{paper} and 0.12 kg_{CO2}/t_{paper} .

Implementing fuel switching from coal to alternative fuels in addition to the energy-efficiency measures allows to reach a total technical CO_2-emissions reduction potential of 0.33 kg_{CO2}/t_{paper} in the case of a fuel switch to biomass or green hydrogen, and 0.24 kg_{CO2}/t_{paper} for a switch to natural gas or electricity.

Differences ranging from ±1.6% to above ±200% are observed between the individual and cumulative values obtained for the energy savings, CO_2-emission reduction potential, and the total annual cost which demonstrates the importance of accounting for interactions when analyzing the implementation of multiple CO_2-emissions reduction measures at a site.

Kurzfassung

Die Papiertrocknung ist der energieintensivste Schritt in der Papierherstellung und führt zu erheblichen CO_2-Emissionen in den Papierfabriken, in denen fossile Brennstoffe zur Erzeugung der erforderlichen Wärme eingesetzt werden. Die Mehrzylinder-Papiertrocknung ist die weltweit verbreitetste Methode zur Papiertrocknung und entspricht etwa 90 % der installierten Trocknungskapazität. Die technisch-ökonomische Analyse von Energieeffizienz- und CO_2-Minderungsmaßnahmen in der Mehrzylinder-Papiertrocknung ist daher von zentraler Bedeutung für den Papiersektor, um seine Emissionsreduktionsziele zu erreichen.

Als Ausgang der Arbeit wurde die vorhandene Literatur zur Analyse von Maßnahmen zur Energieeinsparung und CO_2-Emissionsminderung bei der Mehrzylinder-Papiertrocknung gesichtet. Nach dieser Recherche existiert kein Modell, welches alle für die Bewertung von CO_2-Einsparungsmaßnahmen erforderlichen Prozesskomponenten umfasst. Außerdem wurden die Nutzung der Abwärme aus der Haubenabluft mit Hilfe von Wärmepumpen und die Wechselwirkungen zwischen verschiedenen Maßnahmen in der Trockenpartie von Mehrzylinder-Papiermaschinen bisher nur wenig untersucht.
Darauf aufbauend wurde ein Modell zur Darstellung der Energie- und Stoffströme in einer Mehrzylinder-Trockenpartie in MATLAB erstellt, das Black-Box-Modelle der Haube, des Wärmerückgewinnungssystems, der Dampfkaskade und des Energieversorgungssystems sowie ein Grey-Box-Modell der Trockner umfasst. Das Trocknermodell wurde mit Datensätzen aus der Literatur für vier Papierstandorte validiert.
Anschließend wurden auf der Grundlage des Modells Methoden für die energetische und wirtschaftliche Bewertung von Maßnahmen und Maßnahmenkombinationen entwickelt. Zudem wurde eine neue Methodik für die Erstellung von Energieeinspar- und CO_2-Minderungskostenkurven unter Berücksichtigung der Wechselwirkungen zwischen den Maßnahmen vorgeschlagen, um die Modellergebnisse grafisch darzustellen.
Das entwickelte Gesamtmodell wurde zur Analyse verschiedener Maßnahmen auf die Trockenpartie einer existierenden Papierfabrik in Deutschland angewandt. Die Modellergebnisse zeigen, dass nach Umsetzung der Energieeffizienzmaßnahmen eine Reduzierung des Dampfbedarfs der Trockenpartie um 51,3 % (1,79 GJ_{th}/t_{papier}) bei gleichzeitiger Erhöhung des Strombedarfs um 72,1 % (0,2 GJ_{el}/t_{papier}) durch den Betrieb der Wärmepumpen zu erwarten ist. Die berechneten technischen und ökonomischen CO_2-Reduktionspotenziale liegen bei 0,16 kg_{CO2}/t_{papier} und 0,12 kg_{CO2}/t_{papier}.
Wird zusätzlich zu den Energieeffizienzmaßnahmen ein Brennstoffwechsel von Kohle zu alternativen Brennstoffen durchgeführt, kann ein technisches CO_2-Reduktionspotenzial von insgesamt 0,33 kg_{CO2}/t_{papier} im Falle eines Brennstoffwechsels zu Biomasse oder grünem Wasserstoff, und 0,24 kg_{CO2}/t_{papier} im Falle eines Brennstoffwechsels zu Erdgas oder Strom erreicht werden.
Zwischen den einzelnen und den kumulierten Werten, die für die Energieeinsparungen, das CO_2-Reduktionspotenzial und die jährlichen Gesamtkosten ermittelt wurden, sind Unterschiede von ±1,6 % bis über ±200 % zu beobachten, welches zeigt, wie wichtig es ist, Wechselwirkungen bei der Untersuchung mehrerer CO_2-Minderungsmaßnahmen an einem Standort zu berücksichtigen.

1 Introduction

In 2020, the average global temperature[1] was about 1.2 °C above the level of pre-industrial times (WMO 2021). The acceleration of global warming in the last decades is accompanied by growing physical and financial impacts (WMO 2020). Climate model projections show possible consequences of a 1.5°C and 2°C global warming and highlight the importance of adopting rapid and far-reaching measures to mitigate the occurrence of climate and weather extremes, sea level rise, losses of biodiversity and ecosystems and the associated effects on the world's population in terms of health, livelihoods, water supply and food and human security (IPCC 2018). The main cause of global warming is the increase of anthropogenic greenhouse gas (GHG) emissions which have "unequivocally" enhanced the greenhouse effect of the Earth's atmosphere. CO_2-emissions constitute around 75% of anthropogenic greenhouse gas emissions (WRI 2016) and have made the "largest contribution to the increased anthropogenic forcing in every decade since the 1960's (Myhre et al. 2013).

The discovery of the greenhouse effect in the atmosphere dates back to the 19th century with experimental works conducted by Tyndall (1861), and was followed a few decades later by first quantitative predictions of global warming due to variations in atmospheric carbon dioxide concentration related to fuel combustion by Arrhenius (1896).
However, consensus-building in the scientific community on anthropogenic global warming only really began with pioneering work using computer models in the late 1960's and grew stronger through the observation of global temperature rise in the 1970's and the steady improvement of climate models (Powell 2017).
Thereafter, the topic of climate change shifted from a scientific concern to a pressing political issue and entered the intergovernmental arena. Counting 197 Parties, the UN Framework Convention on Climate Change (UNFCC) launched by the UN General Assembly and adopted in 1992, was the first global agreement aiming to "stabilize greenhouse gas concentrations in the atmosphere at a level that would prevent dangerous anthropogenic interference with the climate system." Industrialised countries were given the major responsibility for fighting against climate change, without specifying how (Hirst 2020). Since 1992, "Conferences of the Parties" are held annually to review the Convention and make decisions regarding its implementation. Consequently, the first binding GHG reduction targets were set for industrialised countries in the 1997 Kyoto Protocol.
As of January 2021, 189 states and the EU, representing about 97% of global greenhouse gas emissions, have signed the Paris agreement and thereby committed to "pursue efforts to limit the temperature increase to 1.5°C". The parties agreed to submit a nationally determined contribution (NDC)[2] and to update it with more ambitious targets at five-year intervals. The implementation of the NDCs and the achievement of set targets is however not legally binding (Rajamani and Brunnée 2017). Until now[3] 190 parties have submitted their first NDCs but only 40 submitted their due 2020 NDCs, of which at least 8 did not increase their ambition (CAT 2021). At the European level, the NDC submitted by the European Commission on 17th December 2020 rises the overall greenhouse gas emission reduction target across sectors from 40 to 55% in 2030 compared to 1990. Additionally, a target of zero net GHG emissions in 2050

[1] Defined as the combined surface air and sea surface temperatures

[2] national plans that include mitigation goals at country-level, the actions undertaken to reach those goals, and measures to adapt to the impacts of climate change.

[3] Last update 04.02.2021

was set in the European Green Deal (EC 2019) and the elaboration of a first European Climate law containing those targets is in progress, to ensure that all EU policies contribute to this goal and that all sectors of the economy and society play their part.

To address the causes and effects of climate change, decision-makers take recourse to numerous policy instruments applied to the different sectors. Those instruments include market-based instruments which incorporate externalities, like carbon taxes or the cap-and-trade European Union Emission Trading System (EU ETS), and non-market-based instruments which encourage/discourage certain behaviors, or impose obligations, like emission standards, product bans, or research funds.

1.1 CO_2-mitigation in the industry

CO_2-emissions represent around 91.5% of the industry's total GHG emissions (WRI 2016). As shown in Figure 1.1 the industry sector caused 43% of world's CO_2-emissions in 2018, of which 16% are so-called process emissions, which result from chemical reactions during industrial processes, and 84% are energy-related.

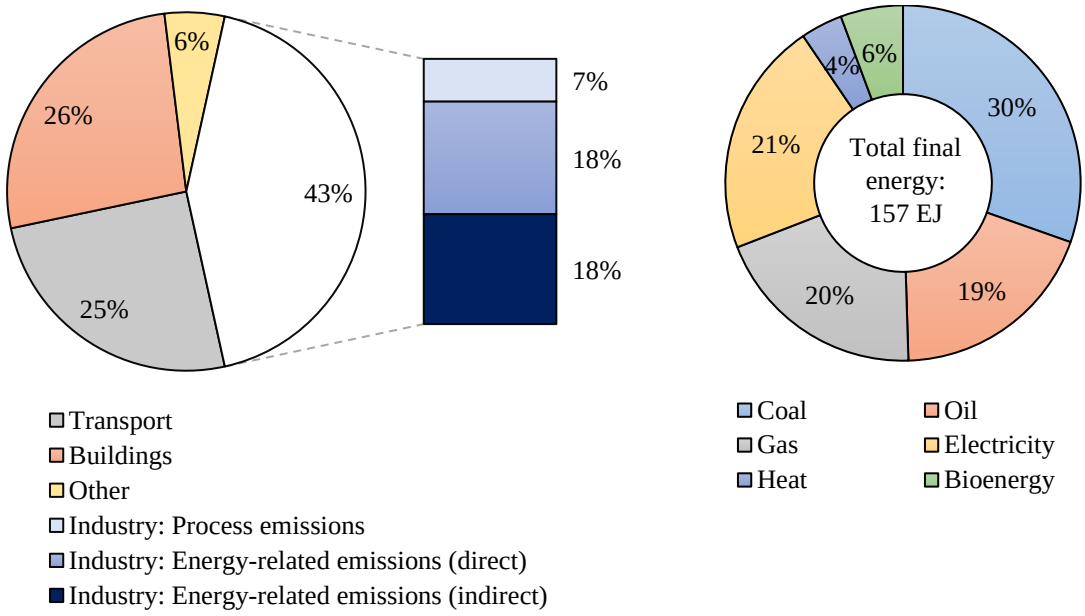

Figure 1.1: Anthropogenic CO_2-emissions distribution across end uses in 2018 with electricity and heat reallocated (left) and final energy consumption in the industry in 2018, including fuel used for blast furnace, coke ovens and feedstock (right). Source: own representation based on data from (IEA 2020a, 2020c, 2020e).

The industry sector accounted for 37% (157 EJ) of total global final energy use in 2018 (including energy use for blast furnaces, coke ovens and feedstock). Large amounts of direct energy-related emissions arise because of the local combustion of fossil fuels to cover the energy demand (see right chart in Figure 1.1), and in particular the heat demand, which corresponds to 67% of the energy demand (IEA 2018). Indirect emissions are generated off-site, mainly in the power generation sector.

CO_2-emission mitigation strategies in the industrial sector include a wide scope of options which aim to either prevent the emissions from arising, or to capture the generated emissions (Guminski et al. 2017; Fischedick et al. 2014).

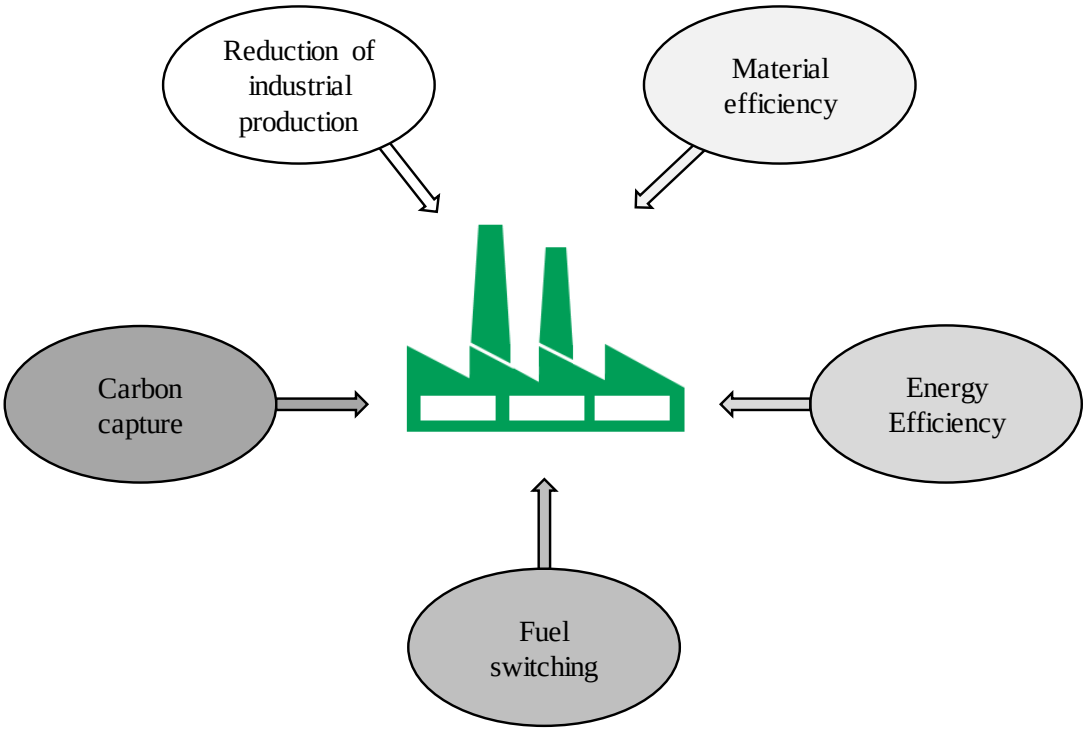

Figure 1.2: The five pillars of CO_2-mitigation in the industry. Source: adapted from (Leipprand et al. 2020)

As shown in Figure 1.2, one way of reducing the amount of generated emissions consists in the reduction of industrial production. A lower product demand can be reached through the more intensive use of the products, for example by sharing products between consumers and extending the product's lifetime through improved design and material properties (Fischedick et al. 2014).

Furthermore, increased efficiency of material flows usually leads to energy savings and can be achieved by increasing the use of secondary raw materials for production, reducing yield losses during production, and adapting the design of the products so that less amounts of materials are required (e.g. lighter cars) (Allwood et al. 2012).

A third and essential pillar for CO_2-mitigation strategies in the industry is the implementation of energy efficiency measures. Those measures comprise the operational optimization of processes (e.g. avoiding unnecessary start-up/shutdowns) and energy management practices, technology retrofit, addition or replacement in the core production processes, and passive and/or active heat recovery.

Finally, fuel switching to renewable fuels for local heat and power generation and the implementation of technologies to capture and utilize or store CO_2-emissions represent further ways to achieve emissions reductions at an industrial site.

Various obstacles are associated with the implementation of emission reduction options, of which the most obvious certainly are technological aspects, which include technical risks of individual technologies and physical aspects like the limited availability of waste materials and biomass for energy substitution in industry, or a lack of CO_2 pipeline infrastructure in the case of carbon capture (Fischedick et al. 2014; IEA 2009).

Financial aspects, like the access to capital in case of high capital expenditure, short investment payback requirements, high fuel prices, hidden costs or liability risk also play a major role in decision-making regarding the implementation of emission mitigation options. Worth mentioning is that the cost of CO_2-mitigation rises with the exhaustion of low hanging fruits solutions and the implementation of more complex and costly technologies (Mehling 2020).
Financial aspects lead certain measures which are relevant from a system-wide perspective to be hardly applicable at the plant-level. For example, in the paper industry, there is a clear trend of increasing the production capacity at paper mills to remain competitive, which globally translates into a shift towards bigger average mills and the closure of smaller ones (Suhr et al. 2015; CEPI 2019).
Taking into account the financial value of co-benefits of mitigation measures (e.g. new business opportunities or health benefits for employees) can help reducing financial barriers in many cases but the monetisation, quantification or even measurement of those non-energy benefits is often a complex task (Campbell et al. 2014; Fleiter 2012).

Obstacles due to the institutional and legal context like market barriers, rapidly changing regulatory frameworks or effects of non-energy policies constitute a further type of barrier to emission mitigation in the industry.

Last but not least, cultural i.e. organisational, behavioural, competence-related, and information-related barriers also slow down the diffusion or hamper the adoption of mitigation options. These barriers have been assessed to play a major role in the so-called “energy-efficiency gap”, i.e. the empirical evidence of high potentials of economic energy-efficiency measures across sectors remaining untapped (Fleiter et al. 2011; Cagno and Trianni 2014).

1.2 Problematic, objectives and methodology

The pulp and paper industry emitted around 296.4 megatons of CO_2 in 2016 worldwide which were caused by its high final energy consumption (WRI 2016). Energy costs account for approximately 10 to 30% of total paper production costs and the steam demand of the paper drying step is often responsible for more than 65% of the energy demand in the papermaking process (Laurijssen et al. 2010; Suhr et al. 2015; Mujumdar 2006)

From the different technologies used for paper drying, multi-cylinder paper drying is the most widespread method constituting around 90% of the installed capacity (Stenström 2020). In multi-cylinder drying sections, steam is required in the drying cylinders and to preheat the hood air to temperatures of around 100°C, which carries away the large amounts of humidity released from the paper web. At non-integrated paper mills, the high steam demand for paper drying is in many cases covered using fossil fuels, causing large amounts of CO_2-emissions.

Paper machines have long lifetimes ranging from 20 to 50 years (Laurijssen et al. 2010) which leads to a slow uptake of innovations and limits the overall impact new papermaking processes can have on the overall branch decarbonisation until 2050. Since new paper machines are highly capital-intensive, incremental changes and the refurbishment and improvement of an existing plant is often the favored option over the installation of a new paper machine (EC 1994; Crotogino 2001; Rogers 2018; Laurijssen et al. 2010).

The implementation of energy-efficiency measures at the drying sections and the switch to greener fuels is therefore of key importance for the reduction of CO_2-emissions related to paper drying, and the quantification of the effect of different options is essential for decision-making processes related to those options. Modelling tools are required for the analysis of CO_2-mitigation measures due to the wide scope of possible measures and the interdependences between the concerned units. Due to large fluctuations in economic parameters, the cost-effectiveness of measures is often hard to determine, especially when combinations of measures are considered.

In this context the following objectives have been defined for this thesis:

- Development of a modelling framework for the quantification of potential energy savings and CO_2-emission reductions reached through the implementation of retrofit measures at a multi-cylinder drying section and fuel switching for the generation of the steam supplied to the drying section of a paper machine.
- Extension of the framework to include the economic analysis of these measures and combinations of measures for different scenarios, and the graphical representation of energy-saving and emissions reduction costs using energy-efficiency cost curves and marginal abatement cost curves.
- Application of this framework to a paper mill in Germany for site-relevant measures, and the analysis of the effect of measure's interactions on the results, or in other words, a comparison between the cumulative effect of measure's combinations and the sum of the effects of individual measures.

A path consisting of seven main steps was chosen to fulfil the presented objectives:

1. Screening of previous studies on the analysis of energy-saving and CO_2-emission reduction measures related to the energy demand of multi-cylinder drying sections in order to identify main shortcomings of existing models and better define the model scope and objectives.
2. Development of a drying model for the determination of the temperature and humidity profiles of the paper web in a multi-cylinder drying section and validation of the model with literature data sets from four different mills.
3. Extension of the model to include the heat recovery system of the drying section, the steam cascade, and the energy supply system in order to determine the overall heat demand of the drying section.
4. Incorporation of methods for the energy and economic assessment of measures and combinations of measures into the framework.
5. Development of a methodology for the construction of marginal energy-saving cost curves and marginal abatement cost curves which account for the measure's interactions.

6. Application of the developed framework to the drying section of a German mill in order to assess the effect of selected measures and measures combinations under three distinct economic scenarios.
7. Sensitivity analysis: evaluation of the robustness of the model against variations in the tuning parameters of the drying model on one hand, and uncertainties in the economic parameters on the other.

1.3 Structure of this work

The structure of this thesis is graphically represented in Figure 1.3.
Chapter 2 provides background information on the paper industry, the paper production process and on the on-going research on material efficiency and new paper production methods.
Main paper drying techniques and fundamentals of paper drying with a focus on multi-cylinder paper drying are described in Chapter 3.
In the fourth chapter is presented the State of the Art of multi-cylinder drying models and their application to the analysis of CO_2-mitigation measures, process integration techniques for assessing retrofits at industrial processes, and energy-efficiency cost and marginal abatement cost curves developed for plant-level analysis.
The core part of the present work, i.e. the developed framework is detailed in Chapter 5, followed by the application of the framework to the analysis of measures at the drying section of a German paper mill in Chapter 6. Finally, a summary of the main results, scope for future work and final remarks are provided in the concluding Chapter 7.

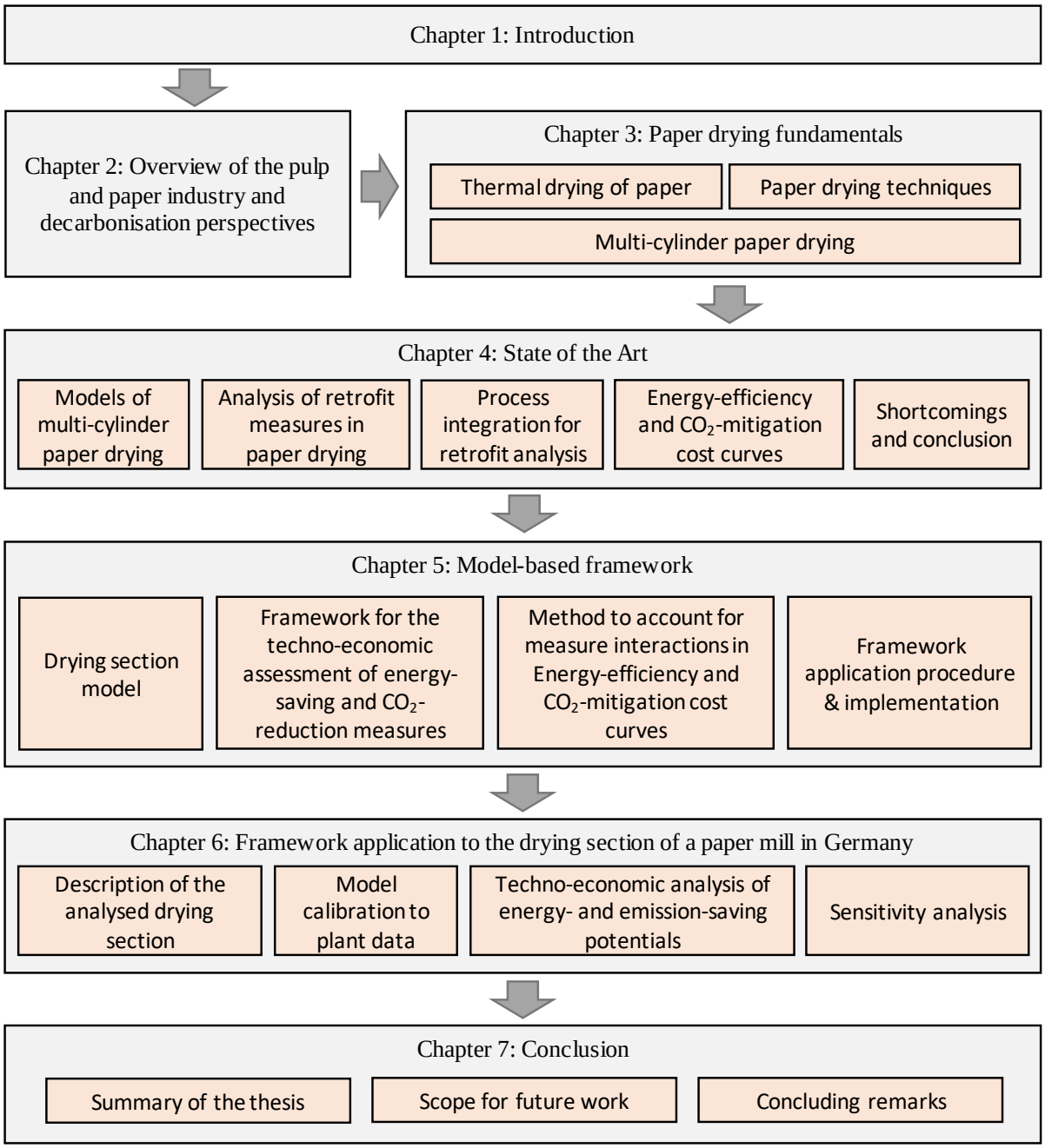

Figure 1.3: Graphical representation of the Thesis' structure

2 Overview of the paper industry and decarbonisation perspectives

This chapter starts with a short description of the paper industry and the paper production process, followed by an overview of the mitigation options identified as game changers in different roadmaps for the decarbonisation of the industry. Finally, a quick analysis of possible improvements on material efficiency and new paper production methods is presented.

2.1 The pulp and paper industry

Around 420 million tons of paper and board were produced worldwide in 2018, of which 26% in China, 17% in the USA, 6% in Japan and 5% in Germany. The paper production in the European Union (EU28) constituted 22% of the global production in the same year (VDP 2020). As shown in Figure 2.1 packaging paper grades represent around 60% of the produced paper and their production is expected to grow further in the coming years with the increase of electronic commerce (VDP 2020). On the other hand, a steady decline in the production of graphic papers has been observed in the last years, due to the transition to paperless communication and digital media. This shift is the driver for paper machine conversion projects from newsprint or other graphics to containerboard and speciality paper (Berg and Lingqvist 2019; Moore 2017; Toto 2019).

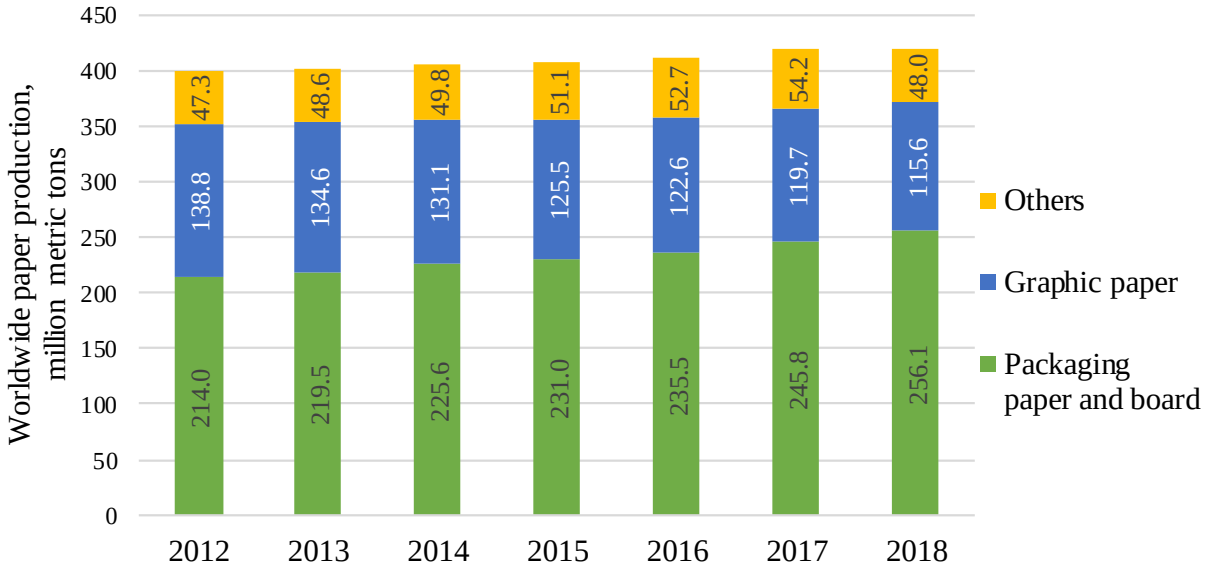

Figure 2.1: Paper and Board Production by main paper types in 2012-2018. Source: own representation based on data from VDP (2020).

As shown in Figure 2.2, the rise in worldwide paper production was accompanied by a rise of the final energy demand of the pulp and paper industry which was equivalent to 7 EJ in 2018. This represents 1.7% of the global final energy consumption in 2018 and makes the pulp and paper industry the fourth biggest industrial energy consumer. (IEA 2020d, 2020b)
The share of its CO_2-emissions is comparatively low with 0.6 % of the global CO_2-emissions, due to low process emissions and the relatively high share of biomass and biomass-based by-products of the pulping processes like bark or black liquor as energy carrier (WRI 2016; IEA 2020b). Merely 45% of the raw wood supplied to the chemical pulping processes is returned as pulp (Cheremisinoff and Rosenfeld 2010) and the wood components lignin and hemicelluloses

which are discarded in the process are transformed into a liquor qualified as “black liquor” for the Kraft, and “brown liquor” for the sulphite process. In modern chemical pulp mills, the combustion of the liquor usually generates enough energy to cover the entire energy demand of the chemical process and a significant part of the energy required for papermaking, in the case of integrated pulp and paper production. (Moya, J. A., Pavel, C. C. 2018)
However, in many cases, fossil fuels, mainly gas and coal, are utilized to cover the high thermal demand of paper production.

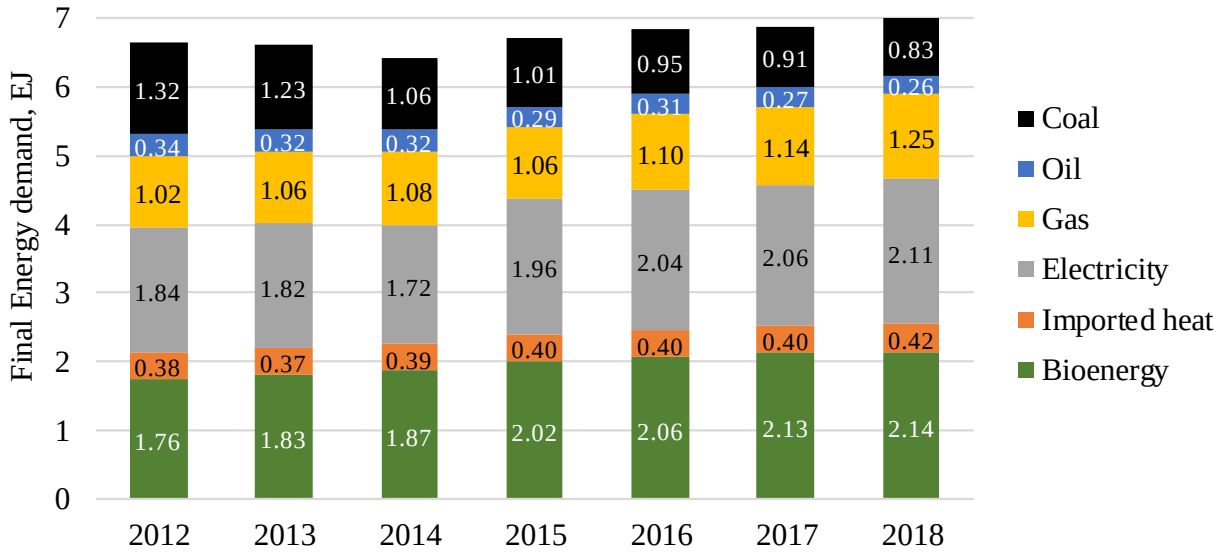

Figure 2.2: Fuel shares of the final energy demand in the Pulp and Paper industry in 2012-2018. Source: own representation based on data from (IEA 2020b).

As shown in Table 2.1, the specific energy consumption of paper production differs between paper grades, in particular because of the influence of the product grammage on the steam demand in the drying section, the effect of machine speed on the power consumption (Valmet 2015a), the use of different paper drying techniques and specific technologies to reach product properties, like calenders or coating units. Furthermore, the presented values constitute averages for European paper mills and great variations of the energy consumption (sometimes up to 40%) have been reported across different paper mills even to produce a same paper grade, due to different paper machine speeds and unit efficiencies (e.g. heat recovery system, motors).

Table 2.1: Typical values for the overall specific heat and electricity demand of the production of different paper grades. Sources: own assessment based on Suhr et al. (2015), Laurijssen (2013), Fleiter et al. (2013), Moya, J. A., Pavel, C. C. (2018) and Bajpai (2016).

Paper grade	Specific heat demand in GJ_{th}/t_{paper}	Specific electricity demand in GJ_{el}/t_{paper}
Newsprint	5.2	1.9
Woodfree	6.4	2.5
Mechanical	6.4	2.3
Tissue (w/o through-air Drying)	6.7	1.7
Cartonboard	6	2
Case Materials	5.2	1.7
Wrappings	6.5	1.9

2.2 The paper production process

In conventional papermaking, fibres and fillers are mixed with around 100 times their weight of process water to a suspension which is subsequently dewatered in multiple steps, in order to obtain a finished paper with a solids content of 90 to 98% (Beer et al. 1998). Despite technological differences at the level of the individual units, the overall sequence of unit operations remains same for the production of all types of papers and boards. First, in the stock preparation step, different types of pulp and additives are mixed and refined to form the papermaking furnish. This suspension is then further diluted to obtain a uniform and constant consistency in a step called "approach flow", before being uniformly distributed across the width of the wire belt via the headbox of the up to 250 meters long paper machine. In the wire section, also called former, the suspension becomes a sheet with a solids content of approx. 15 – 25 % by means of gravity and vacuum. At the end of this stage about 97 % of the water initially present in the suspension at the headbox is already separated from the paper web. The paper web is then conducted through the press section where it is dewatered using nips formed by rolls pressing against each other, and felts that support the sheet and absorb the water, until a moisture content of 45 to 55 %. A last the paper web undergoes thermal drying at the drying section using one or several steam-filled drying cylinders to reach a target solids content of the paper web between 90 and 98 %. Additional process units for surface treatment and finishing, such as size presses, coaters and calenders are placed either between the drying section and the reel (online) or outside the paper machine (offline), depending on the paper and board quality. The steps of the paper production process and the dry substance content of the paper web at the end of those steps are summarized in Figure 2.3.

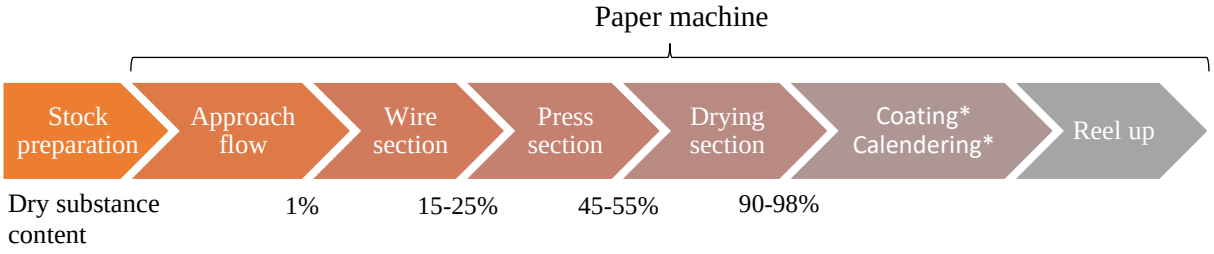

*Figure 2.3: Main steps of the paper production process. The process steps marked with * are optional. Source: own representation.*

Table 2.2 shows typical values for the energy consumption of the process steps involved in the production of case materials. The steam demand of the paper drying step is responsible for more than 85% of the heat demand and 65% of the overall energy demand, although merely 1% of the water discarded during the overall process is removed in that section of the paper machine. Consequently, the relative dewatering costs of the drying section are high and estimated to represent around 78% of the dewatering costs (Ghosh 2011).

*Table 2.2: Typical specific energy demand of the different process steps for case materials production in Europe. Note: The process steps marked with * are optional. Source: own assessment based on Suhr et al. (2015), Laurijssen (2013), Bajpai (2016), Moya, J. A., Pavel, C. C. (2018) and Fleiter et al. (2013).*

Process step	Specific electricity demand in GJ_{el}/t_{paper} and share of total electricity demand	Main electricity consumer	Specific heat demand in GJ_{th}/t_{paper} and share of total heat demand	Main heat consumer
Stock preparation	0.27 / 15.5%	Refiner	-	
Approach flow	0.23 / 13.2%	Pumps	-	
Wire section	0.13 / 7.5%	Vacuum at the couch roll	-	
Press section	0.36 / 20.7%	Vacuum at the press suction rolls, Uhle boxes and drives	-	
Drying section	0.37 / 21.3%	Drives for dryers and hood ventilation	4.55 / 87.5%	Dryers
Coating*	0.07 / 4%	Coat nozzles	0.27 / 5.2%	Infrared dryer
Calendering*	0.13 / 7.5%	Drives	0.21 / 4%	Calender rolls
General mill services	0.185 / 10.6%	Compressed air, water treatment	0.16 / 3.1%	Shrink oven
Total	1.74		5.2	

2.3 Decarbonisation roadmaps and the pulp and paper industry

Numerous studies are being conducted to propose deep decarbonisation pathways and assess their economic impact. Those studies are helpful for decision-making processes of policy makers and are therefore often commissioned by governments. Table 2.3 shows key information on the contribution of the pulp and paper industry for a selection of such decarbonisation roadmaps in different regions. These studies all consider an 80% CO_2-emission reduction until 2050, however the analysis scope varies from the pulp and paper industry only (e.g. CEPI (2011)) to all sectors (e.g. Gerbert et al. (2018) and Bernath et al. (2017)).

The resulting emission reduction target in the pulp and paper industry ranges from a 66% to 98% CO_2-emission reduction below base year (1990) level.

To reach these targets a combination of measures at different levels is systematically proposed. The included measures cover not only changes at the plants like material efficiency in production, energy efficiency measures to reduce the energy demand of the plants, and fuel switching in the local energy generation, but also systemic changes, like increased recycling of products and decarbonisation of national electricity production, on which the paper industry only has a limited influence. The use of carbon capture and usage or storage is however absent from the list of proposed solutions for the paper industry, because these technologies are either not included in the studies due to the high operating and investment costs or are restricted to the capture of process emissions in the industry and/or energy-related emissions for the power generation sector.

In the roadmap proposed by the Confederation of European Paper Industries (CEPI), 31% of the decarbonisation in the branch is reached via fuel mix and the use of best available techniques

(BAT), a large share of the decarbonisation is outsourced to the grid decarbonisation (27%) and very high expectations are set on the development of breakthrough technologies (29%).

Table 2.3: Contribution of the Pulp and Paper industry to the CO_2-emission reduction goals set in diverse decarbonisation roadmaps developed for different regions and scopes. The reference year for the energy saving and emission reduction goals is 1990.

	General information		Information relative to the pulp and paper sector		
Reference / Commissioner	**Region / Roadmap timeline**	**80% CO_2-reduction target in**	**Para-meter**	**Reduction target in the Pulp and Paper industry**	**Measures to reach for CO_2-emission reduction goal**
(Gerbert et al. 2018) Federation of German Industries (BDI)	Germany 1990-2050	All sectors	CO_2-emissions	95%	Biomass, Recycling, Energy Efficiency (in the continuity of the last 10-15 years)
(Bernath et al. 2017) German Federal Ministry of Economics and Technology (BMWi)	Germany 2010-2050	All sectors	CO_2-emissions Energy demand	66% 42.5%	Fuel switching, energy efficiency, recycling
(Bründlinger et al. 2018) German Energy Agency (Dena)	Germany 2015-2050	All sectors	Energy demand	29%	Fuel switching, Heat recovery and waste heat utilization (Heat pumps), recycling
(Repenning et al. 2015) German Federal Ministry for Environment, Nature Conservation and Nuclear Safety (UBA)	Germany 2010-2050	All sectors	Fuel demand Power demand	43% 48%	Fuel switching, energy efficiency, recycling
(Lenaghan and Mill 2015) Scottish Government	Scotland 2012-2050	Industry	CO_2-emissions	98%	Energy efficiency (40%), biomass (40%), grid decarbonisation (20%)
(CEPI 2011) European association representing the paper industry (CEPI)	Europe 1990-2050	Pulp and Paper	CO_2-emissions	80%	Breakthrough technologies (29%), grid decarbonisation (27%), Best available technologies (21%), Fuel mix (10%), transport (10%)
(Wising et al. 2015) Government of the United Kingdom	UK 2012-2050	Pulp and Paper	CO_2-emissions	80%	Biomass, Heat recovery on hoods, Improved process control

2.4 Material efficiency and new paper production methods

The aim of this section is to provide some general information on material efficiency potentials before presenting a brief overview on alternative production methods, which are still in the development stage.

2.4.1 Increasing the share of recycled paper as raw material for paper production

The production of recycled pulp requires approximately 5.7 times less energy than the mechanical pulp and 8.3 times less than chemical pulp production (Moya, J. A., Pavel, C. C. 2018). Thus, the reduction of the energy demand in the pulp and paper industry goes hand in hand with an increased use of recycled paper as a raw material. This difference in energy consumption is even greater when accounting for the energy consumption of the upstream processing steps, i.e. cutting, transporting, and sawing the wood for virgin pulp, compared to transporting recycled paper to the processing plant for secondary fibres.
Beyond energy savings, using recycled paper for paper production has further environmental advantages, since it helps reduce pressure on the world's forests, reduces the use of chemical and allows to save up to 60% water (UBA 2012). In 2019, the recycling rate of paper was equal to 78% in Germany, 72% in Europe, while the global average was 59.1% (ICFPA 2021; EPRC 2020; VDP 2020).

Unfortunately, paper cannot be recycled endlessly. The quality and length of the fibres decreases with each recycling loop and a share of secondary fibres is therefore discarded continuously. However, despite a widespread information according to which fibres can be recycled up to maximum 6 or 7 before becoming too short and therefore useless in papermaking (UBA 2012), recent discussions with industrials as well as tests conducted by Putz and Schabel (2018) suggest that this number is much underestimated and certain grades like cartons can be recycled up to 25 times, or even more. Average use of paper fibres is 3.6 times in Europe, whereas the world average is around 2.4 times (EPRC 2020).

An increase in the use of recycled fibres in paper production depends on the availability and quality of recovered paper and on the potential for the use of secondary fibres in the paper industry.
Regarding the availability of recycled fibres, it is important to note that certain types of paper are not available for collection in first place, like most hygiene papers and those used as component for other products as e.g. insulation materials, that cannot be recycled back into new paper products.
Moreover, increasing the availability of collected paper highly depends on the local collection infrastructure and policies, the tools used to communicate and enforce the rules, and of course, on the behaviours. Increasing the amount of collected paper often goes hand in hand with a decrease of the collected paper quality. This is especially true when the collection rates are already high, since industrial and trade sources are then already tapped and possibilities to increase recovery lies only in the waste coming from households.
Maintaining quality standards for collected paper is however essential for the recycling process. Not all the consumed paper and board is recyclable due to different types of contaminants, like plastics, adhesive substances, food waste and grease. The contaminated paper is either discarded in the sorting plant, or often also in the paper mill itself, during the pulping step.

The quality issue is made worse when so-called commingled collection systems are in use, in which all recyclable materials are collected in a single container. Waste paper obtained after sorting such mixed waste typically includes up to 20% of unusable materials like glass or cans, compared to 1% when a source separated collection method is used (Miranda et al. 2013). Waste paper of such a low quality is difficult to use as a raw material in paper mills since it can significantly lower the product quality and even damage the mill equipment (Miranda et al. 2013). Consequently, in the last decades, low-quality paper waste was usually sent to processing plants in Asia, in particular China. However, the "National Sword" policy enacted in January 2018 in China, set new quality requirements on the imported paper (as well as on other types of waste), which led to the saturation of the wastepaper market with low-quality paper in Europe (which used to send around 5% of collected paper to China), and in other regions. The consequence is critical price drops for wastepaper and an endangered profitability of paper collection. Such events highlight the importance of improving the collection methods to minimize wastepaper contamination as far as possible and reducing the international dependence on waste processing infrastructures.

On the demand side, all paper and board products, apart from high grade paper, can be produced, at least partly, from secondary fibres. In fact, many mills that produce corrugated board, cardboard packaging or newsprint use almost exclusively secondary fibres. Other grades are often produced with a mixture of primary and secondary fibres, to meet paper strength specifications (CEPI 2019; Hillman et al. 2015). Higher quality secondary fibres are typically used for higher grades, whereas low quality recycled paper is used for newsprint or board.
The increase in packaging paper and board i.e. low grade production compared to other grades shall lead to an increased demand for secondary fibres, and to a decline in the quality of recovered paper as a consequence of a higher proportion of non-paper materials in wastepaper.

In general, in order to achieve even higher recycling targets and maintain the production of primary fibres as low as possible, actions should be taken on the product design, to account for both the intended purpose as well as the end-of-life of the product. Examples to prevent “upstream” contamination are the reduced use of plastic layers in paper packaging and colouring chemicals, and using more soluble inks from renewable and recyclable raw materials (CEPI 2020).

2.4.2 Alternative raw materials to wood-pulp

Before the middle of the nineteenth century, herbaceous biomass like cotton, straw and flax were mainly used as a raw material for paper production.
Later on, the increasing paper demand led in most countries to a shift to wood as a raw material, among others because of its year-round availability and its high density which facilitates its transport and storage (Eugenio et al. 2019; Ashori 2006).
China and India constitute an exception in this regard since they belong to the very few countries where non-wood materials, such as corn straw, bamboo, reed and bagasse are currently used in great extent and make up to 70% of the used cellulose fibre in the local paper industry (Liu et al. 2018).

The shortage of wood fibres, long transport routes, and the high energy and water consumption in paper production, have caused a renewed interest for alternatives to wood-fibres (Eugenio et al. 2019; Hanecke 2019; Abd El-Sayed et al. 2020).

Non-wood plant fibres used in pulp and paper industry come from three main types of sources. First, the cheap agricultural residues such as straw of rice, corn or wheat plants, sugarcane bagasse and banana pseudo-stem which have a moderate quality and are abundant at a specific time of the year, after the harvest. Then, the annual plants such as bamboo, reeds or grass and, lastly, the non-wood crops grown for their fibre, like cotton or jute.
These raw materials typically grow faster and have a more porous structure than wood and, in most cases, a lower lignin content, which means less energy and chemical requirements for separating fibres during pulping (Ashori 2006).
As for fibres coming from different wood types, fibres from non-wood plants have varying chemical compositions and physical properties, which have a big impact on the properties of the final paper product. Since wood fibres have particularly good strength properties, the incorporation of non-wood fibres is likely to play the role of a partial substitution and not a complete replacement of wood fibres.

One promising example for the use of non-wood pulp in the paper and board industry is the use of grass as a substitution for wood pulp and recycled pulp up to 50% in packaging (Cruse et al. 2015). The company Creapaper holds a patent for processing grass into pellets which are now used at several plants in Germany (Cruse et al. 2015). Grass presents volume-generating properties, which leads to substantial material savings compared to normal fibre mixtures to achieve a certain paper basis weight and grass paper can be recycled like other paper types (Hanecke 2019). Furthermore, the energy required for preparing this raw material was assessed to be around 50% lower than in RCF pulp production, and 90% lower than in wood pulp production (Terlau et al. 2017).

As a conclusion, there is clearly some untapped potential regarding the use of non-wood fibres in papermaking (Ashori 2006) which could lead to significant costs- and energy-savings. More research is needed to develop adequate pulping processes and pulp mixtures which allow to reach the desired product properties (Liu et al. 2018).

2.4.3 Increasing the share of fillers in paper production

Although fibres constitute the main raw material used for paper production, diverse chemicals are added in significant amounts to the process. The Confederation of European Paper Industries assessed the share of non-fibrous materials to be equal to 12.7% of the total mass of input raw materials in paper production in Europe in 2018 (CEPI 2019).
Additives that improve the operation of the paper machine, like biocides and defoamers, are mostly used at the wet end of the paper machine and qualified as process additives.
On the other hand, functional additives, like mineral fillers and dyes, contribute to reaching specific product properties, such as printability or opacity (Dulany et al. 2011).

The advantages of mineral fillers are presented in Hubbe and Gill (2016), one of which is their low price, which represents typically 10% of the price of the same amount of fibre (Stumm 2007). This explains their increased use in paper production in the past decades to rise the basis weight of paper cost-effectively.
The production of common fillers, like kaolin and calcium carbonate, also requires significantly less energy than pulp production and can therefore have a positive impact of the energy demand in the paper sector.

However, beyond a certain filler content, which differs across the grades, the mechanical product properties are impaired. Modification on fibres and filler particles, and the addition of chemicals to reach higher filler content are object of ongoing research and development works and provide good hopes that further innovations can be expected in the decades to come (Hubbe and Gill 2016; Kong et al. 2016a).

2.5 Alternative papermaking methods

Beyond the modification of raw materials composition, several research projects are dedicated to developing new papermaking processes, in order to increase product properties and/or resource efficiency.
In the current papermaking process, large quantities of water are used to prevent lumps from forming in the fibre suspension. This leads to high energy requirements since on the one hand, the water has to be pumped and cleaned in the loop and, on the other hand, it needs to be removed from the paper web.

Dry-sheet-forming, DryPulp and Cure Forming are alternative processes which aim to reduce the use of water in the paper industry.
In the Dry-sheet-forming process, fibres are dispersed either mechanically or by so-called air laying techniques. In air laying, the fibres are dispersed in the air to form a sheet, which are then bonded to each other either by resins or by a polymer latex sprayed on the web (Beer et al. 1998). In the first case, the resins are polymerized by air-heating or hot pressing of the sheet, and in the second case, the web is dried in a drying chamber filled with hot air.
The air laying technology allows a higher production rate and better control of air flows compared to mechanical processes. A typical production line consists of fibre preparation, web formation, web consolidation and finishing. Dry-sheet-forming is implemented at 15 locations worldwide but only for specific sanitary and speciality papers (Beer et al. 1998). Also, despite the fact that significant savings in thermal energy of 50% might be achieved at the cost of a low rise in the electricity consumption in the range of 150-250 kWh/t paper, this technique has not been transferred to papers produced in larger quantities, because of technical issues regarding the paper quality and a lower production speed (Kong et al. 2016a).

Another possible process for waterless papermaking is the process of dry pulping and cure forming, which was among the finalists of the innovation challenge “Two Team project” conducted by the CEPI (2013). First, the fibres are treated to protect them from shear forces, and, in a next step, they are dissolved in a highly viscous solution called "DryPulp", which has a maximum fibre concentration of 40 %. The DryPulp is then hardened by mechanical forces in the so-called cure forming process to achieve a fibre content of approx. 80 %. Depending on the requirements of the end product, the paper web is also treated with additives or further processes. The combination of these two technologies ("DryPulp" and "Cureforming") enables the sheet to be produced as a layered product with specific properties.
Further research is needed for the development of the optimal DryPulp composition, for the process technology for mixing and pumping the viscous solution and for the technology for forming and curing (CEPI 2013).

At last, it is also conceivable to replace the water in the fibre-water suspension in conventional papermaking by another medium, such as foams, ethanol, or supercritical carbon dioxide, that can be separated from the fibres with less energy input.

Results from a pilot installation of a conventional paper machine, adjusted for foam-forming at VTT in Finland, showed that the dryness of the web may be increased by 2 to 3% at the end of the press section, when compared to the traditional water-laid technique (Kiiskinen et al. 2019; Lehmonen et al. 2019). Since a 1%-unit increase in web dryness, leads to around 4% less water to be removed and subsequently around 4% of required drying energy, this indicates that savings of around 10% could be achieved in the drying energy. According to the authors, this technology can be implemented on conventional paper machines without the replacement of any major component, merely some adjustments are required, in particular at the headbox.
With foam-forming different paper structures and properties can be achieved compared to traditional papermaking, such as uniform and lightweight webs from coarser fibres, thereby achieving material savings. Furthermore, it allows the use of other types of fibres in the process to manufacture novel products. The start-up company Paptic in Finland has recently taken foam-forming to an industrial scale by starting the production of a material having characteristics similar to plastic but made of wood fibres (Paptic 2021).

Even greater savings are expected in the thermal energy required for dewatering the web using ethanol or supercritical CO_2 (CEPI 2013). However, to the author's knowledge, no tests have been conducted in pilot installations yet. It remains uncertain whether overall energy savings would be actually achieved, in particular because of the difficult assessment of the additional electricity needed in those cases.

In conclusion, several alternative paper production processes are in development which may, in the long term, contribute to the decarbonisation of the branch. However, whether one of these processes will constitute a real competitor to the current papermaking process remains highly uncertain.

3 Paper drying fundamentals

The first part of this chapter deals with fundamental notions of paper drying and the following one is dedicated to the implementation of paper drying in the industry. The last section provides key information on diverse aspects of multi-cylinder paper drying which are relevant to the developed model presented in Chapter 5.

3.1 Thermal drying of paper

Drying is the removal of a liquid, usually water, from a solid, gas or liquid, by means of a carrier gas, or sometimes under vacuum (Keey 1992).
Thermal drying is one type of drying process, where the moisture is evaporated by transferring heat to the product via convection, conduction or radiation (Neikov et al. 2009). It is a complex process that involves simultaneous heat and mass transfer, accompanied by physicochemical transformations. The driving force for the mass transfer of water is the difference between the vapor pressure in the product and the partial pressure of water vapor in the carrier gas (Olson 2013). Thus, maintaining a low partial vapor pressure in the carrier gas through proper circulation is the second important process-controlling factor for thermal drying, apart from efficient heat transfer (Earle 1983).

The drying rate is determined by an ensemble of factors affected by heat and mass transfer. Its evolution throughout the drying process is typically represented as a drying curve, like the theoretical representation shown in Figure 3.1. For constant drying conditions over the whole drying process, three distinct drying phases take place: the warm-up, followed by a period of constant evaporation and finally a phase of falling evaporation rate.

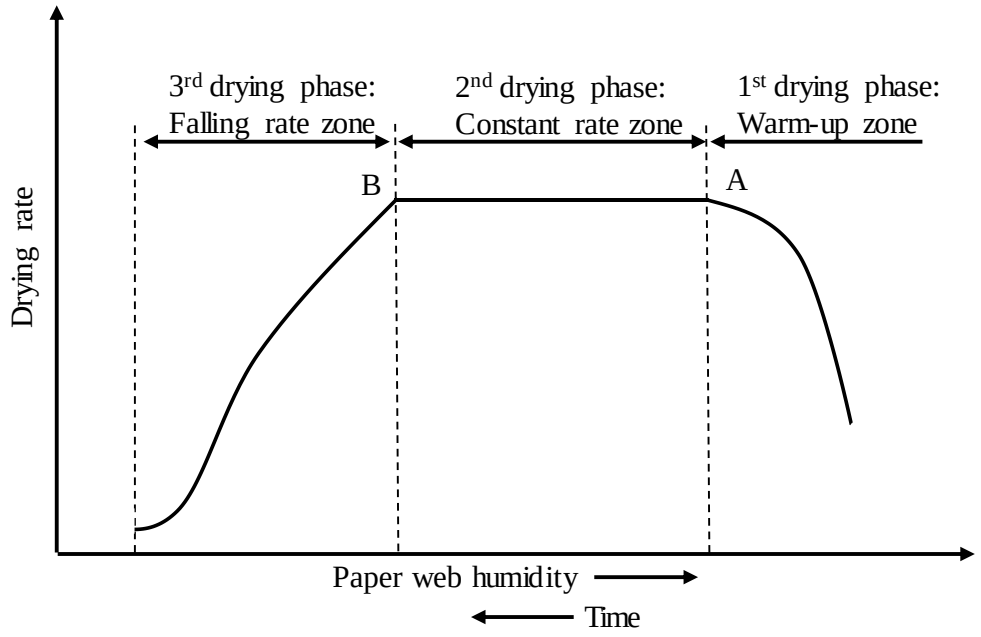

Figure 3.1: Typical Drying curve. Source: adapted from (Ghosh 2011)

Knowledge on the structure of wet paper is essential to understand those different drying stages in the case of paper drying. Paper fibres have a cylindrical shape with a hollow centre called lumen. The fibre walls are porous and made of intricate cellulose and hemicellulose fibrils arranged into layers called lamellas. Both the type of wood used and the pulping method have a large influence on the fibre porosity (Tysen 2018; Karlsson 2006).
In moist paper, water resides in inter-fibre pores, in the lumen, and within the fibre wall, divided into macro- and micro- intra-fibre pores. Those locations are illustrated in Figure 3.2. The water in inter-fibre pores, in the lumen and in the macropores is called free water. Bound water is located in the micropores in the cell walls and in hydrophilic groups (Maloney and Paulapuro 1999; Heikkilä and Paltakari 2010). These various water locations and interactions with the fibre lead to different transport mechanisms of the water within the paper web and play a major role in the drying kinetics of the different drying phases (Weise 1997).

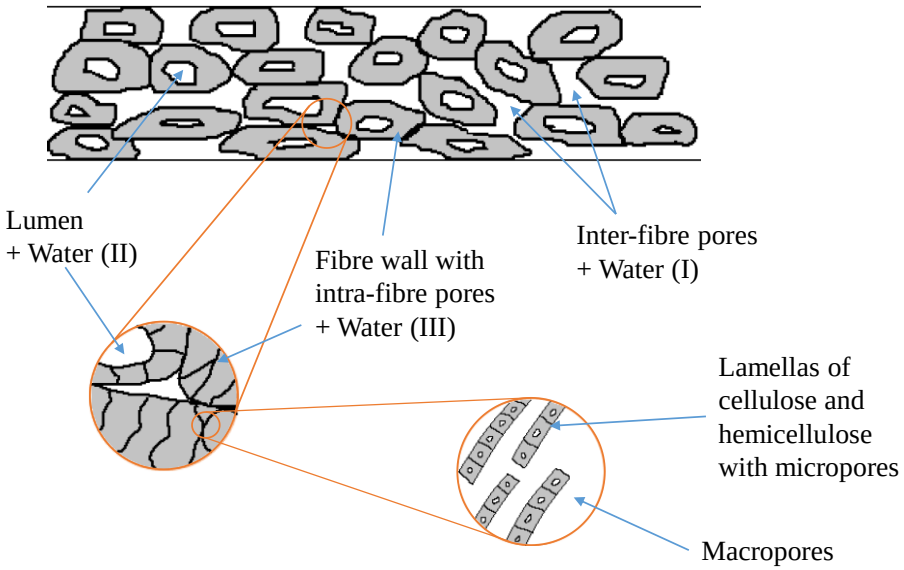

Figure 3.2: Different locations of water in a moist paper web. Source: adapted from (Baggerud and Stenström 2000)

During the first drying phase, the rate of water evaporation increases with the rise in the web temperature, until equilibrium is reached between heat transfer to the web and water evaporation, represented as point A in Figure 3.1.
There starts the second drying phase, in which evaporation further occurs at the web-air interface and continues as long as water is present as a continuous phase in the web (Schneeberger 2014). The water is transported from the web bulk to the surface as a liquid, due to a gradient of the capillary pressure. At this stage, the removed water termed as “unbound water” is located between the fibres or in large pores.
In the 3rd drying phase, all the remaining water is physically or chemically bound to the fibres, the waterfront recedes into the sheet, which causes the water located in micropores to evaporate within the sheet and to travel to the web surface via diffusion through the gas-filled pores of the web (Baggerud 2004). The slower gas diffusion process as compared to capillary flow, the increasing distance between waterfront and web surface, stronger water-to-fibre bonds, as well as the decreasing thermal conductivity of the sheet and higher contact resistance between the cylinder and the paper web all contribute to the falling drying rate in this last drying phase (Ghosh 2011). Since water is removed at very high energy costs in this last drying phase, special attention should be given to not overdry the paper.

It is important to note, that the three drying phases are part of a theoretical scheme and that in practice, the constant rate phase rarely exists, because the drying conditions vary over the drying process (Ghosh 2011).

3.2 Drying techniques in the paper industry

As seen in the previous section, energy needs to be supplied to the paper web in order to heat the water and the fibres, vaporize the water, and desorb the water bound to the fibres. Paper drying techniques that are commonly used in industrial systems are presented in section 3.2.1 and alternative technologies subject of past or ongoing research are described in section 3.2.2.

3.2.1 Industrial paper drying techniques

Industrial techniques for paper drying are based on different types of heat transfer processes, namely convection, radiation, and conduction.

Because of its cost-effectivity, contact drying using the latent heat of condensation of steam is the mechanism used in multi-cylinder drying which constitutes around 90% of the installed paper drying capacity (Slätteke 2006; Stenström 2020). Multi-cylinder drying is largely used for paper, board and coat drying as shown in Table 3.1. More information on this drying technique is provided in Section 3.3.

Both conductive and convective heat transfer modes are used in tissue production, where the paper is typically dried using one big steam-filled cylinder, the Yankee cylinder, around which hot air at a temperature in the range between 250 and 700°C is circulated. The use of this technology for tissue paper is due to the necessity of creping the paper web in order to obtain the required lower paper density and increased caliper.

Convective drying using hot air, called impingement, is also common in the production of coated papers where contactless drying technologies are needed. Sometimes convective drying is used for increasing the capacity of multi-cylinder paper machines.
To improve the bulk and absorbency of the product, the pressing step in tissue production is in a few cases (at around 10 mills in Europe, according to Stenström (2020)) replaced by an energy-intensive through-air drying unit, in which hot and relatively dry air is drawn through the web.

Finally, heat transfer through radiation using electric or gas-heated infrared (IR) drying is common for moisture profiling of the paper web and contactless drying of coated papers. In certain cases, it also used for capacity extension in dryers with limited space because of the high heat fluxes generated on a comparatively compact system (Stenström 2020; Lucidi 2020). However, the efficiency of IR units is rather low (between 25 and 55%) and electricity and gas remain expensive energy sources.

Table 3.1: Distribution of drying technologies used in the paper industry. Source: (Karlsson 2010)

Dryer	Industry share (%)	Grades	Distribution (%)
Multi-cylinder	85-90%	Tissue	5
		Paper	95
		Board	95
		Coating	35
Yankee	4-5	Tissue	84
		Paper	0
		Board	3
		Coating	0
Infrared	3-4	Tissue	0
		Paper	1
		Board	1
		Coating	15
Impingement	2-3	Tissue	0
		Paper	4
		Board	0
		Coating	50
Through-air	1-2	Tissue	11
		Paper	0
		Board	0
		Coating	0

3.2.2 Alternative paper drying technologies

The development of alternative paper drying technologies in order to increase drying rates (and thereby the production capacity) and energy efficiency has been the target of numerous research projects. The technologies reviewed in the present section are based on different heat transfer mechanisms, heat sources and energy carriers. While certain technologies are meant to replace entirely the cylinder drying system, others are conceived as an add-on to the conventional drying section.

In the Condebelt process, the paper web is compressed between two steel belts at pressures of up to 10 bars. The upper side of the paper web is put in direct contact with a steel belt heated by steam at 110 to 160°C whereas the lower side of the web is supported by a wire. Water escapes from the lower side of the web, travels through the wire, condenses on the second steel belt located below the wire, which is cooled with water at around 80°C, and is evacuated using pressure and suction. This technology was developed over 40 years ago and was applied twice at industrial scale, of which only one is still running, in Finland. Although the drying rates are increased and steam savings are estimated to around 15% compared to the traditional paper drying process, the fact that steel bands are moved at high speed leads to complicated and costly design, which may be the reason that the technology did not spread over the years (Stenström 2020).

Impulse drying combines mechanical and thermal drying by pressing the paper web under 2 to 10 MPa against a roll heated with electricity at temperatures between 250 and 450°C. Experiments suggest that the dry solid content of paper may reach 65% using this process which could lead to substantial steam savings in the drying section (Kong et al. 2016a). Although significant resources have been spent on the development of this technology, impulse drying

has not been implemented at industrial scale yet, because of issues in paper quality and the use of the expensive energy carrier electricity (Stenström 2020).

A further possibility to increase the heat flux to the paper web is to fire a fuel (e.g. natural gas) inside the drying cylinders to reach higher surface temperature. Drying rates increased by 2 to 4 times compared to steam-heated cylinders for drum temperatures up to 320°C have been reported (Stenström 2020; Chudnovsky 2004). Since the development of this technology in the 1980s, a few gas-fired dryers have been installed in the United States and Canada and they may be installed in new or existing systems, to increase the production capacity, or reduce the energy consumption. The payback period was estimated to be below 1 year by Chudnovsky (2004). The fact that this technology supposes individual units for gas combustion and flue gas circulation at each cylinder and an efficient heat recovery system for the exiting flue gases to not loose in efficiency constitute obstacles to its implementation in particular for retrofit cases (Stenström 2020).

In microwave drying, the energy is directly absorbed in the material containing water. This technology has been tested successfully for paper drying several times since the 1960s and no damage to paper quality was reported. High drying rates can be achieved, and interesting applications are to heat the web in the press or drying section, in particular for high basis weight paper grades since the energy absorption efficiency increases with greater water loads.
Although a feasibility study showed that paper machine speeds could be increased by 30% and the energy consumption reduced by 20% (Ahrens et al. 2003), microwave paper drying has not been implemented in industrial systems so far, because of the low energy efficiency of the microwave generator, the high electricity consumption and high capital costs (Kong et al. 2016a).

The combination of convective drying using hot air impingement and multi-cylinder drying allows to have more compact systems and a higher drying rate, a good flexibility in terms of speed variations which is beneficial for fast grade changes, and, in the case of single-tier configurations, more uniform moisture profiles throughout the web thickness. (Stenström 2020). Such concept is implemented in the OptiDry Vertical proposed by the company Valmet which is an impingement dryer with gas burners that is installed under the existing drying section and has been installed in numerous paper machines in order to increase production capacity (Valmet 2015b). No significant reduction of the specific energy consumption has been reported compared to an extension of the drying section (Valmet 2010; Williamson 2015; Mende 2009).
Similarly, the Pulp and Paper Research Institute of Canada developed and successfully tested the so-called Papridryer on a pilot machine where large cylinders similar to the Yankee cylinders used in tissue drying are enclosed in an impingement hood. Ten times higher drying rates were reported than in conventional dryers (Poirier et al. 2004; Pikulik 2006). The three Papridryers that were installed in industrial paper machines were removed after rebuilds due to high fuel costs and efficiency issues (in a specific case of heavy weight coated paper). This technology has good potential for new paper machines or capacity improvements (Stenström 2020; Poirier et al. 2004; Crotogino 2001).

As an alternative for hot air, impingement with superheated steam has also been investigated (McCall and Douglas 2006). However, avoiding that the paper web entrains too much air when entering the hood filled with steam is a clear challenge (Stenström 2020).

In summary, several alternatives to the conventional paper drying techniques based on different heat transfer techniques have been developed in the last sixty years which failed to conquer the market so far due to a variety of reasons of technical and economic order.
The initial motivation for the development of several of these technologies was to increase the drying rate as compared to the double-tier cylinder configuration installed in the drying sections in the 1960's for which the production capacity could not be increased due to speed limits. The successful development of single-tier dryers (see section 3.3.1) in the 1980's which allowed smaller incremental changes at the paper machines was a disincentive for the implementation of successfully developed alternatives like the Papridryer and the impulse dryer (Crotogino 2001). In general, because it is highly capital-intensive, the paper industry is risk-averse and many small incremental developments are thus preferred above bold changes (Crotogino 2001). Whether one of the alternative technologies would lead to significant energy-savings at the drying section of paper machines remains unclear.

3.3 Multi-cylinder paper drying

In the drying section of a multi-cylinder paper machine, the paper web is conducted at speeds up to 2000 m/min through 20 to 170 iron or steel drying cylinders with a typical diameter of 2 meters filled with slightly over-saturated steam (Stenström 2020; Suhr et al. 2015).
For grades of paper and board that will be coated or printed, the drying section consists of a pre- and a post-drying section. After entering the drying section, the paper web is dried a first time, until it reaches the moisture content of the final product. Then it goes through a size or a film press, where a starch solution is applied to increase its surface strength. To remove the high humidity of the starch solution, the paper is dried a second time, in the post-drying section. If the paper web is subsequently coated, it goes through a third final drying step, based on cylinder, infrared, impingement, or a combination of those drying techniques.

3.3.1 Cylinder layout

Traditionally, the drying cylinders are placed in two rows in a so-called double-tier configuration, where the paper web is conveyed through the drying section and maintained in close contact with the dryers using two distinct dryer fabrics for the upper and lower cylinder rows (see left chart in Figure 3.3). The sections between the rows are called free draws, and the paper web is unsupported in those zones. Those free draw areas are the cause of a bottleneck for the capacity increase of the paper machine since the risk of paper breaks in the earlier part of the paper machine is high. To address this issue, the single-felted configuration was developed, in which a single fabric wraps both the top and bottom cylinder rows. However, in that configuration the dryer fabric is sandwiched between the cylinder and the paper web in one of the dryer rows, which reduces the heat transfer from the cylinders to the paper web (TAPPI 1992). For this reason, single-felt sections nowadays run as single-tier configuration where the cylinders in the bottom row are either empty or vacuum rolls of a smaller diameter than the dryers, in order to counteract the effect of centrifugal force and to increase the wrapping angle of the dryer row (Ghosh 2011; Holik 2013).

Although the drying section of many production sites has been modified to have at least the first cylinder groups, where the paper web is most fragile, operated as single-run, the double-tier configuration remains the most common cylinder configuration.

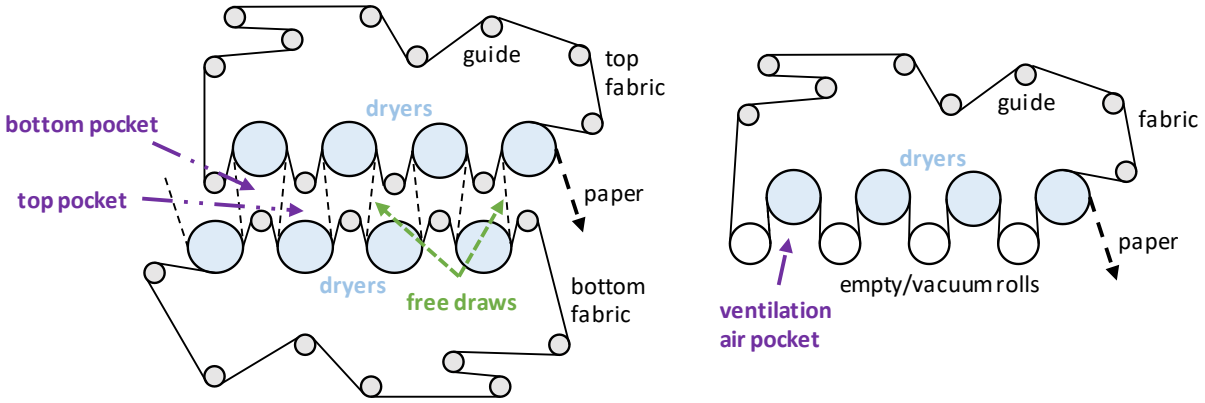

Figure 3.3: Double-tier (left) and single-tier (right) drying section configurations. Source: adapted from (Ghosh 2011)

The drying cylinders are arranged in groups, where all dryers of a group have a common steam-supply header. The steam groups at the beginning of a drying section are operated at low pressure, from slightly below atmospheric pressure up to 5 bar, for a smooth heating of the paper web, whereas the cylinders in the steam groups at the end of the drying section are supplied with steam at pressures between 3 and 10 bar, to remove the bound water from the paper (Karlsson and Oyj 2000). Higher steam pressures in drying cylinders are not common due to the need of more expensive materials and higher security requirements (Berlin 2020). The rotation speed of the cylinders is the same within each group and adjusted between the groups to control the contraction of the paper web occurring during drying throughout the drying section (Li 2001).

3.3.2 Condensate behaviour and removal

The condensate in the drying cylinder has a different behaviour, depending on the dryer speed, the steam pressure, the dryer diameter and the volume of condensate in the dryer (TAPPI 1983). At slow speeds, a puddle of condensate forms at the bottom of the dryer, which moves in the direction of dryer rotation and widens with increasing speed. At higher speed, the puddle extends over the horizontal centreline and cascades, as gravity forces overcome centrifugal forces. Beyond a certain speed (around 300-400 m/min for a dryer of 1.5 m diameter according to (TAPPI 1992)), centrifugal forces overcome gravity and the condensate forms a layer of uniform thickness called rim along the dryer wall. Those three behaviours are illustrated in Figure 3.4.

Figure 3.4: Different condensate behaviours in drying cylinders. Source: adapted from (Olson 2013)

The behaviour of the condensate that forms in the dryers highly affects the overall heat transfer from the steam to the paper web. Although the very turbulent conditions in the cylinder in the cascading stage lead to the best heat transfer, most modern paper machines are operated at speeds well above rimming (Valmet 2012).

Since the thickness of the condensate rim highly impacts the heat transfer, the good functioning of the condensate removal system is of central importance. Condensate is collected from the cylinder wall and channelled out using a siphon, which works with a pressure differential between the dryer steam supply and condensate return headers.
The two main types of siphons used in drying cylinders of paper machines are represented in Figure 3.5.

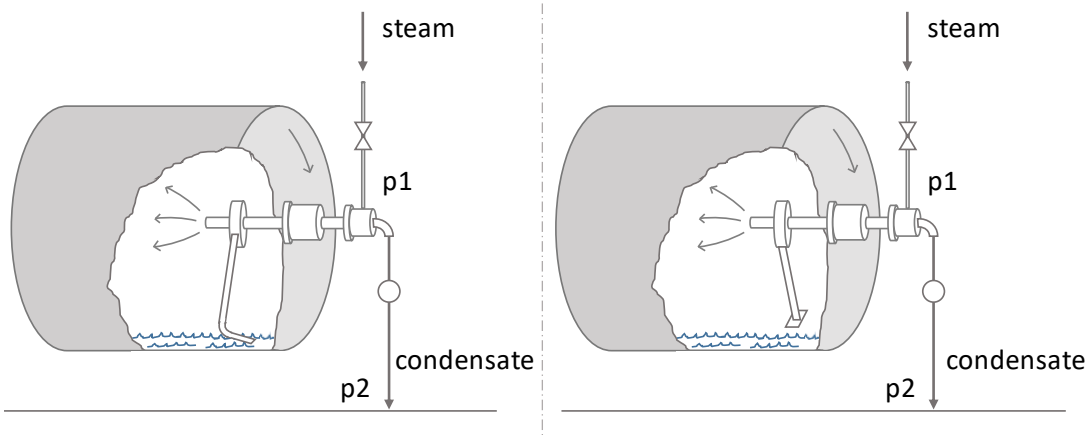

Figure 3.5: Schematic of a stationary siphon (left) and a rotating siphon (right) in a drying cylinder of a paper machine. Source: adapted from (Othen 2014)

Stationary siphons are fixed to a point outside the cylinder and consequently do not rotate with the cylinder. The required differential pressure ($p_1 - p_2$) of such siphons has to be sufficient to overcome frictional resistance and to lift the condensate against the gravity to the centre of the dryer (TAPPI 1983).
Rotating siphons are attached to the inside surface of the dryer shell and require higher differential pressures than stationary siphons at high speeds since they must overcome frictional resistance and lift the condensate against the centrifugal force to the centre of the dryer (TAPPI 1983).
To ensure the continuous removal of condensate, operating differential pressures are kept above the minimum required. This causes a share of the inlet steam, called “blow-through” steam to exit the dryer without condensing. The ratio of blow-through steam to condensing load typically represents 10-15% for stationary and 15-25% for rotating siphons (TAPPI 1983; Ghosh 2011).

The installation of spoiler bars at regular intervals along the cylinder wall in machines operated at speeds above rimming speed, leads to increased turbulent conditions in the condensate rim. Increases by up to 50% of the overall heat transfer coefficient were reported for machine speeds of 1400 m/min (Polat and Mujumdar 2006; Ghosh 2011).

3.3.3 The steam cascade

After leaving the drying cylinders, the mixture of condensate and blow-through steam of each steam group is conducted to a steam-condensate separator as shown in Figure 3.6. Since the pressure in the separators is lower than the pressure of the inlet mixture, a share of the condensate flashes. The condensate stream is often used for heat recovery before being conducted to the boiler house, whereas the steam from the separator is reused in the process.
In most cases the flashed steam from higher steam groups is supplied to lower steam groups in a so-called steam cascade. This configuration is particularly beneficial for dryers equipped with stationary siphons since the pressure differential is rather low (in the range 0.1-0.2 bars) in such cases. The use of thermocompressors to boost the flashed steam using high pressure steam and thereafter feeding it back to the same steam group is a common technique for the Yankee cylinder in tissue production and for certain multi-cylinder paper machines equipped with rotary siphons.

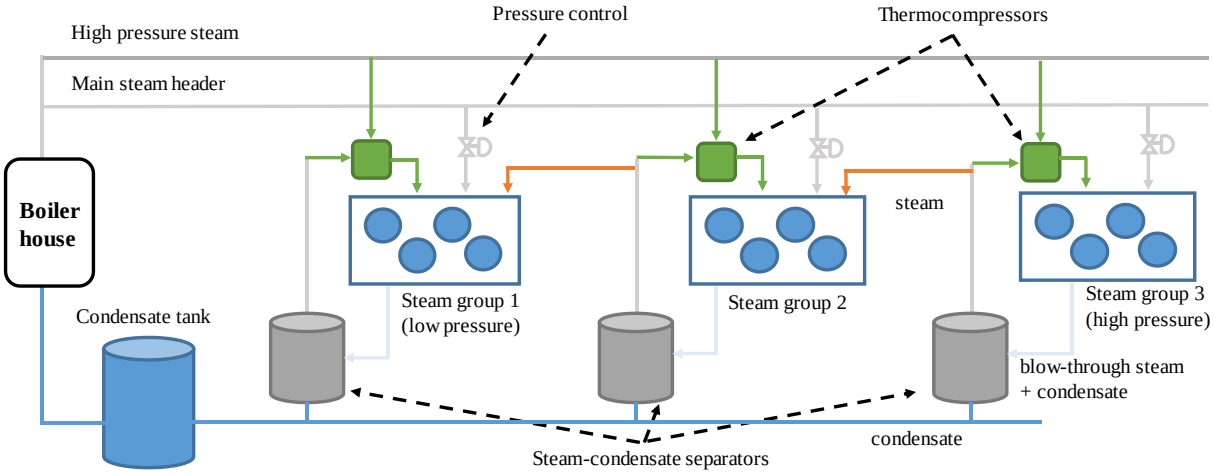

Figure 3.6: Schematic of steam system configurations at the drying section of a paper machine. The steam cascade is represented in orange colour and the configuration based on thermocompressors in green. Source: adapted from (Körting 2010)

3.3.4 Heat and mass transfer resistance

Although the condensate layer often constitutes the major resistance to heat transfer in dryers with rimming condensate (TAPPI 1992), other aspects need to be considered when trying to improve the heat transfer efficiency between the steam and the paper sheet.
As illustrated in Figure 3.7, the cylinder shell (usually made of iron cast), the space between the dryer shell and the paper web, and the paper web itself do also constitute barriers to heat transfer. The tension applied on the paper web through the dryer fabric minimizes the air layer between the dryer and the sheet and thus increases heat transfer (TAPPI 1992).

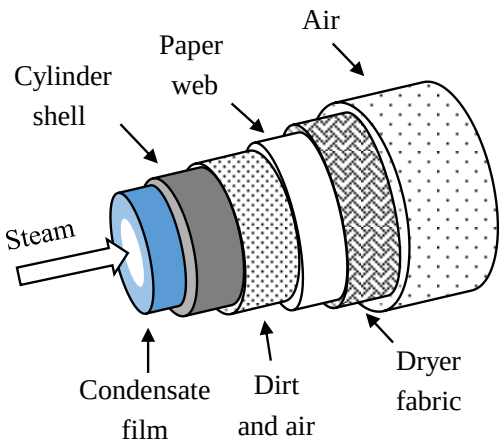

Figure 3.7: Cut-away drawing of a dryer cylinder showing layers exerting heat and mass transfer resistance. Source: adapted from (Ghosh 2011; Mujumdar 2006)

Convective heat transfer between the sheet and the air plays only a minor role in multi-cylinder drying because of rather low air speeds and temperature differences (Lang 2009). Experimental work conducted by Wilhelmsson and Stenström (1995a) showed that the fabric, when it is placed between the sheet and the air has a negligible influence on the heat transfer between the web and the air. This is the case at all dryers in the double-tier configuration and in the free draw areas and the upper cylinders in the single-tier configuration, as shown in Figure 3.8. Furthermore, the same authors, showed that the fabric acts as a barrier to the migration of water vapor to the surroundings and reduces mass transfer by 30% to 50% (Wilhelmsson et al. 1996).

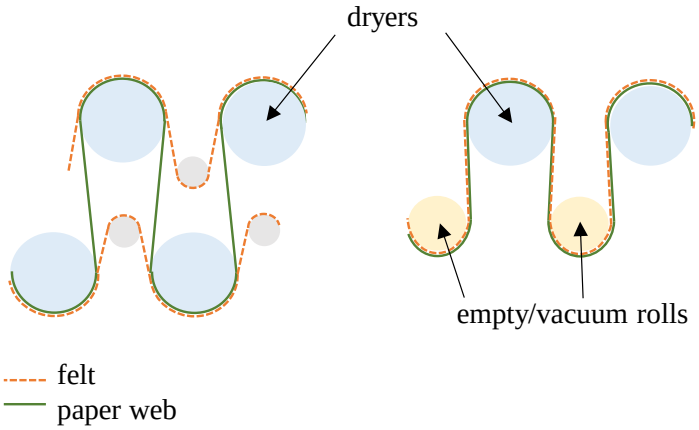

Figure 3.8: Location of the fabric in double- and single-tier (right) drying section configurations. Source: own representation.

3.3.5 Heat and mass transfer in paper drying

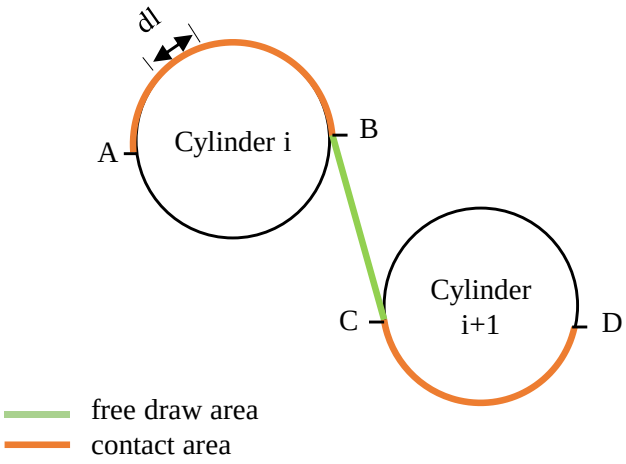

Figure 3.9: Schematic representation of the paper web in the contact and free draw areas. Source: own representation.

In multi-cylinder paper machines, the drying process takes place through the combination of web heating, in the zones where the paper web is in contact with a drying cylinder, and mass transfer of the water in the web to the surrounding air, mainly in the areas between the cylinders (called free draw areas) and at vacuum rolls in single-tier configurations. A schematic representation of the paper web in the contact and free draw areas is provided in Figure 3.9.

These physical processes can be mathematically expressed as an ordinary differential equation (ODE) system of the variation of paper web humidity x_p and temperature T_p along an infinitesimal length element dl in the paper machine direction.
In the literature, the expression for the variation of the humidity along dl is expressed either using the Fick's law (Ghosh 2011; Yin et al. 2016) or the Stefan's law (Wilhelmsson et al. 1996; Roonprasang 2008; Kong and Liu 2012).
In the first case, the vapor mass flow at the web-air interface is caused purely through diffusion of vapor in air, which is considered a realistic assumption for low vapor concentrations.
On the other hand, the Stefan's law considers air diffusion that occurs in the opposite direction of the vapor mass flow (towards the web-air interface) as a result of the concentration gradient of vapor in air. As the web-air (liquid/vapor) interface is impermeable to air molecules, an upward bulk flow, called Stefan flow, maintains the vapor pressure at the interface. These mass transfer processes are illustrated in Figure 3.10.

Considering the high amounts of evaporated water in the paper drying process, the approach using the Stefan's law is preferred for this work. According to the Stefan's law, and assuming that water evaporation occurs only at the paper web surface, the evaporation rate of water of the paper web $\dot{q}_{evap}$ is expressed as follows (Persson 1998; Slätteke 2006)[4]:

$$\dot{q}_{evap} = \frac{K M_w p_{tot}}{R T_p} \cdot ln\left(\frac{p_{tot} - p_{aw}}{p_{tot} - p_{pw}}\right) \qquad \text{(SI Units)} \qquad (1)$$

[4] The detailed derivation of equation (1) is presented in Appendix A.

where p_{aw} and p_{pw} correspond to the partial pressure of vapor in air and at the paper web surface respectively, K represents the convective mass transfer coefficient of vapor between the paper web and the surrounding air, T_p the temperature of the paper web, M_w the molecular weight of water, R the ideal gas constant, and p_{tot} the atmospheric pressure.

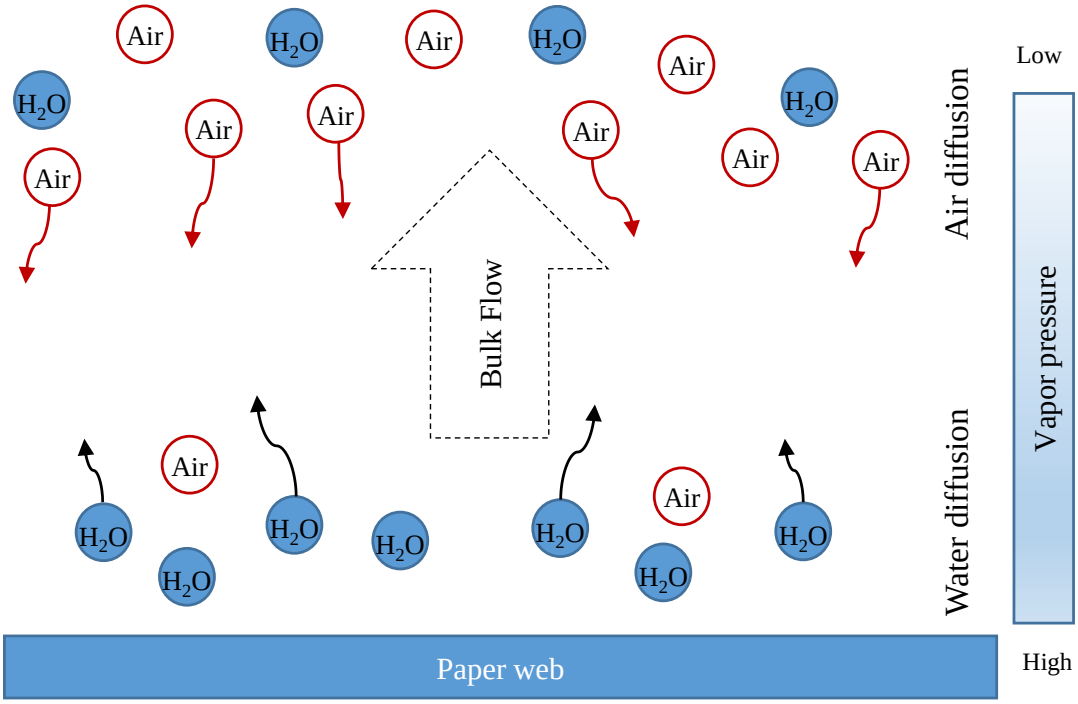

Figure 3.10: Schematic of the evaporation induced Stefan flow at the paper web-air interface. Source: adapted from (Zhang et al. 2020)

At the contact areas, mass transfer occurs only on one side of the paper web, and thus the evaporation rate can be written as:

$$\dot{q}_{evap} = \frac{dm_p}{dA \cdot dt} \tag{2}$$

where dA is an infinitesimal area of the paper web of length dl and width w, and dm_p the variation in mass of paper web along the infinitesimal element dl.
At free draw areas, water evaporation takes place on both sides of the web. Assuming that the temperature and humidity is same on both sides of the paper web, the evaporation rate can be expressed as:

$$\dot{q}_{evap} = \frac{dm_p}{2dA \cdot dt} \tag{3}$$

Additionally, the variation in mass of paper web dm_p is related to the difference in web humidity dx_p along dl:

$$dm_p = -dA \cdot G_{dry} \cdot dx_p \tag{4}$$

where G_{dry} is the dry basis weight of paper in $kg_{dry\ solid}/m^2$.

The variation of the temperature of the paper web along an infinitesimal element of paper web is determined using an energy balance. At the drying cylinders, the energy balance includes condensation heat of the steam transferred via conduction, the energy exchanged with the surrounding air via convection, and the energy of phase change of the water evaporated from the web:

$$-G_{dry}v\left(c_f + c_w x_p\right)\frac{dT_p}{dl} + U_{sp}\left(T_s - T_p\right) + h_{pa}\left(T_a - T_p\right) + G_{dry}v\Delta H_{evap}\frac{dx_p}{dl} = 0 \qquad (5)$$

where T_s is the temperature of steam, v the speed of the paper machine, U_{sp} the heat transfer coefficient between the steam and the paper web, h_{pa} the convective heat transfer coefficient between the paper web and the air, c_f the specific heat of the fiber, c_w the specific heat of water and ΔH_{evap} the enthalpy of water evaporation.

In the free draw areas and the empty/vacuum rolls in single-tier, only the two latter types of heat transfer (convective and latent) occur.

3.3.6 Humid air and drying section hood

The driving force of mass transfer in multi-cylinder paper drying is the difference in the partial pressure of water vapor at the web surface and the surrounding air.
Assuming an ideal air-water vapor mixture, the partial pressure of water vapor in air p_{aw} is related to the absolute humidity of air x_a by the following relationship (Heo et al. 2011; Slätteke 2006)[5]:

$$p_{aw} = \frac{x_a}{x_a + 0.62}p_{tot} \qquad (6)$$

The dew point temperature of air is the temperature below which air is saturated with water vapor and condensation occurs. The relationship between the dew point temperature and the corresponding vapor pressure at saturation is given by the Antoine's equation (Nilsson 2004b; Yin et al. 2016):

$$p_{sat}(T) = 0.133322 \cdot \exp\left(18.3036 - \frac{3816.44}{T + 227.03}\right) \qquad (7)$$

The enthalpy of humid air H_a may be approximated to the sum of the sensible heat of dry air and water vapor, and the latent heat of water vapor (Yin et al. 2016; Pflugradt et al. 2009) :

$$H_a = (c_{pa} + x_a\, c_{pv})T_a + x_a L_{vap0} \qquad (8)$$

Where L_{vap0} is the vaporization enthalpy of water at 0 °C at atmospheric pressure in kJ/kg$_{water}$ and H_a the enthalpy of humid air in kJ/kg$_{dry\ air}$.

The drying section in paper machines is usually enclosed by a hood through which air is blown at a temperature of at least 90-100°C in order to remove the evaporated water in the vicinity of

[5] The detailed derivation of equation (6) is presented in Appendix A.

the sheet and to control the temperature, humidity and air flow around the sheet (Slawtschew 2020). A dew point temperature above which no condensation occurs in the hood is usually guaranteed by hood manufacturers (Laurijssen et al. 2010). This is an important parameter since condensation in the hood can lead to paper quality issues and inefficient drying (TAPPI 1979). Despite higher requirements in terms of hood inlet air temperature, a high operation dew point is a desired characteristic of drying section hoods since in that case the drying air can take up more water (as per equations (6) and (7)) which allows the dimensioning of the hood air circulation system at reduced air flow, and thus leads to lower investment costs and lower operating costs for ventilation. Furthermore, exhaust air flows at higher temperature lead to higher heat recovery potentials.

Different types of drying section hoods are represented in Figure 3.11 and their main characteristics are provided in Table 3.2. Open-canopy hoods typically have a roof with four walls extending from the roof down to around 2.5 meter above the operating flour, whereas closed hoods present movable and sheet opening doors to better isolate the drying section from the machine room and often enclose the basement level for a controlled drying environment (TAPPI 1979).

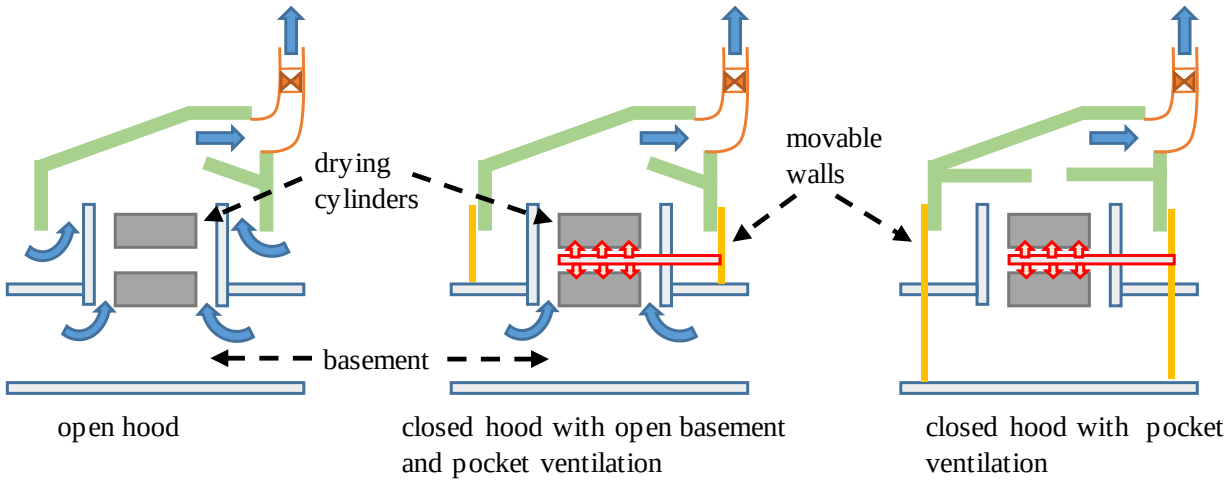

Figure 3.11: Types of hoods in the drying section of multi-cylinder paper machines. Source: adapted from (TAPPI 1979)

Table 3.2: Dew point temperature and exhaust air humidity and temperature for different types of drying section hoods. Source: based on (Karlsson 2010)

	High-performance closed hood	**Medium-humidity closed hood**	**Open-canopy hood**
Typical exhaust air humidity, kg_{water}/kg_{dryair}	0.168 - 0.180	0.120 - 0.140	0.050 - 0.100
Dew point, °C	60.8 - 62.8	55.7 - 58.5	40.3 - 52.5
Typical exhaust air temperature, °C	80 - 90	75 - 85	50 - 70
Typical leakage air ratio, % of exhaust air mass flow	10 - 30	20 - 40	50 - 70

A Mollier chart (as the one in Figure 3.12) provides a convenient way to visualize the different states of humid hood air during the paper drying process, as well as the effect of the dew point temperature on the heat recovery potential. The horizontal axis represents the absolute humidity and the vertical axis the dry bulb temperature. Curves of constant relative humidity are plotted, and the curve of 100% relative humidity (marked in red in Figure 3.12) is the saturation curve for which the dry bulb temperature corresponds to the dew point temperature, and the absolute humidity to the maximum humidity which air can take up before condensation occurs. A transformation at constant specific enthalpy of air happens along the oblique isenthalpic curves.

The evolution of the hood air temperature and humidity for an open-canopy and a closed drying section hood is represented in Figure 3.12. The hood air comprises the hood supply air which is heated before entering the hood and the leakage air from the machine room (see "leakage air ratio" in Table 3.2). Since the drying process in multi-cylinder paper occurs because of conductive heat transfer (and not of convective heat transferred from the hood inlet air), the evolution of the humid air during the drying process (indicated with number 2) is non-isenthalpic. At the end of the drying phase the hood air humidity is equal to the maximum humidity tolerated for the hood, which in the case of the closed hood with dew point 63°C is equal to 0.177 $kg_{water}/kg_{dry\ air}$, more than double the amount tolerated for an open hood with dew point 50°C (0.0863 $kg_{water}/kg_{dry\ air}$).
At the end of the drying phase a part of the energy from hood exhaust air is recovered to preheat the hood supply air. As a consequence, the hood exhaust air is cooled down, first without any condensation occurring (phase number 3) and then, once the dew point temperature is reached, along the saturation curve (phase number 4).
Since the temperature of the hood exhaust air is higher in the case of the closed hood (67.5°C vs. 60.4°C for the considered case), the supply air can be preheated to higher temperatures during heat recovery, which leads to a lower steam demand for air conditioning.
Furthermore, the temperature of the hood exhaust air after heat recovery is at a higher temperature which increases the waste heat recovery potential.

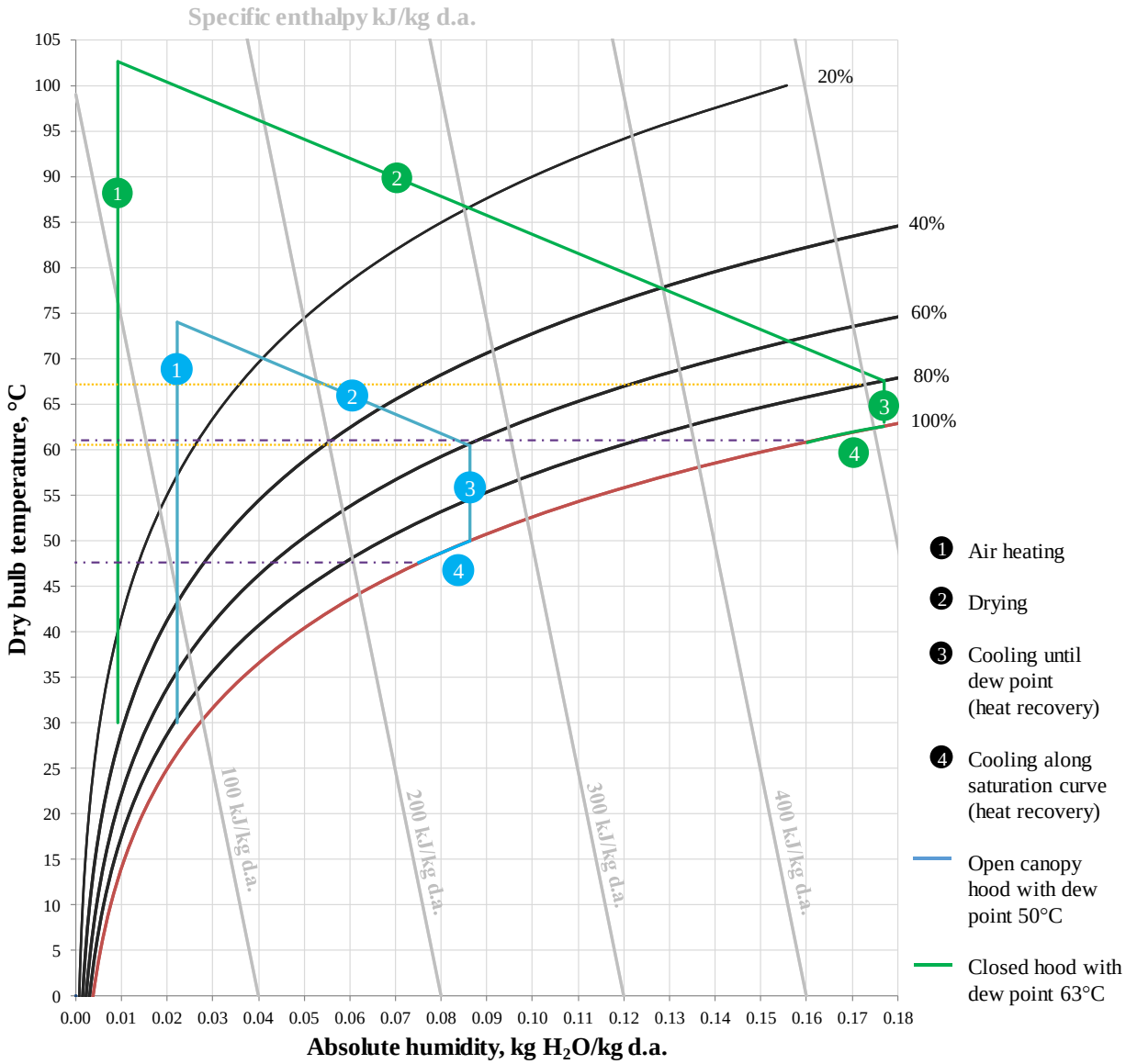

Figure 3.12: Mollier chart featuring the states of hood air during paper drying in an open-canopy and a closed drying section hood. Source for Mollier chart: formulas presented in (Gatley 1997)

4 State of the Art

In this chapter, an overview of existing models of multi-cylinder dryers is presented, followed by the description of previous works on the effect of retrofit measures in multi-cylinder paper drying. The shortcomings of those studies and the underlying models are analysed in regard to the goals of the present work.
Then, process integration and more specifically the use of this ensemble of techniques for retrofit design and CO_2-emission mitigation in the industry is briefly discussed.
The next section deals with the use of energy-efficiency and CO_2-emission abatement cost curves as a decision-making tool for individual industrial sites, and in which extent measure's interactions have been accounted for in past studies.
Finally, key directions for the present work are derived based on the literature review in the last section of this chapter.

4.1.1 Models of multi-cylinder drying sections

Because of the importance of the drying step on the product quality and the overall energy consumption of the papermaking process, numerous models of the multi-cylinder drying section are available in the literature.
First modelling attempts date back to the middle 1950's with the works of Nissan and Knye (1955). Their definition of the four phases of conventional cylinder drying remains a keystone of many current models.
In a detailed model review, Wilhelmsson et al. (1993) observed that the models of the drying section initially focused on improving the energy use and the design of dryers, instead of the paper quality. Since then, models have been extended to include temperature and humidity gradients in the width and thickness of the paper web.
Whether developed to understand phenomenon occurring within the paper web and calculate paper properties at different locations in the paper machine, or to analyse aspects related to energy consumption, most models are based on a detailed description of heat and mass transfer processes between the paper web and the cylinders on one side, and the paper web and the air on the other side.
However, the level of detail differs since models focussing on paper quality (e.g. (Karlsson and Stenström 2005) and (Gaillemard 2006)) often choose a dynamic analysis of the processes within the paper web and include temperature and humidity gradients in the width and thickness of the paper web (three dimensional), whereas the studies focussing on improving the energy efficiency of the drying process (e.g. (Kong and Liu 2012) and (Schneeberger 2014)) favour a static approach and consider gradients within the paper web only along the paper machine direction (one dimensional).
In any case, the choice of heat and mass transfer coefficients have a significant impact on the model results and thus their determination is at the centre of several works (e.g. (Akesson and Ekvall 2006), (Slätteke 2006)). Since the determination of the exact values of these parameters often remains a challenge, it is common practice to use certain heat or mass transfer parameters as fitting parameters when applying the developed model to a real production site (e.g. (Ahrens and Rudman 2003), (Slätteke 2006)).
The effect of the felt used to support the paper web throughout the machine on drying performance was first analysed in the late 50's and is highlighted in (Wilhelmsson and Stenström 1995a) and (Lang 2004). Wilhelmsson and Stenström (1995b) showed that the effect

of the fabric on mass transfer can be summarized in a so-called Fabric Reduction Factor applied on the mass transfer coefficient between the paper web and the air. In addition, the same study showed that the effect of the felt on the heat transfer can be considered negligible.
For models to be adaptable to different paper types (i.e. different basis weights), they must account for the effect of paper thickness on the heat and mass transfer. Wilhelmsson and Stenström (1995b) showed that the use of a lumped parameter accounting for both conduction and evaporation/condensation phenomena within the web gives good results, even for thicker paper grades like board. This approach allows to reduce computing times considerably compared to more detailed approaches.

4.1.2 Previous analysis of CO_2-mitigation measures in multi-cylinder paper drying

A common method to identify energy savings potentials in an industrial process is the energy audit. It allows to make a diagnosis of a process and results in a list of improvement suggestions concerning the operation of the process, but also possible retrofit measures. Good examples of such analysis at paper mills are provided in Li et al. (2012), Chen et al. (2016a) and Kong et al. (2013). Different evaluation methods are used to quantify the effect of the identified energy-saving and CO_2-mitigation measures, as for example the use of estimations derived by experience, benchmark tools and simulation models. Since the first two mentioned methods often lack accuracy and present clear limitations in the case of the assessment of measure's interactions, the overview provided in this section focuses on studies using thermodynamic analysis and simulation tools.

Using thermodynamic analysis and graphical tools Laurijssen et al. (2010) assessed the energy-saving potential of three central energy-efficiency measures at a paper mill, the implementation of which, according to the authors, shall allow to save around 15% of the total primary energy use: applying additives in higher consistencies, increasing the dew point temperature of the drying section hood, and using exhaust air to not only pre-heat the incoming air but also to increase process water temperatures and thereby improving dehydration on the wire. The drawback of this simple calculation method is the use of simplifications for example considering that the cylinder steam is used only for water evaporation, which leads to rather high inaccuracies in the results.

The analysis of the effect of operational and structural changes to be made in processes is one of many applications fields of model-based simulation tools (Chen et al. 2016b). A critical review of some recent works dedicated to the assessment of operational and structural changes using simulations is presented in the following paragraphs.

Ghodbanan et al. (2017) developed a nonlinear programming optimization framework based on a drying section model described in Ghodbanan et al. (2015). In this optimization framework the equality constraints correspond to mass and energy balance relationships on functional blocks of the paper drying process and inequality constraints correspond to process parameters such as production capacity or operating conditions. The objective is to minimize the steam consumption in the whole drying section. The optimization framework was applied to the drying section of a multi-cylinder fluting paper machine plant in Iran, the equivalent cost savings were calculated, and the additional electricity costs due to the ventilation of higher mass flows were assessed.

Chen et al. (2016b) proposed a method based on site-specific benchmarks to identify saving potentials and a simplified drying section model to analyse the impact of changes in process parameters. Later on, Chen et al. (2019) developed a physical model for paper drying in single-tier paper machines including the heat recovery and steam cascade. The application of the model to a mill in China resulted in suggestions regarding the amounts of steam to be supplied to the cylinders and the workload of the ventilation equipment, those measures were implemented, and the steam savings measured. The authors do not mention whether the measured savings match the model predictions. The cost and CO_2-mitigation impact of the process improvements are not mentioned in this work.

Li et al. (2011) calculated the minimum steam consumption required per unit evaporated water and the related economic impact after optimizing process parameters in two different paper machines. Paper drying is modelled as a black box where the relationship between steam consumption and evaporated water is obtained via fitting. The value for the hood supply air temperature is higher than the minimum specified and the obtained values for hood air humidity are rather low compared to usual values.

Yin et al. (2016) assessed the energy savings of the replacement of a semi-closed with a closed hood in the multi-cylinder drying section of a paper machine located in China with a model based on the physical description of the drying process. The model includes the heat recovery system in order to evaluate the steam required for air pre-heating but does not cover the steam cascade and therefore the overall steam demand of the system is not calculated.

Schneeberger (2014) used a simulation tool integrated within the interface of a process control system to perform cost optimization in the drying section of four paper machines in Austria.
The analysis covered the effect of operational changes, like a lower hood air inlet temperature or the impact of a reduction of leakage air in the hood, and structural changes like replacing certain ineffective infrared dryers or integrating thermo-compressors between the steam network and the steam cascade. The cumulative effect of the implementation of several measures is not quantified in this work.

Kong and Liu (2012) built a model covering the drying section, the heat recovery system and the steam cascade of a paper machine. Paper drying is modelled as a black box and the impact of lower hood air temperature and increased exhaust air humidity on the specific heat consumption is described. Later on, Kong et al. (2016b) used the same model to assess the individual effect of changes in parameters like inlet paper temperature and exhaust air humidity on the drying efficiency of a drying section.

Lindell and Stenström (2006) developed a modular process modelling tool which they then used to perform a thermodynamic and economic comparison between a multi-cylinder dryer and a combined multi-cylinder/air impingement dryer coupled with a heat pump to supply heat to a district heating network from the humid exhaust air streams.
Kong et al. (2011) proposed a new waste heat integration scheme for a paper machine after establishing energy and exergy balances on the drying section and for that given plant.

Treppe et al. (2012) analysed waste heat recovery options including heat pump integration at four different paper mills. Whereas the exhaust air from the drying hood after direct heat

recovery is the only heat source considered for the heat pump, the three following heat sinks were considered: process water, steam for the drying cylinders and hood supply air. As a result, the use of a heat pump for heating process water was not recommended due to a limited seasonal demand. Also, a low coefficient of performance of 1.9 due to a large temperature lift was assessed for the heat pump used to generate steam so that the authors came to the same conclusion. A more beneficial picture was drawn in the case of heat pump integration to heat supply air since important steam savings at a reasonable cost were calculated in that case.

Sivill et al. (2005) looked at the effect of operational changes on the heat recovery systems in paper machines using thermodynamic models and thereby demonstrated the need of site-specific solutions and continuous operational optimization to maintain good system performances. Later, Sivill and Ahtila (2009) used the same simulation models to assess the effect of retrofit measures in the existing heat recovery systems on steam consumption.

Manninen et al. (2002) analysed the impact of retrofitting multi-cylinder drying sections with impingement and impulse drying technologies on the efficiency of the local energy system, in that case a combined heat and power (CHP) system. The authors showed that since the efficiency of CHP systems is highly dependent on the fuel to power ratio, radical changes in the process require a redesign of the local energy system, for example by replacing the conventional steam boiler with back pressure turbine with diesel or gas turbines systems (with HRSG units) in order to have an optimal operation.

Following conclusions are drawn from the surveyed literature.

- Previous model-based studies in which both heat demand reduction and improvements of the heat recovery system are investigated, are based on simplified (black box) models of the drying section which limit their applicability for the analysis of a wide scope of options.
- The cumulative effect of several structural changes, in other words, the interaction between several measures, has been very rarely accounted for in previous works, where the effect of structural measures was assessed only for individual measures.
- Most energy models of the drying section include the heat recovery system but only very few include the steam cascade. In order to correctly assess energy-savings and related CO_2-emission reductions at the process level, it is important to include the steam cascade since one ton of steam saved at the dryers is not equivalent to one ton of steam saved in the process.
- Although several studies deal with the improvement of heat recovery networks in paper mills, only little attention has been given to the integration of heat pumps to increase the recovery of waste heat. Since measures reducing the heat demand of the drying section impact the heat recovery and waste heat recovery potentials, wide-scope models are needed for the integrated assessment of measures.

A summary of the reviewed literature is presented in Table 4.1.

Table 4.1: Scope of the developed and reviewed models for the assessment of energy-efficiency and CO_2-emission reduction measures in multi-cylinder paper drying

	Model				**Measures**							**Results**	
	Drying section detail[6]				Object of measure(s)			Type					
	black box	grey box	Steam cascade	Boiler	Heat demand	Heat recovery	Heat supply	Operation	Retrofit	More than 1?	Inter-actions	CO_2 savings	Cost savings
Godin (2022)		x	x	x	x	x	x	x	x	x	x	x	x
Yin et al. (2016)		x			x				x				
Schneeberger (2014)		x	x		x	x	x	x	x	x			x
Ghodbanan et al. (2015) Ghodbanan et al. (2017)		x			x			x					x
Kong et al. (2011) Kong and Liu (2012) Kong et al. (2016b)	x		x		x	x		x	x	x			
Li et al. (2011)	x				x			x					x
Chen et al. (2016b) Chen et al. (2019)		x	x		x			x					
Sivill et al. (2005) Sivill and Ahtila (2009)						x		x	x				x
Manninen et al. (2002)				x	x		x		x				
Treppe et al. (2012)						x			x	x			
Laurijssen et al. (2010)	x				x	x		x	x	x	x		
Lindell and Stenström (2006)	x				x	x			x				x

[6] The energy demand of the drying section is an exogenous variable for the models where the drying section is neither indicated as black box nor as grey box.

4.1.3 Process integration

Since it is an omnipresent subject in scientific (theoretical) works on the assessment of energy-efficiency and ecological improvements of industrial processes, a brief presentation on process integration and its application to retrofit design is provided in this section.

Process integration appeared with the energy crises of the 1970's, under the form of the pinch analysis, a graphical tool for heat integration, and developed over the years to become a family of methodologies based on heuristics, thermodynamics (graphical) and mathematical programming, used to combine several parts of processes or whole processes in manufacturing and power plants for reducing the consumption of resources or harmful emissions into the environment (Klemeš and Kravanja 2013).

Since heuristic methods are not expected to produce accurate results (Nelson and Douglas 1990), graphical and mathematical programming techniques became the two main schools of concepts in process integration and are often used jointly, the pinch analysis for targeting energy savings and generating ideas, and mathematical programming for determining the best of these ideas after including material and costs dimensions to the optimization problem. A good example for the extensive and combined use of different pinch analysis tools for the heat, power, combined heat and power and CO_2-emissions integration at a whole industrial park, called Total Site in the terminology of process integration, is presented by Abdul Aziz et al. (2017). The weakness of the thermodynamic methods is that they cannot be used simultaneously with material balances, thus process streams need to have fixed values of flow rates and temperatures and often non-optimal flow rates and temperatures are obtained (Lang et al. 1990).
In algorithmic methods, the structural alternatives are modelled in a superstructure using mixed integer nonlinear programming (MINLP), where discrete variables typically correspond to structural decisions (e.g. the presence or absence of a heat exchanger) and continuous variables to operational parameters and/or dimensional aspects (e.g. area of heat exchanger). Because of the complexity of the problems, those methods can only guarantee a local optimum to the problem (Kovac and Glavic 1995).

Those techniques were initially mostly utilized for grassroots design (Klemeš and Kravanja 2013) and cannot be directly used for retrofit, since rigorous process models are required in order to describe the current operating process which increases considerably the complexity of the corresponding optimization problem (Klemeš et al. 2013; Lee et al. 2016; Zhelev et al. 1998). To overcome this difficulty, Lee et al. (2016) limited the process alternatives considered for the retrofit of a CO_2 capture pilot plant using a thermodynamic analysis, not without mentioning that this selection could lead to overlooking the optimal solution. Similarly, and to not cause the existing sites too much change, Chen et al. (2013) limited to one the number of additional new units purchased for each type of equipment considered for the retrofit of a existent steam plant in a petroleum refinery.
Although considerable steam savings can be reached by optimizing and retrofitting processes and the related HEN systems, the economic benefit at the plant level is difficult to establish because of strong interactions with the site utility systems. Thus, Varbanov et al. (2004) developed the Top-level analysis, a stepwise optimization procedure based on the accurate simulation model of the utility system, in order to determine the true marginal price of steam at

the different pressure levels. These prices can be used as indicators when taking decisions on process modifications and utility system retrofit.

An interesting contribution because of its ambitious scope was made by Gharaie et al. (2015) who developed a retrofit strategy for the site-wide mitigation of CO_2-emissions in the process industries. The authors adapted the onion diagram for process synthesis proposed by Smith (2005) to the analysis of CO_2-emissions reduction measures (see Figure 4.1) in order to present the sequence for the assessment of retrofit measures at an industrial site. The emission reduction options considered in the case study do not include process changes but the retrofit of heat exchanger networks (HENs), the operational optimization of the utility system and fuel switching at the total site. The generation of retrofit options for the HEN (including structural changes) is carried out using mathematical programming and the most cost-effective retrofit options at the total site level are selected using graphical methods which account for retrofit capital investment, energy costs and CO_2-prices. Afterwards, the operation of the utility system is optimized by minimizing the operating cost (i.e. power import/export costs, fuel cost and the cost associated with CO_2-emissions) under the constraint that the energy requirements of the processes are satisfied. At last, if the set emission reduction target has not been reached after the two previous steps, the most economic fuel switching strategy is determined analysed using a graphical representation. Partial fuel switching is also considered since it may be more beneficial than total fuel switching in certain cases.
Worthy to mention here is that the analysis of fuel switching measures which involve changes at the process level, like the electrification of the glass melting process, should be included in the first step of the assessment procedure, i.e. within the category “process changes”.

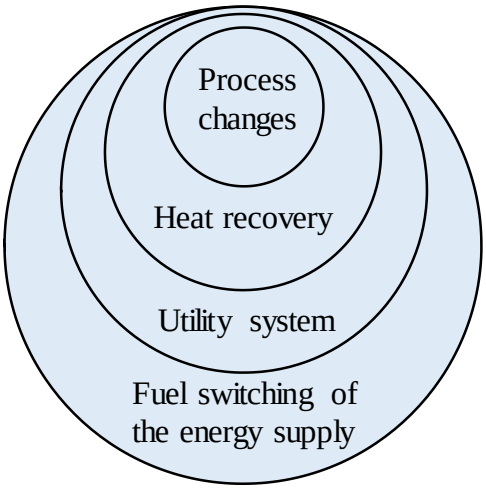

Figure 4.1: CO_2-emissions reduction diagram. Source: adapted from Gharaie et al. (2015).

From the literature reviewed in this section it becomes clear that the generation of retrofit alternatives for heat exchanger networks and utility systems constitutes a highly complex problem which requires a lot of computing resources. It is usually the scope of individual analysis and considered separately from retrofit measures which concern the core processes. Since the focus of this work lies on the assessment of retrofit measures which lead to a reduction of process heat demand, the heat recovery options and other retrofit measures to be analyzed/simulated will be defined a priori, while accepting the risk of missing the optimal design in the case of heat exchanger networks and utility systems. This decision is supported

by the fact that the number of possible retrofit options is usually restricted by a high number of constraints, as for example practical engineering constraints (e.g. limited space for equipment) or limited capital for investment (Min et al. 2015), which leads to a small number of options to be simulated.

4.1.4 Energy-efficiency cost and marginal emission abatement cost curves for the analysis of individual plants

Energy-efficiency cost curves (also called energy conservation cost curves) and marginal abatement cost (MAC) curves are widely used in academia, governments and the industry to capture the economic and technological potential of energy-efficiency and CO_2-emission reduction measures. Differences in regard to the included sectors, regional scope, considered time frame lead, and method for the generation of these curves lead to a wide variety of shapes (Kesicki 2010).

Energy-efficiency cost curves were developed in the continuity of the concept of supply curves of conserved energy proposed by Meier et al. (1982), by extending the notion of economic worthiness of a measure from the only consideration of its investment cost to further economic penalties and benefits, as for example the cost savings induced by reduced fuel consumption. With the growing challenge for policy makers to develop carbon emissions abatement strategies, the supply curves of conserved energy and energy-efficiency cost curves were adapted for the representation of CO_2-mitigation measures from the early 1990s and have become a widespread tool in the last decade, especially due to the abatement cost curves published for various countries by McKinsey and Company (Kesicki and Ekins 2012).

The structure of an energy-efficiency cost curve and marginal abatement cost (MAC) curve is represented in Figure 4.2. For their construction the measures are first ranked in order of increasing marginal cost and then represented as a step function where the y-axis corresponds to the marginal energy-saving cost or marginal CO_2-emission reduction cost of each measure and the x-axis corresponds to the cumulative annual potential final energy savings or cumulative annual potential CO_2-emissions reduction, respectively.
The economic potential corresponds to the value of the cumulative annual potential final energy savings/cumulative annual potential CO_2-emissions reduction for which the marginal cost of measures is negative.

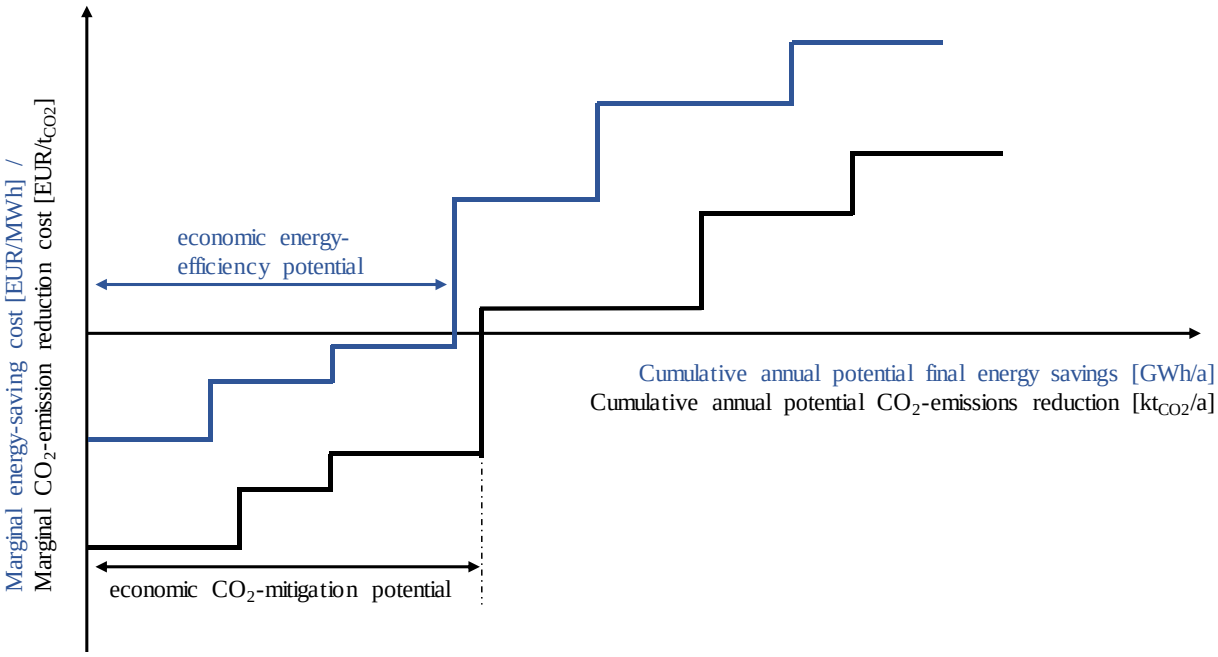

Figure 4.2: Schematic representation of an energy-efficiency cost curve/marginal abatement cost curve. Source: own representation.

Although traditionally used in wide-scoped analysis, for example to display potentials at the scale of a country or a whole industrial sector, several recent studies (e.g. the works of Berghout et al. (2019), Chan et al. (2016) and Min et al. (2015)) show that energy-efficiency cost curves and MAC curves also provide a useful basis for decision-making at the level of individual plants.

Min et al. (2015) developed a high-level screening methodology based on the construction of MAC curves in order to facilitate the comparison between different retrofit options at an industrial site. The methodology was applied to the analysis of four CO_2-emissions reduction options in a refinery: the operational optimization of the site utility system, the retrofit of the heat recovery system, fuel switching from coal to LNG, and end-of-pipe CO_2 capture. The expected savings are based on rough assessments and the interactions between retrofit options are not taken into account.

Chan et al. (2016) built MAC curves to illustrate the impact of energy-efficiency measures, the energy optimization of the utility systems, onsite power generation, fuel switching to natural gas and carbon capture and storage options at the largest Brazilian refinery. There again the effect of measure's interaction is neglected.

The negligence of interactions between measures when assessing specific costs and abatement potential is a common criticism against MAC curves used in policy analysis (Kesicki and Ekins 2012). However, the non-inclusion of interactions seems to be due to the complex quantification of those interactions and missing data, rather than a limitation of the visualization tool itself. Flatau (2019) developed a methodology for the evaluation of interdependent cross-cutting energy efficiency measures, applied it for assessing the energy-saving potential of the German plastics processing industry, and showed that neglecting interactions between measures leads

to an overestimation of the economic final energy saving potential by one third. The results were represented in form of energy-efficiency cost curves.

Berghout et al. (2019) examined four deployment pathways featuring a wide scope of GHG-mitigation measures in a petroleum refinery in Europe using MAC curves. Certain overlaps between the mitigation options in the overall GHG reduction potential and the avoidance costs were assessed by first computing the GHG emission reduction and avoidance cost of the mitigation option that is implemented first, then subtracting the emission reductions of the first mitigation option from the base case emissions, and subsequently computing the GHG emission reduction and avoidance cost of the second mitigation option.
This method is not applicable for MAC curves based on model-based simulation results since in that case the emission reduction related to single measures is not expressed as a percentage of the current emissions or as an amount of emission saved per ton of product but the result of a model-based calculation. Therefore, another method for the construction of energy-saving and MAC curves is needed in order to represent the contributions of individual measures.

4.1.5 Key aspects of the present work derived from the literature review

The review of literature related to the goals presented in the introduction (section 1.2) allowed to better define some key aspects of the present work.
Energy-saving and CO_2-emission reduction options related to paper drying encompass operational and structural changes at the level of the drying process itself, the steam cascade, the air and heat recovery systems, as well as the boiler system, and therefore the simulation model should include these different system parts.
As a result of the works reviewed in section 4.1.2, one of the requirements to the model for paper drying is to be based on a detailed physical description of heat and mass transfer at the paper level to allow the simulation of a wide range of measures at the drying section, and to cover a wide scope of configurational options, in order to be applicable to the drying section of different paper mills.
Also, since only little attention has been given in the past to the effect of waste heat recovery from hood exhaust air using heat pumps and the interactions between measures at different levels, those aspects are in the focus of the present work.
Finally, unlike most energy-efficiency cost and MAC curves built for individual plants using rough assessments for the single options, the model simulation results in the present work will serve as a basis for their construction. The development of a methodology to account for the measure's interactions in the construction of energy-efficiency cost curves and MAC curves based on simulation results constitutes a further objective of this work, since to the author's knowledge no such methodology has been published yet.

5 Framework for the assessment of CO_2-mitigation measures

This chapter deals with the description of the developed model-based framework for the assessment of CO_2-emission reduction measures in multi-cylinder paper drying. First an overview of the process model and a detailed description of the different model blocks are given. Subsequently, the paper drying model is verified with several datasets from the literature. Later, the integration of measures in the framework and the algorithm for the calculation of the energy consumption of paper drying after applying energy efficiency measures are presented.
The translation of the energy-savings into CO_2-emission reductions, the economic analysis and the graphical representation of the results as energy-efficiency cost curves and marginal abatement cost curves are the topics of the next sections.
Finally, the application procedure of the framework and its implementation are described.
Parts of the framework description were previously published and quoted verbatim from (Godin and Radgen 2021) with permission.

5.1 Model of the drying section

The objective of the developed model is to depict the initial energy demand of the analysed drying section accurately in order to serve as a basis for the energy-assessment of various measures in a second step.
The energy demand of a multi-cylinder drying section corresponds to the steam required for the operation of the drying cylinders and the air heating system, and the power consumption of the cylinder drives and the hood ventilation system.
Since heat represents the largest share of the energy demand at the drying section, the scope of energy-efficiency measures analysed in this work is limited to measures which lead to heat demand reductions. Therefore, whereas the steam demand is an output of process model calculation also for the status quo, the power consumption in the initial situation is provided as input and variations in the power consumption for the different combinations of measures is assessed.
The model blocks and calculation sequence for the determination of the overall steam demand in the drying section are shown in Figure 5.1. The calculation sequence is oriented in the opposite direction of the physical flow of energy and starts with the calculation of the energy demand of the dryers.

A grey-box approach was chosen to model the dryers where mass and energy balances are set-up for an infinitesimal length element of paper web along the drying section, and the heat transfer coefficients correspond to physical entities of the system (condensate layer, cylinder shell, etc.). A white-box model covering the time-dependant description of physical mass and heat processes within the paper web, although relevant for the analysis of product-related issues like uneven moisture profiles or web delamination, is not required and considered over-complex for the level of analysis chosen here and would lead to very long solving times. On the other hand, the oversimplification of the processes using a black-box model only based on mass and energy balance over the whole drying section would not allow to quantify the effect of changes on specific parts of the system.
Since details at the physical level do not bring an added-value for the objectives of this model, the hood, steam groups, separators and steam cascade are modelled as black-boxes where the outputs of each entity are calculated based on exogenous variables and energy and mass

balances. As a consequence of these modelling choices, the efforts for model verification in this work are directed towards the dryer model.

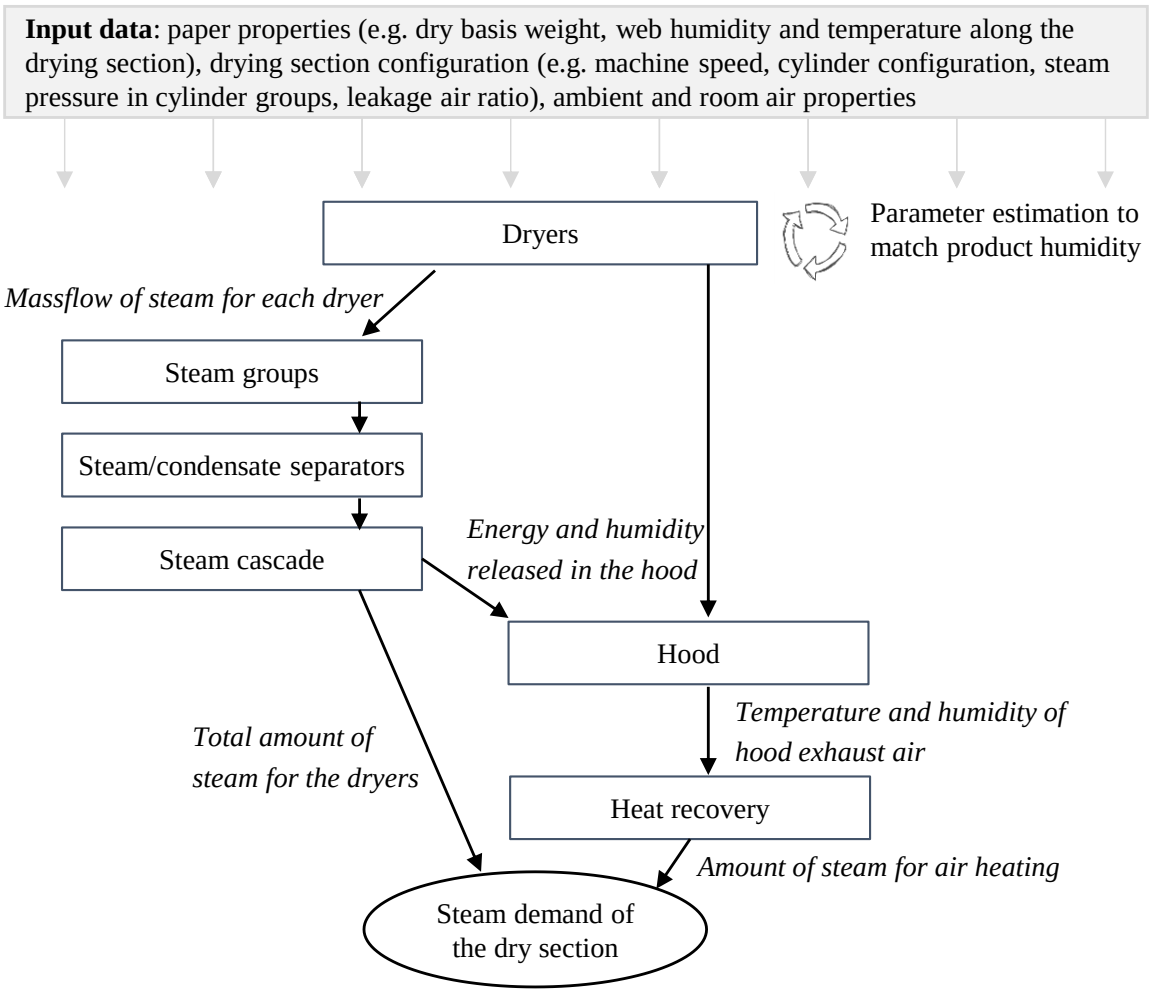

Figure 5.1: Model blocks and calculation procedure of the overall steam demand in multi-cylinder paper drying. Source: (Godin and Radgen 2021), reprinted with permission.

5.1.1 Drying model

The paper drying module is a grey-box model similar to the model presented by Yin et al. (2016): Main differences cover the use of the Stefan's law in the present work instead of the Fick's law to model mass transfer between the web and the air, model extensions to include mixed double- and single-tier cylinder configurations and the fabric reduction factor which accounts for the effect of the fabric on mass transfer, and the use of a lumped parameter to account for conduction and evaporation/condensation phenomena within the paper web, as proposed by Wilhelmsson and Stenström (1995b). A parametric approach is used to calibrate the drying model to the paper web humidity and temperature measured at the paper mill.

As a result of the equations (1) to (5) presented in section 3.3.5 and with $dl = vdt$, following models are obtained for the different drying phases in double-tier and single-tier configurations:

Double-tier

- Contact area

$$\frac{dx_p}{dl} = -\frac{K_{pa}(1-FRF)M_w p_{tot}}{G_{dry} v R T_p} \cdot \ln\left(\frac{p_{tot}-p_{aw}}{p_{tot}-p_{pw}}\right) \tag{9}$$

$$\frac{dT_p}{dl} = \frac{U_{sp}(T_s - T_p) + h_{pa}(T_a - T_p) + G_{dry} v \Delta H_{evap} \frac{dx_p}{dl}}{G_{dry} v (c_f + c_w x_p)} \tag{10}$$

- Free draw area

$$\frac{dx_p}{dl} = -\frac{2K_{pa}M_w p_{tot}}{G_{dry} v R T_p} \cdot \ln\left(\frac{p_{tot}-p_{aw}}{p_{tot}-p_{pw}}\right) \tag{11}$$

$$\frac{dT_p}{dl} = \frac{2h_{pa}(T_a - T_p) + G_{dry} v \Delta H_{evap} \frac{dx_p}{dl}}{G_{dry} v (c_f + c_w x_p)} \tag{12}$$

Single-tier

- Contact area at steam-heated cylinder

$$\frac{dx_p}{dl} = -\frac{K_{pa}(1-FRF)M_w p_{tot}}{G_{dry} v R T_p} \cdot \ln\left(\frac{p_{tot}-p_{aw}}{p_{tot}-p_{pw}}\right) \tag{13}$$

$$\frac{dT_p}{dl} = \frac{U_{sp}(T_s - T_p) + h_{pa}(T_a - T_p) + G_{dry} v \Delta H_{evap} \frac{dx_p}{dl}}{G_{dry} v (c_f + c_w x_p)} \tag{14}$$

- Contact area at non-heated cylinder

$$\frac{dx_p}{dl} = -\frac{K_{pa}M_w p_{tot}}{G_{dry} v R T_p} \cdot \ln\left(\frac{p_{tot}-p_{aw}}{p_{tot}-p_{pw}}\right) \tag{15}$$

$$\frac{dT_p}{dl} = \frac{h_{pa}(T_a - T_p) + G_{dry} v \Delta H_{evap} \frac{dx_p}{dl}}{G_{dry} v (c_f + c_w x_p)} \tag{16}$$

- Free draw area

$$\frac{dx_p}{dl} = -\frac{K_{pa}(2-FRF)\, M_w p_{tot}}{G_{dry} v R T_p} \cdot \ln\left(\frac{p_{tot}-p_{aw}}{p_{tot}-p_{pw}}\right) \tag{17}$$

$$\frac{dT_p}{dl} = \frac{2h_{pa}(T_a - T_p) + G_{dry} v \Delta H_{evap} \frac{dx_p}{dl}}{G_{dry} v (c_f + c_w x_p)} \tag{18}$$

The temperature and humidity of the web at every point in the paper machine are obtained by solving the resulting non-linear coupled ordinary differential equation (ODE) system over the whole length of the paper web in the drying section. The model parameters are described in the next section.

5.1.2 Determination of model parameters

The fabric reduction factor FRF corresponds to the reduction in the mass transfer of vapor between the paper web and the surrounding air due to the presence of the fabric and its value typically lies in the range 0.3-0.5 (Wilhelmsson and Stenström 1995b; Ghodbanan et al. 2015; Gaillemard 2006).
The partial vapor pressure in air p_{aw} is calculated using equation (6) presented in section 3.3.6 with the moisture content of hood inlet air $x_{a,sup}$ and the total pressure p_{tot}.
The partial vapor pressure at the paper web surface p_{pw} is given by following expression (Slätteke 2006; Ahrens and Rudman 2003):

$$p_{pw} = \emptyset(T_p, x_p) \cdot p_{sat}(T_p) \tag{19}$$

where $p_{sat}(T_p)$ is given by the Antoine's Equation (see equation (7), section 3.3.6), and $\emptyset(T_p, x_p)$ is an isotherm correction factor accounting for the sorption of bound water in the paper web for which Heikkilä (1993) proposed the following expression:

$$\emptyset(T_p, x_p) = 1 - \exp\left(-47.58 \cdot x_p^{1.877} - 0.10085 \cdot T_p \cdot x_p^{1.0585}\right) \tag{20}$$

The enthalpy of evaporation ΔH_{evap} is the sum of the vaporization enthalpy and the sorption enthalpy, and is thus given by:

$$\Delta H_{evap} = (L_{vap0} - 2.3237 \cdot T_p) + 0.1 \frac{R}{M_w} \cdot x_p^{1.0585} \cdot (T_p + 273.15)^2 \cdot \frac{1 - \emptyset}{\emptyset} \tag{21}$$

The overall heat transfer coefficients between the steam in the cylinders and the air U_{sa} and between the steam in the cylinders and the paper web U_{sp} are given by:

$$U_{sa} = \frac{1}{\frac{Angle}{360\, h_{sc}} + \frac{Angle}{360\, h_{shell}} + \frac{1}{h_{ca}}} \tag{22}$$

$$\mathrm{U}_{sp} = \frac{1}{\frac{Angle}{360\, h_{sc}} + \frac{Angle}{360\, h_{shell}} + \frac{1}{h_{cp}} + \frac{t_p}{\lambda_p}} \tag{23}$$

Where the heat transfer coefficient of the cylinder shell is related to the thermal conductivity of the cylinder shell by following equation[7]:

[7] The detailed derivation of the equation (24) is presented in Appendix A.

$$h_{shell} = \frac{\lambda_{shell}}{\left(\frac{D}{2} - t_{shell}\right) \cdot \ln\left(\frac{\frac{D}{2}}{\frac{D}{2} - t_{shell}}\right)} \tag{24}$$

And the paper web thickness t_p and density ρ_p are determined based on the grammage and the density of the dry product:

$$t_p = \frac{1 + x_p}{\rho_p} \cdot G_{dry} \tag{25}$$

$$\rho_p = \frac{1 + x_p}{\frac{x_p}{\rho_w} + \frac{1}{\rho_{p,dry}}} \tag{26}$$

λ_p is a lumped parameter for the apparent thermal conductivity of paper formulated by Rhodius and Göttsching (1979) which accounts for conduction and evaporation phenomena within the web:

$$\lambda_p = \lambda_{p,dry} + \frac{0.00057 \cdot x_p^3}{0.0853 + x_p^3} \tag{27}$$

According to Wilhelmsson et al. (1996), the heat transfer coefficient between cylinder and paper h_{cp} can be written as follows:

$$h_{cp} = h_{cp0} + 0.955 x_p \tag{28}$$

The parameter h_{cp0} corresponds to the resistance to heat transfer induced by the thin layer of air and dirt between the cylinder outer surface and the dry paper web. Since the value of this parameter cannot be measured, it is used as second fitting parameter in the model calibration procedure besides the fabric reduction factor, with the constraint that its value lies in the range 0.1-2.2 kW/m^2.K (Yin et al. 2016; Gaillemard 2006).
The convective heat transfer coefficient between the cylinder and the surrounding air h_{ca} and between the paper web and the surrounding air h_{pa} are calculated with a formula combining the Nusselt number for laminar and turbulent parallel flow past a flat plate which has shown to be in good agreement with experimental data (Krischner and Kast 1978):

$$h = Nu \frac{\lambda_a}{l} \tag{29}$$

Where

$$Nu = \sqrt{Nu_{lam}^2 + Nu_{turb}^2}\,, \qquad Re = \frac{\rho_a v_a l}{\mu_a} \quad , \quad Pr = \frac{c_a \mu_a}{\lambda_a} \tag{30}$$

$$Nu_{lam} = 0.664 \cdot Re^{\frac{1}{2}} Pr^{\frac{1}{3}} \qquad \text{and} \quad Nu_{turb} = \frac{0.037 \cdot Re^{\frac{4}{5}} Pr}{1 + 2.443 \cdot Re^{-0.1}\left(Pr^{\frac{2}{3}} - 1\right)} \tag{31}$$

The characteristic length l corresponds to the diameter of the cylinder D for h_{ca} and to the length of the contact or free draw section for h_{pa}. The velocity of air v_a is considered to be same as the speed of the paper machine.
Finally, the mass transfer coefficient from the paper web to the surrounding air is determined based on the widely used Chilton-Colburn analogy which links heat and mass transfer coefficients (Nilsson 2004a; Gaillemard 2006):

$$K_{pa} = \frac{h_{pa}}{\rho_a c_a} Le^{-\frac{2}{3}} \qquad \text{where} \qquad Le = \frac{Sc}{Pr} \quad , \quad Sc = \frac{\mu_a}{\rho_a Diff} \tag{32}$$

And the diffusivity of vapor in air $Diff$ is determined with the formulas presented by Rossié (1953)[8]:

$$\text{If } T_a < 80°C \qquad Diff = 104.91143 \cdot 10^{-6} \cdot \frac{(T_a + 273.15)^{1.774}}{1000 \cdot p_{tot}} \tag{33}$$

$$\text{If } 80°C < T_a < 300°C \qquad Diff = 805.24 \cdot 10^{-6} \frac{(T_a + 273.15)^{2.5}}{(T_a + 190 + 273.15) \cdot 1000 \cdot p_{tot}} \tag{34}$$

5.1.3 Drying model validation

To validate the developed drying model for different paper grades and mill configurations, data sets were taken from the literature and the model was calibrated to each data set by minimizing an objective function corresponding to the quality of the fit between measured and calculated data, using the contact heat transfer coefficient hcp_0 and the fabric reduction factor FRF as tuning parameters.
Some main characteristics of those data sets are summarized in Table 5.1, including the data quality which indicates the number of points within each data set. The measured data points and calculated values at the corresponding locations for the paper web temperature and humidity are represented for all four data sets respectively in Figure 5.2, Figure 5.3, Figure 5.4, and Figure 5.5. The application of a starch solution at the size press of the paper machines analysed in (Yin et al. 2016) and (Chen et al. 2016a) is the reason for the sharp decrease in the paper web temperature at cylinder number 48 in Figure 5.2, and for the sharp rise in the paper web humidity after cylinder number 48 in Figure 5.5.

The results of the error minimization after model calibration are presented in the last line of Table 5.1. Since the web temperature measurements are made after the dryers and thus correspond to peak values of the temperature function, the mean absolute percentage error between measurements and model values is evaluated as the average of the error at those points. Similarly, the error for the humidity is evaluated based on the difference between the measured values and the model values obtained at the same locations.

An average error of 9.8% for the temperature and 4.8% for the humidity of the paper web is obtained across all data sets. Beyond model inaccuracies, these errors may be explained by the

[8] The use of two distinct formulas below and above 80°C is not due to different physical behaviours of the water vapor but to the fact that the diffusivity for temperatures below 80°C was measured and thereby the correlation for low temperatures determined before the additional experiments conducted by Rossié for higher temperatures.

uncertainty in measurement data which is represented with error bars in the figures below. The type of temperature measurement tool has a significant impact on the obtained value (TAPPI 1992). Ghodbanan et al. (2015) used an infrared thermometer, whereas thermal infrared imaging viewers from the same manufacturer were used in the three other studies. These non-contact measurement tools typically have an accuracy of 2°C (Chen et al. 2016a).
The tool used for humidity measurement was documented only in the study conducted by Chen et al. (2016a) and has an accuracy of 5%.[9]
Another reason for discrepancy between measured and calculated values in the case of web temperature lies in the difference between the location of the measurement point, typically a few centimetres after the end of the contact sections, and the model data point, at the end of each contact section. The paper web however undergoes large temperature variations within short distances because of fast heating and cooling through evaporation.
The agreement between measurements and model values is satisfactory for the present purpose of the drying model, which is to provide a basis for further energy calculations.

[9] Because of a lack of error specification in the three further studies, the same error was used as a basis for the error bars in the figures throughout all data sets.

Table 5.1: Literature data sets for dryer model verification

Publication	**(Yin et al. 2016)**	**(Ghodbanan et al. 2015)**	**(Kong and Liu 2012)**	**(Chen et al. 2016a)**
Paper grammage (g/m^2)	120	127	48	147
Name of the paper machine (in this work)	PM1	PM2	PM3	PM4
Paper machine speed (m/min)	375	440	1500	700
Number of cylinders	Pre-drying: 48 Post-drying: 15	35	33	Pre-drying: 47 Post-drying: 20
Type of paper machine	Double-tier	Double-tier	Double-tier	Single- and double-tier
Data quality[10] Temperature Humidity	 ++ -	 ++ ++	 + +	 ++ ++
Measurement tool	Temperature: thermal infrared imaging viewer Humidity: not specified	Temperature: IR-Thermometer. Humidity: not specified	Temperature: thermal infrared imaging viewer Humidity: not specified	Temperature: thermal infrared imaging viewer Humidity: NDC 8100-F system
Measurement location	Temperature: a few cm after each contact zone Humidity: only at beginning and end of drying section	Temperature: not specified Humidity: not specified	Temperature: around 5 cm away from contact zone Humidity: tested at beginning of tail threading	Temperature: At beginning and end of contact zone Humidity: at middle of free draw areas
Mean absolute percentage error				
ΔTemp ΔHum	11.2% 0%	4.6% 5%	14.3% 2.2%	9.2% 12%
Values of fitting parameters				
$\boldsymbol{h_{cp0}}$ (kW/m²K)	0.236	0.454	0.143	0.649 (Single-tier) 1.2 (Double-tier)
$\boldsymbol{FRF}$ $(-)$	0.367	0.65	0.65	0.63

[10] A measurement point is available for each cylinder (‘++’), for each steam group (‘+’), or only for the beginning and the end of the drying section (‘-‘).

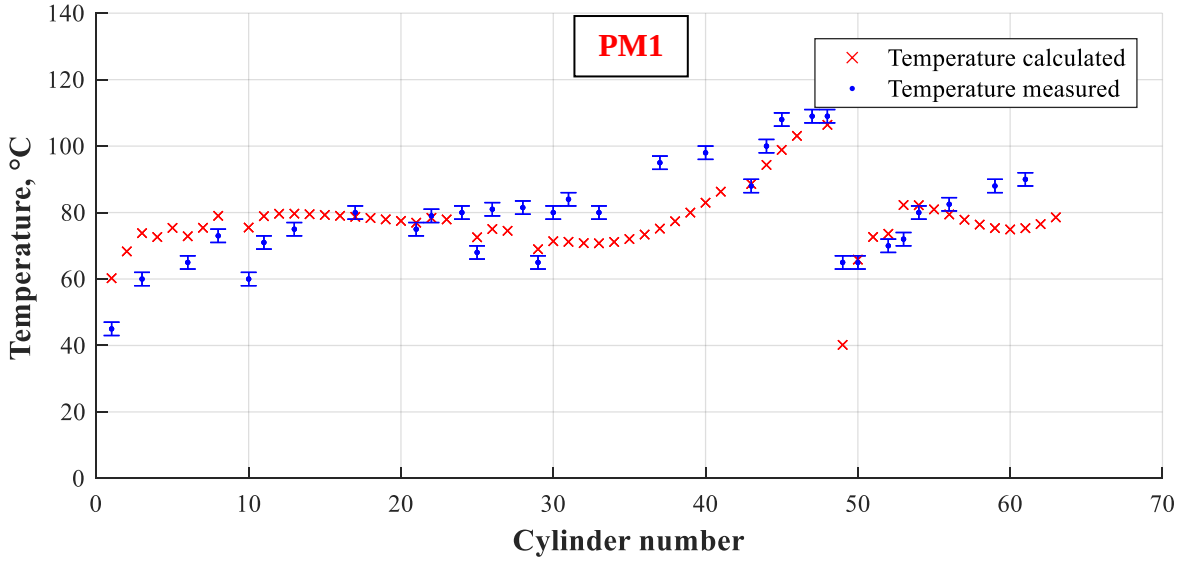

Figure 5.2: Comparison between the calculated and measured temperature of the paper web. [Based on data from Yin et al. (2016)]

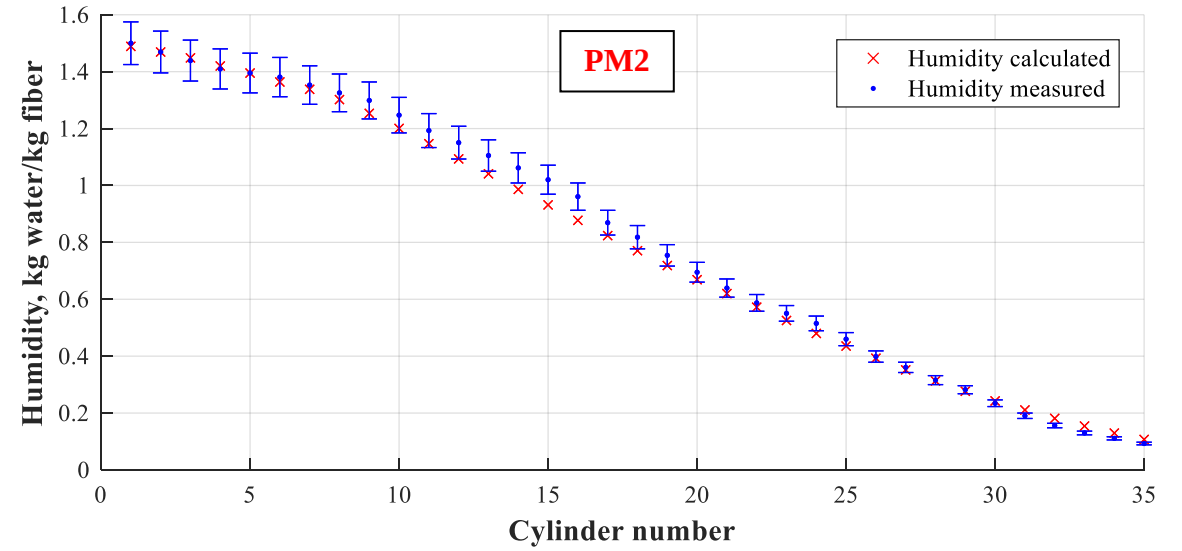

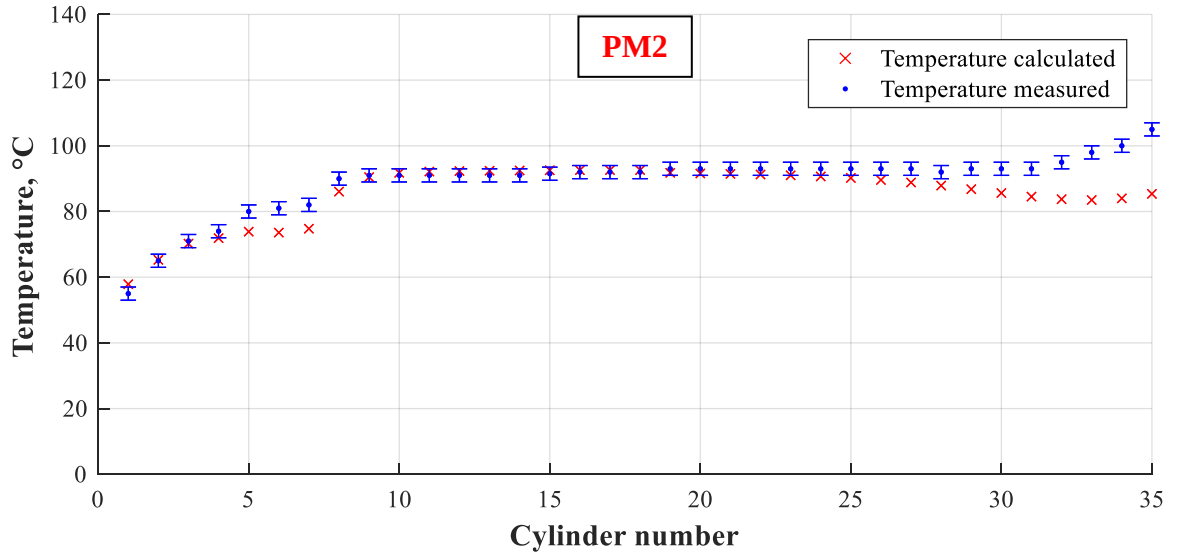

Figure 5.3: Comparison between the calculated and measured humidity (upper chart) and temperature (lower chart) of the paper web. [Based on data from Ghodbanan et al. (2015)]

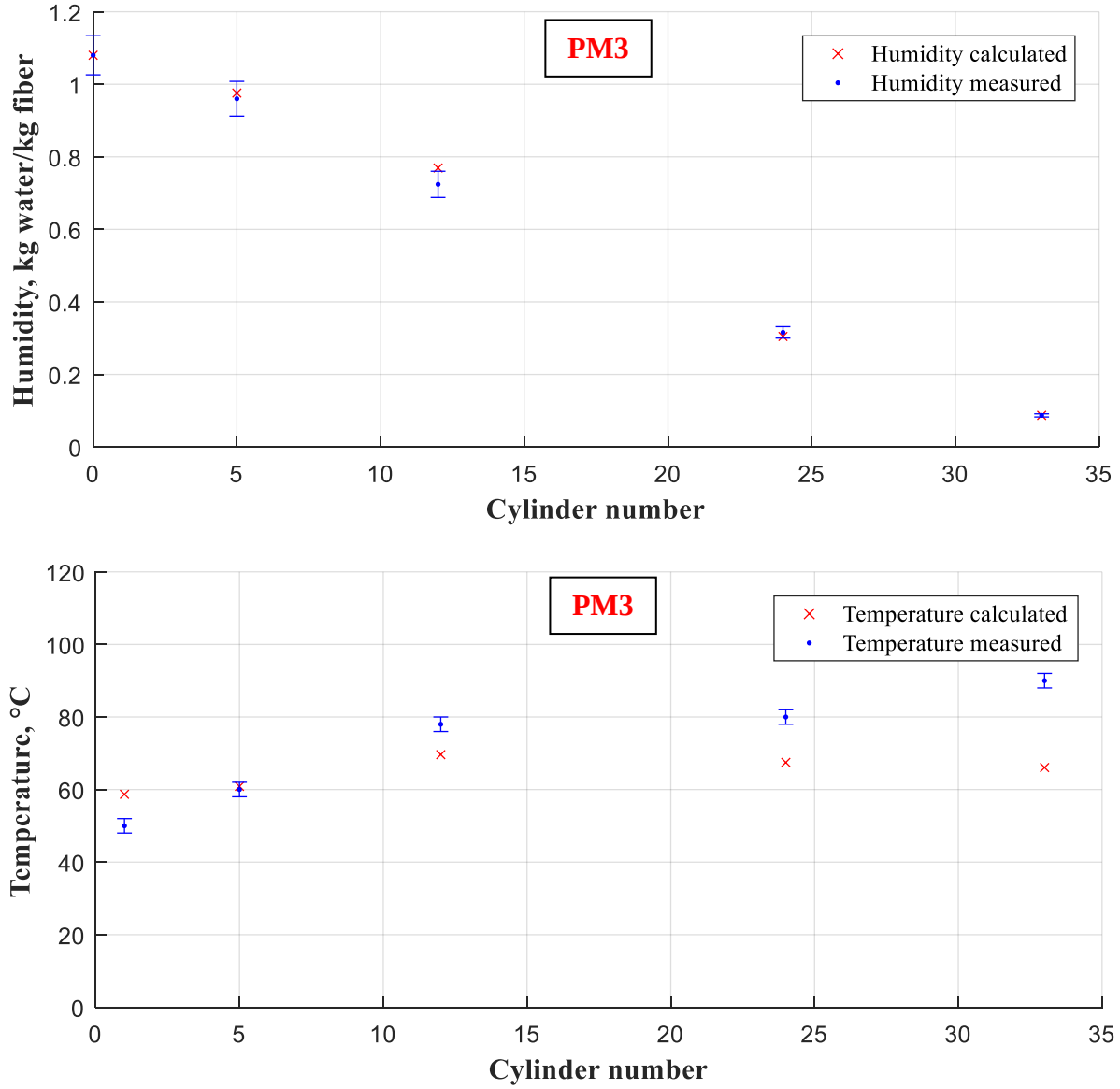

Figure 5.4: Comparison between the calculated and measured humidity (upper chart) and temperature (lower chart) of the paper web. [Based on data from Kong and Liu (2012)]

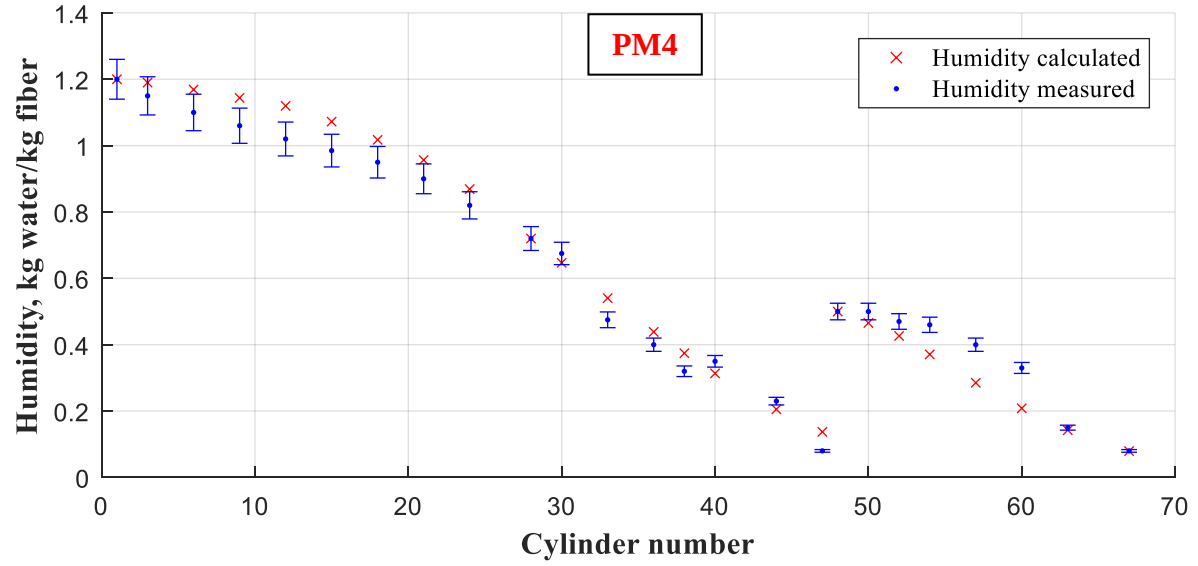

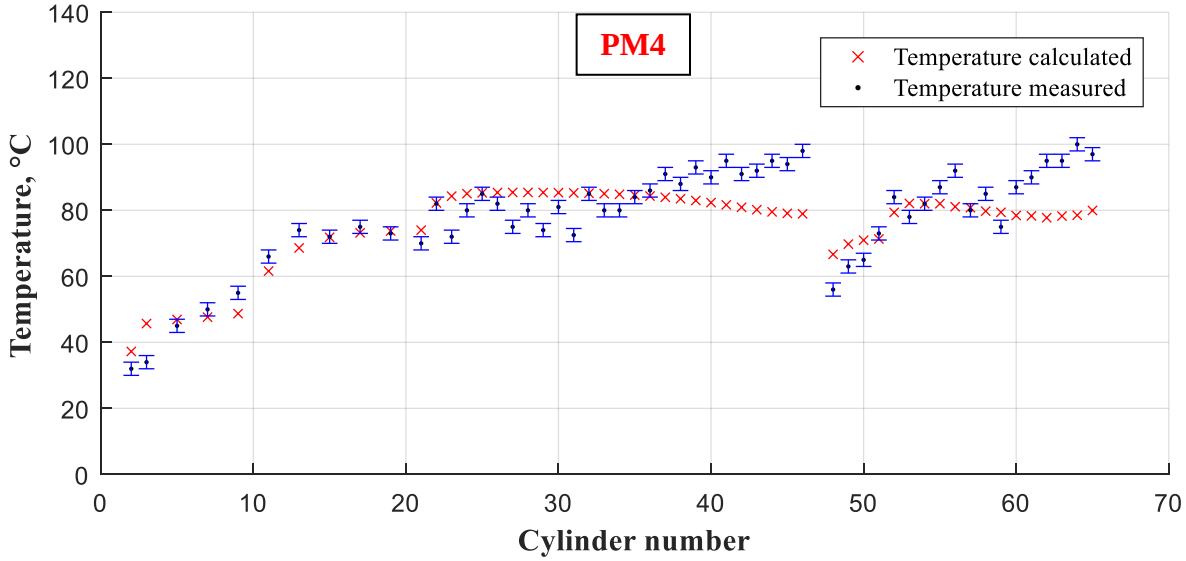

Figure 5.5: Comparison between the calculated and measured humidity (upper chart) and temperature (lower chart) of the paper web. [Based on data from Chen et al. (2016a)]

Additionally, to verify that the developed model gives plausible results, the final paper web humidity was calculated after varying different input parameters by ±15% for the paper machine described in Ghodbanan et al. (2015). The values of the fitting parameters were kept same as in the reference case described above and the results of this analysis are presented in Figure 5.6.

As expected, a lower initial paper web humidity, longer free draw sections, the use of cylinders with a larger diameter, and higher steam pressures in the drying cylinders all lead to a lower paper web humidity at the end of the drying section. The initial paper web humidity and the diameter of the cylinders both have the largest impact on the final paper web humidity.

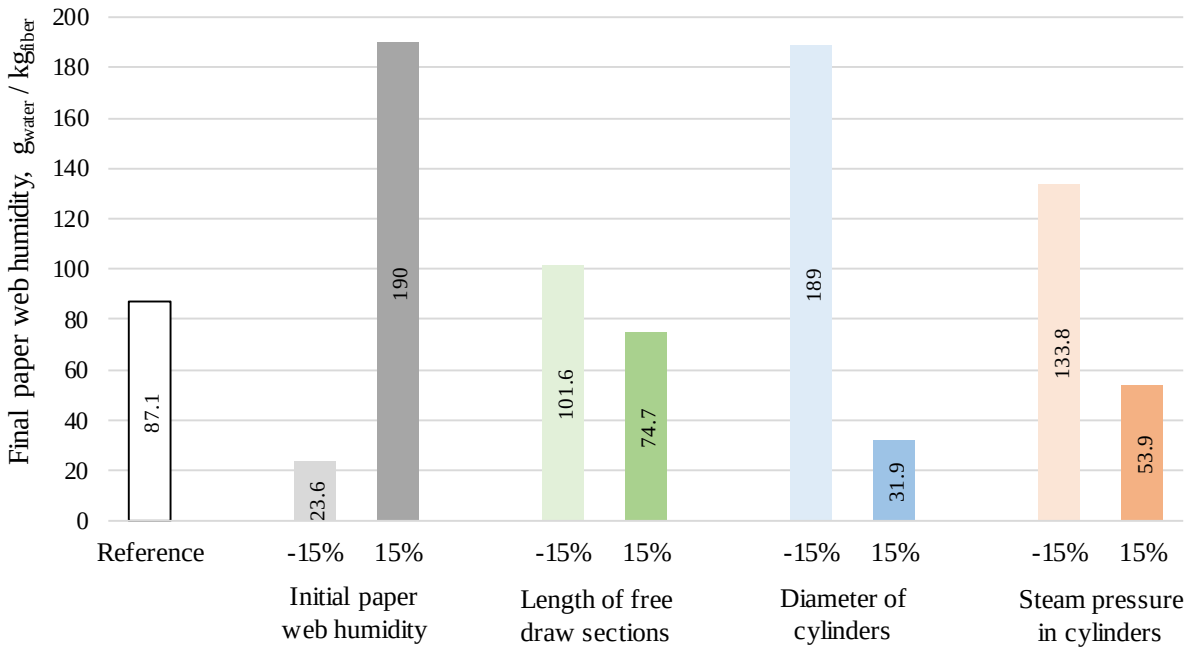

Figure 5.6: Effect of different input parameter values on the paper web humidity at the end of the drying section. [Based on data from Ghodbanan et al. (2015)]

5.1.4 Steam demand of a dryer

The inlet steam, the condensate and the blow-through steam in the cylinders are near saturation conditions (Slätteke 2006). Therefore, the energy transferred to the inner cylinder walls corresponds to the heat released during the condensation of steam.
A large share of this energy is transmitted to the paper web, on the dryer surface area where the web contacts the cylinder. At the bases and the uncovered lateral area of the cylinder, heat is transferred to the surrounding air.

The amount of heat transferred from the cylinder steam to the paper web for each dryer j is the sum of the heat flow rate at each infinitesimal section i of this cylinder:

$$\dot{Q}_{sp,j} = \sum_{i=1}^{l_{cont,j}/dl} U_{sp}\left(T_s - T_{p,i}\right) w dl \tag{35}$$

The heat flow from the steam to the air for each cylinder j is given by:

$$\dot{Q}_{sa,j} = U_{sa}\left(T_{s,j} - T_{a,sup3}\right) \cdot \left(A_{noncovered,j} + 2A_{base,j}\right) \tag{36}$$

Finally, assuming a constant specific enthalpy of the steam $H_{s,j}$ and condensate $H_{c,j}$ in the dryers, the required inlet steam flow per cylinder is given by a mass and energy balance on a cylinder j:

$$\dot{m}_{s,j} = SF \frac{\dot{Q}_{sa,j} + \dot{Q}_{sp,j}}{(1-\alpha) \cdot \left(H_{s,j} - H_{c,j}\right)} \tag{37}$$

Where α is the blow-through steam coefficient and SF a steam margin factor which accounts for additional steam supplied to the dryers during operation in order to reach the targeted paper moisture content.
The expressions for the enthalpy of condensate and saturated steam are obtained by fitting data from Steam tables (Koretsky 2004):

$$H_c = 4.319 \cdot \ln(T_c) - 14.766 \tag{38}$$

$$H_s = 174.87 \cdot \ln(T_s) + 1869.7 \tag{39}$$

5.1.5 Steam demand of the steam cascade

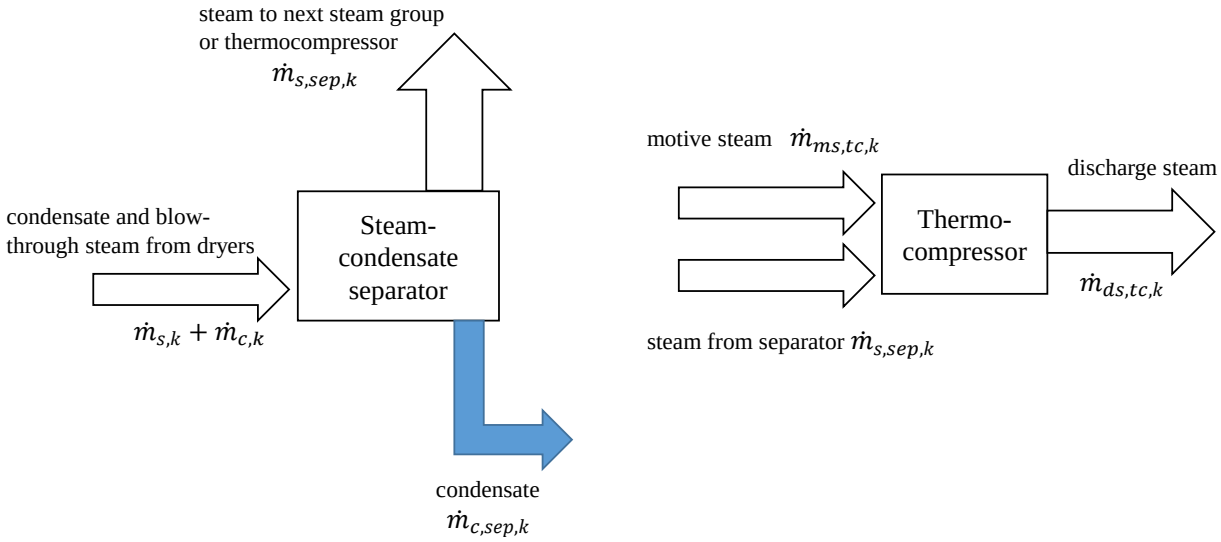

Figure 5.7: Steam and condensate streams at the steam-condensate separator (left) and thermocompressor (right)

The inlet mass flow of the separator module for each steam group k is the sum of the mass flow of steam and condensate from each cylinder j within this steam group. The enthalpy of the condensate and steam entering each separator is thus given by:

$$H_{s,k} = \frac{\sum_j \alpha \dot{m}_{s,j} H_{s,j}}{\dot{m}_{s,k}} \quad \text{and} \quad H_{c,k} = \frac{\sum_j (1-\alpha) \cdot \dot{m}_{s,j} H_{c,j}}{\dot{m}_{c,k}} \tag{40}$$

Knowing the pressure in the separator, the outlet mass flows of steam and condensate of a separator are obtained with mass and energy balances:

$$\dot{m}_{s,sep,k} = \frac{\dot{m}_{c,k}\left(H_{c,k} - H_{c,sep,k}\right) + \dot{m}_{s,k}(H_{s,k} - H_{c,sep,k})}{H_{s,sep,k} - H_{c,sep,k}} \tag{41}$$

$$\dot{m}_{c,sep,k} = \dot{m}_{c,k} + \dot{m}_{s,k} - \dot{m}_{s,sep,k} \tag{42}$$

In the next step the required amount of motive steam $\dot{m}_{ms,tc,k}$ for the thermocompressor is calculated using energy and steam balances on each thermocompressor module:

$$\dot{m}_{ms,tc,k} = \frac{\beta_k \dot{m}_{s,sep,k}(H_{ds,tc,k} - H_{s,sep,k})}{H_{ms,tc,k} - H_{ds,tc,k}} \tag{43}$$

Where

$$\dot{m}_{ds,tc,k} = \dot{m}_{ms,tc,k} + \psi_k \dot{m}_{s,sep,k} \tag{44}$$

If the steam group is working as a conventional steam cascade $\psi_k = 0$ whereas if it uses a thermocompressor $\psi_k = 1$.

The total inlet steam required in a steam group is then given by:

$$\dot{m}_{s,tot,k} = \frac{\dot{m}_{s,k}}{\alpha} - \psi_k \dot{m}_{s,sep,k} - J_k(1 - \psi_k) \tag{45}$$

J_k is equal to zero for the highest-pressure level steam group and to the steam mass flow from the separator of the next steam group $\dot{m}_{s,sep,k+1}$ for lower steam groups.

Finally, the total mass flow of steam for the steam cascade $\dot{m}_{s,tot}$ and the corresponding heat flow rate are obtained:

$$\dot{m}_{s,tot} = \sum_{1}^{k} \dot{m}_{s,tot,k} \tag{46}$$

$$\dot{Q}_{s,tot} = \sum_{1}^{k} \dot{m}_{s,tot,k} \cdot H_{s,tot,k} \tag{47}$$

5.1.6 Steam demand of the air heating system

The hood exhaust air has a high energy content due to its high moisture content and temperatures in the range 50-90 °C. A part of this energy is usually recovered to heat the hood inlet air (as shown in Figure 5.8) and process water. The inlet air, after this first preheating step, is then often heated with the condensate flow from the drying cylinders before being conditioned to the required hood temperature using saturated steam.

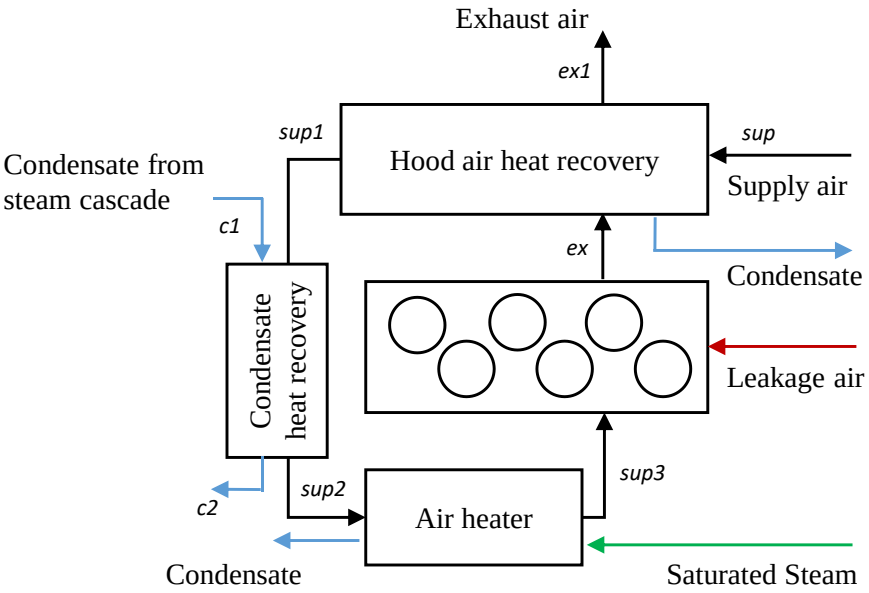

Figure 5.8: Schematic representation of the hood and air heating systems at a drying section. The subscripts used in equations are indicated in italics. Source: (Godin and Radgen 2021), reprinted with permission.

The humidity of the hood exhaust air is determined by calculating the water mass balance of the hood:

$$\dot{m}_{a,ex}x_{a,ex} = \dot{m}_{a,sup3}x_{a,ambient} + \dot{m}_{a,leak}x_{a,room} + G_{dry}vw \cdot \left(\Delta x_{p,pre} + \Delta x_{p,post}\right) \quad (48)$$

And with $r = \frac{\dot{m}_{a,leak}}{\dot{m}_{a,ex}}$:

$$x_{a,ex} = \frac{G_{dry}vw \cdot \left(\Delta x_{p,pre} + \Delta x_{p,post}\right)}{\dot{m}_{a,ex}} + (1-r)x_{a,ambient} + rx_{a,room} \quad (49)$$

The heat flow rate of the exhaust air is obtained with an energy balance on the hood:

$$\dot{Q}_{a,ex} = \dot{Q}_{p,in} + \dot{Q}_{starchsol} + \dot{Q}_{a,leak} + \dot{Q}_{a,sup3} + \dot{Q}_s - \dot{Q}_{p,out} - \dot{Q}_{thlosses} - \dot{Q}_c \quad (50)$$

Where the thermal losses at the hood walls $\dot{Q}_{thlosses}$ are expressed as a share of the energy flow leaving the drying section:

$$\dot{Q}_{thlosses} = \beta(\dot{Q}_{p,out} + \dot{Q}_{a,ex} + \dot{Q}_c) \quad (51)$$

The temperature of hood exhaust air is obtained using equation (8) presented in section 3.3.6:

$$T_{a,ex} = \frac{H_{a,ex} - L_{vap0}x_{a,ex}}{c_a + c_v x_{a,ex}} \quad (52)$$

Assuming that heat recovery from hood exhaust air takes place in a counter-flow heat exchanger with a known delta between the temperature of the inlet flow of hood exhaust air ($T_{a,ex}$) and the outlet flow of hood supply air ($T_{a,sup1}$):

$$T_{a,sup1} = T_{a,ex} - \Delta T_{heatexchanger} \quad (53)$$

The temperature and enthalpy of the supply air after heat recovery $T_{a,ex1}$ and $H_{a,ex1}$ can be determined by the energy balance equation at the heat exchanger:

$$\dot{m}_{a,sup}\left(H_{a,sup1} - H_{a,sup}\right) = \eta_{hr}\dot{m}_{a,ex}(H_{a,ex} - H_{a,ex1} - (x_{a,ex} - x_{a,ex1})c_w T_{a,ex1}) \quad (54)$$

Two successive phases are distinguished during the cooling of the exhaust air: first, the air is cooled down without any condensation until the dew point is reached. Any further cooling occurs along the dew point curve. Therefore, if the air is cooled below its dew point temperature, condensation takes place and the exhaust air after heat recovery is at the saturation humidity corresponding to the temperature $T_{a,ex1}$.
The enthalpy of supply air after the heat recovery from the condensate is expressed as follows:

$$H_{a,sup2} = H_{a,sup1} + \frac{\eta_{hr}(\dot{Q}_{c,1} - \dot{Q}_{c,2})}{\dot{m}_{a,sup}} \quad (55)$$

Finally, the required mass flow of steam for air heating and the corresponding heat flow rate are obtained:

$$\dot{m}_{s,ah} = \dot{m}_{a,sup} \frac{H_{a,sup3} - H_{a,sup2}}{\eta_{ah}\left(H_{s,ah} - H_{c,ah}\right)} \tag{56}$$

$$\dot{Q}_{s,ah} = \dot{m}_{s,ah} H_{s,ah} \tag{57}$$

5.2 Energy assessment of energy-efficiency measures

Measures to reduce the heat demand of the drying section of a paper machine may be classified into the three following categories (Laurijssen et al. 2010):

1) measures which decrease the amount of water to be removed in the drying section
2) measures which decrease the amount of energy needed for water evaporation
3) measures which increase the amount of recovered heat from the exhaust air

This results in a wide scope of measures at various locations of the drying section.

The choice of the measures to be included in the assessement of a specific paper machine depends on the plant configuration, the systems installed, etc. Therefore, it needs to be determined for each mill individually. However, the modeling procedure remains the same, that is identifying the model parameters impacted by the implementation of the measure, assessing the new parameter values through discussions with experts or using literature values, and finally incorporating these effects into the model. For measures which impact the system configuration, e.g. the integration of heat pumps to recover heat from hood exhaust air, the new configuration is stored in a separate module.

To calculate their effect on the energy demand of the drying section, the process model is applied for each combination of energy efficiency measures successively. Mutually exclusive measures are defined as such beforehand to reduce the number of permutations.

In the case of combinations of measures which impact the moisture profile of the paper web in the drying section, the iteration procedure shown in Figure 5.9 is used, in which the number of dryers in the steam group of the highest pressure level is decreased at every loop, starting with the cylinder at the very end of the concerned pre- or post-drying section, until the same final humidity of the paper web is obtained as in the status quo, and no overdrying occurs.

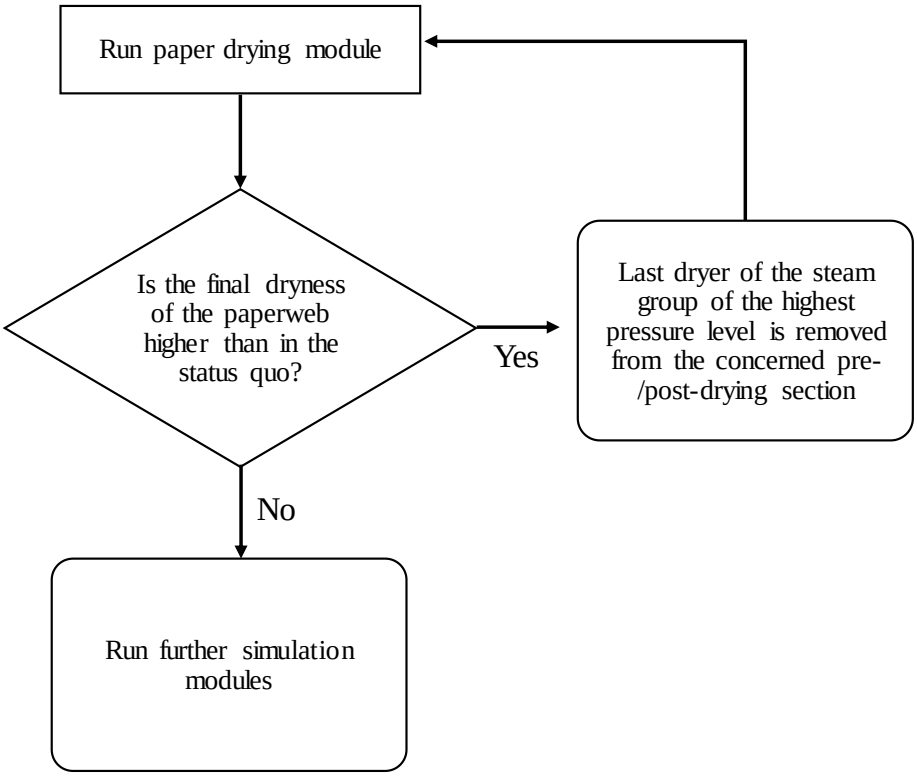

Figure 5.9: Iteration procedure on the number of dryers in the pre- and post-drying sections

The volume flow of hood supply air is determined for each set of measures such that it is higher than the minimum supply air flow, for which the hood exhaust air is at dew point.

The power consumption of fans is adjusted using the third fan law, according to which the power consumption P varies with the cube of the change in air volume flow:

$$P_{ventilation,2} = P_{ventilation,1} \cdot \left(\frac{\dot{m}_{a,2}\rho_{a,1}}{\dot{m}_{a,1}\rho_{a,2}}\right)^3 \quad (58)$$

The electricity consumption of drives is considered to be proportional to the number of cylinders operated at the drying section.
Since the focus of this work was set on heat demand reductions in the drying section, only the difference in power consumption between the initial and final system configurations is considered in this work. The power consumption of process components which are not impacted by the selected energy-efficiency measures is not included.

5.3 Quantification of the CO_2-emissions reduction reached through the implementation of CO_2-mitigation measures

In papermaking, process CO_2-emissions are negligible as compared to the CO_2-emissions due to heat and electricity production (Suhr et al. 2015; CEPI 2019). Those energy-related emissions are usually divided into direct (scope 1) emissions, arising on-site, and indirect (scope 2) emissions, for example from the generation of purchased electricity.

Consequently, the total CO_2-emissions reduction $EMR_{CO2,tot}$ after the implementation of a set of measures is the sum of the direct and indirect CO_2-emissions reduction:

$$EMR_{CO2,tot} = EMR_{CO2,direct} + EMR_{CO2,indirect} \tag{59}$$

Process heat is typically produced on-site so that the (direct) CO_2-emissions reduction related to steam production is given by:

$$EMR_{CO2,direct,heat} = \frac{\dot{Q}_{h,gen,initial}}{\eta_{th,initial}} ef_{fuel,initial} - \frac{\dot{Q}_{h,gen,final}}{\eta_{th,final}} ef_{fuel,final} \tag{60}$$

Where $\dot{Q}_{h,gen}$ corresponds to the amount of heat generated and the initial and final values of η_{th}, the thermal efficiency of the boiler, and ef_{fuel}, the arithmetic mean of the values taken by the emission factor of the fuel over the considered time frame, differ only in the case where a fuel switching measure is implemented.[11]

On the other hand, electricity may be purchased from external providers and/or produced at the paper mill, for example in combined heat and power (CHP) plants. Therefore, the CO_2-emissions reduction due to electricity savings can be expressed as:

$$EMR_{CO2,elec} = EMR_{CO2,direct,elec} + EMR_{CO2,indirect,elec} \tag{61}$$

Where the reduction of direct emissions for electricity produced in a CHP unit is given by:

$$EMR_{CO2,direct,elec} = \frac{P_{elec,gen,initial}}{\eta_{elec,initial}} ef_{fuel,initial} - \frac{P_{elec,gen,final}}{\eta_{elec,final}} ef_{fuel,final} \tag{62}$$

Where η_{elec} stands for the efficiency of electricity generation in the CHP unit and ef_{fuel} for the arithmetic mean of the values taken by the emission factor of the fuel over the considered time frame.
And the reduction in indirect emissions is equal to the differential amount of purchased electricity multiplied by the average value of the emission factor of electricity over the considered time frame:

$$EMR_{CO2,indirect,elec} = -\Delta P_{elec,purchased} \cdot ef_{elec} \tag{63}$$

[11] The variation of the efficiency of steam generation with varying load is considered out of scope of the present work.

5.4 Economic evaluation of measure's implementation

The economic worthiness of the measures is quantified using the Net Present Value which allows to compare the costs and benefits of the combinations of measures in equal terms. In this case, the Net Present Value (NPV) is equal to the difference between the sum of savings in operating costs ($OPEX$) over the lifetime of the measures L_t and the sum of the initial investment costs ($CAPEX$) of those measures:

$$NPV = -\sum CAPEX_{measure} - \sum_{i=t0}^{t0+Lt} \frac{\Delta OPEX_i}{(1+d)^i} \tag{64}$$

Where d stands for the discount rate, and the savings in operating costs $\Delta OPEX$ are determined for each year as the sum of the costs savings related to electricity, fuel and CO_2-emission savings, and other savings for example related to lower maintenance or personnel costs:

$$\Delta OPEX = \Delta OPEX_{elec} + \Delta OPEX_{fuels} + \Delta OPEX_{CO2} + \Delta OPEX_{others} \tag{65}$$

The $OPEX$ terms are determined for each year over the lifetime of the measures as:

$$\Delta OPEX_{elec} = \frac{P_{elec,gen,final}}{\eta_{elec,final}} \cdot price_{fuel,final} - \frac{P_{elec,gen,initial}}{\eta_{elec,initial}} \cdot price_{fuel,initial} + \Delta P_{elec,purchased} \cdot price_{elec} \tag{66}$$

$$\Delta OPEX_{fuels} = \frac{\dot{Q}_{h,gen,final}}{\eta_{th,final}} \cdot price_{fuel,final} - \frac{\dot{Q}_{h,gen,initial}}{\eta_{th,initial}} \cdot price_{fuel,initial} \tag{67}$$

$$\Delta OPEX_{CO2} = -EMR_{CO2,direct} \cdot price_{CO2} \tag{68}$$

The price of purchased electricity in Equation (66) comprises the commodity price as well as the reallocated capacity charge.
The total annualized cost TAC of a measure or combination of measures is then obtained by multiplying the additive inverse of the net present value by the annuity factor AF (Flatau 2019):

$$TAC = -AF \cdot NPV \tag{69}$$

Where $$AF = \frac{(1+d)^{Lt} \cdot d}{((1+d)^{Lt} - 1) \cdot (1+d)} \tag{70}$$

The marginal energy-saving cost $MESC$ is equal to the ratio of the TAC to the energy savings ES at the drying section:

$$MESC = \frac{TAC}{ES} \tag{71}$$

Where the energy savings at the drying section corresponds to the sum of the steam savings for the steam cascade and the air heater and the electric power savings for the ventilation system and cylinder drives:

$$ES = -\Delta\dot{Q}_{s,tot} - \Delta\dot{Q}_{s,ah} - \Delta P_{ventilation} - \Delta P_{drives} \quad (72)$$

Similarly, the marginal CO_2-emissions reduction cost is the ratio of the TAC to the CO_2-emissions reduction:

$$MEMRC = \frac{TAC}{EMR_{CO2,tot}} \quad (73)$$

5.5 Energy-efficiency cost curves and CO_2-emissions reduction cost curves

In this section a methodology is proposed for the construction of energy-efficiency cost curves and MAC curves accounting for the measure's interactions based on model-based simulations of processes.

The challenge with the simulation results obtained in this work is that the energy savings and energy-saving costs are calculated for the combination of measures as a whole and thus need to be split between the different measures.
For that, after choosing the combination of measures to be represented in an energy-efficiency cost curve, the order of measure calculation has to be defined. In order to avoid drawing a completely distorted picture of the contribution of individual measures this calculation sequence is defined here to be the same as the sequence presented in the context of process integration (see Figure 4.1 in section 4.1.3), i.e. in the opposite direction of the energy flow but following the calculation sequence of the simulation model, placing measures which deal with a reduction of the heat demand before those which concern heat recovery and waste heat recovery.
Then the simulation is successively run for the first measure m_1, for the combination of measures $m_1 + m_2$, for the combination $m_1 + m_2 + m_3$, etc. until the combination of all measures has been simulated.

Afterwards, as illustrated in Figure 5.10, the energy savings attributed to a specific measure m are calculated for each measure (apart from m_1) as the difference between the energy savings calculated for the combination of measures where m is the last measure in the sequence and the energy savings assessed for the combination of measures which includes the same measures apart from measure m:

$$ES_m = ES_{measure\ combination} - ES_{measure\ combination\ excluding\ m} \quad (74)$$

Similarly, the total annualized costs for a specific measure are given by:

$$TAC_m = TAC_{measure\ combination} - TAC_{measure\ combination\ excluding\ m} \quad (75)$$

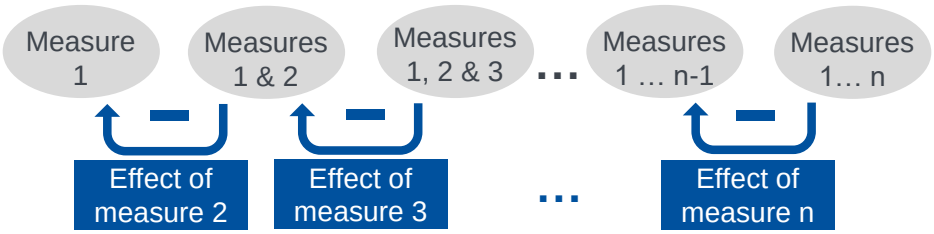

Figure 5.10: Evaluation of the effect of individual measures within a group of measures

Finally, the marginal energy-saving cost of the measure m is obtained:

$$MESC_m = \frac{TAC_m}{ES_m} \tag{76}$$

Since energy-efficiency and MAC curves are constructed by assuming that the measures will be implemented in cost order (Chan et al. 2016), the measures are ranked in terms of growing order of the marginal energy-saving cost and the energy-efficiency cost curve is built using the disaggregated values for the energy savings and energy-saving cost of the individual measures. Exactly the same methodology is applicable for the construction of MAC curves where the CO_2-emission reduction and the marginal CO_2-emission avoidance costs are determined for a measure m:

$$EMR_m = EMR_{measure\ combination} - EMR_{measure\ combination\ excluding\ m} \tag{77}$$

$$MEMRC_m = \frac{TAC_m}{EMR_m} \tag{78}$$

A very important note regarding the construction of the curves using the methodology described above is that the calculation sequence is not necessarily equivalent to the ranking order used when building the energy-efficiency cost and marginal abatement cost curves.
Since the calculation sequence determines the disaggregated values for individual measures, it is therefore highly recommended to indicate the calculation sequence on the curves (e.g. by numbering according to the calculation order). Furthermore, keeping in mind the whole set of measures for which a curve is generated is essential when consulting those curves, since from the measure m where the calculation and "implementation" sequence differ, the values obtained for the measure m are dependent on measures located at the right of this measure on the curves. A cropped vision of the curves, for example by looking only at the first "cheapest" measures, would lead to wrong assessments of the energy savings or CO_2-emissions reduction potentials and related saving costs of those measures, if their ranking order and calculation sequence differs.
Those aspects are illustrated in Figure 5.11. In both curves, the measure indicated by number 2 acts before measure 3 (when considering the opposite direction to the energy flow) and its effect is therefore calculated before measure 3. However, since the calculated energy-saving cost is lower for measure 2 than for measure 3, measure 2 is placed after measure 3 in the MESCC.
Furthermore, the energy savings and marginal energy-saving cost of measure 3 differ between the left and right figures, despite measure 3 being the same. The reason is that the measure

placed before measure 3 in the calculation sequence but after it in the ranking order, is different in both figures (2a and 2b).
On the other hand, the energy savings and marginal energy-saving cost of measure 2 would remain same even if measure 3 is changed, since the results calculated for measure 2 depend only on those calculated for measure 1.

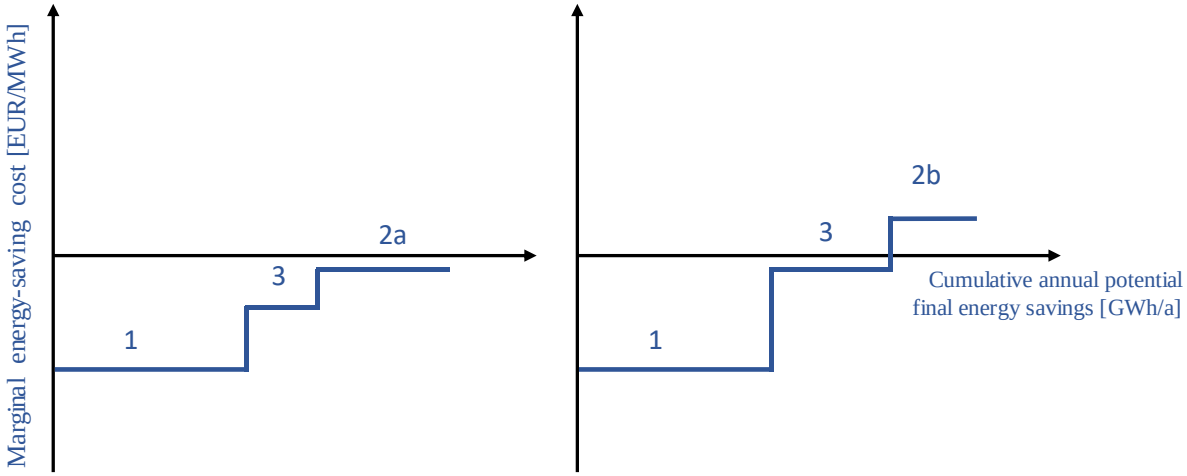

Figure 5.11: Differences in ranking order (from left to right) and calculation sequence (indicated by a number) impact the value of energy savings and marginal energy-saving costs of individual measures.

5.6 Framework application procedure

The overall application procedure of the developed framework is summarized in Figure 5.12. The first step consists in the collection of plant data and feeding the input database accordingly. In the second step the dryer model is calibrated to the plant data by adjusting the values of the tuning parameters to obtain the same humidity and temperature profiles as provided by the mill. In the next step relevant measures are identified, and their influence on process parameters is quantified and fed into the database. Measures which involve configurational changes are modeled and stored as separate modules. Mutually exclusive measures are identified and set as such in the database.

Thereafter a list of possible measure permutations is generated and for each permutation impacting the humidity profiles the iteration described in section 5.2 is executed in order to obtain the same final humidity of the paper web as in the status quo, before the simulation of the other modules of the drying section is carried out. Finally, the economic assessment and the comparison between the different combinations of measures is performed.

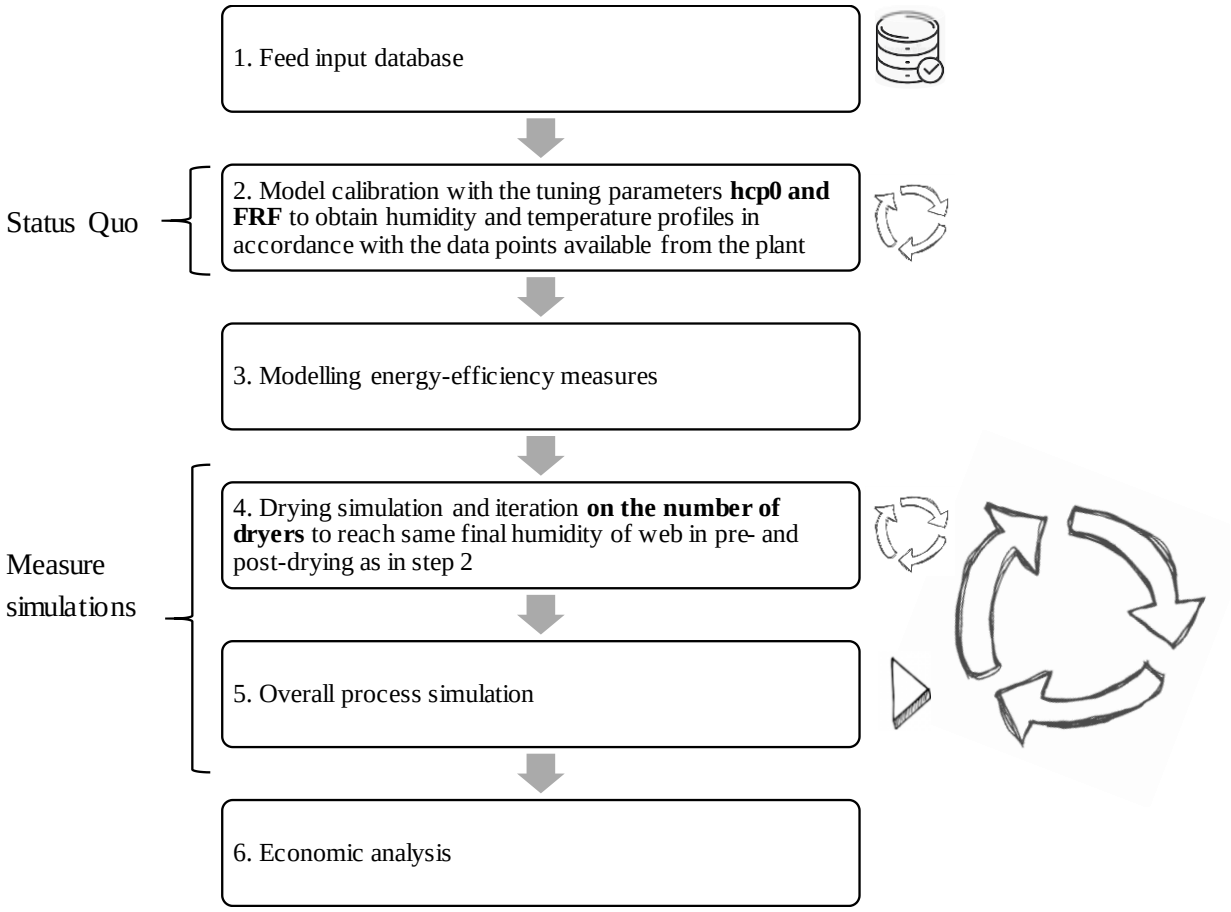

Figure 5.12: Application sequence of the developed framework. Source: own representation.

5.7 Implementation

The input database, which contains all the plant configuration data and parameters related to the energy-efficiency measures is stored in an Excel file. The model was implemented in Matlab R2016b, and the ODE 45 function was used to solve the non-linear differential system of the dryer model. The nonlinear programming solver fmincon was used to calibrate the model results for the temperature and humidity of paper web to the plant measurements by varying the values of certain fitting parameters within a specified range. Since the solver may return a local maximum, the calibration procedure was run multiple times with different initial values for the tuning parameters to gain confidence that a good solution was obtained. The Matlab function fzero which finds the root of a nonlinear function was used to determine the temperature of the hood supply air after heat recovery (Equation (54)).

6 Framework application to the drying section of a German paper mill

The application of the developed framework to the drying section of a German paper mill is demonstrated in this Chapter. First the analysed drying section is described, followed by the results of the model calibration and the selection of relevant energy-efficiency measures.
The results of the measure assessment are presented in the next section, and their sensitivity on several key parameters is analysed and discussed in the final section.
Portions of this chapter were previously published and quoted verbatim from (Godin and Radgen 2021) with permission.

6.1 Description

The studied paper machine is located in Germany, it dates from the 1970's, and produces corrugated board and testliner in the range 90-190 g/m². The configuration of the paper machine and main parameter values are summarized in Table 6.1.

The same mathematical model was used for the vacuum rolls as for the extended free draws in the single-tier sections, since water is removed from both sides of the paper web, and one side is covered with the fabric.
The model was calibrated for a paper grammage of 120 g/m^2 based on the initial and final moisture content of the paper web and following values were obtained for the two fitting parameters: $h_{cp0} = 0.68\ \frac{kW}{m^2.K}$ and $FRF = 0.45$. The exact value of the heat transfer coefficient of steam h_{sc} was not known and set to 2.3 kW/m^2.K in accordance with literature values for this paper machine speed, condensate removal systems equipped with stationary siphons and dryers with spoiler bars (Ghodbanan et al. 2015).

The calculated temperature and humidity profiles of the paper web in the paper machine after model calibration are shown in Figure 6.1. The single-tier sections of the drying sections are characterized by a lower drying rate (i.e. a lower slope of the humidity curve) and a greater distance between two successive temperature peaks, since the paper web is not heated on the vacuum rolls.

Under the current operating conditions, the humidity of hood exhaust air is calculated to be equal to 0.084 kg_{water}/kg_{dryair} and is therefore only slightly below the maximal 0.086 kg_{water}/kg_{dryair} tolerated for the currently installed hood which has a dew point temperature of 50°C.
The minimum leakage air flow required to avoid condensation in the current hood is equal to 79.2 kg_{air}/s which is 6.6 kg_{air}/s below the current level and equivalent to reducing the current leakage to exhaust air ratio from 0.5 to 0.48.

Table 6.1: Configuration of the analysed paper mill and main parameter values

Parameter	**Value**
Range of: Produced grammage Paper machine speed	90-190 g/m^2 700-1050 m/min
Paper web width	5.11 m
Paper web moisture content	46.5% / 28% (beginning of pre-/post-drying sections) 7.5±1.5% (end of pre-/post-drying sections)
Paper web temperature	42 °C (initial) 40 °C (after film press)
Cylinder configuration in pre-drying section	34 cylinders grouped into 3 steam groups #1-6: 240 kPa // #7-14: 340 kPa // #15-34: 400 kPa Single-tier configuration until the 10th cylinder: in total 9 vacuum rolls are located after each of the first 9 cylinders
Cylinder configuration in post-drying section	20 cylinders grouped into 3 steam groups #35-38: 210 kPa // #39-42: 240 kPa // #43-54: 260 kPa Single-tier configuration until the 38th cylinder: in total 3 vacuum rolls are located after the 35th, 36th and 37th cylinders
Dryer material, diameter, thickness, conductivity and wrapping angle of paper web	Cast iron // 1.5 m // 0.03 m // 43 W/m K // 218°
Diameter of vacuum cylinders	1.25 m
Length of free draw sections	1.37 m
Type of condensate removal system, value of blow-through coefficient, condensate heat transfer coefficient and excess steam factor	Stationary siphons and spoiler bars in the dryers // 0.15 // 2.3 kW/m^2 K // 1.05
Type of hood, dew point temperature, leakage air ratio, thermal loss factor and perimeter	Semi-closed hood // 50 °C // 0.5 // 2% // 160 m
Heat recovery system, efficiency of heat exchangers and air heater	Energy from hot hood air and condensate from the steam cascade is partially recovered for air preheating, 95%
Average ambient temperature and air moisture	10 °C // 0.006 $kg_{water}/kg_{dry\ air}$
Room air temperature and moisture	40 °C // 0.039 $kg_{water}/kg_{dry\ air}$

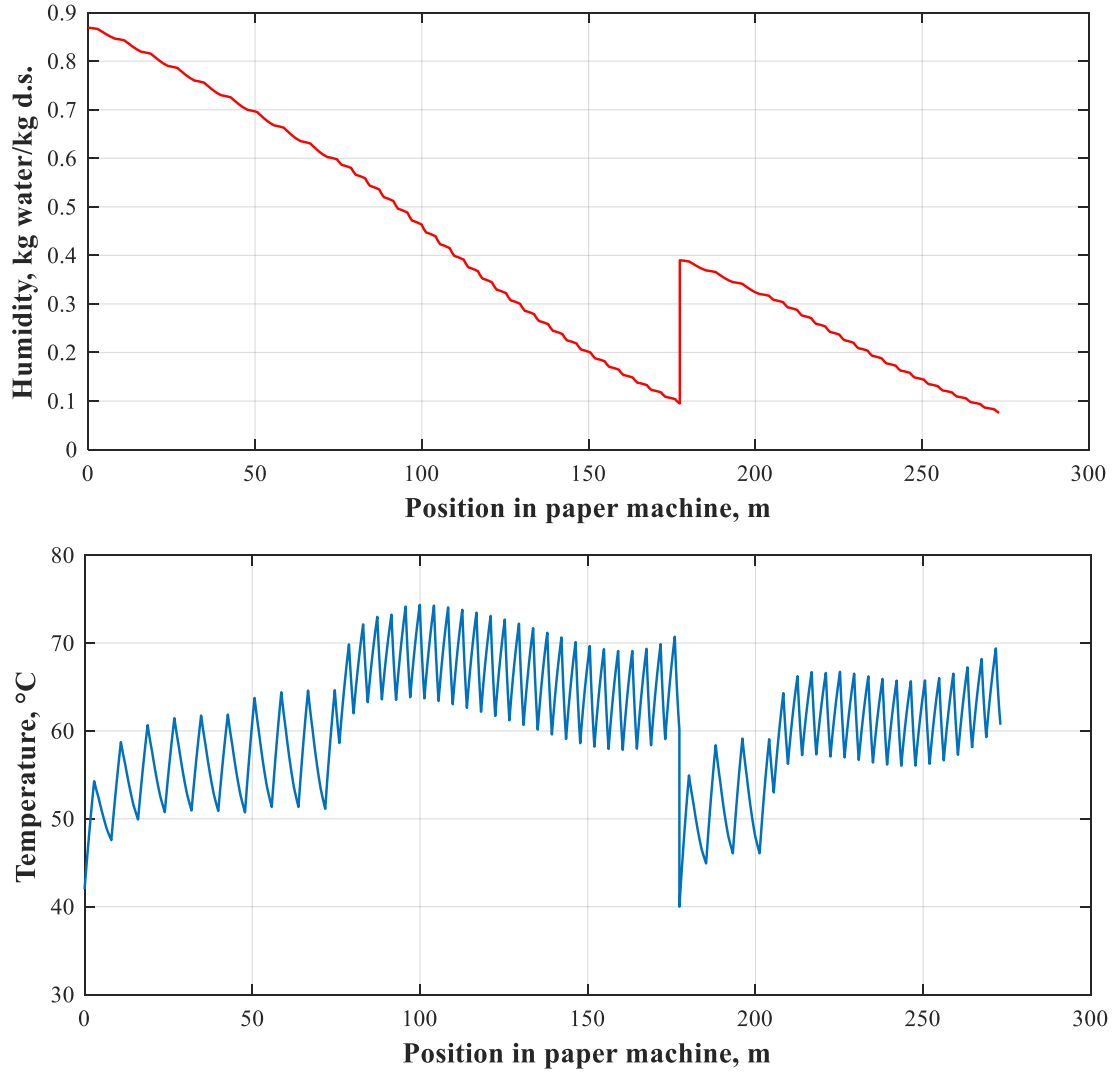

Figure 6.1: Calculated humidity (upper chart) and temperature (lower chart) profiles of the paper web in the paper machine. Source: own representation.

6.2 Energy demand of the analysed drying section

The resulting steam demand calculated for the production of 37.9 t_{paper}/hr of a basis weight of 120 g/m^2 at a paper machine speed of 1030 m/min is equal to 36.7 MW, which is 9 % lower than the 40.1 MW supplied from the boiler to the paper machine according to plant data. This difference is due to the steam consumption for the conditioning of the starch solution and energy losses in the steam supply system between the boiler and the paper machine. Since the calculated amount of evaporated water is equal to 38.2 t_{water}/hr, the specific steam consumption per unit of water evaporated in the current configuration of the drying section amounts to 1.35 $kg_{steam}/kg_{water\ evaporated}$.

A Sankey Diagram featuring the current energy flows in the analyzed drying section is presented in Figure 6.2. In the current state, large amounts of energy are released to the atmosphere in the form of humid saturated air at a temperature of 50 °C. The condensate exiting from the steam cascade and the air heater are conducted back to the boiler. The current electric power consumption of fans and cylinder drives is equal to 0.53 and 2.41 MW_{el} (0.05 and 0.23 GJ_{el}/t_{paper}) respectively.

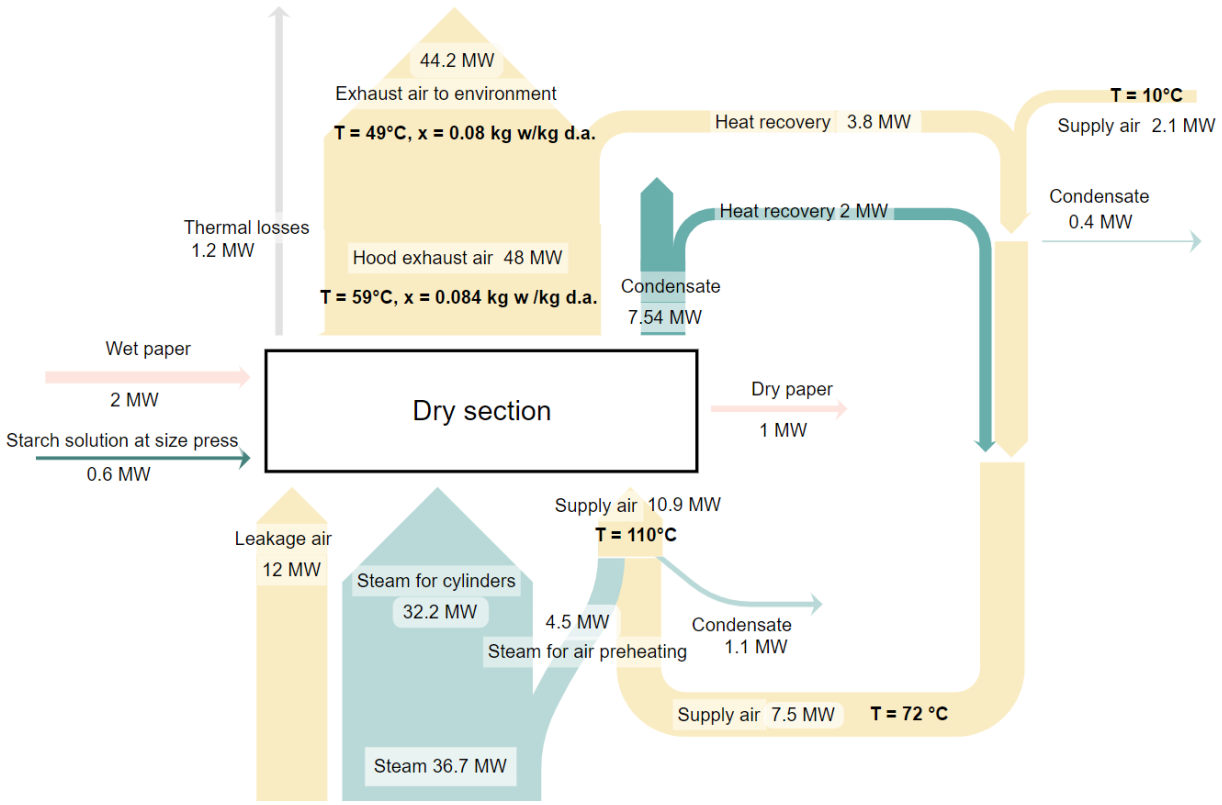

Figure 6.2: Energy flow diagram of the drying section of a German paper mill prior to optimization. Source: Diagram made with the Software Product Sankey Flow Show.

6.3 Selected energy-efficiency measures

Site-relevant measures were identified through discussions with the energy manager of the paper mill and paper machine manufacturers and are represented in Figure 6.3.

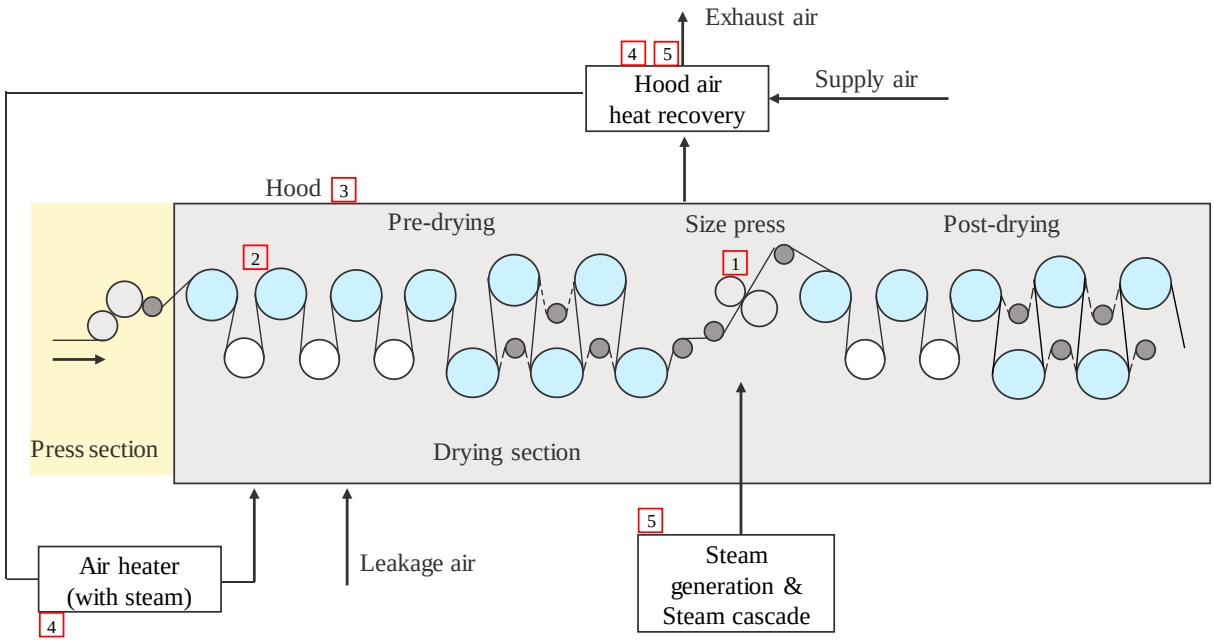

Figure 6.3: Location of the selected energy-efficiency measures at the analysed drying section.

A central measure (indicated with number 1) aims to decrease the amount of water to be removed in the drying section through the application of a starch solution with a higher solid content than the current 16% obtained through film sizing. New technologies like curtain sizing (Valmet 2019) allow the application of the starch solution with dry solid contents up to 40%. An increase of the starch consistency to 37.5% is considered in the present case, which decreases the water share after sizing from 0.39 $kg_{water}/kg_{dry\ solid}$ to 0.175 $kg_{water}/kg_{dry\ solid}$.
The replacement of cast iron dryers with steel cylinders (2) improves the heat transfer between the steam and the paper web, because of the higher thermal conductivity of steel cylinders and the lower thickness of the dryer shell.
The current semi-closed hood has a high exhaust to leakage air ratio and a low operation dew point, which leads to a high heat demand for air heating, high power consumption for the air circulation, and reduces the heat recovery potential (Laurijssen et al. 2010). Thus, one of the measures in the present analysis consists in closing the hood around the drying section (3). In the process model, the mass flow of hood supply air is then determined based on the maximal absolute humidity of air corresponding to the new dew point and leakage to exhaust air ratio.

Key information on the presented measures is summarized in Table 6.2. The model parameters which are directly impacted by the implementation of those measures are specified, as well as the values of the parameters after measure implementation.

Table 6.2: Key information on several site-relevant energy-efficiency measures

Measure	Directly impacted parameters	New value	Reference
Higher starch concentration in the solution applied at size press (1)	Inlet paper humidity at post-drying section	0.175 $kg_{water}/kg_{dry\ solid}$	(Laurijssen et al. 2010), (Valmet 2019)
Replacement of cast iron cylinders with steel cylinders (2)	Thickness Thermal conductivity	0.02 m 48 W/m K	(Stenström 2020), (Voith 2019)
Enclosed paper machine hood with higher dew point (3)	Leakage air ratio Dew point temperature	0.1[12] 63 °C	(Laurijssen et al. 2010), (Karlsson and Oyj 2000)

Furthermore, the integration of compression heat pumps to recover a share of the energy currently released to the atmosphere is analyzed for two distinct applications: heating the air to the required hood temperature (4) and generating steam for the dryers (5). The heat pump integration for both applications is schematically represented in Figure 6.4 and Figure 6.5.

[12] Best value for a very high-performance closed hood

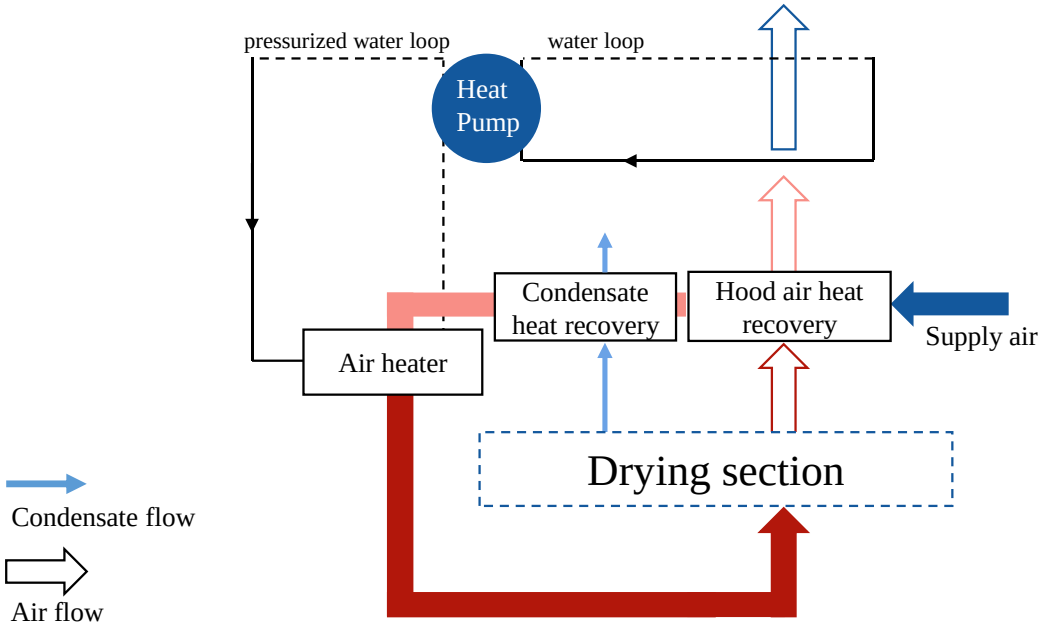

Figure 6.4: Heat pump integration to heat hood air. Source: (Godin and Radgen 2021), reprinted with permission.

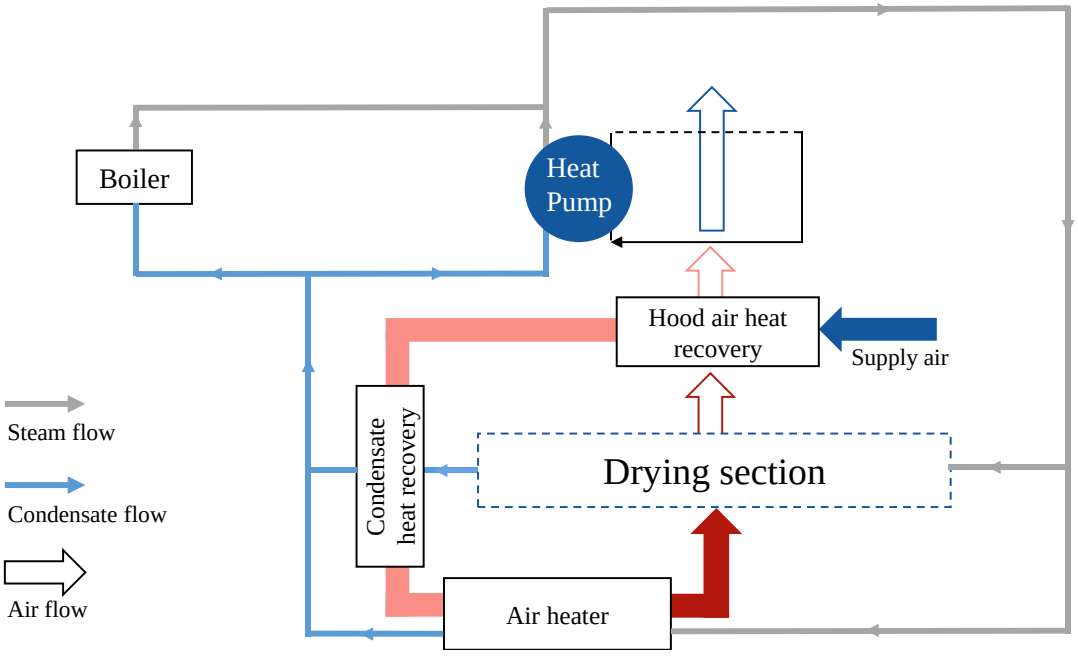

Figure 6.5: Heat pump integration to generate steam. Source: (Godin and Radgen 2021), reprinted with permission.

Additional water loops are used to harvest heat from the exhaust air, and, in the case of air heating, to transfer the heat generated with the heat pump to the supply air. The target temperature is 110 °C for the hood supply air and set to 150 °C for the generated steam since 80% of the energy is used for the higher-pressure steam groups (260, 340 and 400 kPa). A ΔT of 5 K is assumed at the heat exchangers between the inlet temperature of the hot stream and outlet temperature of the cold stream.

The coefficient of performance (COP) of the heat pump is calculated by multiplying the Carnot COP by the secondary efficiency:

$$COP_{real} = \eta_{2nd}\, COP_{Carnot}$$

Where the secondary efficiency η_{2nd} is set to 0.5[13] and the Carnot COP is evaluated with the temperature lift between the target heat sink temperature (of the water loop in the case of air heating) and the temperature of the heat source (water loop on air side) after the heat pump:

$$COP_{Carnot}[-] = \frac{T_{sink,hot}\,[K]}{T_{sink,hot}[K] - T_{source,cold}[K]}$$

In the case of the heat pump used for air heating, the energy to be provided by the heat pump is small compared to the amounts of available waste heat and therefore sets a limitation to the size of the heat pump. In the case of steam generation there is no such limit to the size of the heat pump system, as the amount of steam required for the cylinders is very high. Thus, the mass flow of water used to harvest heat from hood exhaust air is set to 100 kg/s[14] as a constraint for the system size in that case.
In the present case, the two measures related to the use of heat pumps and the four fuel switching measures are set as mutually exclusive. A combined heat pump configuration in which the extracted energy from the hood exhaust air is used successively by two heat pumps for air heating and steam generation is stored in a separate module (as an individual option), since the temperature of the heat source used by the heat pump in second position needs to be calculated anew.

6.4 Results

This section presents the effect of the individual and combined measures on the energy consumption of the analysed drying section (subsections 6.4.1 and 6.4.2). This is followed by the description of the economic assumptions (in 6.4.3) used for the cost analysis and the summary of its results as marginal energy-saving cost curves and marginal abatement cost curves (subsections 6.4.4 to 6.4.9).

6.4.1 Specific energy savings

The calculated steam and power savings for the implementation of individual measures and combinations of measures at the analyzed drying section are shown in Figure 6.6. The steam savings correspond to the amounts of inlet fresh steam saved (and not to the net heat savings).

[13] based on experimental results for a wide range of high temperature heat pumps presented by Arpagaus et al. 2018.

[14] This value is a result of a trade-off between a high amount of recovered waste heat and a not too low COP of the heat pump.

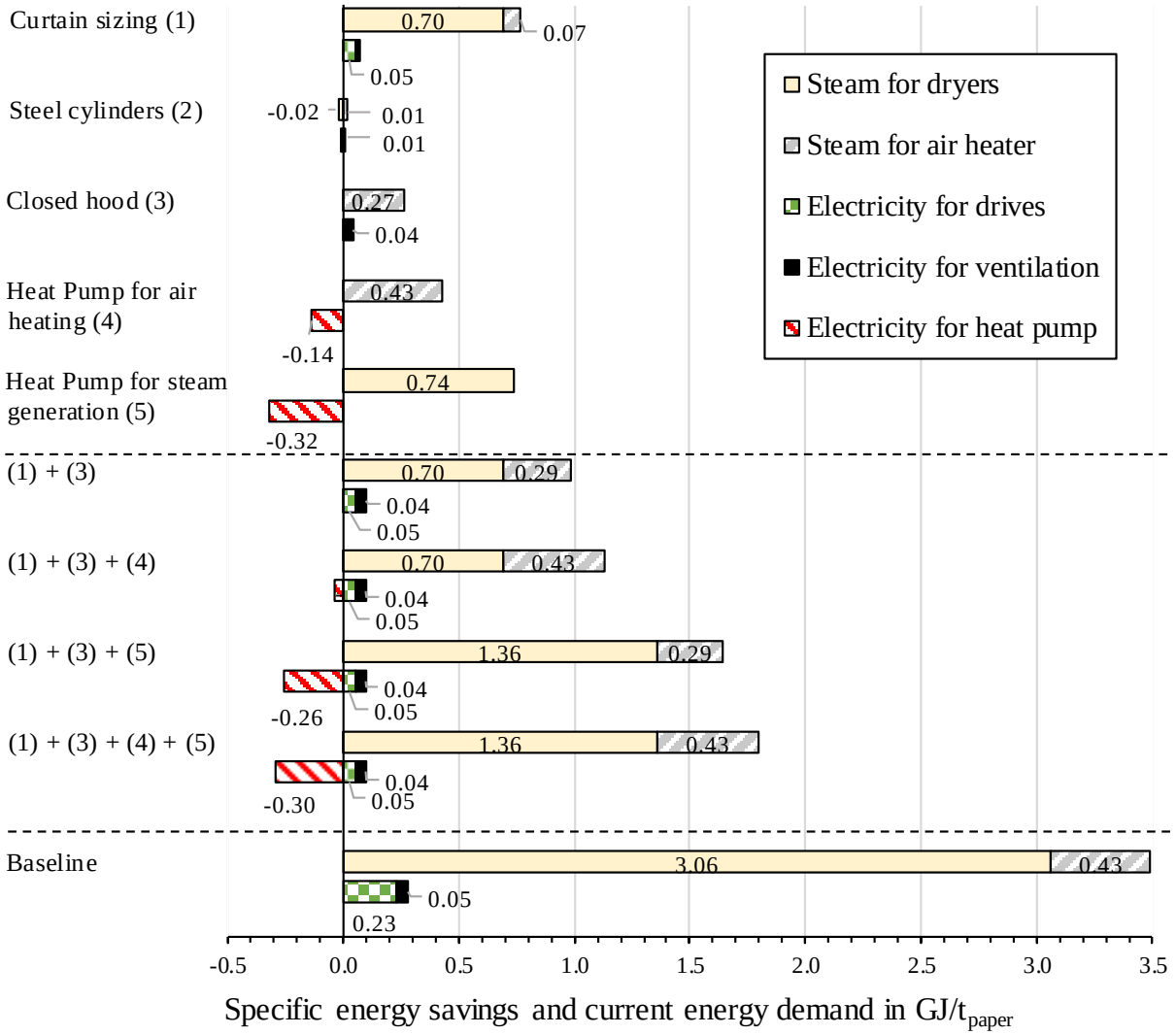

Figure 6.6: Specific steam and electricity savings for individual measures, combinations of measures, and current specific energy demand (indicated as Baseline).

The implementation of curtain sizing as a stand-alone measure leads to a reduction of the steam demand in the drying section by 22% (0.77 GJ$_{th}$/t$_{paper}$). These steam savings are accompanied by power savings, due to lower amounts of air to be circulated through the hood and the removal of 12 redundant drying cylinders in the post-drying section.

Closing the hood allows to reduce the steam demand for air heating by 62% (0.27 GJ$_{th}$/t$_{paper}$) and leads to overall steam savings of 8%. A further benefit of this measure is a reduction of 0.04 GJ$_{el}$/t$_{paper}$ in the power demand for ventilators due to lower mass flows of air in the hood.

Replacing the iron cast cylinders with steel cylinders leads to an improvement of the heat transfer coefficient of the dryer shell by 11.6% and thereby allows to shorten the pre-drying by two and the post-drying section by one cylinder. As a consequence, the power demand for cylinder drives is reduced by 5% (0.011 GJ$_{el}$/t$_{paper}$). On the other hand, the improved heat transfer leads to a small overall increase by 0.6% (0.02 GJ$_{th}$/t$_{paper}$) in the mass flows of steam required for the dryers (see equations (35) and (36)). The 2.8% savings in steam for air heating (0.012 GJ$_{th}$/t$_{paper}$) are the consequence of a by 3.8% higher final humidity of the product compared to the reference case, induced by the method for measure evaluation based on “cylinder removal”. Since the reduction in the number of required cylinders affects both the

pre- and the post-drying sections, this measure can be seen as an opportunity to improve the capacity of the paper machine by increasing the speed of the paper machine compared to the reference case, instead of shortening the drying sections. In the present case, a theoretical speed increase of 7% is calculated which corresponds to additional 2 tons of paper produced per hour. Since this measure leads to a small increase of the overall energy consumption of the drying section it is not included in the further analysis of the following sections.

The heat pump for air heating allows to substitute the steam for air heating and thereby leads to a reduction by 12% (0.43 GJ_{th}/t_{paper}) of the steam demand in the drying section. The temperature lift between the heat source[15] and the heat sink[16] is equal to 78.2°C which leads to a value of 2.48 for the COP, and therefore the steam savings are accompanied by an increase by 48.5% (0.14 GJ_{el}/t_{paper}) of the overall power demand as compared to the status quo.
The high steam savings of 0.74 GJ_{th}/t_{paper} assessed for the implementation of a heat pump for steam generation are accompanied by a high increase of power consumption (0.32 GJ_{el}/t_{paper}) due to a low COP of 1.87[17]. It is important to note that even more steam could be generated using the waste heat available in the exhaust air but that a limitation on this heat pump application was set in order to avoid a too low COP (see section 6.3).
The highest calculated steam savings (1.79 GJ_{th}/t_{paper}) are obtained for the implementation of curtain sizing, closing the hood and a combined heat pump configuration in which the extracted energy from the hood exhaust air is used by a heat pump for air heating and a heat pump for steam generation successively. A disaggregated representation of the steam and electricity savings respective to the different measures is provided as a waterfall chart in Figure 6.7. This combination of measures ((1) + (3) + (4) + (5)) will be noted as “All EEM” in the current and next sections, where EEM stand for energy-efficiency measure.

[15] water loop for the heat recovery from the hood exhaust air, 36.8°C

[16] water loop for heating the hood supply air, 115°C

[17] temperature lift of 113.2°C between the heat source (water loop for the heat recovery from the hood exhaust air, 36.8°C) and the heat sink (steam at 150°C)

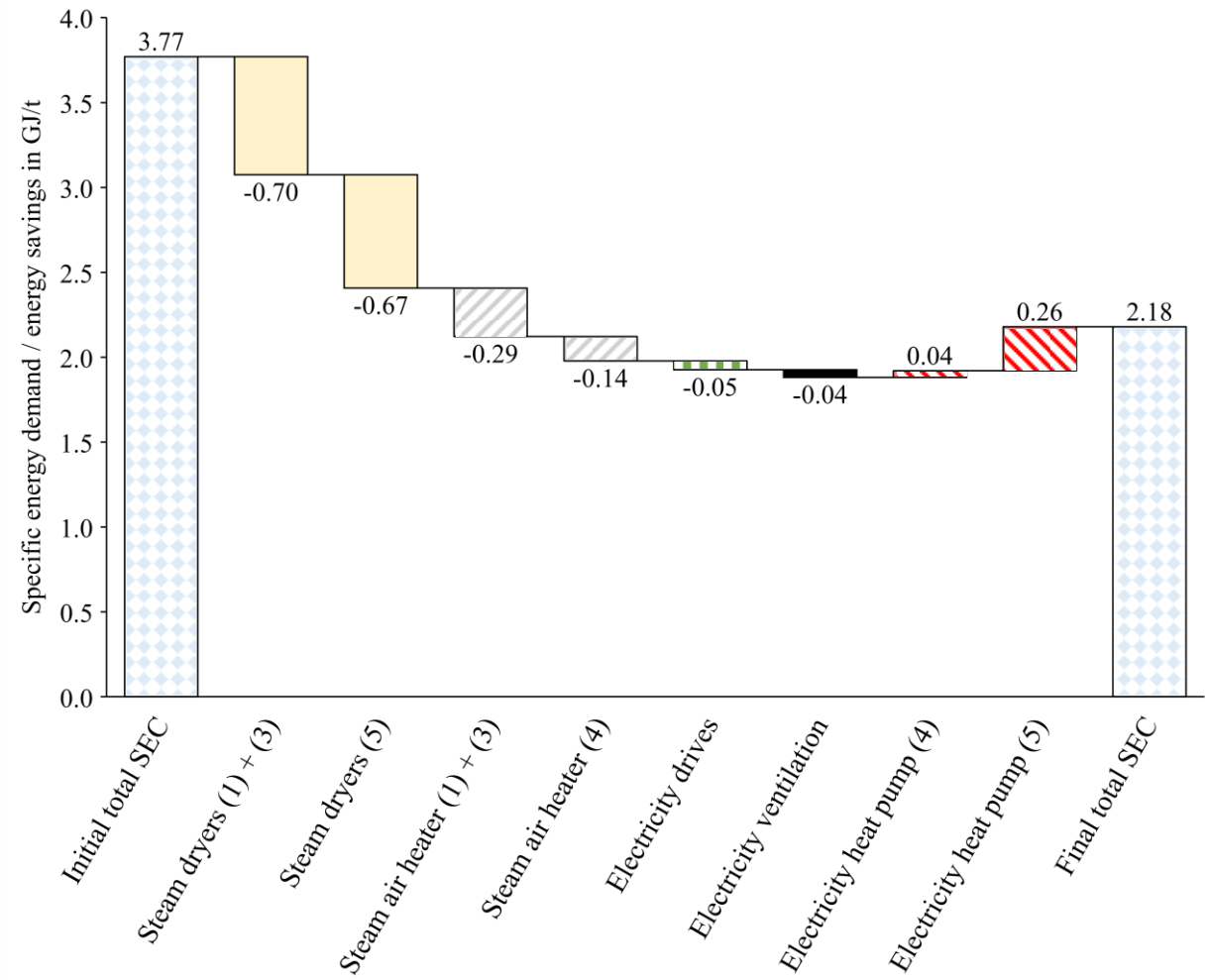

Figure 6.7: Waterfall chart of the calculated energy savings at the level of the energy consumers after implementing the combination of measures "All EEM" (curtain sizing, closure of the hood and heat pumps for air heating and steam generation)

6.4.2 Measure's interactions and energy savings

A comparison between the sum of energy savings of individual measures and their cumulative effect is drawn in Figure 6.8. The sum of individual effects is 4.9% and 13.3% higher than the cumulative value of the steam and power demand respectively, when considering both the curtain sizing and closed hood measures. Interactions at the level of the air mass flow in the hood are the reason for these differences. Even greater gaps are obtained when waste heat recovery measures are considered, since the closure of the hood reduces the heat to be supplied by the heat pump for air heating and leads to an increase of hood exhaust air temperature which improves the COP of the heat pumps.

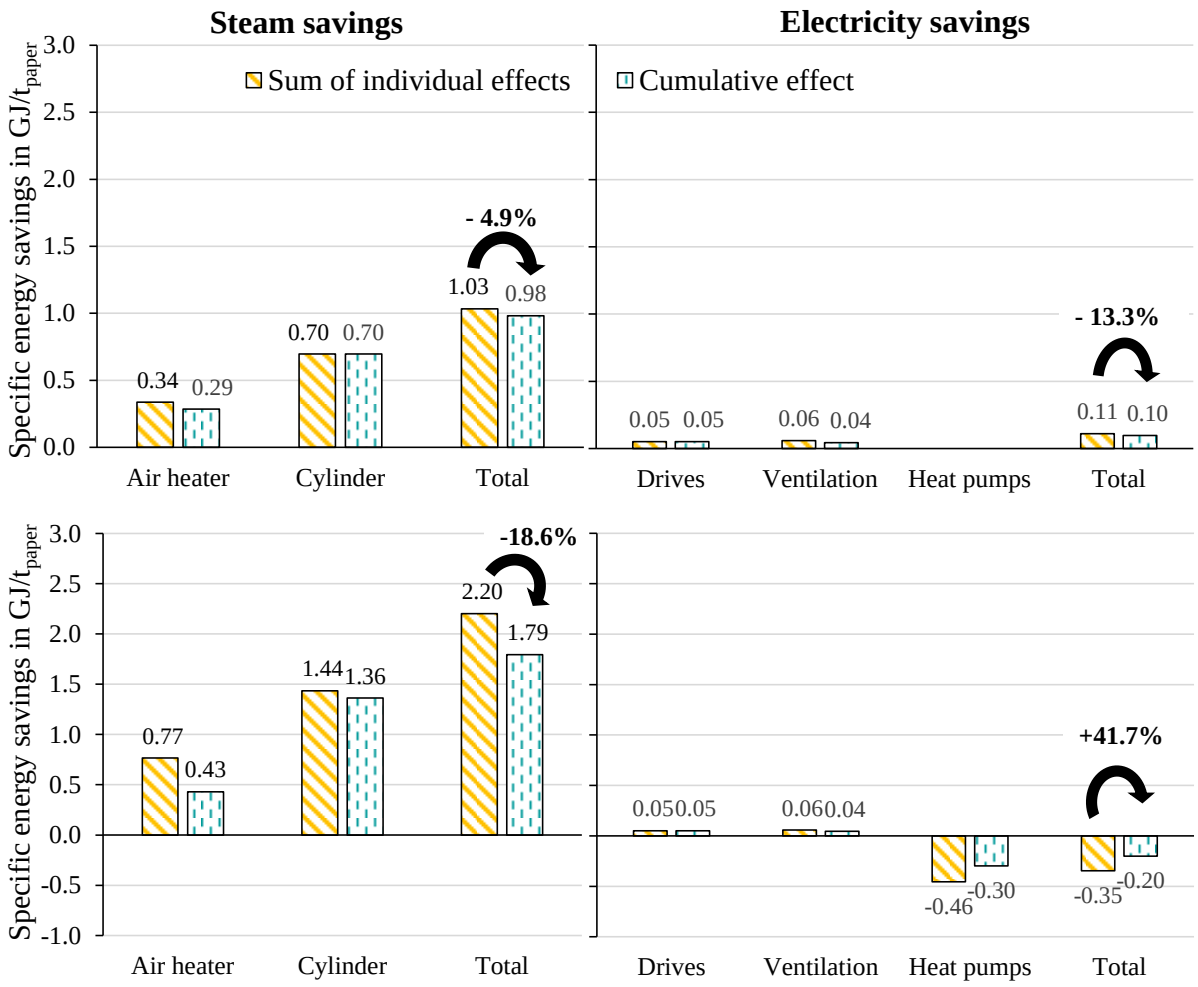

Figure 6.8: Comparison between the sum of energy savings of individual measures and the cumulative value for following combinations of measures: curtain sizing and closed hood (top), "All EEM" (bottom)

6.4.3 Economic parameters and scenario definition

In this section the assumptions on the price components used for the economic assessment of the measures and the scenarios defined to depict the evolution of the economic context are presented.

Information regarding the capital expenditures ($CAPEX$) of the different energy-efficiency measures were collected from manufacturers of the respective technologies and are summarized in Table B.1 in Appendix B. To cover decarbonisation to an extent that cannot be reached only via the implementation of energy efficiency measures, fuel switching options to different fuels were included in this work. The $CAPEX$ for heat generation technologies using those fuels were taken from economic studies or provided by manufacturers and are also presented in Table B.1.

Since only a small share of the electricity demand at the analyzed paper mill is currently covered with local generation, and other parts of the paper machine (as for example the press section) consume higher amount of electric power, the electricity demand of the drying section is considered to be covered with purchased electricity generated off-site. Given the current carbon neutrality objectives of the German government (BMU 2021), a linear decrease is assumed for the emission factor of the purchased electricity, until a value of 0 in 2045. The assumption on emission factors for fuel and electricity, and prices for fuel, electricity, and CO_2 for 2021 are

presented in Table B.2 in Appendix B. The hydrogen considered for fuel switching is green hydrogen produced by water electrolysis using electricity from renewable energy sources, and therefore its emission factor is set to zero. Lignite from neighboring mines is currently used at the paper mill to generate the steam required for the paper machine.
Since it was not possible to obtain reliable values for the non-energy- and CO_2- related savings in operating costs ($\Delta OPEX_{others}$) of the selected measures, the value of this variable is set to zero in the present case study. The economic lifetime of the measures is set to an average value of 20 years and is varied in the sensitivity analysis presented in section 6.5.2.

Three distinct scenarios were considered in the present work to account for different values of the discount rate and evolutions of the fuel and CO_2-prices until the year 2050 as shown in Table 6.3. Common to all three scenarios is the linear evolution of the CO_2- and fuel prices until 2050.
The main scenario called "Trend" is considered the most likely scenario for which the yearly increase of energy prices was set to 0.25% based on Schlesinger et al. (2014) and the discount rate to 15% based on Brunke (2017).
In the "Negative" scenario, which depicts a situation where the economic background has an unfavorable impact on the implementation of energy-efficiency and CO_2-emission reduction measures, no yearly increase of the fuel prices is assumed and high profitability requirements of industrial companies are reflected in a discount rate of 30%, which is at the higher end of the values collected in the literature for this parameter by Brunke (2017).
The "Positive" scenario describes a reverse situation where the economic background encourages the implementation of measures and in which the value of the discount rate is equal to 10% and fuel prices increase yearly by 1%.
A further distinction between scenarios is made for the value of the CO_2-price in 2050 which is set to about current levels, 100 EUR/t_{CO2} and 250 EUR/t_{CO2} for the Negative, Trend and Positive scenarios respectively.

Table 6.3: Scenario description

		Scenarios		
	Unit	Negative	Trend	Positive
Discount rate	%	30	15	10
Yearly price increase fuels	%/a	0	0.25	1
CO_2-price in 2050	EUR/t_{CO2}	55	100	250

6.4.4 Marginal energy-saving costs

A breakdown of the marginal energy-saving cost calculated according to the formulas presented in section 5.4 for each combination of measures is shown in Figure 6.9 for the trend scenario.

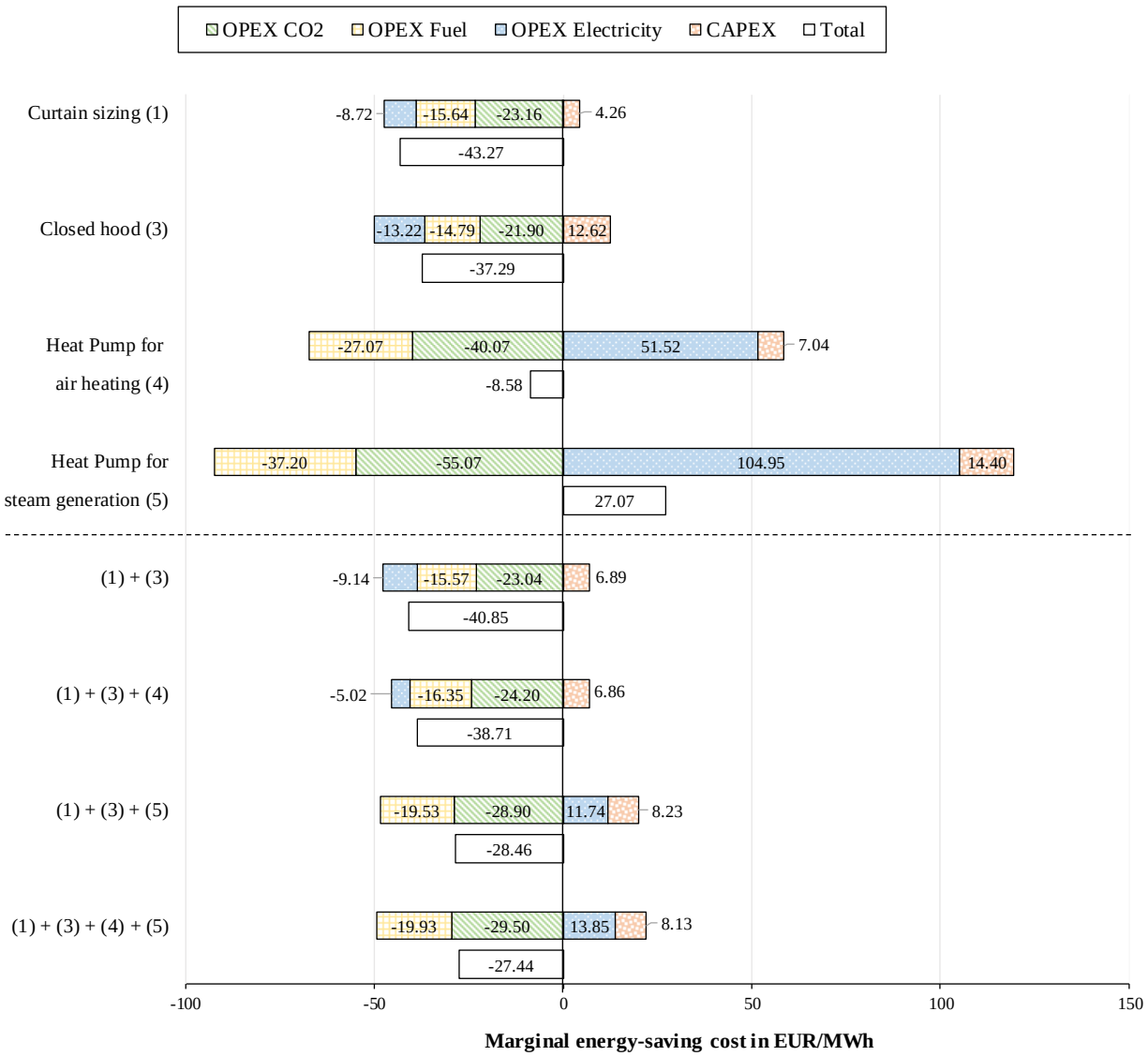

Figure 6.9: Breakdown of the calculated marginal energy-saving cost for different combinations of measures in the trend scenario

Although the $CAPEX$ does reduce the calculated cost savings for each combination of measures, its share in the energy-cost saving lies well below the share of the $OPEX$ related to fuel and electricity consumption and CO_2-emissions.

In most cases the CO_2-related cost constitutes the largest share of the marginal energy-saving cost, which shows that the CO_2-price, if it increases until 100 EUR/t_{CO2} in 2050, constitutes an important motivation for the implementation of energy-efficiency measures at the concerned site (due to the use of lignite to generate steam).

The cost savings related to the implementation of combinations of measures that involve waste heat recovery using heat pumps are lower than for the other energy-efficiency measures due to the additional costs related to the electric power consumption. Apart for the heat pump for steam generation considered individually, the negative costs (i.e. “savings”) outweigh the positive costs and the overall marginal energy-saving cost calculated over the measure lifetime is

negative. Despite the unfavorable electricity to natural gas price ratio (around 3.5), the heat pump for air heating is an economic measure due to the high cost savings of avoided CO_2-emissions.
Since the assumed economic lifetime of the measures of 20 years is higher than the typical value for heat pumps found in the literature (around 15 years), additional model runs were performed for average lifetimes of 10 and 15 years. Resulting marginal energy-saving costs are presented in Figure C.1 and Figure C.2 in Appendix C. Although its marginal energy-saving benefit is around 40% lower than for an assumed lifetime of 20 years, the heat pump for air heating remains a profitable measure, even in the case of a lifetime of 10 years. The reduction from 20 to 10 years of the economic lifetime of the heat pump for steam generation leads to a lower marginal energy-saving cost by 18%.

The marginal energy-saving costs obtained for the different measures when the starting year of implementation is set to 2030 (instead of 2021) are presented in Figure C.3 in Appendix C.
As expected since the assumed CO_2-price rises faster than the fuel prices (2,5%/a increase vs. 0,25%/a), implementing the measures starting from 2030 increases the cost benefit reached with the energy efficiency measures thanks to relatively higher CO_2-related cost savings. However, even in that case the heat pump for steam generation remains a non-economic measure. The $CAPEX$-related costs remain unchanged, since the discount rate and $CAPEX$ for individual measures are assumed to be same as when the starting year is set to 2021.
In order to determine under which economic conditions the use of a heat pump to generate steam is an economic measure, the marginal energy-saving cost was calculated for different values of the electricity to gas price ratio[18]. As shown in Figure 6.10, the break-even point is reached for a ratio of 2.6.
It is also important to highlight the impact of the CO_2-related $OPEX$ in the MESC of the heat pump measures, since the MESC for both heat pump configurations is positive over the whole range of electricity to gas price ratio when CO_2-related $OPEX$ are not accounted for in the calculation.

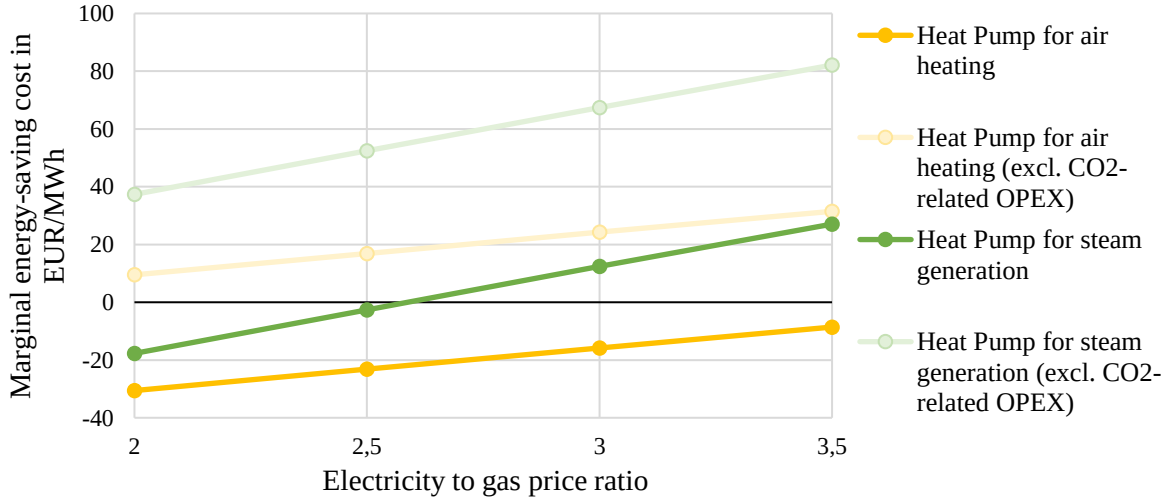

Figure 6.10: Impact of the electricity to gas price ratio on the marginal energy-saving cost related to the implementation of heat pump solutions.

[18] The gas price remained constant while the electricity price was varied. Electricity to gas price ratios of 2 and 3 correspond to electricity to coal price ratios of respectively 3,5 and 5,2.

6.4.5 Energy-efficiency cost curve

The energy-efficiency cost curves for the combination of measures with the highest energy savings ((1) + (3) + (4) + (5)) were built for all three defined scenarios according to the methodology presented in section 5.5 and are shown in Figure 6.11. The curtain sizing measure presents the highest energy saving potential of 65.2 GWh/a and the lowest energy-saving cost of -43.3 EUR/MWh in the trend scenario.
Whereas the calculated final energy savings related to the implementation of each measure remain same, the energy-saving cost of the measures varies greatly throughout the scenarios. The cost savings through measure implementation are higher for higher fuel, electricity, and CO_2-prices, and as a consequence, the marginal energy-saving costs for the positive scenario are 35% to 150% below the trend scenario depending on the measures. The MESC of the negative scenario lies 14% to 60% above the MESC from the trend scenario. Unlike the negative and the trend scenarios, the marginal energy-saving cost of the heat pump for steam generation in the positive scenario is negative, which leads to an increase of the economic potential from 91.46 (for the negative and trend scenarios) to 115.78 GWh/a.

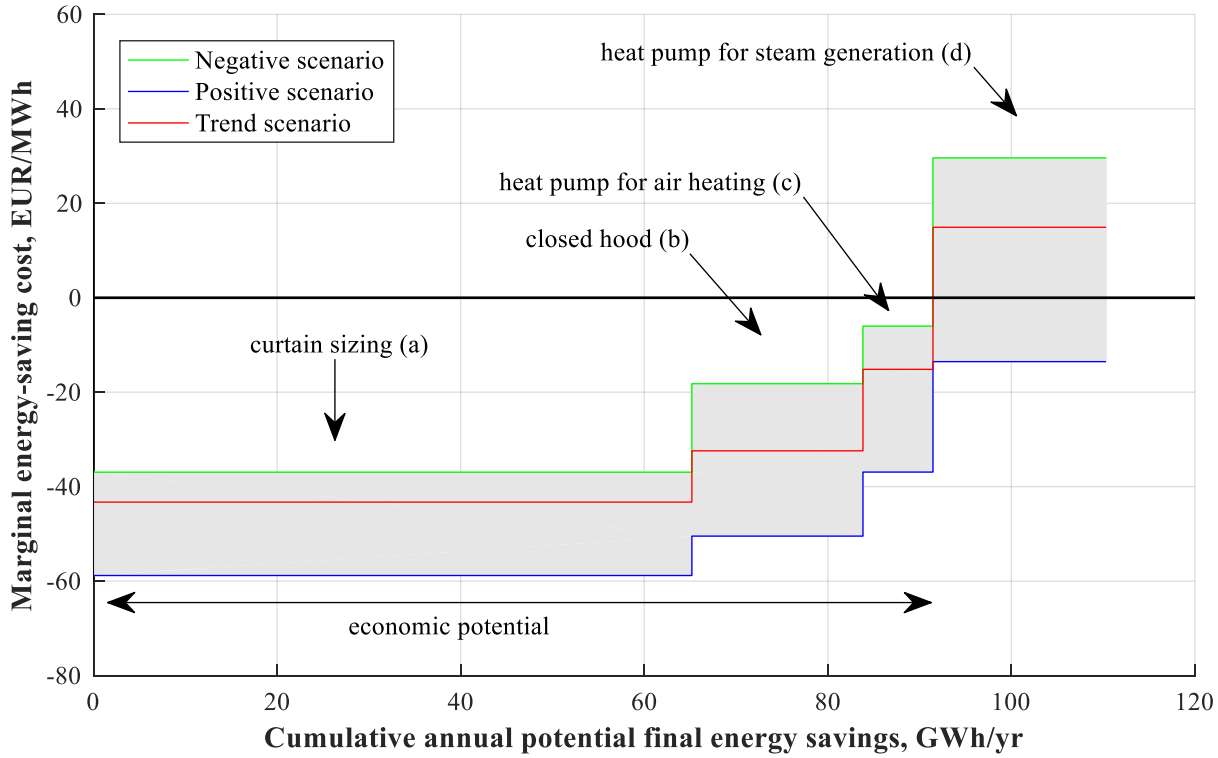

Figure 6.11: Energy-efficiency cost curves for the combination of measures "All EEM" for the three defined scenarios. The economic potential is indicated for the trend scenario. The letters in bracket indicate the calculation sequence.

6.4.6 Measure's interactions and energy-efficiency cost curve

In the continuity of section 6.4.2 in which a comparison was drawn between the cumulative effect and the sum of the individual effects of measures on the calculated energy savings, Figure 6.12 shows the energy-efficiency cost curve built in both cases for the combination of measures "All EEM". The sum of individual energy savings is higher than the cumulative value and the difference in the calculated annual energy saving potential increases for every additional

measure considered: it is equal to 5.15 GWh/a for the combination (1) + (3) and to 18.5 GWh/a for "All EEM".
On the other hand, no clear trend is observed for the marginal energy-saving cost since the cumulative MESC is 4.88 EUR/MWh higher for the closed hood measure than its individual value, but 6.7 EUR/MWh and 12.1 EUR/MWh lower for the heat pump for air heating and steam generation respectively. The latter difference is explained by the fact that closing the hood leads to a reduction of the heat to be supplied by the heat pump, and therefore to a cost reduction in the $OPEX$ for electricity.

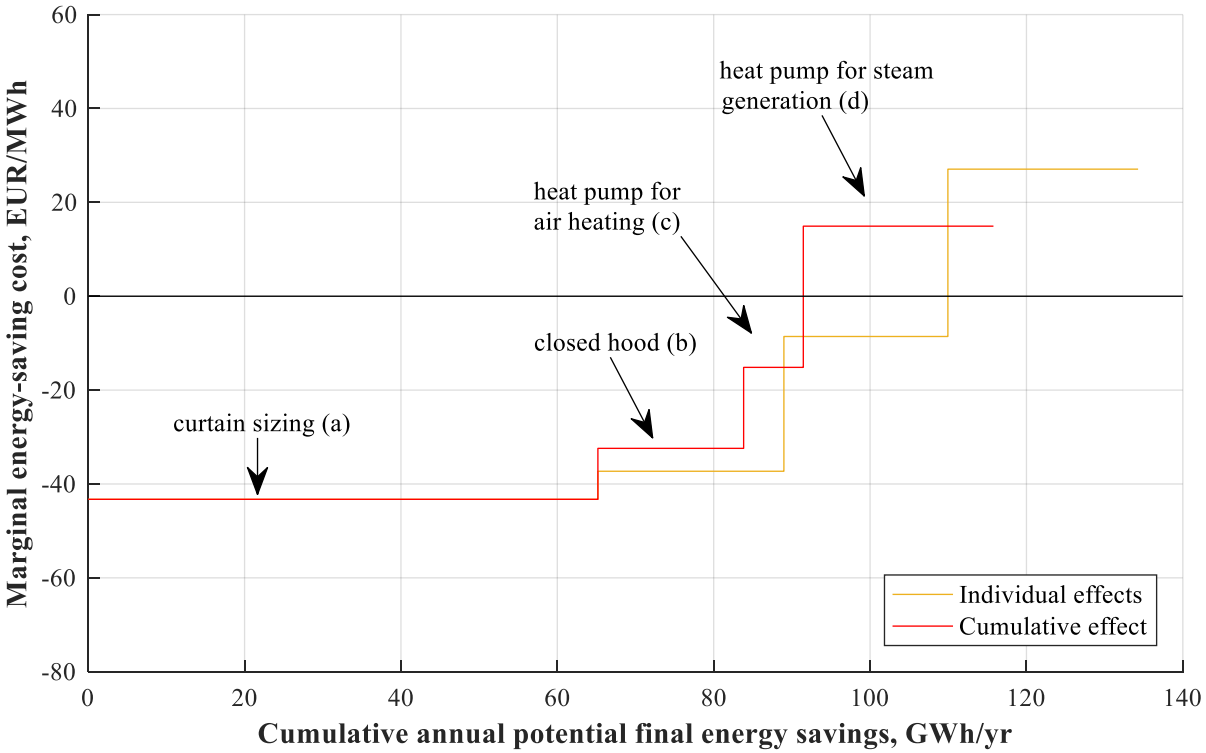

Figure 6.12: Energy-efficiency cost curves including the cumulative and individual effect of the combination of measures "All EEM" in the trend scenario. The letters in bracket indicate the calculation sequence.

6.4.7 Marginal CO_2-emissions reduction costs

The marginal energy-saving costs of the previously considered energy-efficiency measures were translated into CO_2-emissions reduction costs using the formulas presented in sections 5.3 and 5.4, and with the values for the emission factors, boiler efficiencies and prices presented in section 6.4.3. Furthermore, options for fuel switching to green hydrogen, natural gas, electricity, and biomass were added to the analysis to cover in-depth decarbonisation options.
The resulting marginal CO_2-emissions reduction costs for the different combinations of measures in the trend scenario are represented in Figure 6.13.
As expected, the marginal CO_2-emissions reduction cost is negative for all energy-efficiency combinations of measures and the CO_2-related $OPEX$ represents a large share of the cost savings in those cases.
The calculated marginal CO_2-emissions reduction cost of the individual fuel switching options is negative in the case of biomass and natural gas (-29.5 and -11.1 EUR/t_{CO2} respectively), and positive in the case of electricity and green hydrogen (293.3 and 268.5 EUR/t_{CO2}

respectively). In the case of biomass and natural gas the cost savings due to CO_2-emissions reduction coupled with the higher efficiency of heat generation from natural gas, outweigh the additional expenses due to the higher price of biomass and natural gas compared to lignite.
On the other hand, high additional costs are calculated in the case of a fuel switching to electricity and green hydrogen due to the very high assumed prices for electricity and hydrogen. As shown in Figure 6.14 a lower total CO_2-emissions reduction is reached through electrification than through fuel switch to green hydrogen. This is due to the indirect emissions of electricity production and the assumption that the emission factor of the electricity from the grid is only equal to zero from 2045 onwards. Thus, despite a 37.5% lower assumed fuel price for the switch to electricity as compared to green hydrogen, a higher marginal CO_2-emissions reduction cost is reached in the case of the electrification measure.
The implementation of energy-efficiency measures jointly to fuel switching options leads to a reduction in the marginal CO_2-emissions reduction cost ranging from 7.9 EUR/t_{CO2} for a switch to biomass to 247.1 EUR/t_{CO2} for a switch to electricity.
Interestingly, unlike in the individual consideration the calculated marginal CO_2-emissions reduction cost for the combination of measures "All EEM + Electricity" is equal to 46.2 EUR/t_{CO2} and thereby lower than the marginal cost of 108.6 EUR/t_{CO2} obtained for "All EEM + green hydrogen", since in this case the cumulative CO_2-emissions reduction is high enough for the fuel price difference to be determinant on the cost hierarchy.
On the other hand, the lower overall CO_2-emissions reduction for the combination of measures "All EEM + Natural" gas as compared to "All EEM + Biomass" leads to a lower marginal CO_2-emissions reduction cost (-42.5 vs -37.4 EUR/t_{CO2}) despite a 4% higher fuel price.

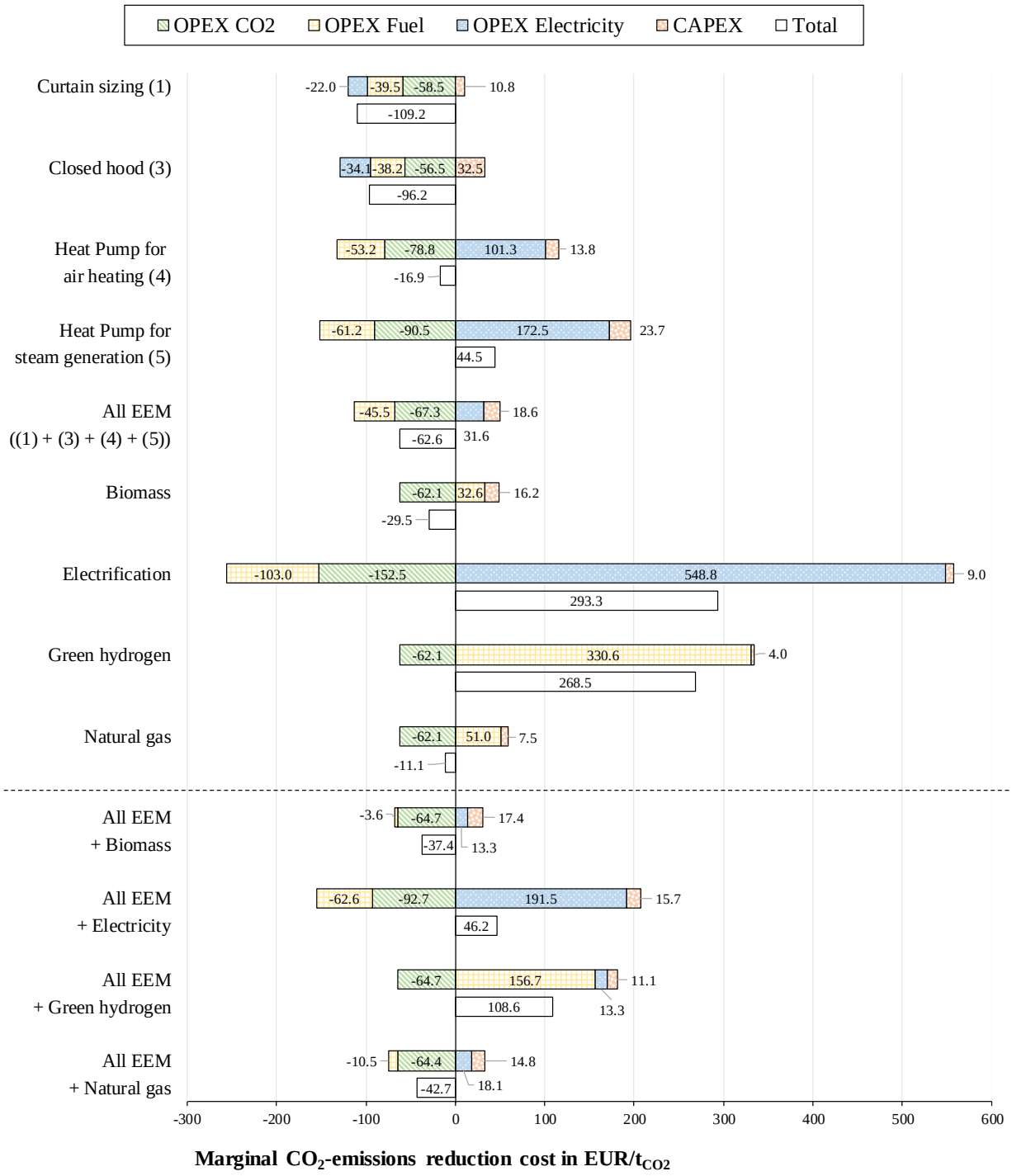

Figure 6.13: Breakdown of the calculated marginal CO_2-emissions reduction cost for different combinations of measures in the trend scenario.

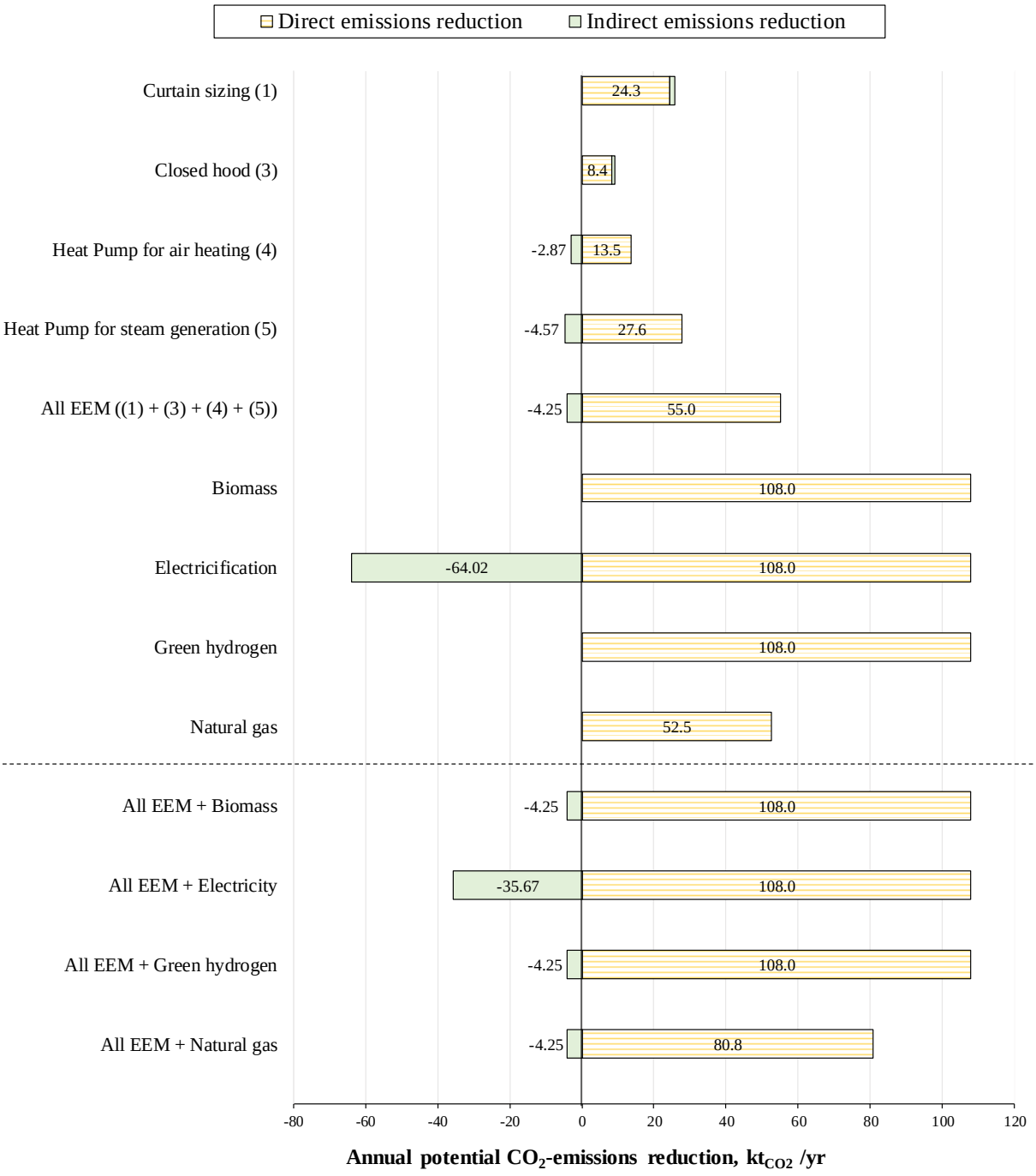

Figure 6.14: Calculated direct and indirect CO_2-emissions reduction for different combinations of measures in the trend scenario.

6.4.8 Marginal abatement cost curves

Marginal abatement cost curves for each fuel switching measure coupled with the combination of energy-efficiency measures with the highest energy savings are presented in Figure 6.15, Figure 6.16, Figure 6.17 and Figure 6.18 for all three previously defined scenarios.

The combinations of measures which include fuel switching to biomass and green hydrogen allow to reach a cumulative potential CO_2-emissions reduction of 103.7 t_{CO2}/a (equivalent to 0.33 kg_{CO2}/t_{paper}) which corresponds to a complete reduction of the energy-related emissions of the drying section. Through the electrification of steam generation and the fuel switching with natural gas coupled with energy efficiency measures, potential emissions reduction of 72.3 kt_{CO2}/a (i.e. 0.23 kg_{CO2}/t_{paper}) and 76.5 kt_{CO2}/a (i.e. 0.243 kg_{CO2}/t_{paper}) are obtained respectively. In the trend scenario the economic potential equals 36.9 kt_{CO2}/a (i.e. 0.12 kg_{CO2}/t_{paper}) in the case of the green hydrogen and electrification pathways since only energy-efficiency measures contribute to this potential, and 62.8 kt_{CO2}/a for the natural gas and 89.8 kt_{CO2}/a (i.e. 0.285 kg_{CO2}/t_{paper}) for the biomass.

For the biomass and natural gas pathways, the fuel switching measures are characterized by a lower marginal CO_2-emissions reduction cost than the heat pump for steam generation and are therefore placed to the left of this latter measure according to the common guidelines for building MAC curves. This allows a direct visualization of the economic potential related to these combinations of measures on one hand, but also brings risks of misinterpretation in the present case where the interactions between measures are accounted for: the CO_2-emissions reduction potential indicated for the fuel switching measures would in fact be higher if no heat pump for steam generation was included in the combination of measures, since more emissions would remain after the implementation of the other energy-efficiency measures, and therefore the potentials indicated for the fuel switching measures are meaningful only for the considered combination of measures and great care should be given when extracting information from the MAC curve.

As for the energy-saving cost curve, the cumulative annual potential CO_2-emissions reduction remains same for a specific combination of measures throughout the scenarios, but the emission reduction cost varies greatly. The cost savings are higher for higher fuel, electricity and CO_2-prices, and the calculated emission reduction cost for the positive scenario lies 36% to 145% below the trend scenario for the energy-efficiency measures. The marginal emission reduction cost of the negative scenario lies 14% to 60% above the trend scenario for the same measures. The marginal energy-saving cost of the heat pump for steam generation in the positive scenario is negative, unlike for the negative and trend scenario. Regarding the fuel switching measures, the difference between scenarios varies from low (-7% for the positive and +2.5% for the negative compared to the trend scenario) in the case of the fuel switching to green hydrogen, to very high for the switch to natural gas (-960% for the positive and +356% for the negative compared to the trend scenario).

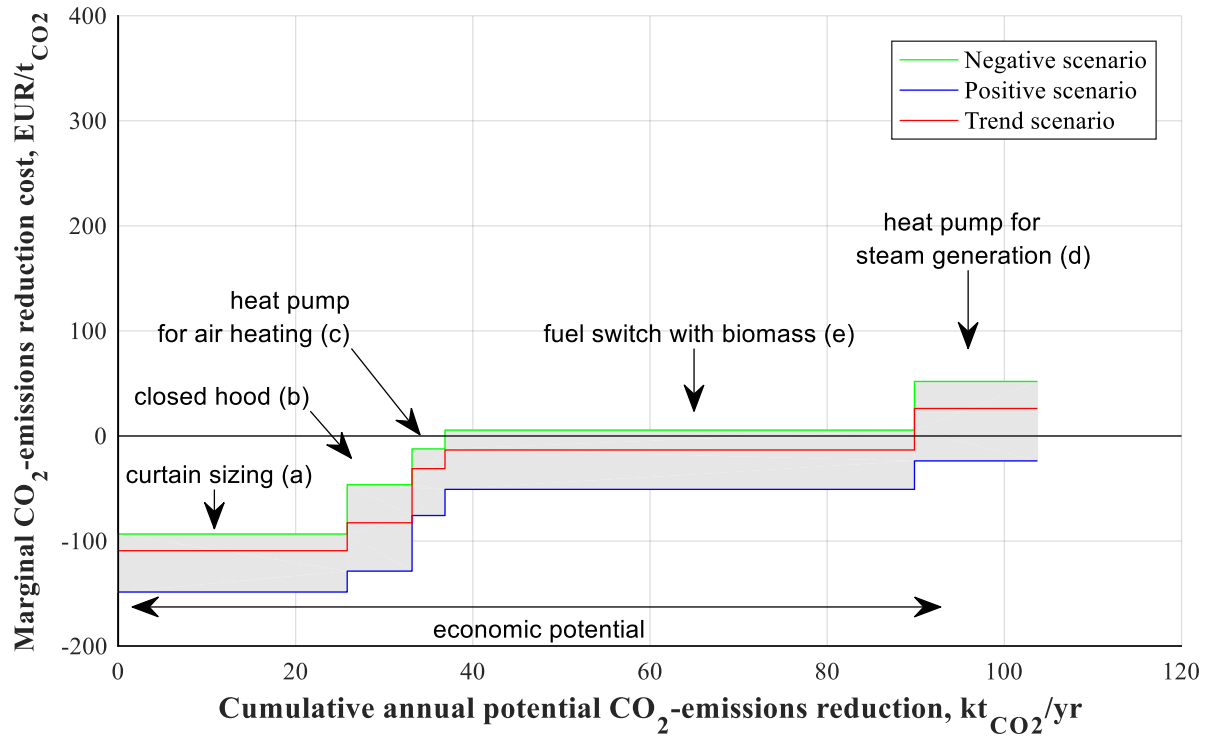

Figure 6.15: Marginal abatement cost curve of the analyzed drying section for the combination of measures "All EEM + fuel switching to biomass". The economic potential is indicated for the trend scenario. The letters in bracket indicate the calculation sequence.

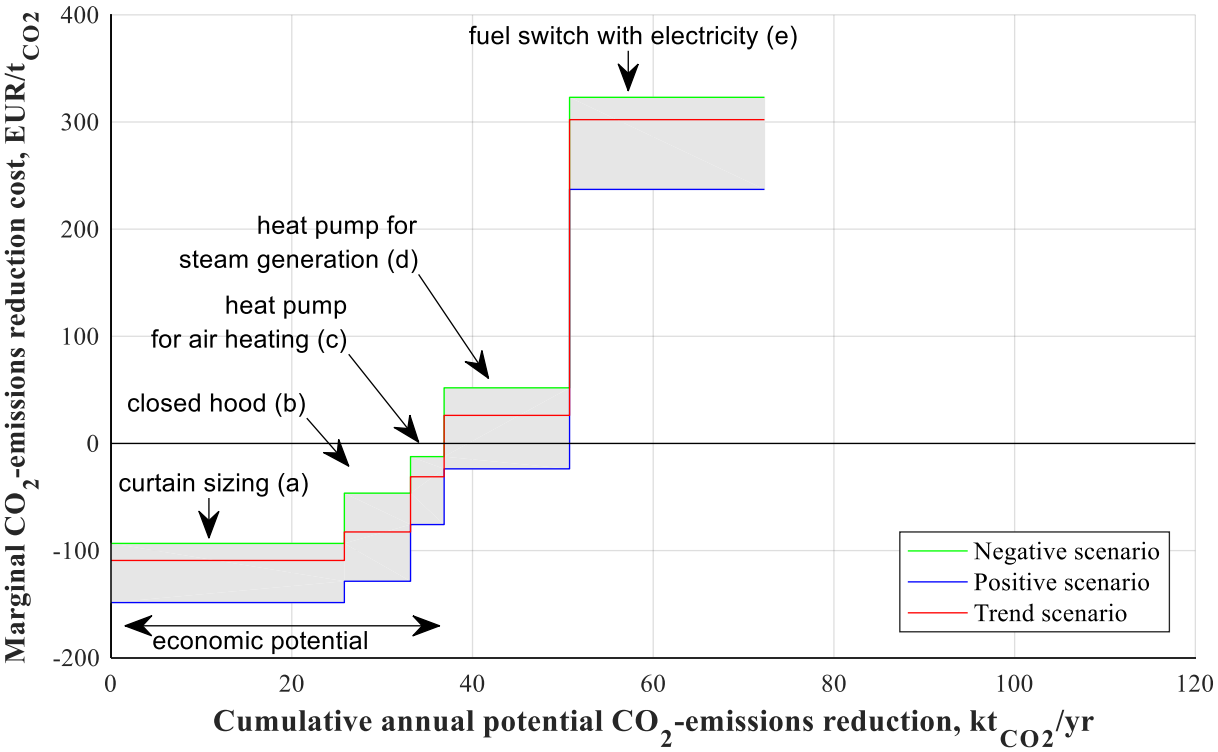

Figure 6.16: Marginal abatement cost curve of the analyzed drying section for the combination of measures "All EEM + electrification of steam generation". The economic potential is indicated for the trend scenario. The letters in bracket indicate the calculation sequence.

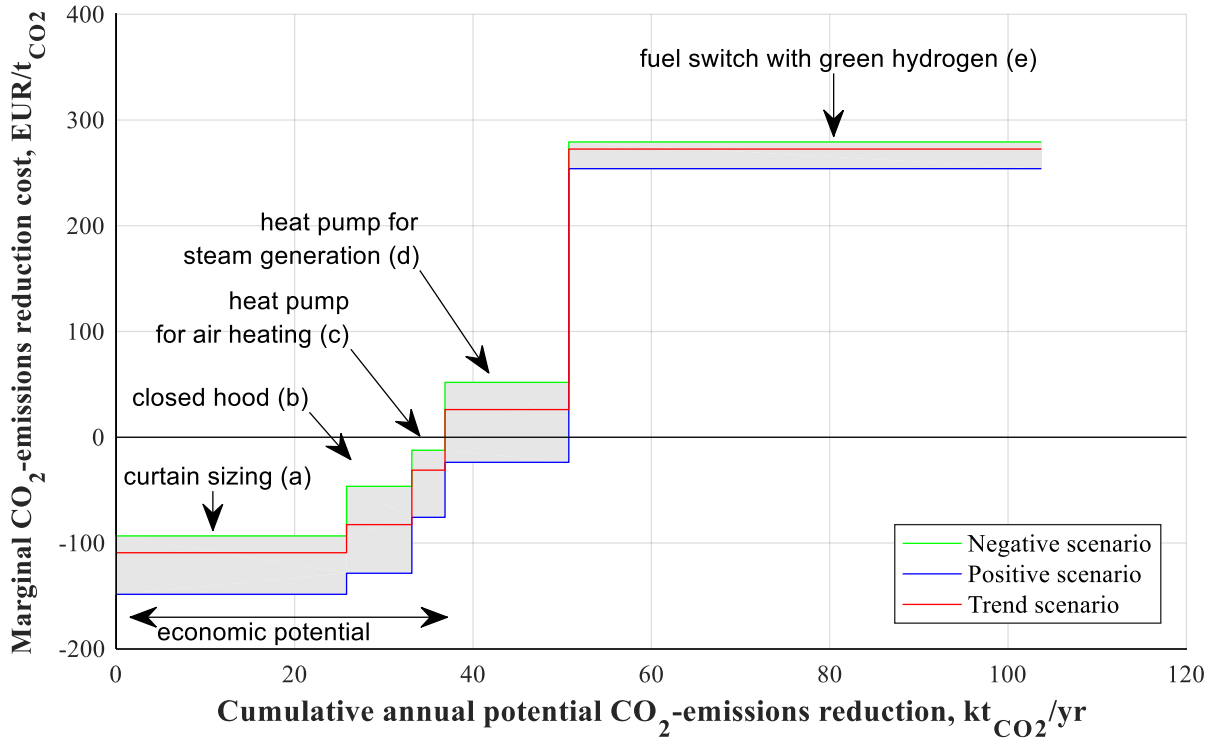

Figure 6.17: Marginal abatement cost curve of the analyzed drying section for the combination of measures "All EEM + fuel switching to green hydrogen". The economic potential is indicated for the trend scenario. The letters in bracket indicate the calculation sequence.

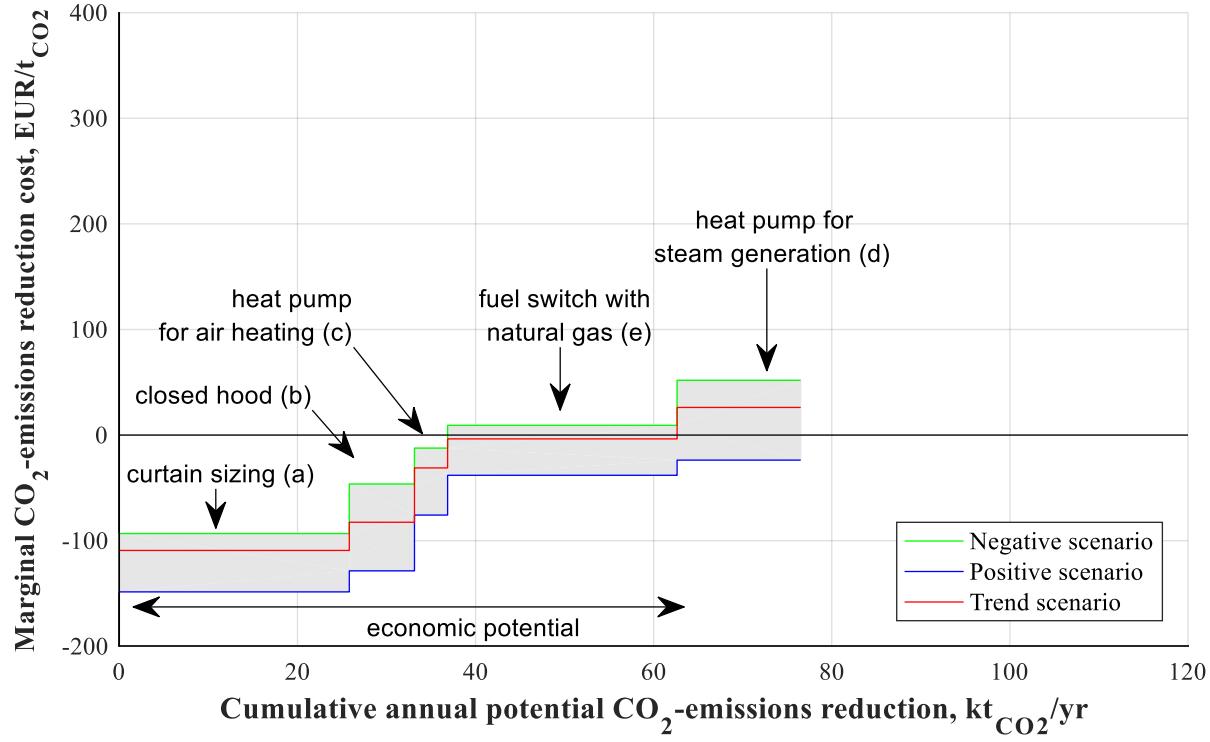

Figure 6.18: Marginal abatement cost curve of the analyzed drying section for the combination of measures "All EEM + fuel switching to natural gas". The economic potential is indicated for the trend scenario. The letters in bracket indicate the calculation sequence.

6.4.9 Measure's interactions and marginal abatement cost curves

The MACC for the cumulative and individual effects of the energy-efficiency measures combined with fuel switching to biomass, electricity, green hydrogen or natural gas are represented in Figure 6.19, Figure 6.20, Figure 6.21 and Figure 6.22 respectively.
The sum of the CO_2-emissions reduction potential for individual measures is systematically higher than the cumulative value for the same combination of measures, by 19.25% for "All EEM", 44.47% (32.16 kt_{CO2}/a) after adding the electrification of steam generation and 62.43% (64.76 kt_{CO2}/a) for "All EEM + the fuel switching to biomass or green hydrogen".

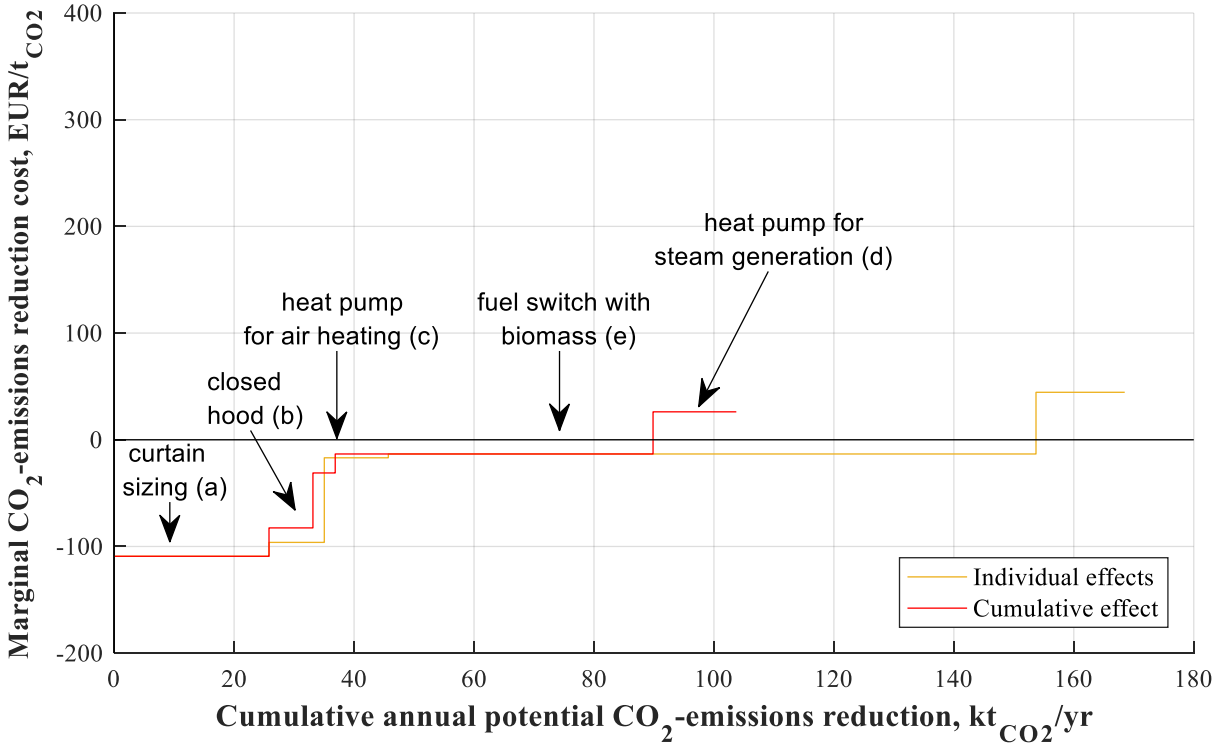

Figure 6.19: Marginal abatement cost curves of the analyzed drying section for the cumulative and individual effects of combination of measures "All EEM + fuel switching to biomass" in the trend scenario. The letters in bracket indicate the calculation sequence.

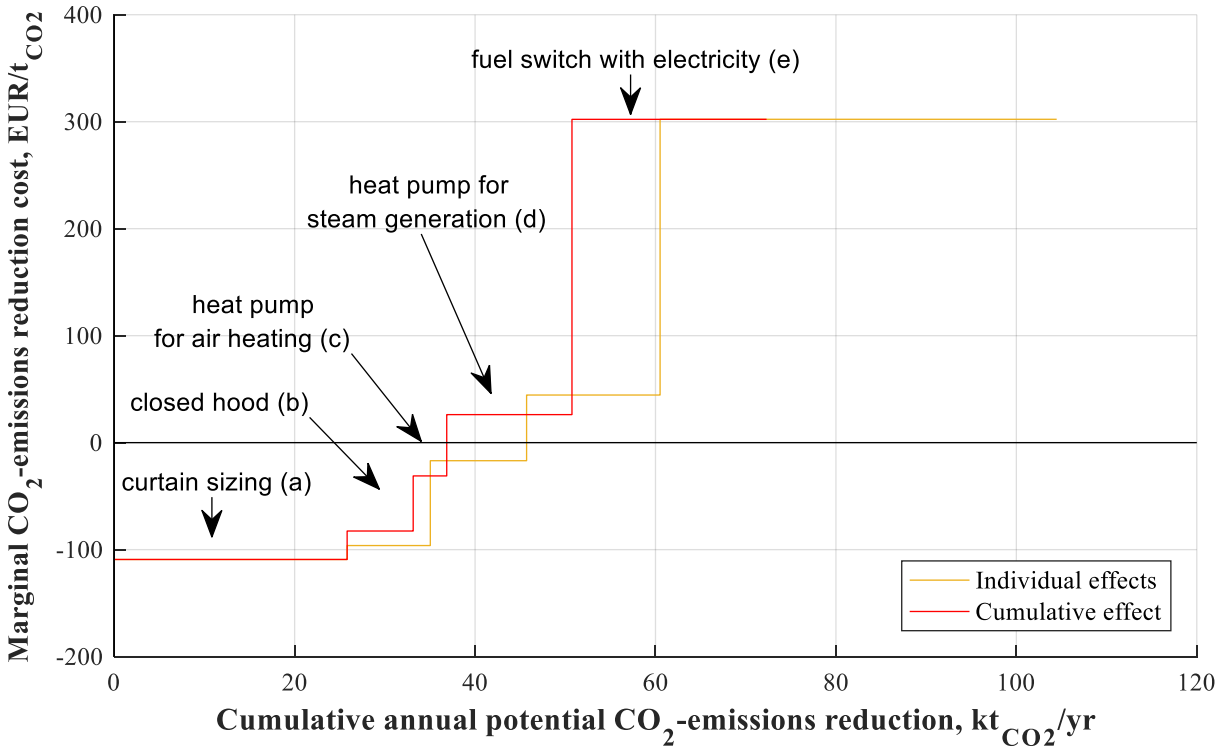

Figure 6.20: Marginal abatement cost curves of the analyzed drying section for the cumulative and individual effects of the combination of measures "All EEM + electrification of steam generation" in the trend scenario. The letters in bracket indicate the calculation sequence.

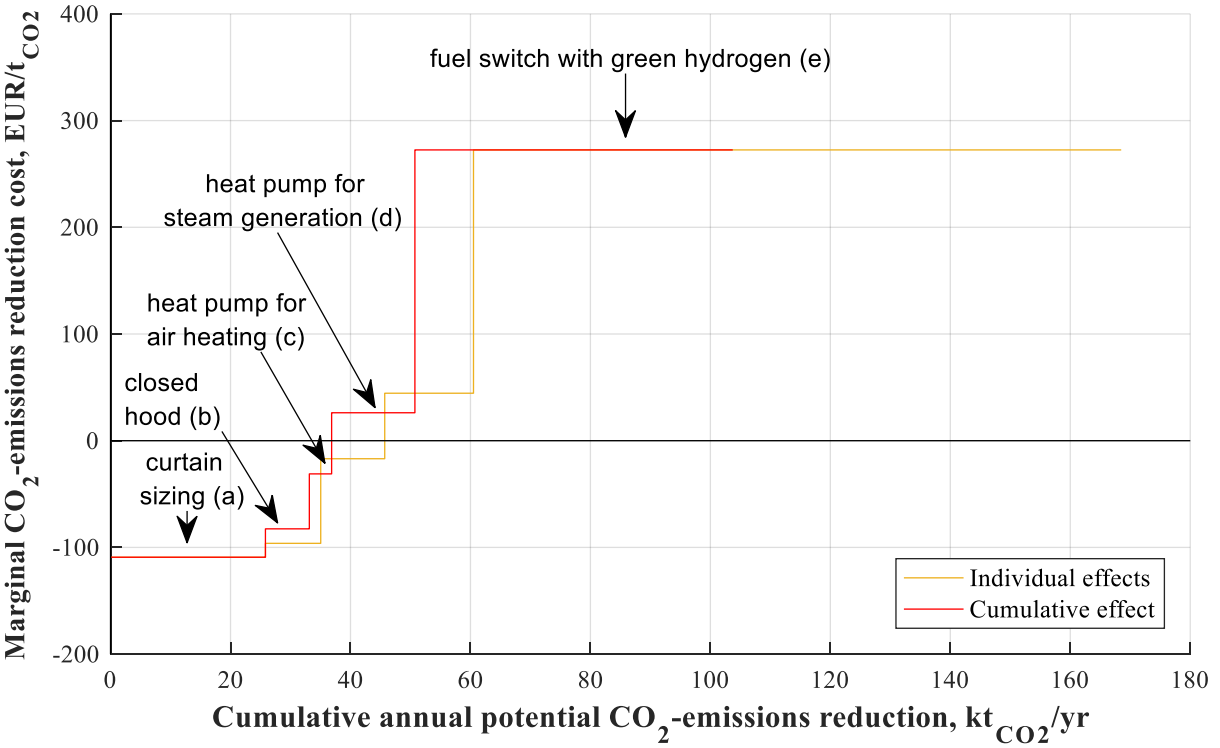

Figure 6.21: Marginal abatement cost curves of the analyzed drying section for the cumulative and individual effects of the combination of measures "All EEM + fuel switching to green hydrogen" in the trend scenario. The letters in bracket indicate the calculation sequence.

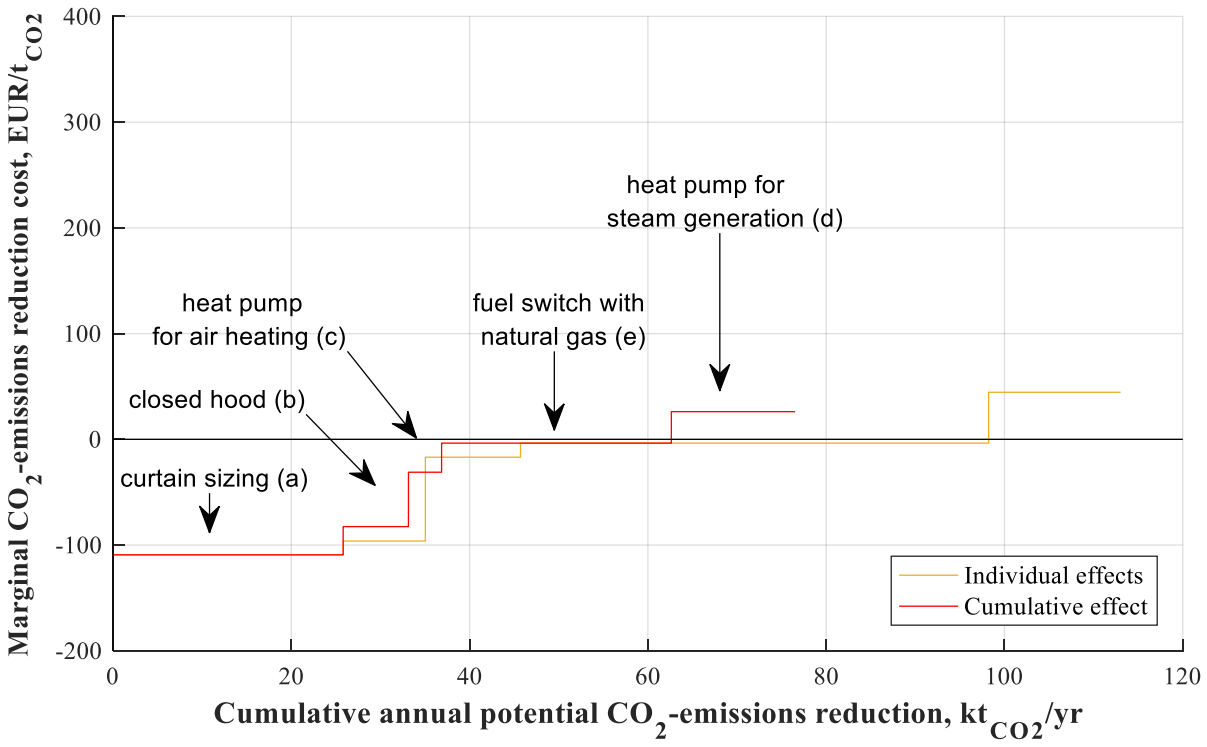

Figure 6.22: Marginal abatement cost curves of the analyzed drying section for the cumulative and individual effects of the combination of measures "All EEM + fuel switching to natural gas" in the trend scenario. The letters in bracket indicate the calculation sequence.

6.5 Sensitivity analysis

In order to test the robustness of the model results presented in section 6.4, the effect of tuning parameter values and parameters involved in the economic analysis is presented successively in sections 6.5.1 and 6.5.2.

6.5.1 The effect of tuning parameter values on energy savings

In the present case study, only a few data points were available at the paper mill for the humidity and the temperature of the paper web along the paper machine. As a consequence, the model was calibrated with a very limited data set, and the uncertainty on the values of the tuned parameters is high.

However, different sets of tuning parameter values which lead to the same overall amount of humidity removed from the paper web as in the status quo, only affect the savings related to changes in heat transfer at the cylinder level or the amount of water to be evaporated, i.e. the implementation of curtain sizing and steel cylinders in the present case.

For those cases, a sensitivity analysis was performed by calculating the impact of different sets of tuned parameters on the energy savings of those measures, where all sets of tuned parameters fulfill the condition that the resulting mean absolute percentage error between the measured and calculated paper web humidity in status quo lies below 5%.

Values below 0.53 and above 0.73 kW/m^2.K for the contact heat transfer coefficient (h_{cp0}) do not allow to calibrate the humidity of the paper web to the measurements with a maximum error of 5%. In the reference case, the value for the heat transfer coefficient of the condensate (h_{sc}) was not used for the model calibration step and was set to 2.3 kW/m^2.K in accordance with literature values for this paper machine speed, condensate removal systems equipped with

stationary siphons and dryers with spoiler bars (Ghodbanan et al. 2015). However, since the exact value of this parameter is not known, the variation of this parameter to a low and high value of 1.5 and 4 kW/m^2.K (Appel and Hong 1975; Kadant Johnson Inc. 2005) was included in the present sensitivity analysis. No additional scenario is considered for the fabric reduction factor FRF since its minimum and maximum values (0.3 and 0.5) are already covered in other scenarios.

The resulting energy savings for the different scenarios (i.e. sets of tuned parameters) are shown in Table 6.4. The gaps obtained between the different scenarios and the reference scenario are lower than 0.18% in the case of the replacement of iron cast cylinders with steel cylinders. Regarding the implementation of curtain sizing, a maximum difference of 2.6% for the steam savings in the high h_{sc} scenario and 2% for the power savings is obtained for the low h_{cp0} scenario as compared to the reference scenario.

This shows that despite variations in the tuned values, the chosen set does not greatly affect the calculated energy savings, as long as the model is fitted with reasonable accuracy to plant data. This can be explained by compensation effects occuring between the parameters, since reaching the same overall drying effect is a condition for determining the sets of tuned parameters.

Table 6.4: Sensitivity analysis: effect of tuning parameter sets on calculated energy savings. The steam and power savings are expressed as a percentage of the steam and power demand in status quo.

	Curtain sizing		**Steel cylinders**	
Scenario **Set of tuning parameters**	Total steam savings	Total power savings	Total steam savings	Total power savings
Reference: $\boldsymbol{h_{cp0}}$ = 0.68 / $\boldsymbol{FRF}$ = 0.45 / $\boldsymbol{h_{sc}}$ = 2.3[1)]	22%	25.6%	-0.22%[2)]	3.9%
Low $\boldsymbol{h_{cp0}}$: $\boldsymbol{h_{cp0}}$ = 0.535 / $\boldsymbol{FRF}$ = 0.3 / $\boldsymbol{h_{sc}}$ = 2.3	19.6%	27.6%	-0.08%	3.9%
High $\boldsymbol{h_{cp0}}$: $\boldsymbol{h_{cp0}}$ = 0.73 / $\boldsymbol{FRF}$ = 0.5 / $\boldsymbol{h_{sc}}$ = 2.3	21.9%	25.4%	-0.26%	3.9%
Low $\boldsymbol{h_{sc}}$: $\boldsymbol{h_{cp0}}$ = 0.78 / $\boldsymbol{FRF}$ = 0.3 / $\boldsymbol{h_{sc}}$ = 1.5	22%	25.4%	-0.16%	3.9%
High $\boldsymbol{h_{sc}}$: $\boldsymbol{h_{cp0}}$ = 0.55 / $\boldsymbol{FRF}$ = 0.43 / $\boldsymbol{h_{sc}}$ = 4	19.4%	27.2%	-0.22%	3.9%

[1)] The heat transfer coefficient of the condensate in the drying cylinders, although not used as a tuning parameter for the model validation (5.1.3), is varied here due to the high uncertainty regarding its value in the present case study.

[2)] The negative steam savings are caused by the improvement of the heat transfer coefficient of the cylinder shell, more details are provided in section 6.4.1.

6.5.2 The effect of selected parameters on the results of the economic analysis

To assess the robustness of the economic analysis against uncertainties in the parameter definition several additional models runs were performed in which the value of one parameter was changed at every run to be either 25% lower or 25% higher than in the trend scenario.

Following parameters were selected since they are characterized by a particularly high uncertainty (Brunke 2017; Flatau 2019; Zuberi and Patel 2019): the discount rate, the yearly fuel price, the increase of the CO_2-price for the year 2050 (the evolution remains linear in the considered time frame), and the economic lifetime of the measures.
The resulting energy-efficiency and CO_2-emission reduction cost curves for the combination of energy-efficiency measures with the highest energy savings combined with the different fuel switching measures are shown in Figure 6.23, Figure 6.24, Figure 6.25, and Figure C.4 and Figure C.5 in Appendix C. The impact of variables on key parameters is summarized in Table 6.5.

As expected, since this variable does not depend on the selected parameters, no variation of the cumulative annual potential final energy savings is obtained throughout the different simulations. No sensitivity of the selected parameters is observed on the economic energy-saving potential due to a higher difference between the individual marginal energy-saving cost of the measures and zero, than between the different values calculated after parameter variation. However, the total annual cost for the same combination of energy-efficiency measures is sensitive to the variation of several parameters, in particular to the CO_2-price and the discount rate where the difference to the trend scenario reaches ±8%. An extension of the economic lifetime of the measures by 25% leads to 2.4% lower total annual costs and a decrease by 25% leads to 4.4% higher costs[19]. A variation of 25% in the yearly fuel price increase leads to a very small difference of ± 0.1% compared to the trend scenario.

The average economic lifetime of measures is the only varied parameter which is used for the calculation of the cumulative CO_2-emissions reduction and its influence on this variable is rather low (between ±0.7% and ±1.4%) for the energy-efficiency measures combined with fuel switching to hydrogen, biomass and natural gas. The impact of this parameter is higher (±8.5%) for the energy-efficiency measures combined with a fuel switching to electricity, which is due to the fact that the value for the average emission factor of electricity is calculated over the measure's lifetime.
As for the economic energy-saving potential, the economic CO_2-emissions reduction potential depends on the difference between the individual marginal CO_2-emission reduction cost of the measures and zero. An important sensitivity for this variable is obtained for the set of measures "All EEM + fuel switching to natural gas", since the fuel switching measure is uneconomic for a lower CO_2-price.
Small variations of the economic CO_2-emissions reduction potential in the range ±0.2-0.6% are also obtained for all combinations of measures when the economic lifetime of the measures is varied, due to a slight variation of the potential CO_2-emissions reduction.

At last, the total annual cost of the considered combinations of measures is sensitive to all varied parameters due to the impact those parameters have on the marginal CO_2-emission reduction cost of the individual measures. The sensitivity of this parameter is the highest for changes in the CO_2-price for which the annual cost variation ranges from ±4.4% for the combination of measures which includes fuel switching to hydrogen, to ±12.9% for the combinations of measures including fuel switching to electricity and biomass. The total annual cost is also

[19] The asymmetry in the variation of the TAC despite a symmetric variation of the economic lifetime of the measures is due to the non-linear relationship between the annuity factor and the discount rate and the economic lifetime of the measures (see Equation (70)).

sensitive to the discount rate since the absolute value of the variations to the trend scenario lies between 2.6% for the combination of measures which includes fuel switching to hydrogen, and 11.7% for the combination of measures that includes a fuel switching to biomass due to the high $CAPEX$ which characterize this fuel switching measure.

The effect of changes in the yearly price increase on the total annual cost is low with a maximum of ±0.78% for the combination of measures that includes the electrification of the steam generation. In this case the importance of the $OPEX$ related to electricity purchase among the other components of the annual cost makes this combination of measures more sensitive to assumptions related to fuel prices.

Finally, variations of the average economic lifetime of measures impact the total annual cost of combinations of measures for which the $CAPEX$ represents an important share of the annual cost. This is the case for a fuel switching to biomass for which the calculated annual cost is 3.7% lower and 6.8% higher than in the trend scenario. On the other hand, for combinations of measures with low $CAPEX$ the impact is limited, as for example the combination of measures that includes fuel switching to hydrogen for which a variation of -0.9% and +1.7% is obtained for an increase and decrease of the average lifetime of measures by 25% respectively. The total annual cost for the combination of measures that includes steam generation with electricity is impacted by -2.94% and +5.16% for an increased and decreases economic lifetime of the measures, due to the relation between the average emission factor of electricity and the average lifetime of the measures.

Table 6.5: Sensitivity analysis: effect of parameter variations on the results of the economic analysis for the trend scenario. The values correspond to the percentage difference between the parameter value for the given scenario and the reference situation.

		CO_2-price in 2050		**Discount rate**		**Yearly fuel price increase**		**Measure's lifetime**	
Parameter	Combination of measures	-25%	+25%	-25%	+25%	-25%	+25%	-25%	+25%
Technical final energy-saving potential	All EEM[1)]	NC[2)]	NC	NC	NC	NC	NC	NC	NC
Economic final energy-saving potential	All EEM	NC	NC	NC	NC	NC	NC	NC	NC
Technical CO_2-emissions reduction potential	All EEM	NC	NC	NC	NC	NC	NC	-1.4%	1.4%
	All EEM + biomass	NC	NC	NC	NC	NC	NC	-0.7%	0.7%
	All EEM + electricity	NC	NC	NC	NC	NC	NC	-8.5%	8.5%
	All EEM + hydrogen	NC	NC	NC	NC	NC	NC	-0.7%	0.7%
	All EEM + natural gas	NC	NC	NC	NC	NC	NC	-1.0%	1.0%
Economic CO_2-emissions reduction potential	All EEM	NC	NC	NC	NC	NC	NC	0.6%	-0.6%
	All EEM + biomass	NC	NC	NC	NC	NC	NC	0.2%	-0.2%
	All EEM + electricity	NC	NC	NC	NC	NC	NC	0.6%	-0.6%
	All EEM + hydrogen	NC	NC	NC	NC	NC	NC	0.6%	-0.6%
	All EEM + natural gas	-41.1%	NC	NC	NC	NC	NC	0.3%	-0.3%
Total annual cost[3)]	All EEM	8.0%	-8.0%	-7.5%	7.1%	0.1%	-0.1%	4.4%	-2.4%
	All EEM + biomass	12.9%	-12.9%	-11.7%	11.2%	-0.1%	0.1%	6.8%	-3.7%
	All EEM + electricity	12.9%	-12.9%	-8.33%	7.80%	-0.77%	0.78%	5.16%	-2.94%
	All EEM + hydrogen	4.4%	-4.4%	-2.8%	2.6%	-0.5%	0.5%	1.7%	-0.9%
	All EEM + natural gas	11.4%	-11.4%	-9.3%	8.8%	-0.1%	0.1%	5.6%	-3.1%

1) All EEM stands for all Energy-efficiency measures, equivalent to the combination of measures (1) + (3) + (4) + (5).
2) *NC stands for "No Change".*
3) *Absolute values of the total annual cost are presented in Table C.1 in Appendix C.*

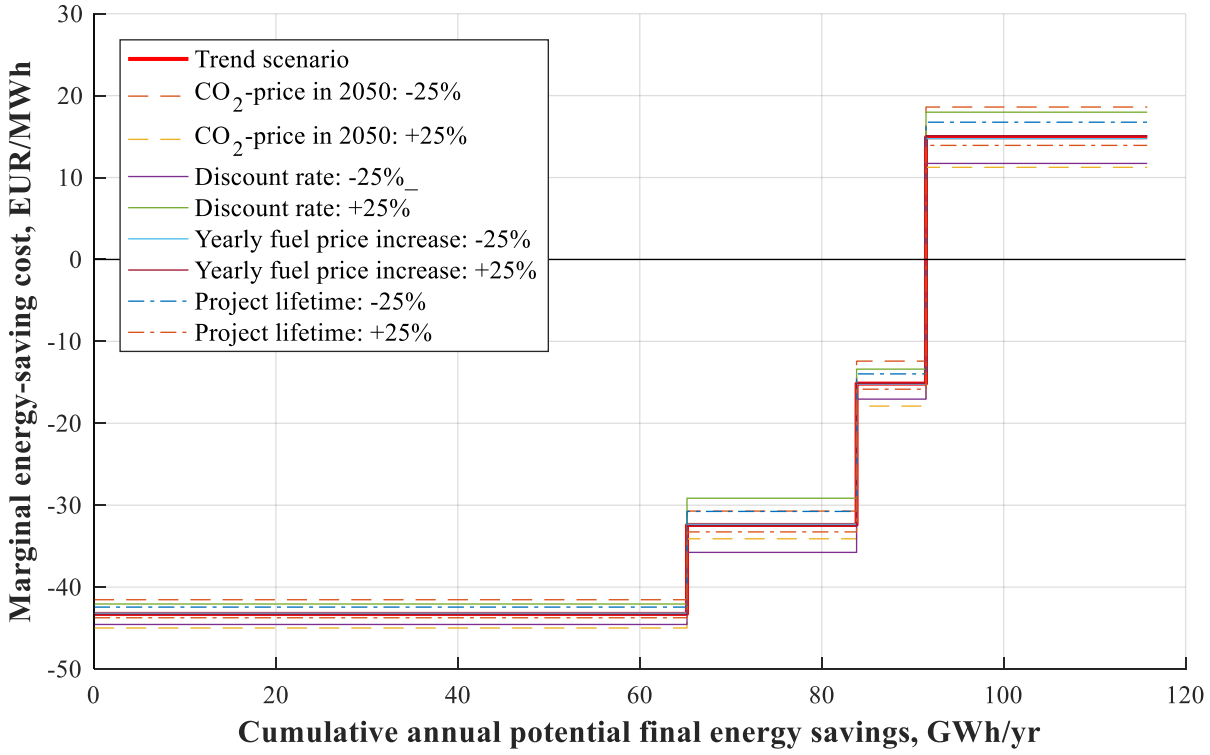

Figure 6.23: Sensitivity analysis of various parameters on the energy-efficiency cost curve of the combination of measures "All EEM" in the trend scenario

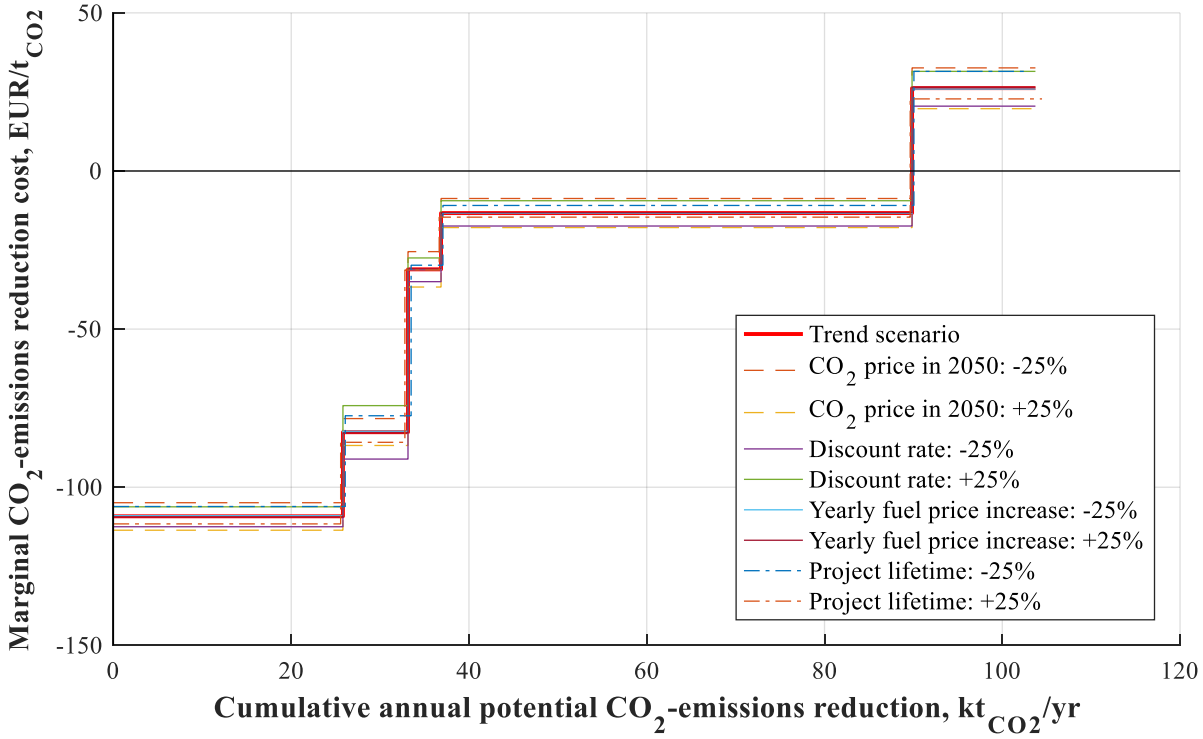

Figure 6.24: Sensitivity analysis of various parameters on the MACC of the combination of measures "All EEM + fuel switching to biomass" in the trend scenario

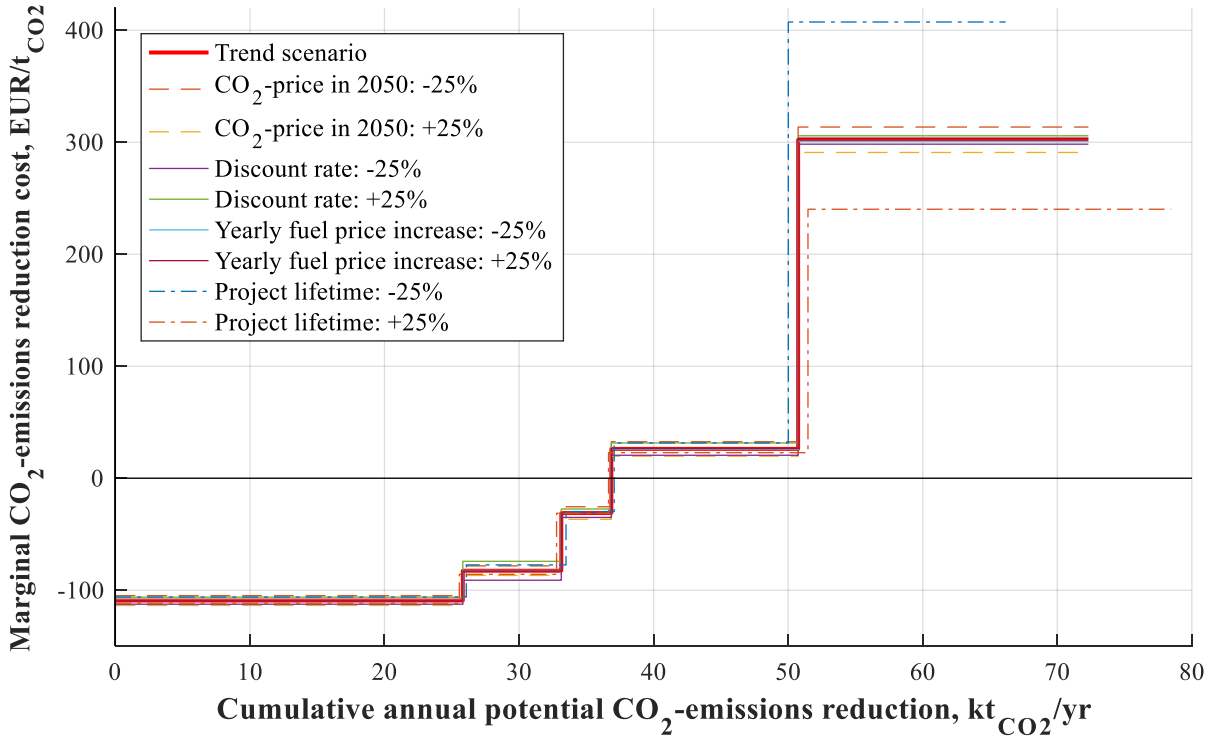

Figure 6.25: Sensitivity analysis of various parameters on the MACC of the combination of measures "All EEM + electrification of steam generation" in the trend scenario

7 Conclusion

This thesis closes with summary of the work undertaken, a presentation of the key results, ideas for future works, and concluding remarks.

7.1 Summary

A multi-step approach was adopted in order to reach the goals of this work, i.e.:

- the quantification of potential energy-efficiency savings and CO_2-emission reductions reached through retrofit measures at the drying section of a paper machine, waste heat recovery measures and fuel switching for the generation of the steam supplied to the drying section.
- the analysis of the economic impact of individual measures and combinations of measures for different scenarios, and the graphical representation of the results using energy-efficiency cost curves and marginal abatement cost curves accounting for the interactions between the measures.
- A comparative analysis between the cumulative effect of combinations of measures and the sum of the effects of individual measures.

In a first step the existing literature on the analysis of energy-saving and CO_2-emission reduction measures related to the energy demand of a multi-cylinder drying section was reviewed. Despite being a requirement for quantifying the impact of various CO_2-mitigation measures at drying sections, no model was found which encompasses a detailed description of the drying process itself, the steam cascade, the air and heat recovery systems, as well as the boiler system.
A further observation drawn from the literature review was that only little attention has been given previously to the analysis of waste heat recovery from hood exhaust air using heat pumps and that the interactions between different measures at the drying section have not yet been quantified.
Besides that, no methodology was found in the literature for the construction of energy-efficiency cost curves and marginal abatement cost curves based on model simulation results which accounts for the interactions between measures.

Following these observations, a model of a multi-cylinder drying section encompassing different modules was developed. The dryers are modelled using a grey-box approach where mass and energy balances are set-up for an infinitesimal length element of paper web along the drying section, and the heat transfer coefficients correspond to physical entities of the system. The integration of the obtained differential equation system over the whole length of the drying section allows to determine the temperature and humidity profiles of the paper web.
The dryer model was validated using literature data sets from four different mills and an average agreement of 9.8% for the temperature and 4.8% for the humidity between measurements and model values was obtained across all data sets.

The model was then extended by black-box modules of the hood, the heat recovery system, the steam cascade and the energy supply system in order to determine the overall heat and fuel demand of the drying section.

In the next step, methods for the energy and economic assessment of measures and combinations of measures were built on top of the model.
Key to the energy assessment are an iteration on the number of drying cylinders for measures which impact the moisture profile of the paper web, in order to obtain the same final humidity of the paper web as in the status quo, and the adjustement of the volume flow of hood supply air such that it is higher than the minimum supply air flow for which the hood exhaust air is at dew point. The difference in power consumption between the initial and final system configurations is assessed for process components impacted by the selected energy-efficiency measures, i.e. the fans used for circulating hood air and the cylinders drives.
A methodology for the construction of marginal energy-saving cost curves and marginal abatement cost curves accounting for interactions between measures was also proposed to graphically represent the model results.

The developed framework was then applied to the drying section of a German mill. The dryer model was calibrated to plant data using two heat transfer coefficients as tuning parameters and the effect of following site-relevant energy-efficiency measures was subsequently analysed: the replacement of film sizing with curtain sizing, the replacement of iron cast cylinders with steel cylinders, the closure of the current semi-closed hood, and the integration of heat pumps using hood exhaust air as a heat source to heat the hood supply air to the required hood temperature and generate steam for the dryers. The model results showed that a reduction of the steam demand by 28% (0.98 GJ_{th}/t_{paper}) and the electricity demand by 34.4% (0.1 GJ_{el}/t_{paper}) is expected at the drying section after replacing film sizing with curtain sizing and enclosing the drying section with a high-performance closed hood. The integration of a heat pump to heat air on top of those measures should allow to save additional 0.14 GJ_{th}/t_{paper} at the cost of an increase in the electricity consumption by 0.04 GJ_{el}/t_{paper}. Generating a part of the steam for the drying section with a second heat pump on top of the implementation of the three previously mentioned measures could allow additional steam savings of 0.67 GJ_{th}/t_{paper} at the cost of an increase of the power demand by 0.26 GJ_{el}/t_{paper}. In other words, a potential decrease of 51.3% of the steam demand and an increase by 72.1% of the power consumption uniquely with energy-efficiency and waste heat recovery measures was calculated for the analyzed drying section.

In the next step, the CO_2-emission reduction potentials related to the implementation of the analysed energy-efficiency measures and fuel switching options to biomass, natural gas, electricity, and green hydrogen, were assessed based on the previously calculated energy saving potentials and data of the current energy generation system of the analysed paper mill. An economic analysis was subsequently carried out for three economic scenarios characterized by different underlying assumptions on the discount rate, the yearly price increase of fuels and the CO_2-price in 2050.
Whereas the technical energy and CO_2-emission saving potentials are identical across the scenarios for each combination of measures (see column marked as “a.” in Table 7.2), high differences are obtained for the economic potentials, total annual cost and the average marginal CO_2-emissions reduction cost as shown in Table 7.1.
The cost obtained for the negative scenario, which depicts a situation where the economic background has an unfavorable impact on the implementation of energy-efficiency and CO_2-emission reduction measures, are 13 to 54% higher than in the trend scenario. For the opposite (positive) scenario the assessed costs lie 28 to 108% below the cost of the trend scenario. The differences in the economic potentials are due to the heat pump for steam generation being an

economic option in the positive scenario, and fuel switching to biomass and natural gas being uneconomic in the negative scenario.

As shown in Table 7.2 large differences ranging from ±1.6% to above 200% are observed between the individual and cumulative values obtained for the energy savings, CO_2-emission reduction potential, and the total annual cost.

These differences are explained among others by interactions between energy-efficiency measures on the amounts of air to be circulated in the drying hood and the heat sink temperature calculated for the heat pumps.

This demonstrates the importance of accounting for interactions when analyzing the implementation of multiple CO_2-emissions reduction measures at a site.

Table 7.1: Results of the economic analysis of different measure combinations at the drying section of the analysed paper mill

	Unit	Negative scenario	Trend scenario	Positive scenario
Discount rate	*%*	*30*	*15*	*10*
Yearly price increase fuels[1)]	*%/a*	*0*	*0.25*	*1*
CO_2-price in 2050	*EUR/t_{CO2}*	*55*	*100*	*250*
Measure combination				
Curtain sizing + closed hood				
Economic CO_2-emissions reduction potential	k_{tCO2}/a	33.14	33.14	33.14
TAC[2)]	$kEUR_{2021}$/a	- 2747.37	- 3424.63	- 4774.44
MEMRC[3)]	EUR_{2021}/t_{CO2}	- 82.91	- 103.35	- 144.08
***TAC, MEMRC*: % change to trend scenario**		+ 19.78%		- 39.41%
All EEM[4)]				
Economic CO_2-emissions reduction potential	k_{tCO2}/a	36.86	36.86	50.74
TAC	$kEUR_{2021}$/a	- 2073	- 3177.2	- 5385.19
MEMRC	EUR_{2021}/t_{CO2}	- 40.85	- 62.62	- 106.13
TAC, MEMRC: % change to trend scenario		+ 34.77%		- 69.48%
All EEM + Biomass				
Economic CO_2-emissions reduction potential	k_{tCO2}/a	36.86	89.85	103.73
TAC	$kEUR_{2021}$/a	- 1778.09	- 3882.55	- 8077.17
MEMRC	EUR_{2021}/t_{CO2}	-17.14	- 37.43	-77.87
TAC, MEMRC: % change to trend scenario		+ 54.21%		- 108.04%
All EEM + Electrification				
Economic CO_2-emissions reduction potential	k_{tCO2}/a	36.86	36.86	50.74
TAC	$kEUR_{2021}$/a	4895.21	3343.02	- 270.4
MEMRC	EUR_{2021}/t_{CO2}	67.69	46.23	-3.74
TAC, MEMRC: % change to trend scenario		+ 46.42%		- 108.09%
All EEM + Green hydrogen				
Economic CO_2-emissions reduction potential	k_{tCO2}/a	36.86	36.86	50.74
TAC	$kEUR_{2021}$/a	12723.79	11264.34	8074
MEMRC	EUR_{2021}/t_{CO2}	122.66	108.59	77.84
TAC, MEMRC: % change to trend scenario		+ 12.96%		- 28.32%
All EEM + Natural gas				
Economic CO_2-emissions reduction potential	k_{tCO2}/a	36.86	62.83	76.51
TAC	$kEUR_{2021}$/a	- 1836.1	- 3269.79	- 6366.2
MEMRC	EUR_{2021}/t_{CO2}	- 24	- 42.74	- 83.21
TAC, MEMRC: % change to trend scenario		+ 43.85%		- 94.69%

1) In the trend scenario the fuel price in 2050 is **7.5% higher** than in 2021, whereas in the positive scenario the fuel price in 2050 is **33.5% higher** than in 2021.
2) Total annual cost related to the implementation of measures
3) Average marginal CO_2-emissions reduction cost
4) "All EEM" stands for all Energy-efficiency measures, equivalent to the combination of measures: curtain sizing + closed hood + heat pump for air heating + heat pump for steam generation.

Table 7.2: Calculated energy and emission savings potential with and without considering interactions for different measure combinations at the drying section of the analysed paper mill. The total annual cost corresponds to the value calculated for the trend scenario. In this table the potential refers to the technical potential and is therefore independent from economic parameters. The specific steam and power savings potentials are not indicated for the combination of measures that include "All EEM" and a fuel switching option since they are equivalent to the values indicated for "All EEM".

Measure combination	Unit	a. No interaction	b. Interactions considered	Percentage change between b. and a.
Curtain sizing + closed hood				
Specific steam savings potential	GJ_{th}/t	1.03	0.98	+ 5.15%
Specific power savings potential	GJ_{el}/t	0.11	0.1	+ 15.29%
CO_2-emissions reduction potential[1)]	kt_{CO2}/a	35.04	33.14	+ 5.75%
Total annual cost[2)]	$kEUR_{2021}/a$	-3707.69	-3424.63	- 8.26%
All EEM[3)]				
Specific steam savings potential	GJ_{th}/t	2.2	1.79	+ 22.78%
Specific power savings potential	GJ_{el}/t	-0.35	-0.2	- 71.5%
CO_2-emissions reduction potential	kt_{CO2}/a	60.51	50.74	+19.25%
Total annual cost	$kEUR_{2021}/a$	-3229.26	-3177.2	- 1.64%
All EEM + Biomass				
CO_2-emissions reduction potential	kt_{CO2}/a	168.49	103.73	+ 62.43%
Total annual cost	$kEUR_{2021}/a$	-4666.65	-3882.6	- 20.2%
All EEM + Electrification				
CO_2-emissions reduction potential	kt_{CO2}/a	104.47	72.31	+ 44.47%
Total annual cost	$kEUR_{2021}/a$	10057.84	3343	+ 200.86%
All EEM + Green hydrogen				
CO_2-emissions reduction potential	kt_{CO2}/a	168.49	103.73	+ 62.43%
Total annual cost	$kEUR_{2021}/a$	26200.17	11264.3	+132.59%
All EEM + Natural gas				
CO_2-emissions reduction potential	kt_{CO2}/a	113.02	76.51	+ 47.72%
Total annual cost	$kEUR_{2021}/a$	-3417.94	-3269.79	- 4.53%

1) Includes direct and indirect emissions
2) Related to the implementation of measures
3) "All EEM" stands for all Energy-efficiency measures, equivalent to the combination of measures: curtain sizing + closed hood + heat pump for air heating + heat pump for steam generation.

At last, a sensitivity analysis was conducted. On the one hand, the robustness of the values calculated for the energy savings was evaluated against different sets of dryer model tuning parameters. It showed that the chosen set has very little effect on the calculated energy savings, as long as the model is fitted with reasonable accuracy to plant data.

On the other hand, the value of key economic parameters characterized by a high uncertainty (i.e. the CO_2-price in 2050, the discount rate, the yearly fuel price increase and the economic lifetime of the measures) were varied individually by ±25% to assess their effect on the results of the techno-economic analysis.

One result of this analysis was that the technical and economic final energy-saving potential are not impacted by variations in those parameters. An important impact on the technical CO_2-emissions reduction potential is observed for an increase and decrease of the measure's lifetime in the case of fuel switching to electricity since the average emission factor of electricity is calculated over the measure's lifetime.

A lower CO_2-price makes fuel switching to natural gas an uneconomic measure and leads thereby to a 41% lower economic CO_2-emissions reduction potential. However, since the EU ETS is at the heart of the ambitious decarbonization agenda of the EU Commission (ICAP 2021), the CO_2-price is unlikely to decrease in Europe in the upcoming decades.
The total annualized cost is rather sensitive to variations of the CO_2-price and the discount rate with variations up to ± 13%. Variations in the discount rate affect the most the combination of measures that includes fuel switching to biomass due to the high related $CAPEX$.
A sensitivity of the annual total cost to high $CAPEX$ measures is also observed for variations in the average economic lifetime with variations up to +6.8% in the case of biomass. In the case of the combination of measures that includes steam generation with electricity, the relation between the average emission factor of electricity and the economic lifetime of the measures leads to a sensitivity of -2.94% and 5.15% of the total annual cost in the case of increased and decreased measure lifetime respectively.

7.2 Future work

Several topics were identified in the course of this work which were not in the focus of the defined goals, but do offer potential for future research. A short selection of some of the main topics includes:

- the analysis of the feasibility of the selected measures: the implementation of energy-efficiency measures is in practice subject to different constraints of practical order. For example, the drives of the paper machine may limit the possible increase in the paper machine speed, and high electricity prices, high investment costs and space availability all constitute obstacles to the implementation of high temperature heat pumps at the drying section of paper machines. The evaluation and quantification of obstacles for example in terms of economic penalties is recommended for future work.
- the validation of the calculated energy-savings through measurements after the implementation of the selected measures at the considered mill. Although the sensitivity analysis presented in section 6.5.1 attests of the robustness of the calculated energy-savings for different sets of tuning parameters, it can't be considered a sufficient proof for the predictive value of the model. Therefore, the verification of the calculated energy savings after measure implementation is recommended for future work.
- extensions of the model to cover other heat and electric power consumers beyond the drying section at the paper mill. The focus in this work was set on the depiction of the energy demand of the drying section and the invesment cost for the steam generation capacities were defined according to the steam demand of the drying section and therefore correspond to a lower cost limit. A global picture on the energy consumers would allow a more realistic economic depiction of the fuel switching measures.
- a more accurate description of the local energy generation system (e.g. accounting for coupled heat and power production, part-load behavior), and the linkage to the temporal dynamics of the "off-site" energy system in particular regarding energy prices and fuel availability. Increasing the level of detail would allow among others to gain insights on the economic potentials of a flexible energy demand and supply, and to quantify "negative" side-effects of energy-efficiency measures due to the induced part-load behavior of the local energy generation system.
- the analysis of the effect of seasonal temperature and humidity fluctuations on the calculated energy savings in particular regarding waste heat recovery potentials.

7.3 Concluding remarks

The developed model-based framework can be used for improving drying sections with various configurations. Its application to the drying section of a German paper mill showed that very high energy savings can be reached at the analysed drying section with a small selection of energy-efficiency measures. In a way these high saving potentials were to be expected since the considered paper machine was installed several decades ago, and paper machines have been improved since then. Because of their high capital-intensity, old paper machines are replaced with newer paper machines only at the end of their lifetime which means that many old paper machines are still in operation and high energy saving potentials still remain untapped.
Also, certain energy-efficiency measures considered in this case study apply to recently installed paper machines as well, like the implementation of curtain sizing and waste heat recovery using heat pumps, which means that the energy performance of newer systems can be improved too.
However, the fact that the integration of heat pump for steam generation was assessed to be a non-economic solution at the analysed drying section will apply to other paper mills as well, due to high temperature lifts and unfavourable economic conditions.

The remaining CO_2-emissions after implementing energy-saving measures may be fully mitigated using fuel switching options but the rentability of the measures highly depends on the prices of fuels and CO_2-certificates. In the case study, fuel switching to electricity and green hydrogen do not constitute competitive options for the three defined scenarios, even in the case of a high CO_2-price. For these measures to be economic, hydrogen and electricity prices would have to be considerably lower than assumed in this work, to an extent where high subsidies seem unavoidable.
Although rising CO_2-prices shall encourage industries to implement fuel switch measures, recent high fluctuations in fuel prices constitute obstacles to investments in fuel switch projects. And with a growing concurrence around green fuels, prices are expected to grow further. This shall increase even more the role to be played by energy efficiency in the decarbonisation of industrial systems.

The large differences obtained between the individual and cumulative values for the energy savings, CO_2-emission reduction potential, and the total annual cost in the case study demonstrate the importance of accounting for interactions when modeling multiple CO_2-emissions reduction measures, be it at the scale of an industrial site, or at regional level.

8 Bibliography

Abd El-Sayed, E. S.; El-Sakhawy, M.; El-Sakhawy, M. A.-M. (2020): Non-wood fibers as raw material for pulp and paper industry. In *Nordic Pulp and Paper Research Journal* 35 (2), pp. 215–230. DOI: 10.1515/npprj-2019-0064.

Abdul Aziz, E.; Wan Alwi, S. R.; Lim, J. S.; Abdul Manan, Z.; Klemeš, J. J. (2017): An integrated Pinch Analysis framework for low CO2 emissions industrial site planning. In *Journal of Cleaner Production* 146, pp. 125–138. DOI: 10.1016/j.jclepro.2016.07.175.

Ahrens, F.; Rudman, I. (2003): The Impact of Dryer Surface Deposits and Temperature Graduation in the First Dryer Section on Drying Productivity. In : Proceedings of TAPPI Spring Technical Conference 2003. Chicago, USA, May 8-10.

Ahrens, F. W.; Habeger, C.; Loughran, J.; Patterson, T. (2003): Application of a Device for Uniform Web Drying and Preheating Using Microwave Energy. Final Report of the Project No. DE-FC07-00ID13872 funded by the U.S. Department of Energy Office of Scientific and Technical Information. Washington, DC.

Akesson, J.; Ekvall, J. (2006): Parameter optimization of a paper machine model. In : Proceedings of Reglermöte 2006. Stockholm, Sweden.

Allwood, J. M.; Cullen, J. M.; Carruth, M. A. (2012): Sustainable Materials with both eyes opened: UIT Cambridge Ltd.

Appel, D. W.; Hong, S. H. (1975): Optimizing heat transfer using bars in dryers. In *Paper Technology and Industry* 16 (4), pp. 264–269.

Arpagaus, C.; Bless, F.; Uhlmann, M.; Schiffmann, J.; Bertsch, S. S. (2018): High temperature heat pumps: Market overview, state of the art, research status, refrigerants, and application potentials. In *Energy* 152, pp. 985–1010. DOI: 10.1016/j.energy.2018.03.166.

Arrhenius, S. (1896): On the Influence of Carbonic Acid in the Air upon the Temperature of the Ground. In *Philosophical magazine and Journal of Science* 41 (5), pp. 237–276.

Ashori, A. (2006): Nonwood Fibers—A Potential Source of Raw Material in Papermaking. In *Polymer-Plastics Technology and Engineering* 45 (10), pp. 1133–1136. DOI: 10.1080/03602550600728976.

Baggerud, E. (2004): Modelling of Mass and Heat Transport in Paper – Evaluation of Mechanisms and Shrinkage. Ph.D. Thesis. Lund University, Lund, Sweden.

Baggerud, E.; Stenström, S. (2000): Modeling of Moisture Gradients for Convective drying of Industrial Pulp Sheets. Paper no. 308. In : Proceedings of the 12th International Drying Symposium (2000). Noordwijkerhout, the Netherlands.

Bajpai, P. (2016): Pulp and Paper Industry: Energy Conservation: Elsevier Science Publishing Co Inc.

Beer, J. de; Worrell, E.; Blok, K. (1998): Long-term energy-efficiency improvements in the paper and board industry. In *Energy* 23 (1), pp. 21–42. DOI: 10.1016/S0360-5442(97)00065-0.

Berghout, N.; Meerman, H.; van den Broek, M.; Faaij, A. (2019): Assessing deployment pathways for greenhouse gas emissions reductions in an industrial plant – A case study for a complex oil refinery. In *Applied Energy* 236 (2013), pp. 354–378. DOI: 10.1016/j.apenergy.2018.11.074.

Berg, P.; Lingqvist, O. (2019): Pulp, paper, and packaging in the next decade: Transformational change. Paper and Forest Products Practice. Mc Kinsey and Company.

Berlin, K. (2020): Discussion with a senior expert in the design of steam systems in the pulp and paper industry and author of the book "Handbuch Dampf- und Kondensatanlagen" published in 2009. Phone Call, 2020.

Bernath, C.; Bossmann, T.; Deac, G.; Elsland, R.; Fleiter, T.; Kühn, A. et al. (2017): Langfristszenarien für die Transformation des Energiesystems in Deutschland_Modul 3. Fraunhofer Institut ISI, Consentec GmbH, IFEU, TU Wien, M-five, TEP Energy Gmbh for the German Federal Ministry of Economics and Technology (BMWi).

Biedermann, F.; Kolb, M. (2014): Faktenblatt Dampfkessel. FFE GmbH. München, Germany.

BMU (2021): Lesefassung des Bundes-Klimaschutzgesetzes 2021 mit markierten Änderungen zur Fassung von 2019. Bundesministerium für Umwelt, Naturschutz und nukleare Sicherheit. Bonn, Germany.

Bründlinger, T.; Elizalde-König, J.; Frank, O.; d. Gründig; Jugel, C.; Kraft, P. et al. (2018): Dena-Leitstudie Integrierte Energiewende Impulse für die Gestaltung des Energiesystems bis 2050. Deutsche Energie-Agentur GmbH. Berlin, Germany.

Brunke, J. C. (2017): Energieeinsparpotenziale von energieintensiven Produktionsprozessen in Deutschland. Eine Analyse mit Hilfe von Energieeinsparkostenkurven. Ph.D. Thesis. Universität Stuttgart, Stuttgart, Germany. Institut für Energiewirtschaft und Rationelle Energieanwendung. Available online at http://dx.doi.org/10.18419/opus-9242.

Cagno, E.; Trianni, A. (2014): Evaluating the barriers to specific industrial energy efficiency measures: an exploratory study in small and medium-sized enterprises. In *Journal of Cleaner Production* 82 (1), pp. 70–83. DOI: 10.1016/j.jclepro.2014.06.057.

Campbell, N.; Ryan, L.; v. Rozite; Lees, E.; Heffner, G. (2014): Capturing the Multiple Benefits of Energy Efficiency. A guide to quantifying the value added. International Energy Agency. Paris. Available online at https://doi.org/10.1787/9789264220720-en.

CARMEN e.V. (2021): Marktpreise Hackschnitzel. Preisentwicklung bei Waldhackschnitzeln. Centrale- Agrar-Rohstoff-Marketing- und Energie-Netzwerk. Available online at https://www.carmen-ev.de/service/marktueberblick/marktpreise-energieholz/marktpreise-hackschnitzel/.

CAT (2021): CAT Climate Target Update Tracker. Available online at https://climateactiontracker.org/climate-target-update-tracker/, updated on 2/3/2021, checked on 2/3/2021.

CEPI (2020): Paper-based packaging. Recyclability Guidelines. With assistance of citpa, ace, FEFCO. Confederation of European Paper Industries. Brussels, Belgium. Available online at https://www.cepi.org/paper-based-packaging-recyclability-guidelines/.

CEPI (2019): Final Key Statistics 2018. Confederation of European Paper Industries. Brussels, Belgium. Available online at https://www.cepi.org/key-statistics-report-2018-out-now/.

CEPI (2013): The Two Team Project. Confederation of European Paper Industries. Brussels, Belgium.

CEPI (2011): The forest fibre industry: 2050 Roadmap to a low-carbon bio-economy. Unfold the future. Confederation of European Paper Industries. Brussels, Belgium.

Chan, W. N.; Walter, A.; Sugiyama, M. I.; Borges, G. C. (2016): Assessment of CO2 emission mitigation for a Brazilian oil refinery. In *Braz. J. Chem. Eng.* 33 (4), pp. 835–850. DOI: 10.1590/0104-6632.20160334s20140149.

Chen, C.-L.; Lin, C.-Y.; Lee, J.-Y. (2013): Retrofit of steam power plants in a petroleum refinery. In *Applied Thermal Engineering* 61 (1), pp. 7–16. DOI: 10.1016/j.applthermaleng.2013.04.001.

Chen, X.; Man, Y.; Zheng, Q.; Hu, Y.; Li, J.; Hong, M. (2019): Industrial verification of energy saving for the single-tier cylinder based paper drying process. In *Energy* 170, pp. 261–272. DOI: 10.1016/j.energy.2018.12.152.

Chen, X.; Li, J.; Liu, H.; Yin, Y.; Hong, M.; Zeng, Z. (2016a): Energy system diagnosis of paper-drying process, Part 1: Energy performance assessment. In *Drying Technology* 34 (8), pp. 930–943. DOI: 10.1080/07373937.2015.1087022.

Chen, X.; Li, J.; Liu, H.; Yin, Y.; Zhang, Y. (2016b): Energy system diagnosis of paper-drying process, Part 2: A model-based estimation of energy-saving potentials. In *Drying Technology* 34 (10), pp. 1219–1230. DOI: 10.1080/07373937.2015.1095206.

Cheremisinoff, N. P.; Rosenfeld, P. E. (2010): Handbook of Pollution Prevention and Cleaner Production. Best Practices in the Wood and Paper Industries. Chapter 6 - Sources of air emissions from pulp and paper mills: Elsevier.

Chudnovsky, Y. (2004): Laboratory Development of a High Capacity Gas-Fired Paper Dryer. Final Technical Report. Gas Technology Institute. USA.

Crotogino, R. (2001): The mysteries of technology transfer. Luck versus good planning. In *Drying Technology* 19 (10), pp. 2559–2575. DOI: 10.1081/DRT-100108254.

Cruse, F.; Dietz, W.; Höller, M.; Szafera, S. (2015): Entwicklung eines Verfahrens zur Gewinnung von Gras als Rohstoff und Verarbeitung für die Herstellung von Papierprodukten unter besonderer Berücksichtigung des Aufbaus einer nachhaltigen Wertschöpfungskette. Final report, project No 300990/01 funded by the Deutsche Bundesstiftung Umwelt. Projektgesellschaft C+G Papier GmbH. Hennef, Germany. Available online at https://www.dbu.de/projekt_30990_db_2409.html.

Dulany, M. A.; Batten, G. L.; Peck, M. C.; Farley, C. E. (2011): Papermaking additives. In *Kirk-Othmer Encyclopedia of Chemical Technology*, pp. 1–28. DOI: 10.1002/0471238961.1601160504211201.a01.

Earle, R. L. (1983): Unit Operations in Food Processing: Elsevier Ltd.

EC (2019): Communication from the Commission to the European Parliament, the European Council, the Council, the European Economic and Social Committee and the Committee of the regions. The European Green Deal. European Commission. Brussels.

EC (1994): Merger Decision IV/M.478 of 29/07/1994. DG IV/B Merger Task Force. European Commission. Brussels, Belgium.

EPRC (2020): Monitoring Report 2019. European Declaration on Paper Recycling 2016-2020. European Paper Recycling Council. Brussels, Belgium.

Eugenio, M.; Ibarra, D.; Martín-Sampedro, R.; Espinosa, E.; Bascón, I.; Rodríguez, A. (2019): Alternative Raw Materials for Pulp and Paper Production in the Concept of a Lignocellulosic Biorefinery. In A. Rodriguez Pascual, M. E. Eugenio Martin (Eds.): Cellulose. London, UK: IntechOpen, pp. 12–78.

Fattler, S.; Conrad, J.; Regett, A.; Böing, F.; Guminski, A.; Greif, S. et al. (2019): Kurzbericht zum Projekt Dynamis: Dynamische und intersektorale Maßnahmenbewertung zur kosteneffizienten Dekarbonisierung des Energiesystems. Datenanhang. Project funded by the German Federal Ministry of Economics and Technology. FFE GmbH, TU München.

Fischedick, M.; Roy, J.; Abdel-Aziz, A.; Acquaye, A.; J. M. Allwood; J.-P. Ceron, Y. Geng, H. Kheshgi, A. Lanza, D. Perczyk; L. Price, E. Santalla, C. Sheinbaum, and K. Tanaka (2014): Industry. In: Climate Change 2014: Mitigation of Climate Change. Contribution of Working Group III to the Fifth Assessment Report of the Intergovernmental Panel on Climate Change. With assistance of O. Edenhofer, R. Pichs-Madruga, Y. Sokona, E. Farahani, S. Kadner, K. Seyboth et al. Cambridge, UK and New York, USA.

Flatau, R. (2019): Integrierte Bewertung interdependenter Energieeffizienzmaßnahmen. Ph.D. Thesis. Universität Stuttgart, Stuttgart, Germany. Institut für Energiewirtschaft und Rationelle Energieanwendung. Available online at http://dx.doi.org/10.18419/opus-10707.

Fleiter, T.; Schlomann, B.; Eichhammer, W. (2013): Energieverbrauch und CO2-Emissionen industrieller Prozesstechnologien. Einsparpotenziale, Hemmnisse und Instrumente. Fraunhofer-Institut für Systemtechnik und Innovationsforschung. Stuttgart, Germany (ISI-Schriftenreihe "Innovationspotenziale").

Fleiter, T. (2012): The adoption of energy-efficient technologies by firms. An integrated analysis of the technology, behavior and policy dimensions. Ph.D. Thesis. Utrecht University and Fraunhofer Institute for Systems and Innovation Research ISI, Karlsruhe, Germany.

Fleiter, T.; Worrell, E.; Eichhammer, W. (2011): Barriers to energy efficiency in industrial bottom-up energy demand models—A review. In *Renewable and Sustainable Energy Reviews* 15 (6), pp. 3099–3111. DOI: 10.1016/j.rser.2011.03.025.

Gaillemard, C. (2006): Modelling the Moisture Content of Multi-Ply Paperboard in the Paper Machine Drying Section. Ph.D. Thesis. KTH Royal Institute of Technology, Stockholm, Sweden.

Gatley, D. P. (1997): Understanding Psychrometrics. Atlanta, GA, USA: W. Stephen Comstock (ASHREA Fundamentals Handbook).

Gerbert, P.; Herhold, P.; Burchardt, J.; Schönberger, S.; Rechenmacher, F.; Kirchner, A. et al. (2018): Klimapfade für Deutschland. BCG and Prognos for BDI.

Gharaie, M.; Panjeshahi, M. Hassan; Kim, J.-K.; Jobson, M.; Smith, R. (2015): Retrofit strategy for the site-wide mitigation of CO2 emissions in the process industries. In *Chemical Engineering Research and Design* 94, pp. 213–241. DOI: 10.1016/j.cherd.2014.08.007.

Ghodbanan, S.; Alizadeh, R.; Shafiei, S. (2017): Optimization for energy consumption in drying section of fluting paper machine. In *Therm sci* 21 (3), pp. 1419–1429. DOI: 10.2298/TSCI150503141G.

Ghodbanan, S.; Alizadeh, R.; Shafiei, S. (2015): Steady-State Modeling of Multi-Cylinder Dryers in a Corrugating Paper Machine. In *Drying Technology* 33 (12), pp. 1474–1490. DOI: 10.1080/07373937.2015.1020161.

Ghosh, A. K. (2011): Fundamentals of Paper Drying – Theory and Application from Industrial Perspective, Evaporation, Condensation and Heat transfer. With assistance of Dr. Amimul Ahsan (Ed.): InTech.

Godin, H.; Radgen, P. (2021): Model-based framework for the evaluation of energy-efficiency measures in multi-cylinder paper drying. In *Drying Technology* 79, pp. 1–18. DOI: 10.1080/07373937.2021.1958338.

Guminski, A.; Wiener, M.; Roon, S. von (2017): Energiewende in der Industrie: Methodik zur Identifikation und Quantifizierung von Dekarbonisierungsmaßnahmen. In : Energiewirtschaftliche Tagesfragen 67 (12), pp. 8–13.

Hanecke, M. (2019): Graspapier - eine umweltfreundliche Alternative? Interview mit dem Erfinder des Graspapiers, Uwe D'Agnone. Available online at https://printelligent.de/umweltfreundlich-drucken-mit-graspapier/, checked on 9/7/2020.

Heikkilä, P.; Paltakari, J. (2010): Fundamentals of paper drying (Chapter 2). Helsinki, Finland: Paper Engineers' Association / Paperi ja Puu Oy (Papermaking Part 2, Drying, 9).

Heikkilä, P. (1993): A study on the drying process of pigment coated paper webs. Ph.D. Thesis. Helsinki University of Technology, Finland.

Heo, C. Hoe; Cho, H.; Yeo, Y.-K. (2011): Dynamic modeling of paper drying processes. In *Korean J. Chem. Eng.* 28 (8), pp. 1651–1657. DOI: 10.1007/s11814-011-0046-0.

Hillman, K.; Damgaard, A.; Eriksson, O.; Jonsson, D.; Fluck, L. (2015): Climate benefits of material recycling. Inventory of Average Greenhouse Gas Emissions for Denmark, Norway and Sweden. Nordic Council of Ministers. Copenhagen, Denmark. Available online at https://www.norden.org/en/publication/climate-benefits-material-recycling.

Hirst, D. (2020): The history of global climate change negotiations. A short introduction to the history of climate change as an intergovernmental political issue, touching on key international treaties and agreements reached along the way. Available online at https://commonslibrary.parliament.uk/the-history-of-global-climate-change-negotiations/, updated on 6/24/2020, checked on 2/4/2021.

Holik, Herbert (Ed.) (2013): Handbook of Paper and Board. Volume 2. 2 volumes: Wiley-VCH Verlag GmbH and Co. KGaA.

Hubbe, M.; Gill, R. A. (2016): Fillers for papermaking: A review of their properties, usage practices, and their mechanistic role. In *BioResources* 11 (1), pp. 2886–2963.

ICAP (2021): ETS Detailed Information - EU Emissions Trading System (EU ETS). International Carbon Action Partnership. Berlin, Germany.

ICFPA (2021): Global Sustainability Progress Report. International council of forest and paper associations. Washington, DC, USA.

IEA (2020a): Industry direct CO2 emissions in the Sustainable Development Scenario, 2000-2030, updated on 6/4/2020, checked on 2/3/2021.

IEA (2020b): Fuels and Technologies_Pulp and paper. Final energy demand in pulp and paper in the Sustainable Development Scenario, 2000-2030. Available online at https://www.iea.org/data-and-statistics/charts/final-energy-demand-in-pulp-and-paper-in-the-sustainable-development-scenario-2000-2030, updated on 5/29/2020, checked on 8/30/2020.

IEA (2020c): Direct CO2 emissions from selected heavy industry sectors, 2019. Available online at https://www.iea.org/data-and-statistics/charts/direct-co2-emissions-from-selected-heavy-industry-sectors-2019, updated on 9/25/2020, checked on 2/3/2021.

IEA (2020d): Key World Energy Statistics 2020. Paris, France.

IEA (2020e): Tracking Industry 2020. With assistance of Peter Levi, Tiffany Vass, Hana Mandova, Alexandre Gouy, Andreas Schröder. Available online at https://www.iea.org/reports/tracking-industry-2020, updated on 06.2020, checked on 1/17/2021.

IEA (2018): Clean and efficient heat for industry. Available online at https://www.iea.org/commentaries/clean-and-efficient-heat-for-industry, checked on 17.01.

IEA (2009): Energy technology transitions for industry. Strategies for the next industrial revolution. International Energy Agency; Organisation for Economic Co-operation and Development. Paris.

IPCC (2018): Global Warming of 1.5°C. An IPCC Special Report on the impacts of global warming of 1.5°C above pre-industrial levels and related global greenhouse gas emission pathways, in the context of strengthening the global response to the threat of climate change, sustainable development, and efforts to eradicate poverty. Edited by [Masson-Delmotte, V., P. Zhai, H.-O. Pörtner, D. Roberts, J. Skea, P.R. Shukla, A. Pirani, W. Moufouma-Okia, C. Péan, R. Pidcock, S. Connors, J.B.R. Matthews, Y. Chen, X. Zhou, M.I. Gomis, E. Lonnoy, T. Maycock, M. Tignor, and T. Waterfield. Press.

Jossart, J.-M.; Rosenberger, C.; Slente, H. P.; Siegmund, T.; Baù, L.; Backéus, S. et al. (2015): Report on conversion efficiency of biomass. BASIS – Biomass Availability and Sustainability Information System. Project supported by the Intelligent Energy Europe program (IEE/12/830/S12.645698). European Biomass Association, Austrian Biomass Association, Danish Bioenergy Association, German BioEnergy Association, Italian Agroforestry Energy, Swedish Bioenergy Association, Spanish Bioenergy Association, French Biomass Energy, Eclareon Consultants, Imperial COllege for Science, Technology and Medicine.

Kadant Johnson Inc. (2005): Heat transfer performance with dryer bars. Technical White Paper series. Kadant Johnson Inc.

Karlsson, H. (2006): Fibre Guide - Fibre analysis and process applications in the pulp and paper industry. Kista, Sweden: AB Lorentzen and Wettre.

Karlsson, M. (Ed.) (2010): Papermaking Part 2, Drying. 2.th ed. Helsinki, Finland: Paper Engineers' Association / Paperi ja Puu Oy (Papermaking science and technology, 9).

Karlsson, M.; Stenström, S. (2005): Static and Dynamic Modeling of Cardboard Drying Part 1: Theoretical Model. In *Drying Technology* 23 (1-2), pp. 143–163. DOI: 10.1081/DRT-200047954.

Karlsson, M.; Oyj, M. (2000): Papermaking Part 2, Drying. Helsinki, Finland: Paper Engineers' Association (Papermaking Science and Technology Series).

Keey, R. B. (1992): Drying of Loose and Particulate Materials. New York, USA: Hemisphere publishing corporation.

Kesicki, F.; Ekins, P. (2012): Marginal abatement cost curves: a call for caution. In *Climate Policy* 12 (2), pp. 219–236. DOI: 10.1080/14693062.2011.582347.

Kesicki, F. (2010): Marginal abatement cost curves for policy making – expert-based vs. model-derived curves. In : Proceedings of the 33rd IAEE International conference 2010. Rio de Janeiro.

Kiiskinen, H.; Salminen, K.; Lappalainen, T.; Asikainen, J.; Keränen, J.; Hellén, E. (2019): Progress in foam forming technology. In *TAPPI Journal* 18 (8), pp. 499–510.

Klemeš, J. Jaromír; Kravanja, Z. (2013): Forty years of Heat Integration. Pinch Analysis (PA) and Mathematical Programming (MP). In *Current Opinion in Chemical Engineering* 2 (4), pp. 461–474. DOI: 10.1016/j.coche.2013.10.003.

Klemeš, J. Jaromír; Varbanov, P. Sabev; Kravanja, Z. (2013): Recent developments in Process Integration. 122. In *Chemical Engineering Research and Design* 91 (10), pp. 2037–2053. DOI: 10.1016/j.cherd.2013.08.019.

Kong, L.; Hasanbeigi, A.; Price, L. (2016a): Assessment of emerging energy-efficiency technologies for the pulp and paper industry: a technical review. In *Journal of Cleaner Production* 122, pp. 5–28. DOI: 10.1016/j.jclepro.2015.12.116.

Kong, L.; Tao, Z.; Liu, H.; Zhang, D. (2016b): Effect of operating parameters on the drying performance of multicylinder paper machine dryer section. In *Drying Technology* 34 (13), pp. 1641–1650. DOI: 10.1080/07373937.2016.1139588.

Kong, L.; Price, L.; Hasanbeigi, A.; Liu, H.; Li, J. (2013): Potential for reducing paper mill energy use and carbon dioxide emissions through plant-wide energy audits: A case study in China. In *Applied Energy* 102, pp. 1334–1342. DOI: 10.1016/j.apenergy.2012.07.013.

Kong, L.; Liu, H. (2012): A Static Energy Model of Conventional Paper Drying for Multicylinder Paper Machines. In *Drying Technology* 30 (3), pp. 276–296. DOI: 10.1080/07373937.2011.635253.

Kong, L.; Liu, H.; Li, J.; Tao, J. (2011): Waste Heat Integration of Coating Paper Machine Drying Process. In *Drying Technology* 29 (4), pp. 442–450. DOI: 10.1080/07373937.2010.506620.

Koretsky, M. D. (2004): Engineering and Chemical Thermodynamics. Hoboken N.J., USA: John Wiley and Sons, Inc.

Körting (2010): Thermocompressors for the paper industry. Controllable steam jet compressors for the pulp and paper industry. Documentation from Manufacturer. Körting Hannover AG.

Kovac, A.; Glavic, P. (1995): Retrofit of complex and energy intensive processes I. In *Computers and Chemical Engineering* 19 (12), pp. 1255–1270.

Krischner, O.; Kast, W. (1978): Die wissenschaftlichen Grundlagen der Trochnungstechnik. Dritte Auflage. Erster Band. Hamburg: Springer-Verlag.

Lang, I. (2009): Effect of the Dryer Fabric on Energy Consumption in the Drying Section. Canada. In *Pulp and Paper Canada* 110 (5), pp. 33–37.

Lang, I. (2004): Drying performance and fabric tension: Mill trials.

Lang, Y.-D.; Biegler, L. T.; Grossmann, I. E. (1990): Simultaneous optimization and heat integration with process simulators. In *Computers and Chemical Engineering* 12 (4), pp. 311–327.

Laurijssen, J. (2013): Energy use in the paper industry. An assessment of improvement potentials at different levels. Ph.D. Thesis. Utrecht University. Kenniscentrum Papier en Karton.

Laurijssen, J.; Gram, F. J. de; Worrell, E.; Faaij, A. (2010): Optimizing the energy efficiency of conventional multi-cylinder dryers in the paper industry. In *Energy* 35 (9), pp. 3738–3750. DOI: 10.1016/j.energy.2010.05.023.

Lee, U.; Mitsos, A.; Han, C. (2016): Optimal retrofit of a CO2 capture pilot plant using superstructure and rate-based models. In *International Journal of Greenhouse Gas Control* 50, pp. 57–69. DOI: 10.1016/j.ijggc.2016.03.024.

Lehmonen, J.; Rantanen, T.; Kinnunen-Raudaskoski, K. (2019): Upscaling of foam forming technology for pilot scale, TAPPI JOURNAL August 2019. In *TAPPI Journal* 13 (8), pp. 461–471.

Leipprand, A.; Holtz, G.; Schneider, C.; Lenz, V.; Jordan, M.; Lorenz, T. (2020): Auf dem Weg zur klimaneutralen Industrie – Herausforderungen und Strategien. FVEE-Jahrestagung 2020 "Forschung für den European Green Deal". Wuppertal Institut, DBFZ, UFZ, DLR, FZ Jülich, ISFH, KIT.

Lenaghan, M.; Mill, D. (2015): Industrial Decarbonisation and Energy Efficiency Roadmaps: Scottish Assessment. Summary Report. Prepared by: Zero Waste Scotland. Stirling, Scotland.

Li, J.; Kong, L.; Liu, H. (2012): Dryer Section Energy System Measurement and Energy-Saving Potential Analysis for a Paper Machine. In *Measurement and Control* 45 (8), pp. 239–243. DOI: 10.1177/002029401204500803.

Lindell, K.; Stenström, S. (2006): A Modular Process Modeling Tool for the Analysis of Energy Use and Cost in the Pulp and Paper Industry. In *Drying Technology* 24 (11), pp. 1335–1345. DOI: 10.1080/07373930600951109.

Liu, Z.; Wang, H.; Hui, L. (2018): Pulping and Papermaking of Non-Wood Fibers. In Salim Newaz Kazi (Ed.): Pulp and Paper Processing: InTech.

Li, Y.; Liu, H.; Li, J.; Tao, J. (2011): Process Parameters Optimization for Energy Saving in Paper Machine Dryer Section. In *Drying Technology* 29 (8), pp. 910–917. DOI: 10.1080/07373937.2010.548617.

Li, Y. (2001): Développement d'un nouveau modèle de simulation d'une sècherie multi-cylindrique. Master's Thesis. Université du Québec à Trois-Rivières.

Lucidi, G. (2020): Email communication on the application of IR dryers in the paper industry with Mr. Lucidi. President and CEO of the American company Marsden, Inc. specialized in process heating technologies. Email, 2020.

Maloney, T.; Paulapuro, H. (1999): The Formation of Pores in the Cell Wall. In *Journal of Pulp and Paper Science* 25 (12), pp. 430–436.

Manninen, J.; Puumalainen, T.; Talja, R.; Pettersson, H. (2002): Energy aspects in paper mills utilising future technology. In *Applied Thermal Engineering* 22 (8), pp. 929–937. DOI: 10.1016/S1359-4311(02)00010-8.

McCall, J. M.; Douglas, W. J. M. (2006): Use of Superheated Steam Drying to Increase Strength and Bulk of Papers Produced from Diverse Commercial Furnishes. In *Drying Technology* 24 (2), pp. 233–238. DOI: 10.1080/07373930600559183.

Mehling, M. A. (2020): Instrument Choice for Climate Change Mitigation: A Legal Perspective. Ph.D. Thesis. University of Helsinki, Helsinki, Finland.

Meier, A.; Rosenfeld, A.; Wright, J. (1982): Supply curves of conserved energy for California's residential sector. In *Energy* 7, pp. 347–358.

Mende, D. (2009): Trockenpartie Konzepte von Metso. Vereinigung Gernsbacher Papiermacher e.V. 17. - 20. Mai 2009. Metso Paper GmbH. Stadthalle Gernsbach, 2009.

Min, K.-J.; Binns, M.; Oh, S.-Y.; Cha, H.-Y.; Kim, J.-K.; Yeo, Y.-K. (2015): Screening of site-wide retrofit options for the minimization of CO2 emissions in process industries. In *Applied Thermal Engineering* 90, pp. 335–344. DOI: 10.1016/j.applthermaleng.2015.07.008.

Miranda, R.; Monte, M. Concepcion; Blanco, A. (2013): Analysis of the quality of the recovered paper from commingled collection systems. In *Resources, Conservation and Recycling* 72, pp. 60–66. DOI: 10.1016/j.resconrec.2012.12.007.

Moore, B. (2017): Recovered Paper Market Trends. Recycle Florida Today. Moores and Associates. Tampa, Florida, 2017.

Moya, J. A., Pavel, C. C. (2018): Energy efficiency and GHG emissions: Prospective scenarios for the pulp and paper industry. EUR 29280 EN. Joint Research Centre, European Commission. Publications Office of the European Union, Luxembourg.

Mujumdar, Arun (Ed.) (2006): Handbook of Industrial Drying, Third Edition. Boca Raton, Florida: CRC Press.

Myhre, G.; d. Shindell; Bréon, F.-M.; Collins, W.; Fuglestvedt, J.; J. Huang; D. Koch, J.-F. Lamarque, D. Lee, B. Mendoza, T. Nakajima, A. Robock, G. Stephens, T. Takemura and H. Zhang (2013): Anthropogenic and Natural Radiative Forcing. In: Climate Change 2013: The Physical Science Basis. Contribution of Working Group I to the Fifth Assessment Report of the Intergovernmental Panel on Climate Change. Edited by Stocker, T.F., D. Qin, G.-K. Plattner, M. Tignor, S.K. Allen. Intergovernmental Panel on Climate Change.

Neikov, Oleg d.; Naboychenko, Stanislav; Yefimov, N. A.; Lotsko, Dina v. (Eds.) (2009): Handbook of non-ferrous metal powders. Technologies and Applications. 2nd: Elsevier Science.

Nelson, D. A.; Douglas, J. A. (1990): A systematic procedure for retrofitting chemical plants to operate utilizing different reaction paths. In *Ind. Eng. Chem. Res.* 29, pp. 819–829.

Nilsson, L. (2004a): Heat and mass transfer in multicylinder drying Part I Analysis of machine data. In *Chemical Engineering and Processing: Process Intensification* 43 (12), pp. 1547–1553. DOI: 10.1016/j.cep.2004.03.003.

Nilsson, L. (2004b): Heat and mass transfer in multicylinder drying Part II Analysis of internal and external transport resistances. In *Chemical Engineering and Processing: Process Intensification* 43 (12), pp. 1555–1560. DOI: 10.1016/j.cep.2004.03.002.

Nissan, A. H.; Knye, W. G. (1955): An Analytical Approach to the Problem of Drying of Thin Fibrous Sheets on Multicylinder Machines. In *Tappi* 38(7), pp. 385-398.

Olson, J. A. (2013): Papermachine - Drying. Lecture on Papermaking: Topic 15. The University of British Columbia. Vancouver, Canada, 2013.

Othen, R. (2014): Papier machen. Einfach machen. Available online at https://www.papier-machen.de/, updated on 2014, checked on 2/10/2022.

Paptic (2021): Sustainable Alternative to Plastic Materials in Packaging. Available online at https://paptic.com/, checked on 8/4/2021.

Persson, H. (1998): Dynamic Modelling and Simulation of Multi-Cylinder Paper Dryers. licentiate dissertation. Lund University, Lund, Sweden.

Pflugradt, N.; Lehnguth, M.; Schirmer U. (2009): Thermodynamische Grundlagen - Dokumentation des Berechnungsprogramms feuchte Luft. Mollier-hx-Diagramm für feuchte Luft.

Pikulik, I. (2006): Papridry, A New Technique for Drying of Paper and Board. In : Proceedings of Pan Pacific Conference 2006. Seoul, Korea.

Poirier, N.; Pikulik, I.; Sadeghi, M. (2004): Papridry - The future of paper drying? In : Proceedings of the 14th International Drying Symposium. Sao Paulo, Brazil, 22-25 August.

Polat, O.; Mujumdar, A. (2006): Drying of Pulp and Paper. In Arun Mujumdar (Ed.): Handbook of Industrial Drying, Third Edition. Boca Raton, Florida: CRC Press.

Powell, J. (2017): Scientists Reach 100% Consensus on Anthropogenic Global Warming. In *Bulletin of Science, Technology and Society* 37 (4), pp. 183–184. DOI: 10.1177/0270467619886266.

Putz, H.-J.; Schabel, S. (2018): Der Mythos begrenzter Faserlebenszyklen. Über die Leistungsfähigkeit einer Papierfaser. In *Wochenblatt für Papierfabrikation*, pp. 350–357.

Rajamani, L.; Brunnée, J. (2017): The Legality of Downgrading Nationally Determined Contributions under the Paris Agreement: Lessons from the US Disengagement. In *Journal of Environmental Law* 29 (3), pp. 537–551. DOI: 10.1093/jel/eqx024.

Repenning, J.; Emele, L.; Blanck, R.; Böttcher, H.; Dehoust, G.; Förster, H. et al. (2015): Klimaschutzszenario 2050 – 2. Endbericht. Öko-Institut and Fraunhofer ISI for Bundesministeriums für Umwelt, Naturschutz, Bau und Reaktorsicherheit (UBA).

Rhodius, D.; Göttsching, L. (1979): Der Trocknungsverlauf von Papier und Pappe in Abhängigkeit von Trocknungstechnischen und papiertechnologischen Parametem. Teil IV: Trocknung in der Mehrzylinder- Trockenpartie. In *Das Papier* 33, pp. 1–9.

Rogers, J. G. (2018): Paper making in a low carbon economy. In *AIMS Energy* 6 (1), pp. 187–202. DOI: 10.3934/energy.2018.1.187.

Roonprasang, K. (2008): Thermal Analysis of Multi-Cylinder Drying Section with variant Geometry. Ph.D. Thesis. Technische Universität Dresden, Germany.

Rossié, K. (1953): Die Diffusion von Wasserdampf in Luft bei Temperaturen bis 300 °C. In *Forschung im Ingenieurwesen* 19, pp. 49–58.

Schlesinger, M.; Hofer, P.; Kemmler, A.; Kirchner, A.; Koziel, S.; Ley, A. et al. (2014): Entwicklung der Energiemärkte - Energiereferenzprognose. Project Nr. 57/12 funded by the German Federal Ministry of Economics and Technology (BMWi). Prognos AG, EWI, GWS.

Schneeberger, M. (2014): „Energetische Trocknungsoptimierung bei Papiermaschinen mittels Simulation der Stoff- und Wärmeübertragung unter Berücksichtigung der trocknungsrelevanten Eigenschaften der Faserstoffe". Ph.D. Thesis. TU Graz, Austria.

Schuewer, D.; Schneider, C. (2018): Electrification of industrial process heat: long-term applications, potentials and impacts. In : Proceedings of ECEEE Industrial Summer Study 2018. Berlin, Germany, 11-13 June, pp. 411–422.

Sivill, L.; Ahtila, P. (2009): Energy efficiency improvement of dryer section heat recovery systems in paper machines – A case study. In *Applied Thermal Engineering* 29 (17-18), pp. 3663–3668. DOI: 10.1016/j.applthermaleng.2009.06.022.

Sivill, L.; Ahtila, P.; Taimisto, M. (2005): Thermodynamic simulation of dryer section heat recovery in paper machines. In *Applied Thermal Engineering* 25 (8-9), pp. 1273–1292. DOI: 10.1016/j.applthermaleng.2004.09.002.

Slätteke, O. (2006): Modeling and Control of the Paper Machine Drying Section. Ph.D. Thesis. Lund University, Sweden.

Slawtschew, G. (2020): Richtiger Umgang mit heißer Luft. VAP Mitarbeitermagazin der Papierindustrie (Papier + Technik). Available online at https://www.papierundtechnik.de/papiertechnik/richtiger-umgang-mit-%C2%84heisser-luft%C2%93/#slider-intro-3, checked on 2/8/2021.

Smith, R. (2005): Chemical process design and integration. Chichester, UK: John Wiley and Sons, Inc.

Sommerhalder, M.; Schelske, O.; Nussbaumer, T.; Engeli, H.; Membrez, Y. (2007): Wirtschaftlichkeit von heutigen Biomasse-Energieanlagen. Project funded by the Swiss Ministry for Energy. Ernst Basler + Partner AG, Verenum, engeli engineering, EREP S.A. Bern, Switzerland.

Stenström, S. (2020): Drying of paper: A review 2000–2018. In *Drying Technology* 19, pp. 1–21. DOI: 10.1080/07373937.2019.1596949.

Stumm, D. R. K. (2007): Untersuchungen zum chemischen Wasserrückhaltevermögen und zur Trocknungsfähigkeit von Papierstoffen unter besonderer Berücksichtigung der Rolle von chemischen Additiven. Ph.D. Thesis. Technische Universität Darmstadt, Darmstadt.

Suhr, M.; Klein, G.; Kourti, I.; Gonzalo, M. Rodrigo; Santonja, G. Giner; Roudier, S.; Delgado Sancho, L. (2015): Best available techniques (BAT) reference document for the production of pulp, paper and board. Industrial emissions directive 2010/75/EU (integrated pollution prevention and control). Luxembourg: Publications Office of the European Union (JRC science and policy reports, 27235). Available online at http://dx.doi.org/10.2791/370629.

TAPPI (1992): Dryer surface temperature measurement. 5th ed. Technical Association of Pulp and Paper Industry (Technical Information paper, 0404-39).

TAPPI (1983): Recommended dryer differential pressures. 4th ed. Technical Association of Pulp and Paper Industry (Technical Information paper, 0404-31).

TAPPI (1979): Guidelines for the design, operation, performance evaluation, and troubleshooting of a paper machine hood and air systems. 4th ed. Technical Association of Pulp and Paper Industry (Technical Information paper, 0404-24).

Terlau, W.; Fuchshofen, N.; Klement, J. (2017): Ökologischer Vergleich des Einsatzes von Sulfat-Zellstoff, Altpapierstoff und grasbasiertem Zellstoff in der deutschen Papierproduktion. Project funded by Creapaper GmbH. University of Applied Sciences, Bonn-Rhein-Sied and International Centre for sustainable development.

Toto, D. A. (2019): PPRCE 2019: Global shifts in paper and board production. Available online at https://www.recyclingtoday.com/article/pprce-2019-paper-production-globally/, updated on 11/11/2019, checked on 9/6/2020.

Treppe, K.; Zelm, R.; Schinke, L.; Kuitunen, S.; Pinnau, S.; Kamischke, R. et al. (2012): Energetische Optimierung der Trockenpartie Wärmetechnische Bewertung zur Steigerung der Energieeffizienz. Final Report for the Project n°117 funded by the Center of Research and Technology of the German Pulp and Paper Association. Technische Universität Dresden. Bonn, Germany.

Tyndall, J. (1861): On the absorption and radiation of heat by gases and vapours. In *Philosophical magazine and Journal of Science* 22, pp. 169–194.

Tysen, A. (2018): Through air drying - Thermographic studies of drying rates, drying non-uniformity and infrared assisted drying. Ph.D. Thesis. Karlstad University, Karlstad, Sweden. Chemical Engineering Department.

UBA (2021): Entwicklung der spezifischen Kohlendioxid-Emissionen des deutschen Strommix 1990-2020. Umweltbundesamt. Available online at https://www.umweltbundesamt.de/sites/default/files/medien/372/bilder/strommix-2020.png, checked on 8/5/2021.

UBA (2012): Papier - Wald und Klima schützen. Flyer funded by the German Environment Agency. Forum Ökologie und Papier (FÖP).

Vakkilainen, E. Kari (2017): Steam generation from Biomass. Construction and design of large boilers: Elsevier Inc.

Valmet (2019): New opportunities with OptiSizer Hard. Valmet. Available online at https://www.valmet.com/board-and-paper/board-and-paper-machines/sizing/hard-nip-sizing/new-opportunities-with-hard-nip-sizing/, checked on 6/15/2021.

Valmet (2015a): Energy Savings. Technical Paper Series.

Valmet (2015b): OptiDry Vertical impingement drying. Revolutionary technology for drying capacity increase in rebuilds. Available online at https://www.valmet.com/board-and-paper/board-and-paper-machines/drying/impingement-drying/capacity-increase-for-rebuilds/, checked on 8/5/2021.

Valmet (2012): Papermaking Savings Potentials. Technical Paper Series.

Valmet (2010): Steinbeis PM 4 increases its production capacity. Available online at https://www.valmet.com/media/articles/all-articles/steinbeis-pm-4-increases-its-production-capacity/, checked on 8/5/2021.

Varbanov, P.; Perry, S.; Makwana, Y.; Zhu, X. X.; Smith, R. (2004): Top-level Analysis of Site Utility Systems. In *Chemical Engineering Research and Design* 82 (6), pp. 784–795. DOI: 10.1205/026387604774196064.

VDP (2020): Papier 2020 - Ein Leistungsbericht. German Pulp and Paper Association. Bonn, Germany.

Voith (2019): Steel cylinders are the future of drying. EvoDry (Product sheet).

Weise, U. (1997): Characterization and mechanism of changes in wood pulp fibres caused by water removal. Ph.D. Thesis. Helsinki University of Technology, Helsinki, Finland.

Wilhelmsson, B.; Stenström, S.; Nilsson, L.; R. Krook; H. Persson; R. Wimmerstedt (1996): Modeling multicylinder paper drying-validation of a new simulation program. In *TAPPI Journal* 79 (4), pp. 157–167.

Wilhelmsson, B.; Stenström, S. (1995a): Experimental and computational evaluation of mass transfer resistance of paper dryer fabrics. In *Nordic Pulp and Paper Research Journal* 10 (3), pp. 174–182.

Wilhelmsson, B.; Stenström, S. (1995b): Heat and Mass Transfer Coefficients in Computer Simulation of Paper Drying. In *Drying Technology* 13 (4), pp. 959–975. DOI: 10.1080/07373939508916993.

Wilhelmsson, B.; Nilsson, L.; Stenstram, S.; Wimmerstedt, R. (1993): Simulation models of multi-cylinder paper drying. In *Drying Technology* 11 (6), pp. 1177–1203. DOI: 10.1080/07373939308916895.

Williamson, M. (2015): Cartones Ponderosa strengthens its competitive advantage. In *Pulp and paper International* 56 (9), pp. 49–52.

Wising et al. (2015): Industrial Decarbonisation and Energy Efficiency Roadmaps to 2050. Pulp and Paper. Funded by the Government of the UK. Parsons Brinckerhoff and DNV GL.

WMO (2021): 2020 was one of three warmest years on record. Press Release Number: 14012021. World Meteorological Organization. Available online at https://public.wmo.int/en/media/press-release/2020-was-one-of-three-warmest-years-record, updated on 1/15/2021, checked on 2/4/2021.

WMO (2020): State of Global Climate 2020. Provisional Report. World Meteorological Organization. Geneva, Switzerland.

WRI (2016): World Greenhouse Gas Emissions: 2016. Source: Climate Watch, based on raw data from IEA (2018), CO2 Emissions from Fuel Combustion. World Resources Institute. Available online at https://www.wri.org/resources/data-visualizations/world-greenhouse-gas-emissions-2016, updated on 2/1/2020, checked on 2/4/2021.

Yin, Y.; Li, J.; Liu, H.; Chen, X. (2016): An energy-saving assessment approach for hood retrofitting in multi-cylinder dryer sections. In *Drying Technology* 34 (15), pp. 1868–1883. DOI: 10.1080/07373937.2016.1142452.

Zhang, L.; Zhao, L.; Wang, E. N. (2020): Stefan flow induced natural convection suppression on high-flux evaporators. In *International Communications in Heat and Mass Transfer* 110, p. 104255. DOI: 10.1016/j.icheatmasstransfer.2019.03.020.

Zhelev, T. K.; Varbanov, P. S.; Seikova I. (1998): HEN's operability analysis for better process integrated retrofit. In *Hung J Ind Chem* 26, pp. 81–88.

Zuberi, M. Jibran S.; Patel, M. K. (2019): Cost-effectiveness analysis of energy efficiency measures in the Swiss chemical and pharmaceutical industry. In *Int J Energy Res* 43 (1), pp. 313–336. DOI: 10.1002/er.4267.

A. Appendix: Derivation of model equations

Derivation of Equation (1):

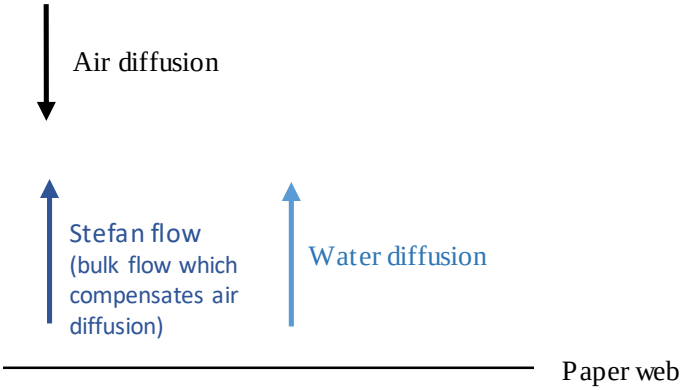

As represented above, the total vapor flux j is the sum of the convective and diffusive flux:

$$j = -D_{wa}\frac{M_w}{RT_p}\frac{dp_w}{dz} + \frac{p_w M_w}{RT_p}V_0$$

Where D_{wa} is the mass diffusivity (m^2/s) from water to air and V_0 is the bulk flow velocity of air (m/s) expressed as:

$$V_0 = \frac{D_{aw}}{p_a}\frac{dp_a}{dz}$$

On the basis of force and counterforce $D_{wa} = D_{aw}$, and with the Dalton's law for an ideal gas mixture $p_w + p_a = p_{tot}$ and $\frac{dp_a}{dz} + \frac{dp_w}{dz} = 0$. Thus, the total vapor flux j can be expressed as:

$$j = \frac{D_{aw}M_w p_{tot}}{RT_p p_a}\frac{dp_a}{dz}$$

After integration on the whole thickness of the diffusion layer Z and with the mass transfer coefficient $K = \frac{D_{aw}}{Z}$, Equation (1) is obtained:

$$\dot{q}_{evap} = \frac{KM_w p_{tot}}{RT_p} \cdot ln\left(\frac{p_{tot} - p_{aw}}{p_{tot} - p_{pw}}\right)$$

Derivation of Equation (6):

According to the ideal gas law:

$$m = \frac{p_{tot}VM}{RT}$$

Furthermore, the Dalton's law states that the total pressure for an ideal gas mixture is equal to the sum of the partial pressures of each individual component at the same temperature (T) and total volume (V) of the mixture. Thus, for a gas mixture composed of water vapor and dry air:

$p_{dry\ air} = p_{tot} - p_{aw}$, $m_{water\ vapor} = \frac{p_{aw} V M_w}{RT}$ and $m_{dry\ air} = \frac{p_{dry\ air} V M_a}{RT}$

The absolute humidity of water in air can thus be expressed as:

$$x_a = \frac{m_{water\ vapor}}{m_{dry\ air}} = \frac{M_w p_{aw}}{M_a (p_{tot} - p_{aw})}$$

Which leads to following expression of the partial pressure of water in air with $M_w = 18\ g/mol$ and $M_a = 29\ g/mol$:

$$p_{aw} = \frac{x_a}{x_a + 0.62} p_{tot}$$

Derivation of Equation (24):

The heat transfer rate for heat conduction across cylinder walls can be expressed as:

$$\dot{Q} = \frac{dQ}{dt} = -\lambda_{shell} \cdot 2\pi r \mathrm{L} \cdot \frac{\mathrm{dT}}{\mathrm{dr}}$$

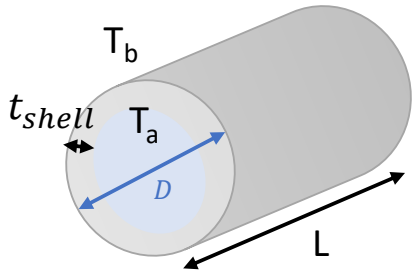

And thus:

$$\frac{dr}{r} = \frac{-\lambda_{shell} \cdot 2\pi \mathrm{L} \cdot dT}{\dot{Q}}$$

The integration of this expression along the thickness of the cylinder shell results in:

$$\dot{Q} = \frac{\lambda_{shell} \cdot 2\pi \mathrm{L} \cdot (\mathrm{T_a} - \mathrm{T_b})}{\ln\left(\frac{\frac{D}{2}}{\frac{D}{2} - t_{shell}}\right)}$$

Furthermore, per definition the heat transfer rate is the product of the heat transfer coefficient, the surface of heat transfer and the temperature difference.

$$\dot{Q} = h_{shell} \cdot \mathrm{A_{ht}} \cdot (\mathrm{T}_a - \mathrm{T_b})$$

Considering the surface of heat transfer as the surface of the inner cylinder:

$$\mathrm{A_{ht}} = 2\pi \mathrm{L} \cdot \left(\frac{\mathrm{D}}{2} - t_{shell}\right)$$

And thus Equation (24) is obtained:

$$h_{shell} = \frac{\lambda_{shell}}{\left(\frac{D}{2} - t_{shell}\right) \cdot \ln\left(\frac{\frac{D}{2}}{\frac{D}{2} - t_{shell}}\right)}$$

B. Appendix: Data and assumptions

Table B.1: Main assumptions on the $CAPEX$ of the selected measures. Source: Own assumptions based on values provided by technology manufacturers, Fattler et al. (2019), Sommerhalder et al. (2007).

	Unit	Value
Curtain sizing	EUR_{2021}/unit	2 000 000
Closed hood with high dew point	EUR_{2021}/meter of hood	13500
Heat pump for air heating	$EUR_{2021}/kW_{th\ output}$	300
Heat pump for steam generation	$EUR_{2021}/kW_{th\ output}$	400[1)]
Biomass boiler	$EUR_{2021}/kW_{th\ output}$	400
Electro-/Electrode boiler	$EUR_{2021}/kW_{th\ output}$	90
Green hydrogen boiler	$EUR_{2021}/kW_{th\ output}$	99
Natural gas boiler	$EUR_{2021}/kW_{th\ output}$	90

1) The difference to the $CAPEX$ assumed for the heat pump for air heating is due to the higher temperature lift.

Table B.2: Assumptions on the thermal efficiency of a boiler system for different fuels, the emission factors for fuel and electricity, and the prices for fuel, electricity, and CO_2 for the year 2021

	Thermal efficiency of boiler system	Emission factor	Price
Unit	%	g/kWh	EUR-ct_{2021} /kWh EUR_{2021} /tCO2
Lignite	87.3[1)]	360	1.5[7)]
Natural gas	95[2)]	201.2	2.6[8)]
Biomass	83[3)]	0	2.5[9)]
Electricity	99[4)]	400.6[6)]	9[10)]
Green hydrogen	95[5)]	0	14.4[11)]
CO_2-price	-	-	53.5[12)]

1) Current thermal efficiency of the local heat generation system
2) Biedermann and Kolb (2014)
3) Jossart et al. (2015), Vakkilainen (2017)
4) Schuewer and Schneider (2018)
5) 10% above thermal efficiency for natural gas system according to technology manufacturer
6) Value obtained for a linear decrease until 0 in 2050, with a value of 434 g_{CO2}/kWh for the domestic power consumption in 2019 taken from (UBA 2021)
7) Local lignite providers
8) Includes grid charges. Based on European Energy Exchange (EEX) stock exchange prices (consulted on 14.07.2021) and discussions with experts from the industry branch.
9) Price for wood chips (CARMEN e.V. 2021)
10) Includes the grid and reallocated capacity charges. Based on European Power Exchange (EPEX) spot market (consulted on 14.07.2021) and discussions with industry experts. In Germany, Paper mills are usually exempted from the renewable energy reallocation charge on the electricity purchase (in German "EEG-Umlage") due to their high energy consumption.
11) Based on the "Hydrogen-Index" proposed by the company E-Bridge Consulting GmbH (consulted on 14.07.2021)
12) OTC EU CO2 Allowances 2022 (consulted on 14.07.2021)

C. Appendix: Additional details on results

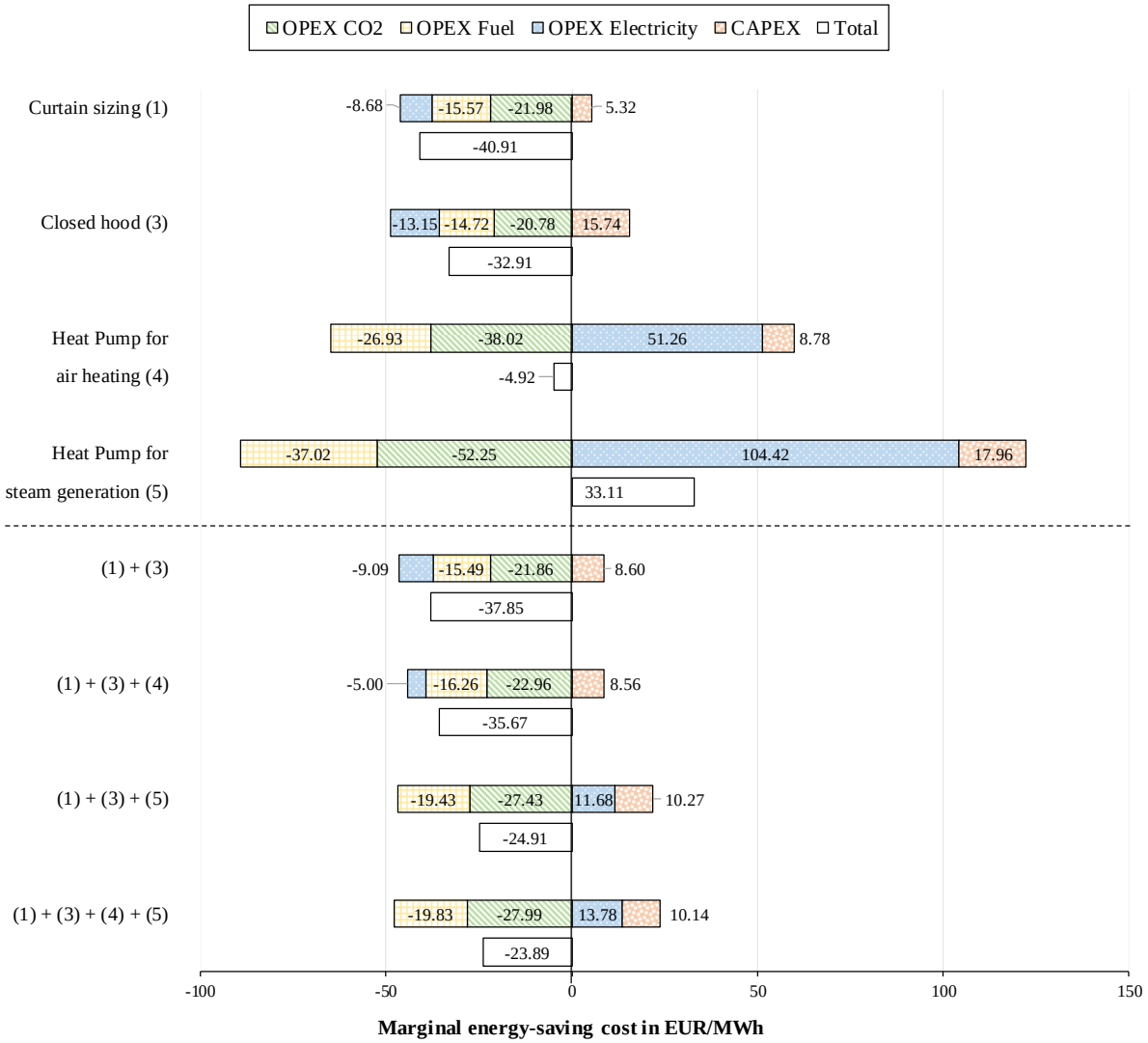

Figure C.1: Breakdown of the calculated marginal energy-saving cost for different combinations of measures in the trend scenario with an average economic lifetime of the measures of 10 years

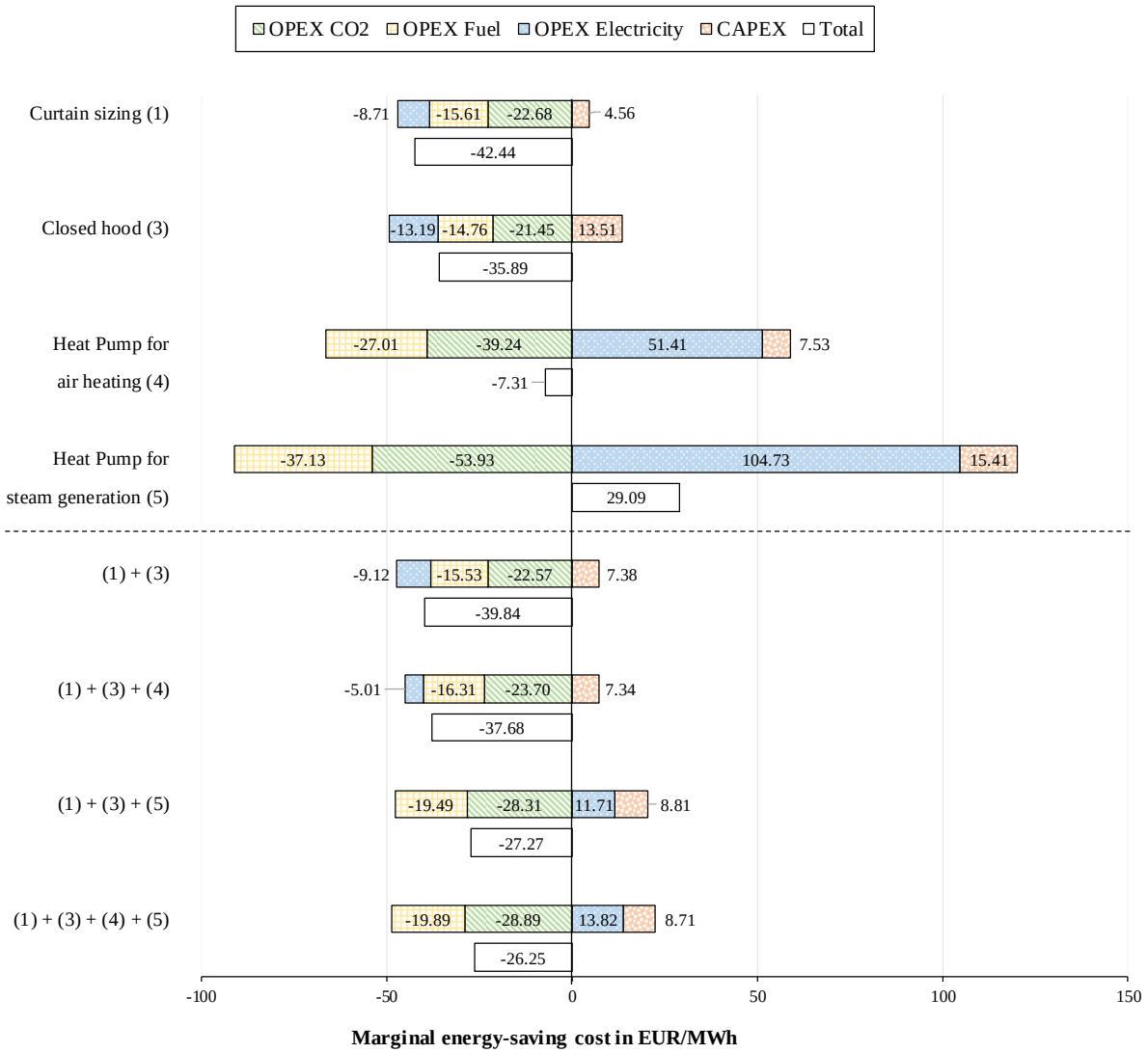

Figure C.2: Breakdown of the calculated marginal energy-saving cost for different combinations of measures in the trend scenario with an average economic lifetime of the measures of 15 years

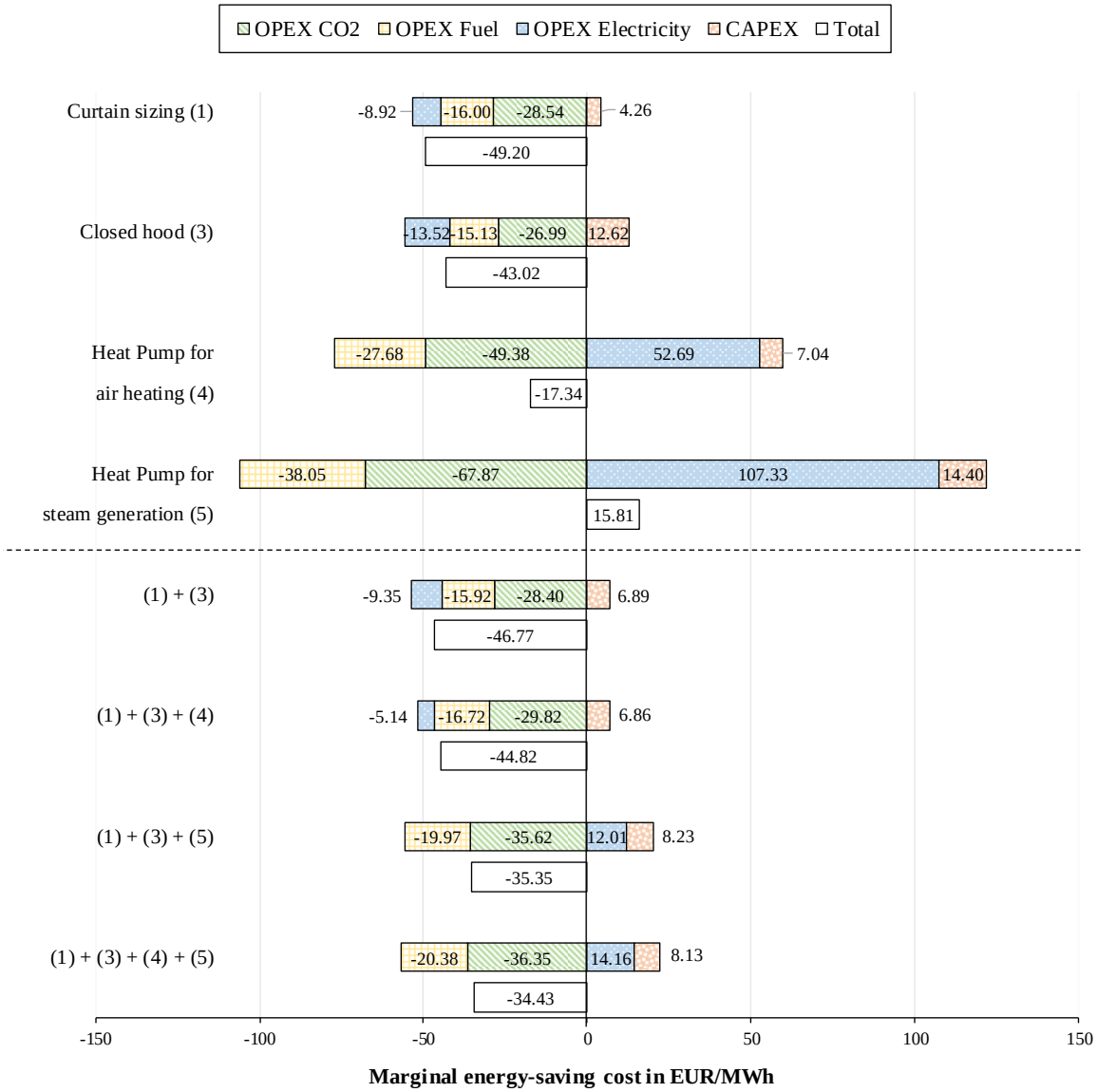

Figure C.3: Breakdown of the calculated marginal energy-saving cost for different combinations of measures in the trend scenario with an average economic lifetime of the measures of 20 years, implementation in 2030

Table C.1: Calculated total annual cost in kEUR$_{2021}$/a for different combinations of measures and parameter variations in the trend scenario

	Trend	CO_2-price in 2050		Discount rate		Yearly fuel price increase[1)]		Project lifetime	
Parameter variation		*-25%*	*+25%*	*-25%*	*+25%*	*-25%*	*+25%*	*-25%*	*+25%*
Measures									
All EE	-3177.2	-2922.8	-3431.6	-3416.1	-2950.4	-3174.8	-3179.6	-3038.9	-3253.7
All EE + biomass	-3882.6	-3383.1	-4382	-4338.5	-3449.6	-3886	-3879.1	-3619.1	-4028
All EE + electricity	3343	3842.5	2843.6	3019.7	3645.9	3313	3373.2	3543.5	3229.1
All EE + hydrogen	11264.3	11763.8	10764.9	10954.2	11556.8	11207.6	11321.4	11450.2	11160.2
All EE + natural gas	-3269.8	-2896.2	-3643.3	-3574.1	-2982.8	-3271.8	-3267.7	-3087.4	-3372.1

1) For a 25% lower yearly fuel price increase than in the trend scenario (0.19%) the fuel price in 2050 is **5.6% higher than in 2021**, whereas for a 25% higher yearly fuel price increase than in the trend scenario (0.31%), the fuel price in 2050 is **9.5% higher than in 2021**.

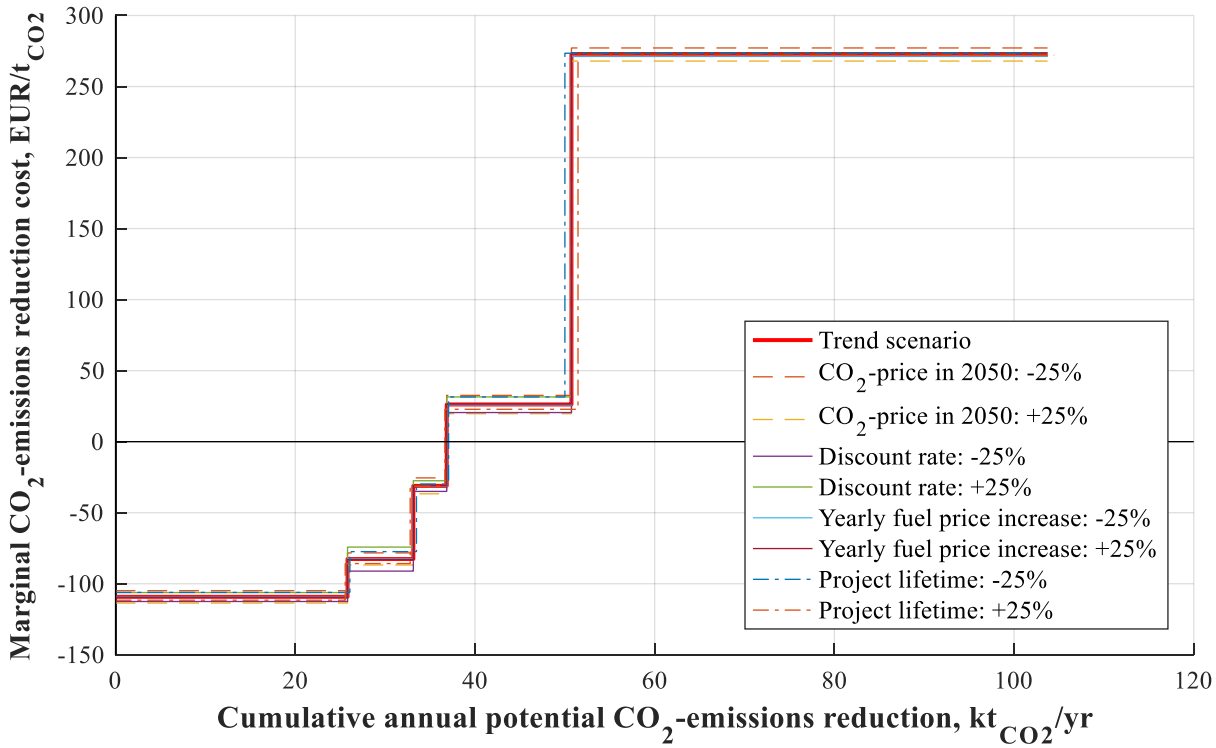

Figure C.4: Sensitivity analysis of various parameters on the MACC of the combination of measures "All EEM + fuel switching to green hydrogen" in the trend scenario

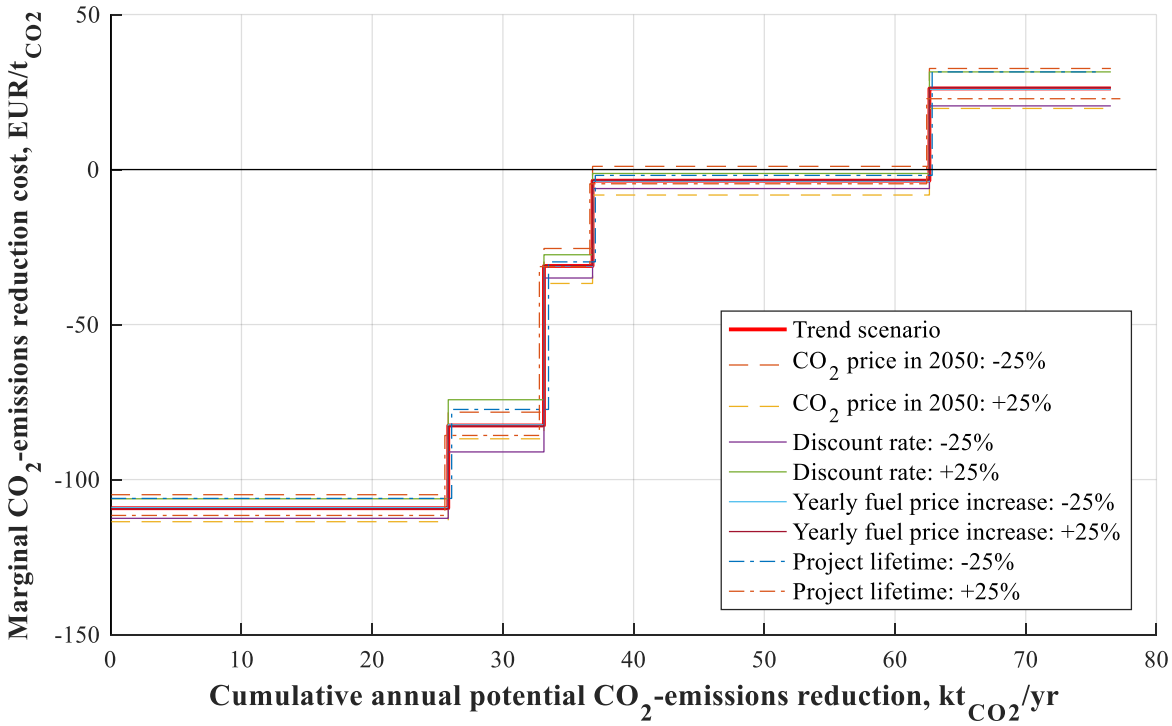

Figure C.5: Sensitivity analysis of various parameters on the MACC of the combination of measures "All EEM + fuel switching to natural gas" in the trend scenario

Forschungsberichte des Instituts für Energiewirtschaft und Rationelle Energieanwendung

Bezugsadresse: Universität Stuttgart
Institut für Energiewirtschaft und Rationelle Energieanwendung
- Bibliothek –
Tel.: 0711 / 685 87861
Fax: 0711 / 685 87873
E-Mail: bib@ier.uni-stuttgart.de

Bestellungen sind auch über Internet möglich:
https://www.ier.uni-stuttgart.de

Band 150 A. Dobbins
System analysis of the significance of energy poverty on household energy use and emissions in Germany
2022, 222 Seiten

Band 149 D. Chudinzow
Modelling the energy yield of bifacial photovoltaic plants and their integration into European power supply systems
2022, 92 Seiten

Band 148 F. Rainer
Methodology for Integrated Impact Assessment of Emissions of Air Pollutants, Noise and Greenhouse Gases in Europe – ExternE Methodology Update 2022
2022

Band 147 D. Turek
Die Standortwahl von Rechenzentren unter Berücksichtigung der Total Cost of Ownership – Ein Framework zur multikriteriellen Entscheidungsanalyse
2022, 114 Seiten

Band 146 N. Seckinger
Methodische Weiterentwicklung dynamischer, prospektiver Treibhausgasemissionsfaktoren zur Analyse von Technologien der Sektorkopplung
2022, 242 Seiten

Band 145 M. Unger
Systematische Analyse von Druckluftleckagen
August 2021, 186 Seiten

Band 144 N. Li, G. Huang, R. Friedrich, U. Vogt, S. Schürmann, D. Straub
Messung und Bewertung der Schadstoffemissionen von Holzfeuerungen in Innenräumen
Juli 2019, 44 Seiten

Band 143 N. Li
Long-term Exposure of European Population Subgroups to PM2.5 and NO2
August 2020, 152 Seiten

Band 142 M. Miller
Wege zur Ermittlung von Energieeffizienzpotenzialen von Informationsund Kommunikationstechnologien
Februar 2020, 391 Seiten

Band 141 R. Flatau
Integrierte Bewertung interdependenter Energieeffizienzmaßnahmen – Eine modellgestützte Analyse am Beispiel von Querschnittstechnologien
Juli 2019, 216 Seiten

Band 140 B. Fleischer
Systemeffekte von Bioenergie in der Elektrizitäts- und Fernwärmewirtschaft – Eine modellgestützte Analyse langfristiger Energiewendeszenarien für Deutschland
April 2019, 190 Seiten

Band 139 B. Mousavi
Analysis of the relative roles of supply-side and demand-side measures in tackling global climate change – Application of a hybrid energy system model
Januar 2019, 167 Seiten

Band 138 S. Bothor
Prognose von Netzverlusten
August 2019, 152 Seiten

Band 137 C. Schieberle
Development of a stochastic optimization approach to determine cost-efficient environmental protection strategies: Case study of policies for the future European passenger transport sector with a focus on railbound and on-road activities
Mai 2019, 218 Seiten

Band 136 J. Welsch
Modellierung von Energiespeichern und Power-to-X im deutschen und europäischen Energiesystem
Dezember 2018, 158 Seiten

Band 135 M. Stenull
Stand und Entwicklungspotenziale der landwirtschaftlichen Biogasnutzung in Baden-Württemberg – ein regionalspezifischer Vergleich
Juni 2017, 171 Seiten

Band 134 J. Brunke
Energieeinsparpotenziale von energieintensiven Produktionsprozessen in Deutschland: Eine Analyse mit Hilfe von Energieeinsparkostenkurven
August 2017, 353 Seiten

Band 133 S. Wolf
Integration von Wärmepumpen in industrielle Produktionssysteme – Potenziale und Instrumente zur Potenzialerschließung
Juli 2017, 177 Seiten

Band 132 S. Marathe
Recognising the Change in Land Use Patterns and its Impacts on Energy Demand and Emissions in Gauteng, South Africa
April 2017, 202 Seiten

Band 131 T. Haasz
Entwicklung von Methoden zur Abbildung von Demand Side Management in einem optimierenden Energiesystemmodell – Fallbeispiele für Deutschland in den Sektoren Industrie, Gewerbe, Handel, Dienstleistungen und Haushalte
April 2017, 177 Seiten

Band 130 M. Steurer
Analyse von Demand Side Integration im Hinblick auf eine effiziente und umweltfreundliche Energieversorgung
April 2017, 230 Seiten

Band 129 S. Bubeck
Potenziale elektrischer Energieanwendungstechniken zur rationellen Energieanwendung
Januar 2017, 255 Seiten

Band 128 R. Beestermöller
Die Energienachfrage privater Haushalte und ihre Bedeutung für den Klimaschutz – Volkswirtschaftliche Analysen zur deutschen und europäischen Klimapolitik mit einem technologiefundierten Allgemeinen Gleichgewichtsmodell
Januar 2017, 211 Seiten

Band 127 M. Ohl
Analyse der Einsatzpotenziale von Wärmeerzeugungstechniken in industriellen Anwendungen
August 2016, 202 Seiten

Band 126 W. Genius
Grüne Bilanzierung - Internalisierung von Umwelt- und Gesundheitsschäden im Rahmen der Input-Output-Rechnung
April 2015, 243 Seiten

Band 125 E. Heyden
Kostenoptimale Abwärmerückgewinnung durch integriert-iteratives Systemdesign (KOARiiS) - Ein Verfahren zur energetisch-ökonomischen Bewertung industrieller Abwärmepotenziale
2016, 121 Seiten

Band 124 K. Ohlau
Strategien zur wirksamen Minderung von Fluglärm in Deutschland - Minderungsmaßnahmen und langfristige Perspektiven
2015, 192 Seiten

Band 123 T. Telsnig
Standortabhängige Analyse und Bewertung solarthermischer Kraftwerke am Beispiel Südafrikas
September 2015, 285 Seiten

Band 122 M. Henßler
Ganzheitliche Analyse thermochemischer Verfahren bei der Nutzung fester Biomasse zur Kraftstoffproduktion in Deutschland
April 2015, 243 Seiten

Band 121 B. Fais
Modelling policy instruments in energy system models - the example of renewable electricity generation in Germany
Januar 2015, 194 Seiten

Band 120 M. Blesl
Kraft-Wärme-Kopplung im Wärmemarkt Deutschlands und Europas – eine Energiesystem- und Technikanalyse
August 2014, 204 Seiten

Band 119 S. Kempe
Räumlich detaillierte Potenzialanalyse der Fernwärmeversorgung in Deutschland mit einem hoch aufgelösten Energiesystemmodell
Juli 2014, 204 Seiten

Band 118 B. Thiruchittampalam
Entwicklung und Anwendung von Methoden und Modellen zur Berechnung von räumlich und zeitlich hochaufgelösten Emissionen in Europa
April 2014, 238 Seiten

Band 117 T. Kober
Energiewirtschaftliche Anforderungen an neue fossil befeuerte Kraftwerke mit CO2-Abscheidung im liberalisierten europäischen Elektrizitätsmarkt
März 2014, 158 Seiten

Band 116 S. Wissel
Ganzheitlich-integrierte Betrachtung der Kernenergie im Hinblick auf eine nachhaltige Energieversorgung
Februar 2014, 230 Seiten

Band 115 R. Kuder
Energieeffizienz in der Industrie – Modellgestützte Analyse des effizienten Energieeinsatzes in der EU-27 mit Fokus auf den Industriesektor
Februar 2014, 286 Seiten

Band 114 J. Tomaschek
Long-term optimization of the transport sector to address greenhouse gas reduction targets under rapid growth – Application of an energy system model for Gauteng province, South Africa
Dezember 2013, 263 Seiten

Band 113 B. Rühle
Kosten regionaler Energie- und Klimapolitik - Szenarioanalysen mit einem Energiesystemmodell auf Bundesländerebene
November 2013, 196 Seiten

Band 112 N. Sun
Modellgestützte Untersuchung des Elektrizitätsmarktes - Kraftwerkseinsatzplanung und -investitionen
August 2013, 173 Seiten

Band 111 J. Lambauer
Auswirkungen von Basisinnovationen auf die Energiewirtschaft und die Energienachfrage in Deutschland - Am Beispiel der Nano und Biotechnologie
März 2013, 303 Seiten

Band 110 R. Barth
Ökonomische und technisch-betriebliche Auswirkungen verteilter Elektrizitätserzeugung in Verteilungsnetzen - eine modellgestützte Analyse am Beispiel eines Mittelspannungsnetzes
März 2013, 234 Seiten

Band 109 D. Bruchof
Energiewirtschaftliche Verkehrsstrategie - Möglichkeiten und Grenzen alternativer Kraftstoffe und Antriebe in Deutschland und der EU-27
März 2012, 226 Seiten

Band 108 E. D. Özdemir
The Future Role of Alternative Powertrains and Fuels in the German Transport Sector - A model-based scenario analysis with respect to technical, economic and environmental aspects with a focus on road transport
Januar 2012, 194 Seiten

Band 107 U. Kugler
Straßenverkehrsemissionen in Europa - Emissionsberechnung und Bewertung von Minderungsmaßnahmen
Januar 2012, 236 Seiten

Band 106 M. Blesl, D. Bruchof, U. Fahl, T. Kober, R. Kuder, B. Götz, A. Voß
Integrierte Szenarioanalysen zu Energie- und Klimaschutzstrategien in Deutschland in einem Post-Kyoto-Regime
Februar 2011, 200 Seiten

Band 105 O. Mayer-Spohn
Parametrised Life Cycle Assessment of Electricity Generation in Hard-Coal-Fuelled Power Plants with Carbon Capture and Storage
Dezember 2009, 210 Seiten

Band 104 A. König
Ganzheitliche Analyse und Bewertung konkurrierender energetischer Nutzungspfade für Biomasse im Energiesystem Deutschland bis zum Jahr 2030
Juli 2009, 194 Seiten

Band 103 C. Kruck
Integration einer Stromerzeugung aus Windenergie und Speicher-systemen unter besonderer Berücksichtigung von Druckluft-Speicherkraftwerken
Mai 2008, 162 Seiten

Band 102 U. Fahl, B. Rühle, M. Blesl, I. Ellersdorfer, L. Eltrop, D.-C. Harlinghausen, R. Küster, T. Rehrl, U. Remme, A. Voß
Energieprognose Bayern 2030
Oktober 2007, 296 Seiten

Band 101 U. Remme, M. Blesl, U. Fahl
Global resources and energy trade: An overview for coal, natural gas, oil and uranium
Juli 2007, 108 Seiten

Band 100 S. Eckardt
Energie- und Umweltmanagement in Hotels und Gaststätten: Entwicklung eines Softwaretools zur systematischen Prozessanalyse und Management-unterstützung
Mai 2007, 152 Seiten

Band 99 U. Remme
Zukünftige Rolle erneuerbarer Energien in Deutschland: Sensitivitätsanalysen mit einem linearen Optimierungsmodell
August 2006, 336 Seiten

Band 98 L. Eltrop, J. Moerschner, M. Härdtlein, A. König
Bilanz und Perspektiven der Holzenergienutzung in Baden-Württemberg
Mai 2006, 102 Seiten

Band 97 B. Frey
Modellierung systemübergreifender Energie- und Kohlenstoffbilanzen in Entwicklungsländern
Mai 2006, 148 Seiten

Band 96 K. Sander
Potenziale und Perspektiven stationärer Brennstoffzellen
Juni 2004, 256 Seiten

Band 95 M. A. dos Santos Bernardes
Technische, ökonomische und ökologische Analyse von Aufwindkraftwerken
März 2004, 228 Seiten

Band 94 J. Bagemihl
Optimierung eines Portfolios mit hydro-thermischem Kraftwerkspark im börslichen Strom- und Gasterminmarkt
Februar 2003, 138 Seiten

Band 93 A. Stuible
Ein Verfahren zur graphentheoretischen Dekomposition und algebraischen Reduktion von komplexen Energiesystemmodellen
November 2002, 156 Seiten

Band 92 M. Blesl
Räumlich hoch aufgelöste Modellierung leitungsgebundener Energiever-sorgungssysteme zur Deckung des Niedertemperaturwärmebedarfs
August 2002, 282 Seiten

Band 91 S. Briem, M. Blesl, M. A. dos Santos Bernardes, U. Fahl, W. Krewitt, M. Nill, S. Rath-Nagel, A. Voß
Grundlagen zur Beurteilung der Nachhaltigkeit von Energiesystemen in Baden-Württemberg
August 2002, 138 Seiten

Band 90 B. Frey, M. Neubauer
Energy Supply for Three Cities in Southern Africa
Juli 2002, 96 Seiten

Band 89 A. Heinz, R. Hartmann, G. Hitzler, G. Baumbach
Wissenschaftliche Begleitung der Betriebsphase der mit Rapsölmethylester befeuerten Energieversorgungsanlage des Deutschen Bundestages in Berlin
Juli 2002, 212 Seiten

Band 88 M. Sawillion
Aufbereitung der Energiebedarfsdaten und Einsatzanalysen zur Auslegung von Blockheizkraftwerken
Juli 2002, 136 Seiten

Band 87 T. Marheineke
Lebenszyklusanalyse fossiler, nuklearer und regenerativer Stromerzeugungs-techniken
Juli 2002, 222 Seiten

Band 86 B. Leven, C. Hoeck, C. Schaefer, C. Weber, A. Voß
Innovationen und Energiebedarf - Analyse ausgewählter Technologien und Branchen mit dem Schwerpunkt Stromnachfrage
Juni 2002, 224 Seiten

Band 85 E. Laege
Entwicklung des Energiesektors im Spannungsfeld von Klimaschutz und Ökonomie - Eine modellgestützte Systemanalyse
Januar 2002, 254 Seiten

Band 84 S. Molt
Entwicklung eines Instrumentes zur Lösung großer energiesystem-analytischer Optimierungsprobleme durch Dekomposition und verteilte Berechnung
Oktober 2001, 166 Seiten

Band 83 D. Hartmann
Ganzheitliche Bilanzierung der Stromerzeugung aus regenerativen Energien
September 2001, 228 Seiten

Band 82 G. Kühner
Ein kosteneffizientes Verfahren für die entscheidungsunterstützende Umweltanalyse von Betrieben
September 2001, 210 Seiten

Band 81 I. Ellersdorfer, H. Specht, U. Fahl, A. Voß
Wettbewerb und Energieversorgungsstrukturen der Zukunft
August 2001, 172 Seiten

Band 80 B. Leven, J. Neubarth, C. Weber
Ökonomische und ökologische Bewertung der elektrischen Wärmepumpe im Vergleich zu anderen Heizungssystemen
Mai 2001, 166 Seiten

Band 79 R. Krüger, U. Fahl, J. Bagemihl, D. Herrmann
Perspektiven von Wasserstoff als Kraftstoff im öffentlichen Straßen-personenverkehr von Ballungsgebieten und von Baden-Württemberg
April 2001, 142 Seiten

Band 78 A. Freibauer, M. Kaltschmitt (eds.)
Biogenic Greenhouse Gas Emissions from Agriculture in Europe
Februar 2001, 248 Seiten

Band 77 W. Rüffler
Integrierte Ressourcenplanung für Baden-Württemberg
Januar 2001, 284 Seiten

Band 76 S. Rivas
Ein agro-ökologisches regionalisiertes Modell zur Analyse des Brennholz-versorgungssystems in Entwicklungsländern
Januar 2001, 200 Seiten

Band 75 M. Härdtlein
Ansatz zur Operationalisierung ökologischer Aspekte von "Nachhaltigkeit" am Beispiel der Produktion und Nutzung von Triticale (×*Triticosecale* Wittmack)-Ganzpflanzen unter besonderer Berücksichtigung der luftgetragenen N-Freisetzungen
September 2000, 168 Seiten

Band 74 T. Marheineke, W. Krewitt, J. Neubarth, R. Friedrich, A. Voß
Ganzheitliche Bilanzierung der Energie- und Stoffströme von Energieversorgungstechniken
August 2000, 118 Seiten

Band 73 J. Sontow
Energiewirtschaftliche Analyse einer großtechnischen Windstromerzeugung
Juli 2000, 242 Seiten

Band 72 H. Hermes
Analysen zur Umsetzung rationeller Energieanwendung in kleinen und mittleren Unternehmen des Kleinverbrauchersektors
Juli 2000, 188 Seiten

Band 71 C. Schaefer, C. Weber, H. Voss-Uhlenbrock, A. Schuler, F. Oosterhuis, E. Nieuwlaar, R. Angioletti, E. Kjellsson, S. Leth-Petersen, M. Togeby, J. Munksgaard
Effective Policy Instruments for Energy Efficiency in Residential Space Heating - an International Empirical Analysis (EPISODE)
Juni 2000, 146 Seiten

Band 70 U. Fahl, J. Baur, I. Ellersdorfer, D. Herrmann, C. Hoeck, U. Remme, H. Specht, T. Steidle, A. Stuible, A. Voß
Energieverbrauchsprognose für Bayern
Mai 2000, 240 Seiten

Band 69 J. Baur
Verfahren zur Bestimmung optimaler Versorgungsstrukturen für die Elektrifizierung ländlicher Gebiete in Entwicklungsländern
Mai 2000, 154 Seiten

Band 68 G. Weinrebe
Technische, ökologische und ökonomische Analyse von solarthermischen Turmkraftwerken
April 2000, 212 Seiten

Band 67 C.-O. Wene, A. Voß, T. Fried (eds.)
Experience Curves for Policy Making - The Case of Energy Technologies
April 2000, 282 Seiten

Band 66 A. Schuler
Entwicklung eines Modells zur Analyse des Endenergieeinsatzes in Baden-Württemberg
März 2000, 236 Seiten

Band 65 A. Schäfer
Reduction of CO_2-Emissions in the Global Transportation Sector
März 2000, 290 Seiten

Band 64 A. Freibauer, M. Kaltschmitt (eds.)
Biogenic Emissions of Greenhouse Gases Caused by Arable and Animal Agriculture - Processes, Inventories, Mitigation
März 2000, 148 Seiten

Band 63 A. Heinz, R. Stülpnagel, M. Kaltschmitt, K. Scheffer, D. Jezierska
Feucht- und Trockengutlinien zur Energiegewinnung aus biogenen Festbrennstoffen. Vergleich anhand von Energie- und Emissionsbilanzen sowie anhand der Kosten
Dezember 1999, 308 Seiten

Band 62 U. Fahl, M. Blesl, D. Herrmann, C. Kemfert, U. Remme, H. Specht, A. Voß
Bedeutung der Kernenergie für die Energiewirtschaft in Baden-Württemberg - Auswirkungen eines Kernenergieausstiegs
November 1999, 146 Seiten

Band 61 A. Greßmann, M. Sawillion, W. Krewitt, R. Friedrich
Vergleich der externen Effekte von KWK-Anlagen mit Anlagen zur getrennten Erzeugung von Strom und Wärme
September 1999, 138 Seiten

Band 60 R. Lux
Auswirkungen fluktuierender Einspeisung auf die Stromerzeugung konventioneller Kraftwerkssysteme
September 1999, 162 Seiten

Band 59 M. Kayser
Energetische Nutzung hydrothermaler Erdwärmevorkommen in Deutschland - Eine energiewirtschaftliche Analyse -
Juli 1999, 184 Seiten

Band 58 C. John
Emissionen von Luftverunreinigungen aus dem Straßenverkehr in hoher räumlicher und zeitlicher Auflösung - Untersuchung von Emissionsszenarien am Beispiel Baden-Württembergs
Juni 1999, 214 Seiten

Band 57 T. Stelzer
Biokraftstoffe im Vergleich zu konventionellen Kraftstoffen - Lebensweganalysen von Umweltwirkungen
Mai 1999, 212 Seiten

Band 56 R. Lux, J. Sontow, A. Voß
Systemtechnische Analyse der Auswirkungen einer windtechnischen Stromerzeugung auf den konventionellen Kraftwerkspark
Mai 1999, 322 Seiten

Band 55 B. Biffar
Messung und Synthese von Wärmelastgängen in der Energieanalyse
Mai 1999, 236 Seiten

Band 54 E. Fleißner
Statistische Methoden der Energiebedarfsanalyse im Kleinverbrauchersektor
Januar 1999, 306 Seiten

Band 53 A. Freibauer, M. Kaltschmitt (Hrsg.)
Approaches to Greenhouse Gas Inventories of Biogenic Sources in Agriculture
Januar 1999, 252 Seiten

Band 52 J. Haug, B. Gebhardt, C. Weber, M. van Wees, U. Fahl, J. Adnot, L. Cauret, A. Pierru, F. Lantz, J.-W. Bode, J. Vis, A. van Wijk, D. Staniaszek, Z. Zavody
Evaluation and Comparison of Utility's and Governmental DSM-Programmes for the Promotion of Condensing Boilers
Oktober 1998, 156 Seiten

Band 51 M. Blesl, A. Schweiker, C. Schlenzig
Erweiterung der Analysemöglichkeiten von *NetWork* - Der Netzwerkeditor
September 1998, 112 Seiten

Band 50 S. Becher
Biogene Festbrennstoffe als Substitut für fossile Brennstoffe - Energie- und Emissionsbilanzen
Juli 1998, 200 Seiten

Band 49 P. Schaumann, M. Blesl, C. Böhringer, U. Fahl, R. Kühner, E. Läge, S. Molt, C. Schlenzig, A. Stuible, A. Voß
Einbindung des ECOLOG-Modells '*E³Net*' und Integration neuer methodischer Ansätze in das *IKARUS*-Instrumentarium (*ECOLOG II*)
Juli 1998, 110 Seiten

Band 48 G. Poltermann, S. Berret
ISO 14000ff und Öko-Audit - Methodik und Umsetzung
März 1998, 184 Seiten

Band 47 C. Schlenzig
PlaNet: Ein entscheidungsunterstützendes System für die Energie- und Umweltplanung
Januar 1998, 230 Seiten

Band 46 R. Friedrich, P. Bickel, W. Krewitt (Hrsg.)
External Costs of Transport
April 1998, 144 Seiten

Band 45 H.-D. Hermes, E. Thöne, A. Voß, H. Despretz, G. Weimann, G. Kamelander, C. Ureta
Tools for the Dissemination and Realization of Rational Use of Energy in Small and Medium Enterprises
Januar 1998, 352 Seiten

Band 44 C. Weber, A. Schuler, B. Gebhardt, H.-D. Hermes, U. Fahl, A. Voß
Grundlagenuntersuchungen zum Energiebedarf und seinen Bestimmungsfaktoren
Dezember 1997, 186 Seiten

Band 43 J. Albiger
Integrierte Ressourcenplanung in der Energiewirtschaft mit Ansätzen aus der Kraftwerkseinsatzplanung
November 1997, 168 Seiten

Band 42 P. Berner
Maßnahmen zur Minderung der Emissionen flüchtiger organischer Verbindungen aus der Lackanwendung - Vergleich zwischen Abluftreinigung und primären Maßnahmen am Beispiel Baden-Württembergs
November 1997, 238 Seiten

Band 41 J. Haug, M. Sawillion, U. Fahl, A. Voß, R. Werner, K. Weiß, J. Rösch, W. Wölfle
Analysis of Impediments to the Rational Use of Energy in the Public Sector and Implementation of Third Party Financing Strategies to improve Energy Efficiency
August 1997, 122 Seiten

Band 40 U. Fahl, R. Krüger, E. Läge, W. Rüffler, P. Schaumann, A. Voß
Kostenvergleich verschiedener CO_2-Minderungsmaßnahmen in der Bundesrepublik Deutschland
August 1997, 156 Seiten

Band 39 M. Sawillion, B. Biffar, K. Hufendiek, R. Lux, E. Thöne
MOSAIK - Ein EDV-Instrument zur Energieberatung von Gewerbe und mittelständischer Industrie
Juli 1997, 172 Seiten

Band 38 M. Kaltschmitt
Systemtechnische und energiewirtschaftliche Analyse der Nutzung erneuerbarer Energien in Deutschland
April 1997, 108 Seiten

Band 37 C. Böhringer, T. Rutherford, A. Pahlke, U. Fahl, A. Voß
Volkswirtschaftliche Effekte einer Umstrukturierung des deutschen Steuersystems unter besonderer Berücksichtigung von Umweltsteuern
März 1997, 82 Seiten

Band 36 P. Schaumann
Klimaverträgliche Wege der Entwicklung der deutschen Strom- und Fernwärmeversorgung - Systemanalyse mit einem regionalisierten Energiemodell
Januar 1997, 282 Seiten

Band 35 R. Kühner
Ein verallgemeinertes Schema zur Bildung mathematischer Modelle energiewirtschaftlicher Systeme
Dezember 1996, 262 Seiten

Band 34 U. Fahl, P. Schaumann
Energie und Klima als Optimierungsproblem am Beispiel Niedersachsen
November 1996, 124 Seiten

Band 33 W. Krewitt
Quantifizierung und Vergleich der Gesundheitsrisiken verschiedener Stromerzeugungssysteme
November 1996, 196 Seiten

Band 32 C. Weber, B. Gebhardt, A. Schuler, T. Schulze, U. Fahl, A. Voß, A. Perrels, W. van Arkel, W. Pellekaan, M. O'Connor, E. Schenk, G. Ryan
Consumers' Lifestyles and Pollutant Emissions
September 1996, 118 Seiten

Band 31 W. Rüffler, A. Schuler, U. Fahl, H.W. Balandynowicz, A. Voß
Szenariorechnungen für das Projekt *Klimaverträgliche Energieversorgung in Baden-Württemberg*
Juli 1996, 140 Seiten

Band 30 C. Weber, B. Gebhardt, A. Schuler, U. Fahl, A. Voß
Energy Consumption and Air-Borne Emissions in a Consumer Perspective
September 1996, 264 Seiten

Band 29 M. Hanselmann
Entwicklung eines Programmsystems zur Optimierung der Fahrweise von Kraft-Wärme-Kopplungsanlagen
August 1996, 138 Seiten

Band 28 G. Schmid
Die technisch-ökonomische Bewertung von Emissionsminderungsstrategien mit Hilfe von Energiemodellen
August 1996, 184 Seiten

Band 27 A. Obermeier, J. Seier, C. John, P. Berner, R. Friedrich
TRACT: Erstellung einer Emissionsdatenbasis für TRACT
August 1996, 172 Seiten

Band 26 T. Hellwig
OMNIUM - Ein Verfahren zur Optimierung der Abwärmenutzung in Industriebetrieben
Mai 1998, 118 Seiten

Band 25 R. Laing
CAREAIR - ein EDV-gestütztes Instrumentarium zur Untersuchung von Emissionsminderungsstrategien für Dritte-Welt-Länder dargestellt am Beispiel Nigerias
Februar 1996, 221 Seiten

Band 24 P. Mayerhofer, W. Krewitt, A. Trukenmüller, A. Greßmann, P. Bickel, R. Friedrich
Externe Kosten der Energieversorgung
März 1996, Kurzfassung, 40 Seiten

Band 23 M. Blesl, C. Schlenzig, T. Steidle, A. Voß
Entwicklung eines Energieinformationssystems
März 1996, 76 Seiten

Band 22 M. Kaltschmitt, A. Voß
Integration einer Stromerzeugung aus Windkraft und Solarstrahlung in den konventionellen Kraftwerksverbund
Juni 1995, Kurzfassung, 51 Seiten

Band 21 U. Fahl, E. Läge, W. Rüffler, P. Schaumann, C. Böhringer, R. Krüger, A. Voß
Emissionsminderung von energiebedingten klimarelevanten Spurengasen in der Bundesrepublik Deutschland und in Baden-Württemberg
September 1995, 454 Seiten

Band 20 M. Fischedick
Erneuerbare Energien und Blockheizkraftwerke im Kraftwerksverbund - Technische Effekte, Kosten, Emissionen
Dezember 1995, 196 Seiten

Band 19 A. Obermeier
Ermittlung und Analyse von Emissionen flüchtiger organischer Verbindungen in Baden-Württemberg
Mai 1995, 208 Seiten

Band 18 N. Kalume
Strukturmodule - Ein methodischer Ansatz zur Analyse von Energiesystemen in Entwicklungsländern
Dezember 1994, 113 Seiten

Band 17 Th. Müller
Ermittlung der SO_2- und NO_x-Emissionen aus stationären Feuerungsanlagen in Baden-Württemberg in hoher räumlicher und zeitlicher Auflösung
November 1994, 142 Seiten

Band 16 A. Wiese
Simulation und Analyse einer Stromerzeugung aus erneuerbaren Energien in Deutschland
Juni 1994, 223 Seiten

Band 15 M. Sawillion, T. Hellwig, B. Biffar, R. Schelle, E. Thöne
Optimierung der Energieversorgung eines Industrieunternehmens unter Umweltschutz- und Wirtschaftlichkeitsaspekten - Wertanalyse-Projekt
Januar 1994, 154 Seiten

Band 14 M. Heymann, A. Trukenmüller, R. Friedrich
Development prospects for emission inventories and atmospheric transport and chemistry models
November 1993, 105 Seiten

Band 13 R. Friedrich
Ansatz zur Ermittlung optimaler Strategien zur Minderung von Luftschadstoffemissionen aus Energieumwandlungsprozessen
Juli 1992, 292 Seiten

Band 12 U. Fahl, M. Fischedick, M. Hanselmann, M. Kaltschmitt, A. Voß
Abschätzung der technischen und wirtschaftlichen Minderungspotentiale energiebedingter CO_2-Emissionen durch einen verstärkten Erdgaseinsatz in der Elektrizitätsversorgung Baden-Württembergs unter besonderer Berücksichtigung konkurrierender Nutzungsmöglichkeiten
August 1992, 471 Seiten

Band 11 M. Kaltschmitt, A. Wiese
Potentiale und Kosten regenerativer Energieträger in Baden-Württemberg
April 1992, 320 Seiten

Band 10 A. Reuter
Entwicklung und Anwendung eines mikrocomputergestützte Energieplanungsinstrumentariums für den Einsatz in Entwicklungsländern
November 1991, 170 Seiten

Band 9 T. Kohler
Einsatzmöglichkeiten für Heizreaktoren im Energiesystem der Bundesrepublik Deutschland
Juli 1991, 162 Seiten

Band 8 M. Mattis
Kosten und Auswirkungen von Maßnahmen zur Minderung der SO_2- und NO_x-Emissionen aus Feuerungsanlagen in Baden-Württemberg
Juni 1991, 188 Seiten

Band 7 M. Kaltschmitt
Möglichkeiten und Grenzen einer Stromerzeugung aus Windkraft und Solarstrahlung am Beispiel Baden-Württembergs
Dezember 1990, 178 Seiten

Band 6 G. Schmid, A. Voß, H.W. Balandynowicz, J. Cofala, Z. Parczewski
Air Pollution Control Strategies - A Comparative Analysis for Poland and the Federal Republic of Germany
Juli 1990, 92 Seiten

Band 5 Th. Müller, B. Boysen, U. Fahl, R. Friedrich, M. Kaltschmitt, R. Laing, A. Voß, J. Giesecke, K. Jorde, C. Voigt
Regionale Energie- und Umweltanalyse für die Region Neckar-Alb
Juli 1990, 484 Seiten

Band 4 Th. Müller, B. Boysen, U. Fahl, R. Friedrich, M. Kaltschmitt, R. Laing, A. Voß, J. Giesecke, K. Jorde, C. Voigt
Regionale Energie- und Umweltanalyse für die Region Hochrhein-Bodensee
Juni 1990, 498 Seiten

Band 3 D. Kluck
Einsatzoptimierung von Kraftwerkssystemen mit Kraft-Wärme-Kopplung
Mai 1990, 155 Seiten

Band 2 M. Fleischhauer, R. Friedrich, S. Häring, A. Haugg, J. Müller, A. Reuter, A. Voß, H.-G. Wystrcil
Grundlagen zur Abschätzung und Bewertung der von Kohlekraftwerken ausgehenden Umweltbelastungen in Entwicklungsländern
Mai 1990, 316 Seiten

Band 1 U. Fahl
KDS - Ein System zur Entscheidungsunterstützung in Energiewirtschaft und Energiepolitik
März 1990, 265 Seiten

Inhalt

Paper drying is the most energy-intensive step in paper making and leads to significant CO_2-emissions at paper mills where fossil fuels are used to generate the required heat. From the different technologies used for paper drying, multi-cylinder paper drying is the most widespread method constituting around 90% of the installed capacity.

In this research a model was developed in MATLAB which encompasses all modules needed for the assessment of energy-efficiency and CO_2-saving measures in multi-cylinder paper drying. Methods for the energy and economic assessment of measures and combinations of measures were developed on top of the model, and a new methodology for the construction of marginal energy-saving cost curves and marginal abatement cost curves accounting for interactions between measures was proposed.

The developed framework was applied to the drying section of a German mill to analyse the effect of the replacement of film sizing with curtain sizing, the replacement of iron cast cylinders with steel cylinders, the closure of the current semi-closed hood, and the integration of heat pumps using hood exhaust air as a heat source to heat the hood supply air and generate steam for the dryers. The model results showed that a reduction of the steam demand by 51.3% (1.79 GJ_{th}/t_{paper}) at the cost of an increase of the electricity demand by 72.1% (0.2 GJ_{el}/t_{paper}) due to the operation of heat pumps is expected at the drying section after implementing all energy-efficiency measures. For the same combination of measures, the calculated technical and economic CO_2-emissions reduction potentials are equal to 0.16 kg_{CO2}/t_{paper} and 0.12 kg_{CO2}/t_{paper}. Implementing fuel switching from coal to alternative fuels in addition to the energy-efficiency measures allows to reach a total technical CO_2-emissions reduction potential of 0.33 kg_{CO2}/t_{paper} in the case of a fuel switch to biomass or green hydrogen, and 0.24 kg_{CO2}/t_{paper} for a switch to natural gas or electricity.

Differences ranging from ±1.6% to above ±200% are observed between the individual and cumulative values obtained for the energy savings, CO_2-emission reduction potential, and the total annual cost which demonstrates the importance of accounting for interactions when analyzing the implementation of multiple CO_2-emissions reduction measures at a site.

IER - Institut für Energiewirtschaft
und Rationelle Energieanwendung
Universität Stuttgart
Heßbrühlstr. 49a
D-70565 Stuttgart